Cyclic Nucleotide Signalling in Cardiac Myocytes from the mdx Model of Duchenne Muscular Dystrophy

Marcella Dias Brescia
Green Templeton College



This thesis is submitted for the degree of Doctor of Philosophy at the University of Oxford

Trinity Term 2017

Supervised by Professor Manuela Zaccolo

Department of Physiology, Anatomy and Genetics

Approximate word count: 36.000 words

To my mom, all my family and to Tim.
For their endless and essential support.

A minha mãe, toda família e ao Tim.
Pelo apoio incondicional e essencial.

Abstract

Cyclic nucleotide signalling in cardiac myocytes from the mdx model of Duchenne Muscular Dystrophy

Marcella Dias Brescia, Green Templeton College
Thesis submitted for the degree of Doctor of Philosophy, University of Oxford, Trinity 2017

Background and Aims: Duchenne muscular dystrophy (DMD), the most frequent muscular dystrophy, is caused by mutations in the dystrophin gene resulting in the absence of dystrophin. Loss of cardiac dystrophin eventually leads to dilated cardiomyopathy and congestive heart failure in at least 20% of patients. Previous studies have shown that inhibition of enzymes that degrade cGMP improves cardiac contractility, energy metabolism and cardiac myocyte integrity in the DMD mouse model *mdx*. The aim of this project is to explore whether defective cGMP and cAMP signalling is a feature of mdx cardiac myocytes and whether this may play a role in the pathogenesis of the cardiomyopathy associated with dystrophin deficiency.

Methods: Live-cell fluorescent imaging of Fluoresence Resonance Energy Transfer (FRET) has been used to investigate real-time changes in cAMP and cGMP in specific subcellular compartments of neonatal and adult isolated cardiomyocytes. The IonOptix contractility and force transducer system were used to explore the contractile performance and force generation upon contraction in mdx adult cardiomyocytes.

Results: cAMP and cGMP regulation and compartmentalisation seem to be significantly altered in *mdx* mice cardiomyocytes. The data suggest that the activity of several isoforms of phosphodiesterase and the ability to generate cGMP and cAMP in specific subcellular compartments is altered in neonatal cardiomyocytes (NCM) from the *mdx* model, indicating that not only the cGMP pathway might underpin the cardiomyopathy associated with DMD but disruption of cAMP signalling may also play a role. Analysis of cyclic nucleotide signalling in adult *mdx* cardiac myocytes indicated significantly higher levels of oxidised sGC and PDE mRNA levels. Additionally, adult mdx cardiomyocytes presented lower nNOS expression in the PM and in the ER. Basal levels of cyclic nucleotides significantly changed with age, suggesting that compensatory mechanisms may develop with age. Furthermore, mdx cardiomyocytes showed significantly impaired force of contraction which was abolished upon IBMX treatment suggesting that altered PDE activity might underpin defects in contractility.

Conclusions: In summary, the data presented in this thesis supports the hypothesis that defective cyclic nucleotides signalling might play a role in the cardiomyopathy associated with DMD in the mdx.

Declaration of own work

No portion of the document has been submitted for another degree at this University, or for a degree at any other institution.

This DPhil thesis is entirely my own work, however, two members of the Zaccolo group have contributed to some of the experimental data presented in this thesis:

- Some experimental data (2 graphs) presented in Chapter 3 in improving the isolation protocol were performed in collaboration with Dr. Oliver Lomas who was a DPhil student at the Zaccolo lab at the time when those experiments were performed.

- Dr. Andreas Koschinski, a Postdoctoral fellow at Zaccolo group, has performed many of the ‘in cell' calibration experiments presented in Chapter 4 and has taught me the related techniques.

Marcella Dias Brescia
September 2017

Acknowledgements

Nothing could have been achieved without the presence and support of the wonderful people I encountered along my way. The gratitude and admiration that I feel for all of them are so great that no words can fully convey my sincere thankfulness.

First and foremost, I would like to thank my supervisor Prof. Manuela Zaccolo for her guidance, efforts, input, support and understanding throughout all these years. She has been a tremendous inspiration and an excellent mentor. Her scientific and personal support has been invaluable in bringing this DPhil to completion. I also would like to thank her for opening the doors of her lab for me when I was still an undergraduate student and for allowing me to be part of her excellent team during my PhD. These were life changing experiences which I will be always thankful for.

I am also extremely grateful for the friendly and pleasant work environment of the Zaccolo group. All my labmates, who became the dearest friends, had great impact on my scientific and personal growth. I would like to specially thank Dr. Nicoletta C. Surdo, Dr. Andreas Koschinski and Dr. Stefania Monterisi for opening the doors of the lab for me on my very first day and for having me by their side since then, mentoring and inspiring me. As for them, I am also extremely thankful to Dr. Katharina Schleicher, Nshunge Musheshe, Miguel Lobo and Dr. Oliver Lomas. All the help, advices, discussions and conversations, guidance and friendship provided by each of them were essential. It has been an immense honour and pleasure to work with all of them.

Furthermore, a number of individuals outside the Zaccolo group also contributed to the completion of thesis and my scientific development. I would like to deeply thank Dr. Corinne Betts who has helped me since the very start giving me access to the mdx mice and expert advice on DMD and dystrophin related experiments. I am also very thankful to Dr. Konstantinos Lefkimmiatis for his advice on molecular biology and teaching; Prof. Pawel Swietach and Dr. Alzbeta Hulikova for being great neighbours with constructive discussions and help with confocal imaging. Special thanks go to Prof Barbara Casadei, Prof Matthew Wood and Prof Pawel Swietach for their assessment of progress and insightful input provided during the Transfer of Status and the Confirmation of Status. I would also like to thank Prof Andreia Laura for her support since my undergraduate degree, for inspiring me with science and opening the doors for my scientific growth.

I am grateful for CNPq for funding my studies, for the Department of Physiology, Anatomy and Genetics and the Green Templeton College communities for providing outstanding learning possibilities and engagement, as well as funds to present my work at international conferences. I

am extremely grateful to my college advisor Prof Leanne Hodson, for always being available when I needed guidance and advice, as well as for the scientific and person support and motivational conversation during dinners and meetings. I feel tremendously lucky to have had her as my college advisor.

I would like to deeply thank all my friends, in special Tete, Lele, Tássia, Sâmia, Pri Preta, Naback, Aninha, Bellinha, Ju and Lu for their constant support and for proving that real friendship is never affected by distance. Also, to all my friends in Oxford who have been sharing with me this great adventure called PhD, in special Carol, Luiza, Pri, Sergio, Ari, Willian, Henrique, Lucas, Ivo, Thais and Fabio.

Finally, I wish to dedicate this thesis to my family: minha mãe, Luiz, meu pai, Tia Lucia, Renata, Roberta, Tia Fatinha, Tio, Gabriel, Marina, Mariana, Vovô, Pedro, Tia Junia, Leo and to Tim and his family for their love and immeasurable support. Nothing would be worth if it wasn't for you. A very special thanks to my partner, Tim for the help, motivation, patience, support and love during all my DPhil and specially while I was putting this thesis together.

Acronyms and Abbreviations

AC – Adenylyl cyclase

AKAP – A-Kinase Anchoring Protein

AKAR – A-Kinase Activity Reporter

ATP – Adenosine Triphosphate

BL10 – C57BL/10ScSn

CAR – Coxackie and Adenovirus Receptor

CFP – Cyan Fluorescent Protein

CHO – Chinese Hamster Ovary Cell Line

CNBD – Cyclic Nucleotide Binding Domain

DAPC – Dystrophin Associated Complex

DMD – Duchenne Muscular Dystrophy

DNA – Deoxyribonucleic acid

EPAC – Exchange Protein directly Activated by cAMP

ER – Endoplasmic Reticulum

FRET – Fluoresence Resonance Energy Transfer

GAPDH – Glyceraldehyde 3-phosphate dehydrogenase

GFP – Green Fluorescent Protein

IBMX – 3-Isobutyl-1-Methylxanthine

LTCC – L-Type Calcium Channel

LV – Left Ventricle

MOI – Multiplicity of Infection

NRCM – Neonatal Cardiac Myocytes

NO – Nitric Oxide

NOS – Nitric Oxide Synthase

PDE – Phosphodiesterase

PKA – Protein Kinase A

PKG – Protein Kinase G

RI – Regulatory subunit (Type 1 of PKA)

RIA – Radioimmunoassay

RII – Regulatory subunit (Type 2 of PKA)

ROS – Reactive Oxygen Species

SR – Sarcoplasmic Reticulum

TNI – Troponin I

YFP – Yellow fluorescent protein

WT – Wild Type

cAMP – Cyclic Adenosine MonoPhosphate

eNOS – Endothelial Nitric Oxide Synthase

iNOS – Inducible Nitric Oxide Synthase

nNOS – Neuronal Oxide Synthase

sGC – Soluble Guanylyl Cyclase

Table of Contents

CHAPTER 1. INTRODUCTION 17

1.1. The cyclic nucleotides 17

1.1.1. The generation of cAMP 18

1.1.2. The generation of cGMP 20

1.2. Phosphodiesterases 23

1.3. Cyclic nucleotide's compartmentalisation 28

1.3.1. cAMP compartmentalised signalling 28

1.3.2. NO - cGMP compartmentalised signalling 31

1.4. Role of the PDEs in signalling compartmentalisation 33

1.5. Local inhibition of phosphodiesterase activity 36

1.6. Introduction to Duchenne Muscular Dystrophy 40

1.6.1. The dystrophin associated complex (DAPC) 40

1.6.2. Some molecular pathologies associated to the disease 42

1.6.3. DMD cardiomyopathy 45

1.6.4. DMD animal models 45

1.7. Aim of this thesis 46

1.8. References 49

CHAPTER 2. METHODS 59

2.1. Preparation of isolated cardiomyocytes 59

2.1.1. Adult Mouse Left ventricular cardiomyocyte isolation 59

2.2. Imaging 64

2.2.1. FRET microscopy experiments 64

2.2.2. Immunofluorescence staining and confocal imaging 67

2.2.3. FRET-based sensor calibration 67

2.3. Biochemistry 72

2.3.1. Western blotting 72

2.3.2. Cell fractionation and western blotting 72

2.3.3. cAMP and cGMP ELISA 73

2.3.4. sGC activity assay 73

2.3.5. qPCR 74

2.4. Construction of targeted FRET-based sensors 75

2.5. Sarcomere shortening and force measurements 78
2.6. Statistics 84
2.7. References 86

CHAPTER 3: OPTIMISATION OF ADULT MICE CARDIOMYOCYTES ISOLATION AND INFECTION 87
3.1. Introduction 87
3.2. Initial protocol 89
3.2.1. Characterisation of Isolated cardiomyocytes - Initial protocol 91
3.3. Improved protocol 92
3.3.1. Culture medium and addition of Cytochalasin D 93
3.3.2. Adenovirus infection 95
3.3.3. Heart extraction 98
3.3.4. Contractility 100
3.4. Characterization of isolated MDX cardiomyocytes 104
3.5. Discussion and conclusion 109
3.6. References 113

CHAPTER 4. CONSTRUCTION AND CHARACTERIZATION OF FRET-BASED SENSORS 115
4.1. Introduction 115
4.1.1. Detection of cyclic nucleotides in living cells 115
4.1.2. FRET 116
4.1.3. FRET- based sensors 118
4.1.4. Measuring intracellular cGMP in live cells 124
4.1.5. Targeted FRET-based sensors 129
4.1.6 Calibration of FRET sensors 131
4.2. Aims of this chapter 133
4.3. An attempt to further improve the cGI500 FRET-based sensor 134
4.4. Generation of targeted cGMP and cAMP FRET-based sensors 138
4.4.1. Cloning strategy 139
4.5. Characterization of the new sensors 142
4.6. Discussion and conclusions 146
4.7. References 148

CHAPTER 5. ANALYSIS OF COMPARTMENTALISED CAMP AND CGMP SIGNALLING IN DYSTROPHIC CARDIAC MYOCYTES 155

5.1. introduction on Cyclic nucleotides and Duchenne Muscular Dystrophy ... 155

5.1.1. cAMP and Duchenne Muscular Dystrophy 155

5.1.2. NO - cGMP and Duchenne Muscular Dystrophy 157

5.2. Specific aims 166

5.3. Results 168

5.3.1. nNOS, eNOS and iNOS expression levels in specific cardiomyocyte compartments change with age 168

5.3.2. mdx cardiomyocytes show significant differences in basal cyclic nucleotide levels 181

5.3.3. PDE levels are altered in the cytosol of mdx cardiomyocytes..... 186

5.3.4. mdx cardiomyocytes show compromised ability to generate cAMP and present different levels of PDE activity 192

5.3.5. Adult mdx cardiomyocytes present higher levels of NO insensitive $_{s}$GC .. 199

5.3.6. mdx neonatal cardiomyocytes present altered basal levels of $_{c}$AMP and $_{c}$GMP at specific subcellular compartments. 204

5.3.7. PDE activity is significantly altered at the plasma membrane of neonatal mdx cardiomyocytes 207

5.3.8. The $_{c}$AMP pathway but not $_{c}$GMP is affected at the outer mitochondria membrane of mdx neonatal cardiomyocytes 216

5.4. Summary and Discussion 225

5.5. References 231

CHAPTER 6. CONTRACTILITY ANALYSIS OF MDX CARDIOMYOCYTE UPON CYCLASE STIMULATION 236

6.1. Introduction 236

6.1.1. Cardiomyocyte contractility..... 236

6.1.2. Calcium modulation by beta-adrenergic stimulation 241

6.1.3. Nitric oxide and $_{c}$GMP effect in cardiac contractility..... 244

6.1.4. Sarcomere length, tension and force of contraction relationship..... 245

6.2. Specific aims 246

6.3. Results 247

6.3.1. Unloaded mdx cardiomyocytes contracts similarly to healthy cells upon increase in cAMP however present defective relaxation upon NO donors application. 247

6.3.2. mdx cardiomyocytes generate significantly lower force under tension..... 249

6.4. Discussion **255**
6.5. References **258**
CHAPTER 7. CONCLUDING REMARKS **262**
APPENDIX 1. SOLUTIONS AND REAGENTS **264**

List of Figures and Tables

Chapter 1

Figure 1.1. G-coupled protein receptors and cAMP generation in the heart

Figure 1.2. Membrane-bound and soluble GC generation of cGMP in the heart

Figure 1.3. Hydrolysis of cyclic nucleotides by phosphodiesterases

Figure 1.4. Schematic representation of PDEs

Table 1.1. Biochemical characteristics of PDEs

Figure 1.5. cAMP compartmentalisation in cardiomyocytes

Figure 1.6. The dystrophin associated complex

Figure 1.7. Molecular pathways in heathy and dystrophic cells

Chapter 2

Figure 2.1. Langendorff Perfusion Apparatus and perfused heart

Figure 2.2. Analysis of FRET experiment

Figure 2.3. Microinfusion technique - schematic of ‘in cell’ FRET sensor calibration

Figure 2.4. Saponin calibration schematic

Figure 2.5. qPCR analysis

Figure 2.6. Targeted FRET-based sensor - Cloning strategy

Table 2.1. Monotonic Analysis Parameters used for analysis

Figure 2.7. Unloaded Cardiomyocyte Contractility

Figure 2.8. Analysis of sarcomere shortening and force of contraction

Chapter 3

Figure 3.1. Cardiomyocytes autofluorescence under different conditions

Figure 3.2. Influence of adenovirus infection on the number of contractile cells

Figure 3.3. Fractional shortening comparison of fresh and cultured cardiomyocytes (initial protocol)

Figure 3.4. SYTOX green cell viability assay- M199 vs. MEM

Figure 3.5. SYTOX green cell viability assay quantification and comparison.

Figure 3.6. Adenovirus infection efficiency under M199 and MEM

Figure 3.7. Adenovirus infection efficiency assay quantification and comparison

Figure 3.8. Improvement in cardiomyocytes’ morphology under different isolation protocols

Figure 3.9. Improvement in the initial yield of cells from the different isolation protocols

Figure 3.10. Fractional shortening comparison of fresh and cultured cardiomyocytes (improved protocol)

Figure 3.11. Fractional shortening comparison between different culturing conditions

Figure 3.12. Adenovirus infection and cell viability assay in MDX cardiomyocytes

Figure 3.13. MDX adenovirus infection and cell viability assay quantification and comparison.

Figure 3.14. Fractional shortening comparison of fresh and cultured MDX cardiomyocytes.

Figure 3.15. Fractional shortening comparison of fresh and cultured cardiomyocytes – WT vs. MDX

Table 3.1. Summary of improvements on isolating cardiomyocytes

Chapter 4

Figure 4.1. FRET equations

Figure 4.2. FRET sensor

Figure 4.3. cAMP FRET sensors

Figure 4.4. cGMP FRET sensors

Figure 4.5. Structure of the different targeting strategies

Figure 4.6. Microinfusion technique - schematic of ‘in cell’ FRET sensor calibration

Figure 4.7. Analysis of Cygnet 2.1 performance in cardiomyocytes

Figure 4.8. An attempt to further improve the cGI 500 sensor

Figure 4.9. Plasma membrane targeted FRET-based sensors

Figure 4.10. Outer membrane mitochondria targeted FRET-based sensors

Figure 4.11. pH sensitivity the of sensors

Figure 4.12. Calibration of FRET-based sensors

Chapter 5

Figure 5.1. Schematic of cyclic nucleotide signalling in healthy cardiomyocyte

Figure 5.2. Hypothetical scenario of cGMP and cAMP signalling disruption in dystrophic cardiomyocytes

Figure 5.3. nNOS, eNOS and iNOS Western blotting

Figure 5.4. Comparison between nNOS, eNOS and iNOS expression in isolated cardiomyocytes and left ventricle tissue of mdx and BL10 mice

Figure 5.5. Plasma membrane and Sarcoplasmic Reticulum fractions nNOS, eNOS and iNOS Western blotting

Figure 5.6. Comparison between nNOS, eNOS and iNOS expression at the plasma membrane of cardiac myocytes from mdx and BL10 mice

Figure 5.7. Comparison between nNOS, eNOS and iNOS expression at the sarcoplasmic reticulum fraction of mdx and BL10 cardiac myocytes

Figure 5.8. nNOS detection in intact wt neonatal and adult cardiomyocytes

Figure 5.9. nNOS detection in intact mdx neonatal and adult cardiomyocytes

Figure 5.10. Basal cGMP and cAMP levels in neonatal mdx heart

Figure 5.11. Basal cGMP and cAMP levels in adult mdx heart

Table 5.1. Basal cyclic nucleotide fluctuations with age

Figure 5.12. Basal cGMP PDE activity in neonatal cardiomyocytes

Figure 5.13. Basal cAMP PDE activity in neonatal cardiomyocytes

Figure 5.14. PDE mRNA levels in neonatal and adult mdx heart

Figure 5.15. cGMP PDE activity after cGMP generation in neonatal cardiomyocytes

Figure 5.16. cAMP PDE activity after cAMP generation in neonatal cardiomyocytes

Figure 5.17. cAMP PDE activity after cAMP generation in adult cardiomyocytes and mRNA analysis of AC 5 and 6

Figure 5.18. sGC activity and redox state in adult and neonatal mdx cardiomyocytes

Figure 5.19 Basal cAMP and cGMP concentration at the plasma membrane

Figure 5.20. Basal cAMP and cGMP concentration at the outer mitochondria membrane

Figure 5.21. Basal cGMP PDE activity at the plasma membrane of neonatal cardiomyocytes

Figure 5.22. cGMP PDE activity at the plasma membrane of neonatal cardiomyocytes after cGMP generation via sGC

Figure 5.23. Basal cAMP PDE activity at the plasma membrane of neonatal cardiomyocytes

Figure 5.24. cAMP PDE activity at the plasma membrane of neonatal cardiomyocytes after cAMP generation

Figure 5.25. Basal cGMP PDE activity at the outer mitochondria membrane of neonatal cardiomyocytes

Figure 5.26. cGMP PDE activity at the outer mitochondria membrane of neonatal cardiomyocytes after cGMP generation via sGC

Figure 5.27. Basal cAMP PDE activity at the outer mitochondrial membrane of neonatal cardiomyocytes

Figure 5.28. cAMP PDE activity at the outer mitochondria membrane of neonatal cardiomyocytes after cAMP generation

Figure 5.29a. Summary of findings in schematic figure – Neonatal cardiomyocyte

Figure 5.29b. Summary of findings in schematic figure – adult cardiomyocyte

Chapter 6

Figure 6.1. Calcium transport in ventricular cardiomyocytes

Figure 6.2. PKA-mediated phosphorylation of excitation-contraction coupling proteins

Figure 6.3. Sarcomere shortening analysis of unloaded cardiomyocytes

Figure 6.4. Analysis of force developed upon stretch and isoproterenol and IBMX stimulation

Chapter 1. Introduction

Parts of this chapter have been published in: Brescia, Marcella, and Manuela Zaccolo. "Modulation of compartmentalised cyclic nucleotide signalling via local inhibition of phosphodiesterase activity." International Journal of Molecular Sciences 17, No. 10 (2016): 1672.

This chapter has the aim to give a general introduction on cyclic nucleotide signalling and Duchenne Muscular Dystrophy. A focused and more specific literature review and introduction are available at beginning of each chapter.

1.1. THE CYCLIC NUCLEOTIDES

Significant progress has been made since 1958 when Rall and Sutherland first described adenosine 3'-5'-cyclic monophosphate (cAMP) to be involved in the cellular response to hormones. Today it is well known that cAMP and guanosine 3'-5'-cyclic monophosphate (cGMP) are intracellular second messengers involved in several cellular processes, including secretion, energy metabolism, gene transcription, cell migration, growth and survival and several other cell-specific functions, including immune function, learning and memory and cardiac strength and frequency of contraction. Defects in cyclic nucleotide (CN) signalling are known to be involved in the pathogenesis of multiple diseases and several drugs currently in use target cAMP or cGMP signalling pathways (Keravis and Lugnier 2012).

1.1.1. The generation of cAMP

cAMP is generated by the activation of adenylyl cyclases (ACs). This activation occurs by the binding of a first messenger to a specific G protein-coupled receptor and in turn, activates the ACs. G proteins are a family of GTP binding proteins crucial in mediating transmembrane signalling pathways by recognising an extracellular stimulus and the specific effector which generate the intracellular signal (Bachmann et al 2016). Their heterotrimeric structure consists of an alpha subunit which binds and hydrolyses GTP, plus a beta and a gama subunit which form a strong complex. This heterotrimeric G protein undergoes changes depending on their active state and controls the activity of associated enzymes, such as the adenylyl cyclases. In the resting state, GDP is tightly bound to the alpha-subunit and in association to the beta-gama complex. Sympathetic stimulation of the beta-adrenergic receptor, which is primarily coupled to the G-proteins by the first messenger, such as catecholamines, activates the system by promoting exchange of GDP to GTP on the stimulatory alpha-subunit of the G protein. The GTP-bound alpha-subunit dissociates from the activated receptor, as well as from the beta-gama complex activating the adenylyl cyclases, which in turn, generates cAMP. The activity of the ACs can also be inhibited by a second GTP binding protein, Gi. Cholinergic stimulation of the muscarinic receptors promotes the binding of GTP to the inhibitory alpha-subunit which, when dissociated, stimulated GTPase to break down active alpha-subunit, decreasing the activity of the ACs (Wettschureck and Offermanns 2005) (See Figure 1.1 for schematic).

The adenylyl cyclases are the only enzymes able to generate cAMP and requires adenosine 5'-triphosphate (ATP) as substrate. There are nine membrane-bound isoforms described in mammals (AC1-AC9). Their suggested structure includes three cytoplasmic

domains, one small and two larges, and two hydrophobic transmembrane domains. The two large cytoplasmic domains constitute the catalytic moiety of the enzyme, therefore containing the binding site for alpha-subunit of the G proteins. Additionally, they also present binding site to the protein kinase C (PKC), calmodulin (CaM) kinase II and the inhibitory G_i. AC5 and AC6 are the main isoforms present in the heart. These isoforms present several similar characteristics, such as the negative regulation by low Ca^{2+} concentrations and stimulation upon treatment with Froskolin. Additionally, these isoforms can be inhibited by PKA-mediated phosphorylation, which can account for a negative-feedback loop by cAMP (Hanoune and Defer 2001). Apart from the membrane-bound AC, a soluble version of the enzyme (sAC) is also known exist and play a role in cardiac function (Chen, Levin, and Buck 2012).

The main downstream effector of cAMP signalling is the protein kinase A (PKA). However, the exchange factor for Rap (EPAC) and cyclic nucleotide- gated ion channel are also its effectors (Tasken and Aandahl 2004). PKA is a holoenzyme consisting of two catalytic (C) subunits bound in a noncovalent way to two regulatory (R) subunits. cAMP binds to two specific sites at each R subunits and promotes a conformational change and dissociation into a R subunit dimer and two monomers of catalytic subunit. The catalytic subunits then became active and phosphorylate serine and threonine residues of specific target protein. Two different classes of PKA isozymes are known to exist, PKA-I and PKA-II. Their main difference is found in the R subunits, R-I and R-II, which apart from being differently expressed in distinct tissues, also present different cAMP binding affinities (Tasken and Aandahl 2004; Taylor et al. 2005). cAMP and its effector PKA, regulates sino-atrial cells and excitation-contraction coupling in ventricular myocytes by

phosphorylation of membrane channels, phospholamban and sarcomeric proteins, resulting in positive chronotropic, inotropic and lusitropic effects (Bers 2002).

Figure 1.1. G-coupled protein receptors and cAMP generation in the heart

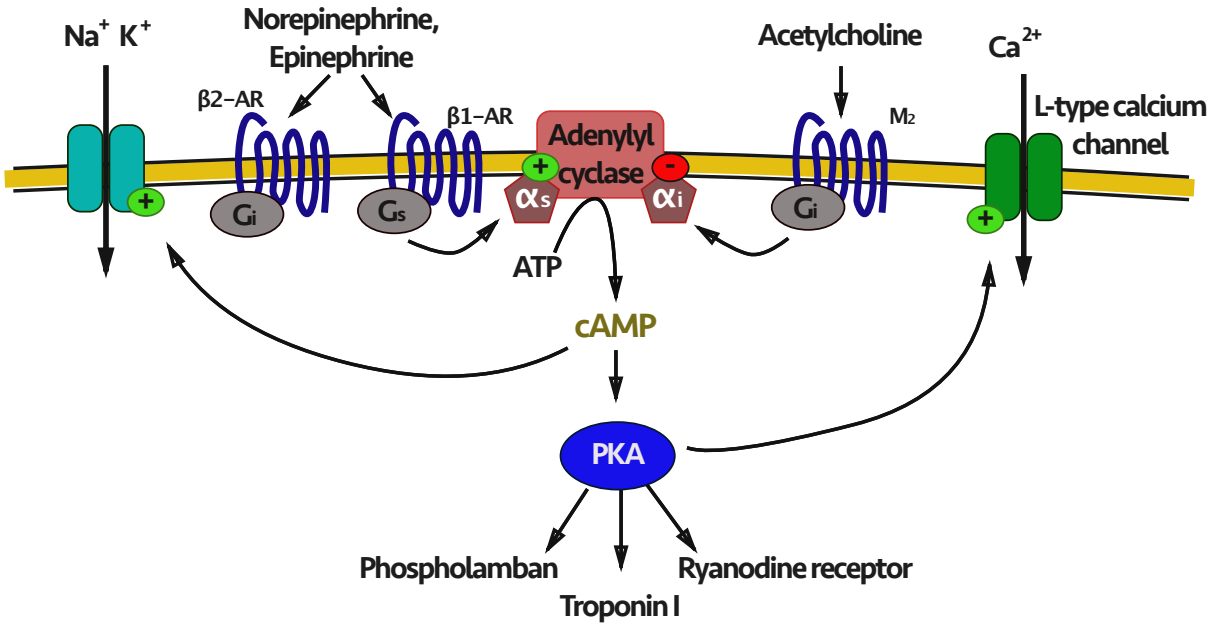


Figure 1.1.
Role of heterotrimeric G proteins in mediating sympathetic and parasympathetic control of heart function via the generation of cAMP and PKA-dependent phosphorylation of excitation-contraction coupling proteins. Abbreviations: β1-AR and β2-AR: β2 and β1-adrenergic receptors; M_2: muscarinic receptor; PKA: protein kinase A.

1.1.2. The generation of cGMP

cGMP is also an important second messenger which plays significant role in cardiac physiology. cGMP, via its effector PKG, tends to have a contrary effect in the heart when comparted to cAMP, acting as a myocardial brake (M. Zhang and Kass 2011), and negatively modulates contractility. Furthermore, cGMP signalling in the cardiovascular system is known to regulate hypertrophy and vascular tone by modulating intracellular calcium concentration, as well as having a role in proliferation and differentiation of smooth muscle cell (Lohmann, Fischmeister, and Walter 1991; M. Zhang and Kass 2011).

cGMP is generated from GTP by different isoforms of guanylyl cyclases (GC) via two pathways: First, via stimulation of a family of membrane-associated or particulate guanylyl clyclases and secondly, via NO stimulation of the soluble guanylyl cyclases. The membrane GCs consist of a transmembrane protein composed of an extracellular ligand domain, a short transmembrane area and an intracellular domain. The last one is where the catalytic domain is located. The extracellular ligand domain is known to encode receptors for the natriuretic peptides (NPs), which are polypeptide hormones secreted by the heart and vasculature. There are three types of NPs: Atrial NP (ANP), B-type (BNP) or C-type (CNP), which bind to GC receptors (pGC) with different specificity. GC-A presents receptors for ANP and BNP, whereas the CG-B for the C-type (CNP). Although at least seven different mammalian membrane GC receptors have been described, GC-A and GC-B are the main isoforms present in the heart. Their main effects are mediated by cGMP, which is generated upon NP stimulation of the receptors (Kuhn 2003).

The soluble GC generated cGMP upon nitric oxide (NO) stimulation, an inorganic free radical synthesized from L-arginine and NADPH by the NO synthases (NOSs). The NOS family is composed of three different isoforms: neuronal NOS (nNOS or NOS1), endothelial NOS (eNOS or NOSIII) and inducible NOS (iNOS or NOSII). The three distinct isoforms are products of different genes, present different localisation, regulation, catalytic properties and inhibition. The corresponding proteins of the three genetic loci identified are named after their original site of identification, as well as their order of purification and isolation (Griffith and Stuehr 1995). NO synthesis requires coenzymes, cofactors, and the presence of calmodulin. The reaction involves two separate steps where in the first, N^{ω}-Hydroxyarginine is formed by a reaction requiring O_2, NADPH and tetrahydrobiopterin (BH_4). This intermediate product, N^{ω}-Hydroxyarginine, is then

oxidised (second step) resulting in the production of NO and L-citrulline (Figure 1.2) (Knowles and Moncada 1994).

The sGC is a heterodimer molecule consisting of two homologous subunits, alpha (α_1 and α_2) and beta (β_1 and β_2) being the α_1 β_1 the most prevalent isoform. The beta subunit contains a heme-binding domain to which NO binds in order to activate the catalytic domain of the enzyme and generate cGMP (Derbyshire and Marletta 2012). NO binding to the ferrous heme iron moiety of the sGC happens in two steps, where in the first, NO binding transforms sGC into an intermediate inactive but NO-responsive enzyme with low basal rate of cGMP generation. The presence of magnesium promotes the second step where NO-binding changes the conformation of the catalytic domain significantly accelerating the basal rate of conversion from GTP to cGMP (Tsai and Kass 2009).
Downstream effectors of this pathway include cGMP dependent protein kinase (PKG), cyclic nucleotide gated cation channels and the phosphodiesterases (PDEs). In the heart, PKG-type I (PKG-I), which is composed of one α and one β subunit, is the prominent isotype. Each subunit consists of a regulatory domain, a kinase domain and an N-terminus domain. The N-terminus domain has the role of regulating PKG homodimerization, as well as supressing the kinase domain in low cGMP levels and interacting target substrates. Upon cGMP binding to the regulatory domain, the N-terminus releases the inhibitory effect on the kinase domain, which in turn, phosphorylates serine and threonine sites of targeted substrate proteins (see Figure 1.2 for schematic) (Tsai and Kass 2009; Lohmann, Fischmeister, and Walter 1991).

Figure 1.2. Membrane-bound and soluble GC generation of cGMP in the heart

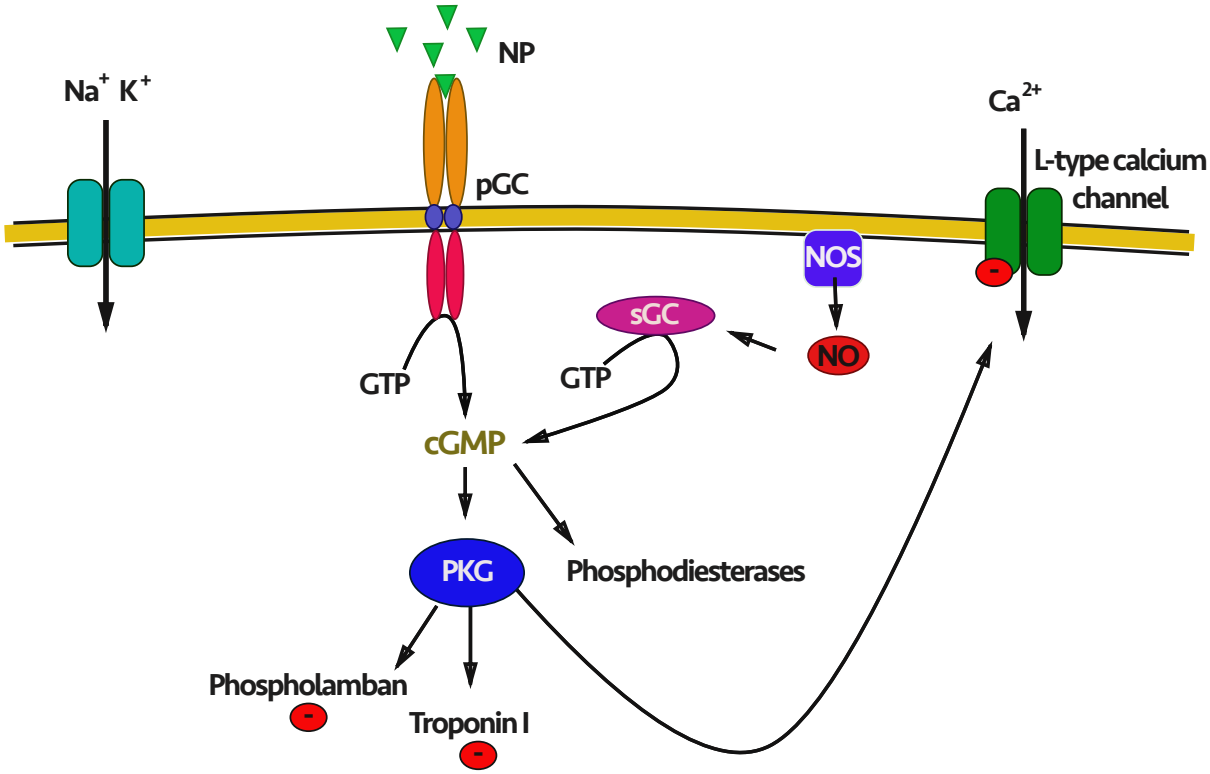
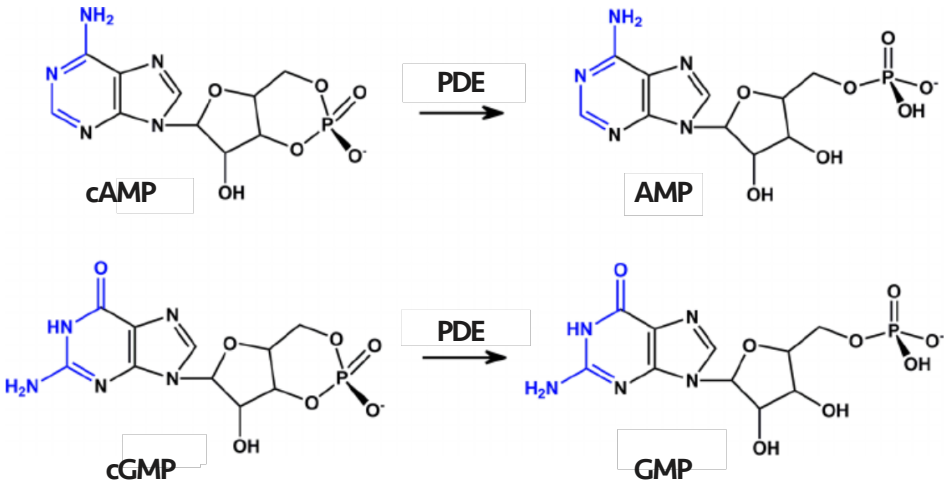


Figure 1.2.
Role of the different guanylyl cyclases in generating cGMP in the heart. The figure also illustrates specific PKG phosphorylation targets which have negative inotropic effect in the heart. Abbreviations: pGC: Particulate guanylyl cyclase or membrane-bound; sGC: soluble guanylyl cyclase; NOS: Nitric Oxide Synthases; NO: Nitric oxide; NP: Natriuretic peptides; PKG: Protein kinase G. The negative sign represents that PKG-mediated phosphorylation of these proteins lead to negative inotropic effect in the heart.

1.2. PHOSPHODIESTERASES

Cyclic nucleotides PDEs play an important role in cellular signalling by degrading cAMP and cGMP (Figure 1.3). Their activity modulates effectors via feedback pathways in coordination with the cyclases. Due to their diverse distribution in different tissues, at the cellular and subcellular levels, and their major role in regulating cellular function, PDEs have been the focus of intense research as potential therapeutic targets.

Figure 1.3. Hydrolysis of cyclic nucleotides by phosphodiesterases

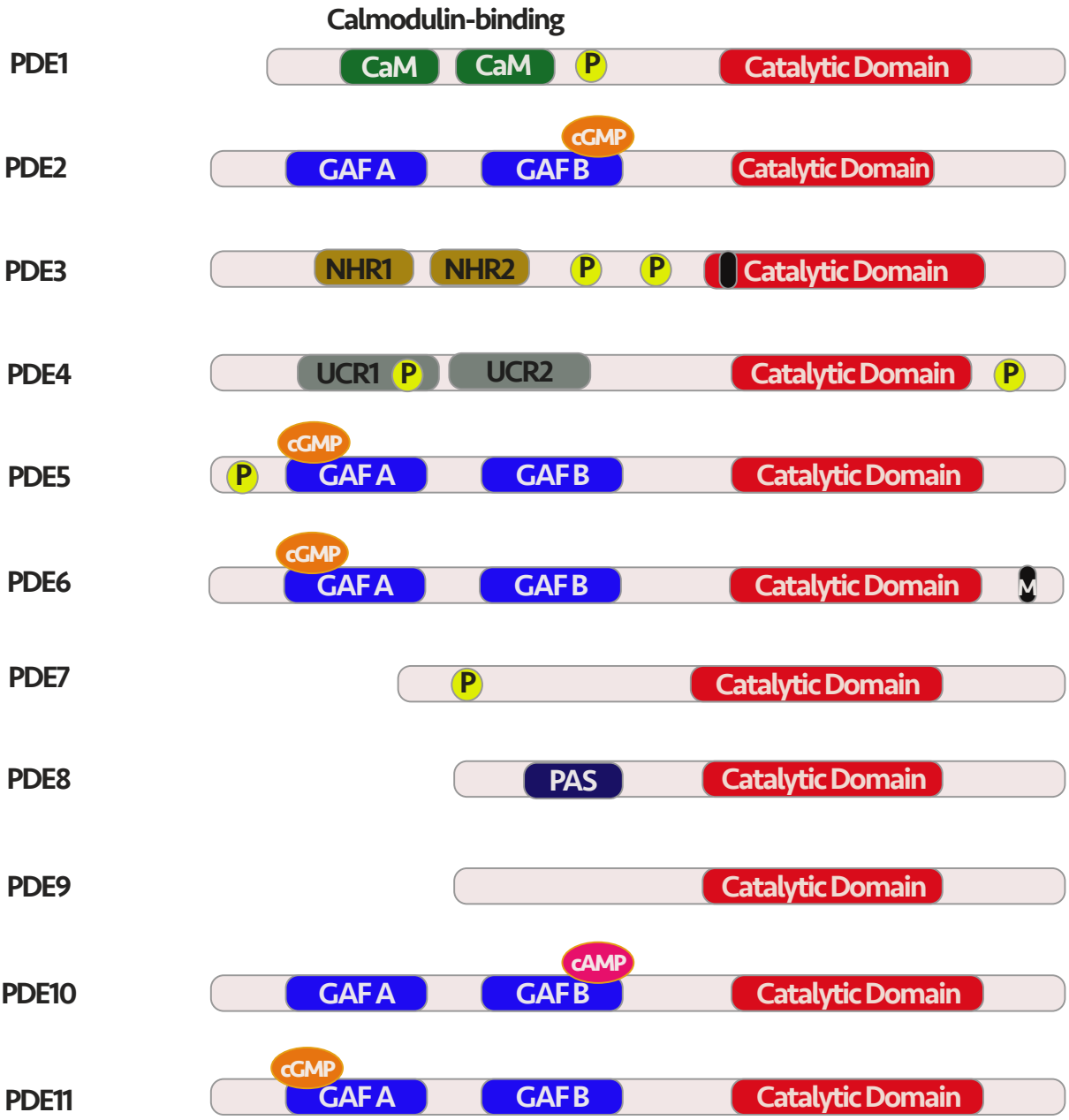


(adapted from: Z. Li et al. 2014)

Figure 1.3.
Molecular structure of cyclic nucleotides before (cAMP and cGMP) and after phosphodiesterases (PDE) hydrolysis (AMP and GMP). Highlighted in blue are the differences between both molecules.

PDEs are the only enzymes that degrade CN and are grouped in a superfamily comprising 21 genes, which constitute 11 distinct PDE families, PDE1 – PDE11. The structural properties of each family are markedly diverse, however, they all share a conserved catalytic domain (Figure 1.4). Although presenting high % of sequence identity, functional proprieties, such as substrate preference and affinities, as well as catalytic rates are variable. Each PDE family may include several genes and at least 100 different PDE isoforms can be generated by different splice variants or alternative transcription start sites (Conti and Beavo 2007). Each isoform shows unique substrate specificity and affinity, kinetics properties, regulatory mechanisms and subcellular localisation (Conti, Mika, and Richter 2014).

Figure 1.4. Schematic representation of PDEs



Adapted from (Francis, Blount, and Corbin 2011)

Figure 1.4.
Depiction of domain organization of 11 mammalian PDE families. All mammalian PDEs share a conserved Catalytic domain located in the COOH-terminal portion of the protein (red rectangles). In GAF-containing PDEs, one or both GAFs can provide dimerization contacts and allosteric cGMP binding (PDE2, PDE5, PDE6, PDE11), allosteric cAMP binding (PDE10), and regulation of catalytic site functions (PDE2, PDE5, PDE6). The encircled P indicates phosphorylation sites. The other families of PDEs have unique complements of various subdomains: CaM stands for calcium/calmodulin binding domain; UCR for upstream regulatory domain; NHR for NH_2- terminal hydrophobic region which provide membrane association; PAS for Per-ARNT-Sim domain; and M for membrane association, that contribute to regulation of activity.

PDE 1, 2, 3, 10 and 11 hydrolyse both cAMP and cGMP, although each of their isoforms presents different affinities for both CN. PDE1A, PDE1B and PDE10A have a higher affinity for cGMP over cAMP, whereas PDE1C, PDE2A and PDE11A have equal affinity for both CN. PDE3A and PDE3B present similar affinity for cAMP and cGMP but much higher catalytic rates for cAMP than for cGMP. PDE4, 7 and 8 degrade cAMP only, and PDE5, 6 and 9 are cGMP specific (Bender and Beavo 2006; Lomas and Zaccolo 2014). PDEs are subject to a complex system of regulatory mechanisms. The activity of some PDEs is regulated by post-translational modification. For example, the N-terminal domain of PDE1, 2, 3, 4 and 5 can undergo phosphorylation and PDE4 isoforms can be ubiquitinated at their C-terminus (X. Li, Baillie, and Houslay 2009). PDE1 is regulated by intracellular Ca^{2+} as this enzyme presents a Ca^{2+}/calmodulin binding site at the N-terminus where binding of $Ca^{2+/}$CaM leads to stimulation of its V_{max} by 10-fold without changing its affinity for the substrate. However, the K_m for the substrate is reduced when the same site is phosphorylated by PKA (Florio et al. 1994). PDE2, 6 and 9 contain allosteric binding sites for cGMP, called GAF domains, from cGMP-binding PDEs, *Anabaena* adenylyl cyclase, and *Escherichia coli* Fh1A, which function as ligand-binding domains or facilitators of protein-protein interaction (Francis, Blount, and Corbin 2011; Ahmad et al. 2015). Binding of cGMP to PDE2 and PDE5 GAF domains increases the hydrolytic activity of the enzyme. This is particularly interesting as it allows cross-talk between the cAMP and cGMP pathways with possible reciprocal regulation. cGMP activates PDE2 which, as previously discussed, degrades both cAMP and cGMP. Therefore, the intracellular levels of cGMP can influence the rate at which PDE2 hydrolyses cAMP. cGMP can also stimulate PDE5 by binding to its GAF domain and thus it can increase the rate of its own degradation. In addition, cGMP binding to PDE5 promotes PKG-mediated phosphorylation, which again increases PDE5 enzymatic

activity. This regulatory mechanism of PDE5 does not seem to be cGMP specific as PKA-mediated phosphorylation appears to have a similar effect (Francis, Blount, and Corbin 2011; Francis and Corbin 1994; Stangherlin and Zaccolo 2012). The regulation of PDE3 is also involved in the interconnection between cAMP and cGMP signalling. This enzyme has dual-specificity and binds with high affinity both cAMP and cGMP, which are mutually competitive substrates. Because PDE3 shows a much higher catalytic rate for cAMP than for cGMP, PDE3 functions principally as a cGMP-inhibited cAMP-hydrolysing enzyme. Consequently, the levels of cGMP can alter the availability of PDE3 to degrade cAMP, thus regulating cAMP concentration. PDE3 can be phosphorylated by PKA, and this phosphorylation enhances its activity (biochemical characteristics of PDEs are summarised in Table 1.1).

Table 1.1. Biochemical characteristics of PDEs

PDE	Substrate	Km (μmol/L)	Unique characteristic	Major tissue expression
PDE1	cAMP cGMP	73–120 2.6–5	Calcium/calmodulin regulated	Brain, smooth muscle, heart, testis
PDE2	cAMP cGMP	30–50 10–30	cGMP stimulated	Adrenal cortex, brain, heart
PDE3	cAMP cGMP	0.02–0.15 0.18	cGMP inhibited	Heart, smooth muscle, adipose tissue, platelets
PDE4	cAMP	2.9–10	cAMP specific	Ubiquitous
PDE5	cGMP	1–6.2	cGMP binding, cGMP specific	Smooth muscle, platelets, cerebellum, heart
PDE6	cGMP	15–17	Photoreceptor	Retina
PDE7	cAMP	0.1–0.2		Skeletal muscle, immune cells, brain
PDE8	cAMP	0.04–0.06	cAMP specific	Immune cells, liver, kidney, testis, thyroid
PDE9	cGMP	0.17–0.39	cGMP specific	Brain, kidney, heart

PDE10	cAMP cGMP	0.26 7.2	cAMP inhibited	Brain, testis
PDE11	cAMP cGMP	1.04-5.7 0.52-4.2		Prostate, testis, skeletal muscle

Data from (Bender and Beavo 2006; Omori and Kotera 2007)

1.3. CYCLIC NUCLEOTIDE'S COMPARTMENTALISATION

The cells have the ability to transform an extracellular stimulus into specific downstream events with specific physiological outcomes. For this to happen, spatial and temporal regulation and organization of signalling proteins is needed.

1.3.1. cAMP compartmentalised signalling

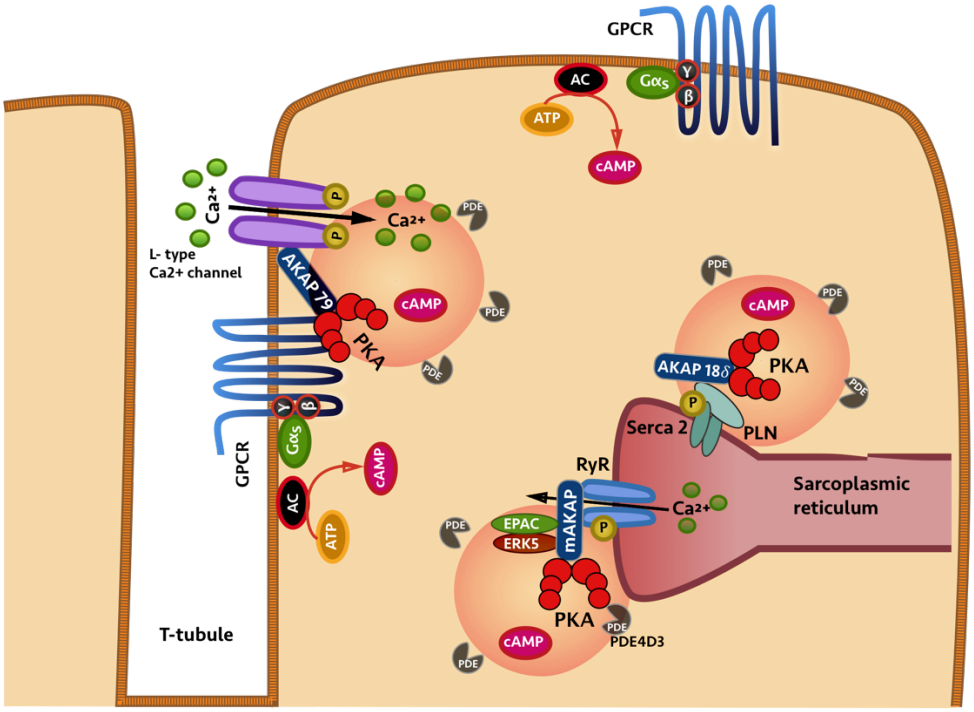
The initial model proposed for cAMP signalling was simple and linear: the first messenger activates a GPCR, cAMP is generated leading to activation of PKA. The PKA-mediated phosphorylation of downstream protein targets results then in the required cellular effect (Sutherland and Robison 1966). However, the idea that cAMP could activate PKA, which in turn could phosphorylate a multiplicity of proteins without any selectivity, appeared unsatisfactory since the early days (Zaccolo 2011). As further research uncovered the complexity of the cAMP signalling pathway, it became apparent that a more sophisticated model was required. The challenge was to reconcile the fact that the same cell can express multiple GPCRs, all signalling via cAMP, and that PKA can phosphorylate a vast number of protein targets within the same cell with the ability of the cell to effectively coordinate its response to a specific extracellular stimulus and achieve the required functional outcome with high fidelity (Zaccolo 2011). To resolve this conundrum, in the early '80s the concept was put forward that cAMP signalling must be compartmentalised. Brunton and co-workers observed that stimulation of cardiac myocytes with either prostaglandin E1 (PGE1) or isoproterenol resulted in the generation

of cAMP but yielded very different functional outcomes: isoproterenol caused an enhanced force of contraction whereas this effect was not detected when the heart was perfused with PGE1 (Hayes et al. 1979). To explain this observation, it was suggested that distinct subsets of PKA are activated in response to different stimuli thus allowing for hormonal specificity of cAMP signalling (Hayes, Brunton, and Mayer 1980). However, a mechanistic understanding of how this could happen remained elusive for several decades.

Research over the past 30 years has clearly established that CN signalling is indeed compartmentalised (McCormick and Baillie 2014). Compartmentalised signalling results from the ability of individual GPCRs to generate spatially distinct pools of cAMP. These, in turn, activate defined subsets of localised PKA which are tethered in proximity to specific targets via binding to anchoring proteins. PDEs play a key role in the spatial regulation of cAMP propagation. They not only contribute to establishing boundaries to cAMP diffusion and to generating cAMP pools where the second messenger is confined within delimited subcellular compartments but they also regulate cAMP levels within individual compartments (McCormick and Baillie 2014). A-kinase anchoring proteins (AKAPs) are scaffolding proteins that anchor PKA to specific subcellular sites and are instrumental in keeping cAMP signalling specific and physically compartmentalised. AKAPs form signalling hubs, or signalosomes, which organise within the same macromolecular complex GPCR, AC, PDEs, PKA and its targets, and phosphatases, ensuring selective phosphorylation and tight local regulation of signal duration (Kritzer et al. 2012). More than 50 AKAPs and their strategic localisation have already been identified. For example, in the heart, several AKAPs involved in the regulation of excitation-contraction coupling have been described. The localisation of AKAP79 at the

plasmalemma is required for PKA-mediated phosphorylation of L-type calcium channels (LTCC) in response to β-adrenergic receptor stimulation (Gao et al. 1997). LTCC are essential in the generation of normal cardiac rhythm and in triggering atrial and ventricular contraction and AKAP79, by tethering PKA in proximity to the channel, plays a crucial role in coordinating the adrenergic regulation of cardiac function (Reuter 1984). As another example, AKAP18δ interacts with SERCA2 at the sarcoplasmic reticulum (SR) and ensures the PKA-dependent phosphorylation of SERCA2-associated phospholamban (Figure 1.5). The disruption of this complex by AKAP18δ knock down compromises the potentiation of Ca^{2+} re-uptake into the SR induced by adrenergic stimulation, confirming that the AKAP18δ/PKA/SERCA2/phospholamban signalosome provides a mechanism for the precise spatiotemporal control of phospholamban phosphorylation (Lygren et al. 2007). mAKAP, muscle specific A kinase anchoring protein, is localised in close proximity to the ryanodine receptor (RyR) and also serves as a scaffold to anchor PDE4D3, EPAC1 and ERK5 in cardiac myocytes (Dodge et al. 2001) (Figure 1.5). Phosphorylation of RyRs, mediated by mAKAP-anchored PKA, has been implicated in the regulation of cardiac myocyte contractility (Edwards, Christian, and Baillie 2012; Gao et al. 1997; Carnegie, Means, and Scott 2009).

Figure 1.5. cAMP compartmentalisation in cardiomyocytes



(Brescia and Zaccolo 2016)

Figure 1.5.
Compartmentalised cAMP signalling by AKAPs and PDEs. Intracellular distribution of three AKAP complexes involved in the cardiac contractility. GPCR indicates G protein-coupled receptor; AC adenylyl cyclase; PKA protein kinase A; AKAP A kinase anchoring protein; PDE phosphodiesterase; P phosphate group; PLN Phospholamban; RyR Ryanodine receptor; EPAC GTPases Exchange Factor directly activated by cAMP. Red shaded areas indicate distinct cAMP pools generated by an AC anchored at the plasma membrane and activated by a GPCR exposed to the extracellular space. PKA anchored to AKAPs and the activity of PDEs, contribute to spatial regulation of cAMP and specific downstream physiological effect as selective PKA phosphorylates the target that is contained within the specific microdomain.

1.3.2. NO - cGMP compartmentalised signalling

cGMP signalling presents mechanisms of spatial organisation similar to cAMP, yet less is known about the details of its compartmentalisation. A role for PDEs in local cGMP regulation has been demonstrated in particular for PDE5, PDE2 and PDE9. There is evidence that these enzymes are differently engaged in degradation of cGMP depending on whether cGMP is generated via particulate or soluble GCs, thus suggesting spatial segregation of these cGMP signalling components; PDE9A and PDE2, unlike PDE5A,

mainly regulate cGMP produced via natriuretic peptides rather than nitric oxide stimulation (Tsai and Kass 2009; Lee et al. 2015; Castro et al. 2006). Furthermore, it has been shown that the generation of cGMP upon ANP stimulation of the pGC results into more readily activation of the CNG channels, one of the cGMP effectors, than cGMP generated upon sGC stimulation in HEK cells (Piggott et al. 2006). The idea that pGC cGMP pool is more readily accessible at the plasma membrane when compared to sGC cGMP pool was also shown to occur in rat cardiomyocytes (Castro et al. 2006). These data suggest that differential spatiotemporal distribution of cGMP pools, regulated by the localisation of pGC and sGC, contribute to the specific effects of NP and NO donors in the heart. However, although pGC cGMP pool is greater detected at the plasma membrane, it is not translated into greater PKG activity and it was not shown to modulate the cGMP-PDE5 beta-adrenergic responses in the heart. This regulation was described to be specifically linked with PKG activity and PDE5 derived from sGC cGMP pool (Takimoto et al. 2007).

PKG and GCs are suggested to be organized in macromolecular complexes, and the localisation of PDEs appears to be important in determining cGMP microdomains (M. Zhang and Kass 2011), as discussed above. Although the presence of anchoring proteins for PKG has not yet been firmly established, studies have suggested that proteins like myosin, atrial natriuretic peptide receptor, and troponin T could act like GKAPs (Vo, Gettemy, and Coghlan 1998), adding another level of compartmentalised cGMP signalling.

The NO signalling, which consequently influence the cGMP signalling, is known to be compartmentalised by the subcellular localisation and isoforms of NOS. This

compartmentalisation has been shown to importantly regulate physiological processes mediated by cGMP. Mislocalisation of nNOS, which localised at the plasmalemma of skeletal muscle in association with the dystrophin complex (Brenman et al. 1995), is known to be responsible for the exaggerated fatigue in response to mild exercise in models of neuromuscular conditions via reduced cGMP-mediated vasomodulation of supply vessels (Kobayashi et al. 2008). In the heart, nNOS is known to be mostly localised at the sarcoplasmic reticulum (Xu et al. 1999), which might play a role in the PKG-mediated phosphorylation of phospholamban (Raeymaekers, Hofmann, and Casteels 1988). eNOS has been shown to traffic between the plasma membrane and the Golgi apparatus and present different NO production rates at each location (Q. Zhang et al. 2006).

1.4. ROLE OF THE PDES IN SIGNALLING COMPARTMENTALISATION

The key role of PDEs in compartmentalisation of CN signalling was firmly established using FRET-based, genetically encoded fluorescent indicators that allow for cAMP (Zaccolo et al. 2000; Ponsioen et al. 2004; Nikolaev et al. 2004) or cGMP (Nikolaev, Gambaryan, and Lohse 2006; Honda et al. 2001; Sato et al. 2000; Russwurm et al. 2007) dynamics to be visualized in real-time in intact, living cells. It was using this technique that it was possible to directly demonstrate for the first time that cAMP generated by β-adrenergic stimulation does not homogeneously equilibrate in the cell but rather is compartmentalised within defined subcellular microdomains. On inhibition of PDEs, the localisation of cAMP was disrupted and the second messenger was able to uniformly distribute in the cytosol of cardiac myocytes. The same effect was observed when the cells were pre-treated with the inhibitor followed by β- adrenergic stimulation, leading to the conclusion that PDEs control cAMP diffusion and concentration in the cytosol,

consequently regulating the local activation of PKA (Zaccolo and Pozzan 2002). A body of work supports the involvement of PDEs in the compartmentalisation of cAMP signalling. The cAMP specific PDE4 family was the focus of some of these studies. PDE4D3 was shown to be compartmentalised with PKA via mAKAP anchoring (Dodge et al. 2001), and PKA was shown to be activated only if the cAMP concentration is sufficiently high to overcome the local cAMP-degrading activity exerted by the local PDE (Dodge et al. 2001). PDE4D5 was found in complex with the scaffold protein β- arrestin which is recruited to the β2-AR upon agonist stimulation, where it plays an important role in attenuating the activity of a local pool of PKA tethered to the β2-AR by AKAP79. This local pool of PKA phosphorylates β2-AR allowing it to switch its coupling from Gs to Gi, leading to the activation of ERK. Therefore, PDE4 in complex with β- arrestin was found to be instrumental in controlling the phosphorylation of β2-AR by AKAP79 tethered PKA (Baillie et al. 2003).

As PDEs are the only route to CN degradation, the specific subcellular localisation of these enzymes represents a fundamental mechanism for regulating locally the magnitude, duration, and specificity of CN-dependent signals. Without PDEs-dependent control of local cAMP levels, stimulation of adenylyl cyclase activity by any hormone would fill up the cells with a uniform concentration of the second messenger. As a consequence, signal specificity would be lost as all PKA subsets present in the cell would be activated (McCormick and Baillie 2014). In this scenario, manipulation of cAMP levels by specific pharmacological inhibition of individual PDE families offers the opportunity to achieve a more specific effect as compared to activation of the upstream GPCR, which may trigger a complex downstream signalling cascade.

Pharmacological inhibition of PDEs is extensively used for experimental work, and it has enormously contributed to our understanding of the role of individual PDE families and the definition of the cAMP compartmentalisation model. For example, the PDE2 inhibitor Bay 60-7550 was used to show that PDE2 is responsible for degradation of cGMP in hippocampal neurons and can improve memory functions by enhancing neuronal plasticity (Boess et al. 2004). The same inhibitor was used to demonstrate that a pool of cAMP, selectively modulated by PDE2A, regulates cardiac myocytes hypertrophic growth (Zoccarato et al. 2015). Studies where PDE3 was inhibited with cilostamide and PDE4 with rolipram showed that reducing by only 10% the total PDE4 activity results in a dramatic increase in cAMP, whereas total PDE3 inhibition has only a marginal effect on the cAMP response to β-AR stimulation, suggesting that compartmentalisation of PDEs is as important as their level of expression in determining their impact on CN levels and cell function (Mongillo et al. 2004).

A number of PDE inhibitors are used in the clinic. PDE3, PDE4 and PDE5 family-selective inhibitors have been approved for clinical use. For example, roflumilast, a PDE4 selective inhibitor is indicated for the treatment of chronic obstructive pulmonary disease (COPD). However, PDE4 inhibitors present adverse emetic effects due to inhibition of PDE4 in the brain and the gut, limiting their use as therapeutics (Hatzelmann and Schudt 2001; Huang et al. 2001; Ahmad et al. 2015). The PDE3 inhibitor cilastazol has been widely used to treat intermittent claudication, a peripheral vascular disease causing pain and cramps in the legs (Ahmad et al. 2015). Milrinone, also a PDE3 inhibitor, is effective in increasing cardiac contractility in failing hearts, although it increases mortality in the long term, most commonly as a consequence of arrhythmias and cardiac arrest (Florio et al. 1994), limiting its indication to the treatment of patients with refractory, acute

decompensated heart failure (Ahmad et al. 2015). The most famous PDE inhibitors available on the market are the PDE5 inhibitors sildenafil (Viagra;Pfizer), vardenafil (Levitra:Bayer/Glaxo SmithKline) and tadalafil (Cialis:Lilly) for treatment of erectile dysfunction (Lugnier 2006). Sildenafil and vardenafil also inhibit PDE6 and for this reason, their use might be accompanied by brief visual disturbances. Other side-effects such as headache, flushing and nasal congestions are mild (Ahmad et al. 2015). PDE5 inhibitors have also been approved for the treatment of pulmonary hypertension and have been evaluated for other indications such as benign prostatic hyperplasia and cardiomyopathies (Bender and Beavo 2006; Isidori, n.d.; Gilead Sciences, n.d.).

1.5. LOCAL INHIBITION OF PHOSPHODIESTERASE ACTIVITY

As discussed above, family-selective PDE inhibitors present limitations for clinical use, mainly due to lack of isoform selectivity resulting in undesirable side effects. Studies are currently under way to circumvent this problem and we briefly outline some of the existing isoform-selective inhibition strategies below.

After the publication of the PDE4 crystal structure (Burgin et al. 2010), new insights into the PDE4 regulatory domains allowed the visualization of a previously unknown binding mode for PDE4 inhibitors involving the upstream conserved region 2 (UCR2), which is part of the regulatory domain, and the third C-terminal (CR3) control region, present in all four PDE4 families. The same study described the generation of PDE4D allosteric modulators, small molecules interacting with UCR2 and CR3 that partially inhibit the enzymatic activity and cAMP hydrolysis. These allosteric modulators showed positive results when assessed for pro-cognitive, anti-inflammatory and antidepressant outcomes with reduced side effects when compared to classical PDE4 inhibitors (Burgin et al. 2010;

Gurney et al. 2011; Ahmad et al. 2015). After further elucidation of the regulatory mechanisms, a new PDE4 subfamily-selective inhibitor was developed. This compound, defined as an atypical inhibitor, recognizes specific folded conformations within the UCR2 domain and the catalytic domain of the PDE4 rather than interacting exclusively with the catalytic domain. This approach provides the possibility of isoform selectivity by exploiting a Thyr/Phe polymorphism in the UCR2 helix of PDE4 isoforms (Pandit 2014).

Small interfering RNA (siRNA) of individual PDEs is significantly more specific than most available pharmacological inhibitors (Sharma, Rungta, and Prasad 2014) allowing for ablation of sub-families of PDEs. Houslay et al. (2004) used this technique to selectively deplete PDE4Bs and PDE4Ds in HEK293B2 cells in order to compare the functional outcome of the interaction of β-2 AR with β-arrestin. The transfection of the designed oligonucleotides was highly efficient with ~95% of each of these PDEs sub-families selectively knocked down (Lynch et al. 2005). The same approach was used to deplete PDE7 and PDE8 and examine the influence of gene silencing on gene expression in human osteoblasts (Pekkinen et al. 2008) and to establish the anti-hypertrophic effect of PDE2 inhibition (Zoccarato et al. 2015). Although very effective for research purposes, siRNA is not likely to be easily adapted for manipulation of PDE activity in the clinical setting.

In a scenario where compartmentalisation of CN signalling is crucial for cell function, techniques that allow specific manipulation of local signalling provide an interesting opportunity to achieve a more targeted intervention. Displacement of specific isoforms of endogenous PDEs by overexpression of their catalytically inactive mutant is one

approach used in the laboratory. This strategy involves engineering specific PDE isoforms by introducing a single point mutation in their catalytic site. The overexpression of these constructs results in the displacement of the endogenous active PDE isoform from its original localisation within the cell. The technique was used to explore the role of specific anchored PDE isoforms in the compartmentalisation of CN signalling. Compared to the siRNA approach described above, expression of catalytically inactive PDEs allows to directly assess the role of PDE subcellular localisation in the regulation of a specific cellular function. The first study to use this technique generated catalytic inactive PDE4A4, PDE4B1, PDE4C2 and PDE4D3 to identify the role of specific tethered PDE4 isoforms in regulating cAMP and PKA-dependent phosphorylation in resting COS1 cells. The study successfully showed that PDE4C2 and PDE4D3 isoforms are constitutively phosphorylated by PKA type-II and, as they are tethered in a complex including AKAP450 and PKA type-II, they play a central role in regulating the activation of AKAP450-bound PKA type-II at the perinuclear region (McCahill et al. 2005). In another study, catalytically inactive mutants of PDE2A, PDE3A2 and PDE4D3 were overexpressed in neonatal rat cardiac myocytes to investigate the role of different pools of cAMP in the regulation of cardiac myocyte hypertrophic growth. It was successfully shown that displacement of PDE4D3 and PDE3A2 results in cardiac myocyte hypertrophy, whereas displacement of PDE2A counteracts the hypertrophic growth induced by chronic β-adrenergic stimulation (Zoccarato et al. 2015).

As previously discussed, different PDEs can localise to different subcellular sites, anchored to AKAPs or via interaction with other proteins. For example, PDE4D3, together with PKA, is localised by the mAKAP-organised signalosome in the perinuclear region (Dodge et al. 2001) and, via interaction with AKAP450, PDE4D3 localises at the

centrosomes (Taskén et al. 2001). PDE4A4/5 interact with plasma membrane receptors (Sachs et al. 2007) and PDE4D3 tethered together with PKA, via interaction with AKAP18δ, localises at aquaporin-2 vesicles regulating vasopressin-mediated water reabsorption (Stefan et al. 2007). As mentioned above, PDE4D5 can form a complex with β-arrestin and the PDE4D5-β-arrestin complex plays an important role in the activation of ERK signalling (Baillie et al. 2003). Another obvious strategy to achieve selective local manipulation of PDE activity, therefore, involves the disruption of the interaction between the PDE and the protein interacting partner. In this approach, a short peptide or small molecule is used to target the interaction surface between the PDE and the anchoring protein. In a proof of principle experiment, this strategy was used to disrupt the interaction of PDE4D5 with HSP20, a heat shock protein with a role in protecting from cardiac dysfunction induced by sepsis and endotoxin in mice via PKA-dependent phosphorylation. In this study, selective local inhibition of PDE activity was achieved by using a synthetic peptide encompassing a short stretch of amino acid residues from the PDE4D5 sequence involved in binding to HSP20 and resulted in attenuated β-agonist induced hypertrophy in neonatal cardiomyocytes (Sin et al. 2011; Klussmann 2016). As another example, PDE3B was found to interact with EPAC1 and p84, a PI3Kγ regulatory subunit. A cell permeable peptide was used to disrupt PDE3B-EPAC1 binding in human aortic endothelial cells (HAEC). The study demonstrates that manipulation of EPAC1-PDE3B interaction results in altered cAMP signalling, thus affecting EPAC1-mediated activation of PI3Kγ and dynamic cAMP-dependent regulation of HAEC cells adhesion, spreading and tubule formation (Wilson et al. 2011).

1.6. INTRODUCTION TO DUCHENNE MUSCULAR DYSTROPHY

Duchenne Muscular Dystrophy (DMD) first described in mid-1800, is the most common and severe human muscular dystrophy, affecting 1 in 3500 live born male. It is a X-linked recessive disease manifesting primarily by progressive muscle weakness as a result of the absence of dystrophin, a large subsarcolemmal protein, which is a part of a multimolecular network, called the dystrophin-glycoprotein complex (DGC) due to out-of-frame mutations on the gene that encodes for dystrophin (Hoffman, Brown, and Kunkel 1987). The first obvious clinical manifestation, proximal muscle weakness, is observed by the age of 3-5 years; subsequently, at approximately 11 years, the patients are wheelchair-bounded due to the progressive loss of muscle strength (Guiraud et al. 2015). Cardiac and respiratory failures represent the major causes of mortality in DMD patients (90%) (Nigro et al. 1990). Although the cardiomyopathy varies between patients, it is prevalent in most patients by 20 years of age and has emerged as the most prevalent cause of death in DMD patients. Improvement of non-invasive respiratory support increased the lifespan and quality of life of the patients by treating respiratory deficit, however, it also increased the incidence of complications and eventual mortality from cardiac failure (Wehling-Henricks et al. 2005).

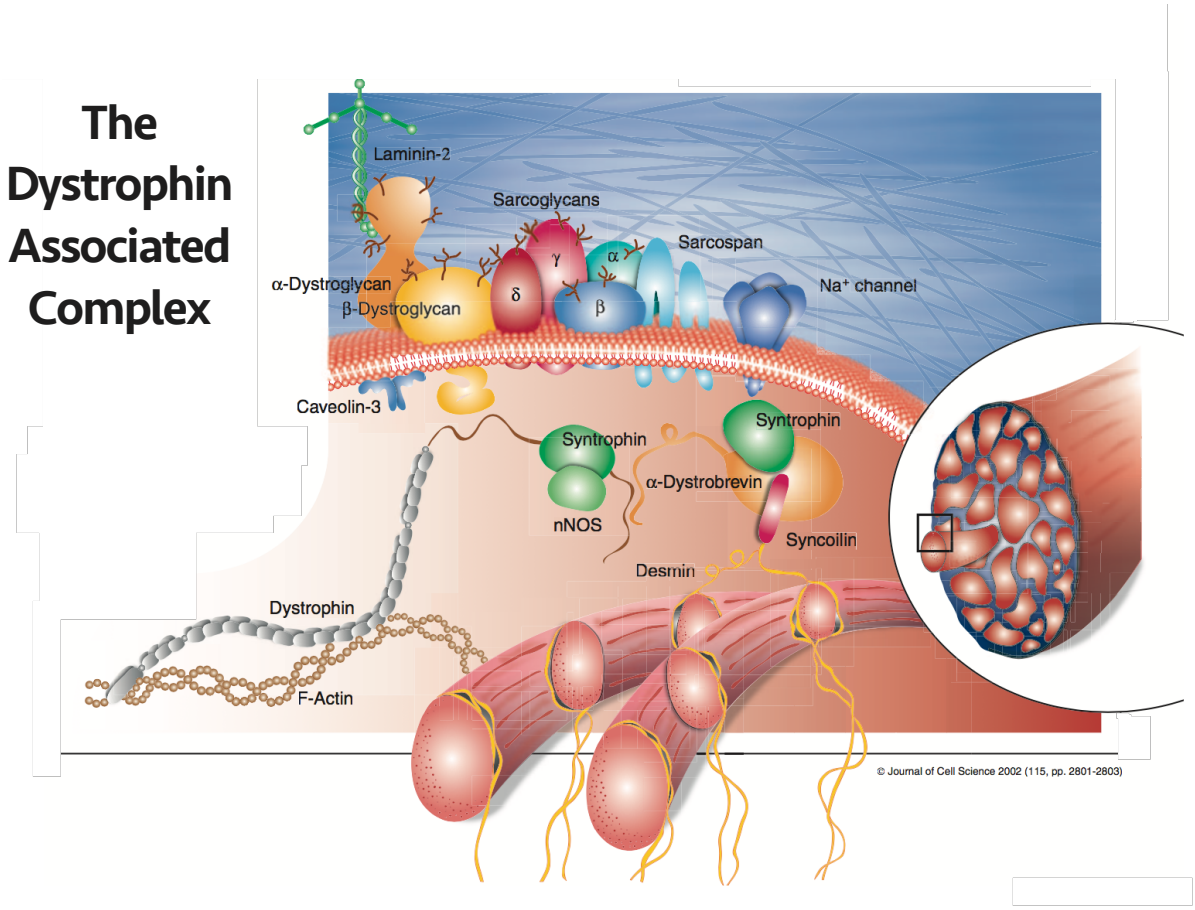
1.6.1. The dystrophin associated complex (DAPC)

In skeletal and cardiac muscle, dystrophin associates with several proteins forming the dystrophin-associated protein complex (DAPC). This complex is known to have a crucial structural role by linking the actin cytoskeleton to the extracellular matrix. The absence of dystrophin causes reduction of other proteins from the complex, disrupting sarcolemma integrity and causing mechanical instability in cell membrane. This

instability results in easily damaged muscle fibres (Ervasti and Campbell 1991; Ervasti et al. 1990).

DGC is composed by (1) α- and β- dystroglycan subunits, which constitute the core of the complex by stablishing the connection between laminin-2 and dystrophin. Additionally, the C-terminus of β- dystroglycan interacts directly with caveolin-3 ; (2) α- and β syntrophins, which interacts with several proteins, such as nNOS, sodium channels and stress-activated kinases (Rando 2001); (3) α- dystrobrevin, which binds to syntrophin and contains several tyrosine kinase consensus sites, is also known to associate with syncoilin. This association is thought to provide a link between the complex and the intermediate filament protein network (Blake and Martin-Rendon 2002); (4) Sarcospan, a protein with four transmembrane domains and intracellular N and C terminus; (5) α-, β-,γ-, δ- and ε-sarcoglycans, five associated transmembrane proteins (Ehmsen, Poon, and Davies 2002) (Figure 1.6). The amino-terminal of dystrophin links the cytoskeletal F-actin filaments to the extracellular matrix and the α-dystroglycan binds to laminin in the basal lamina, stabilising the sarcolemma against stress- induced muscle during the contraction and relaxation (Wallace and McNally 2009). Syntrophins bind nitric oxide synthase (NOS) (Brenman et al. 1996) and also associate DGC to sodium and L-type calcium channels, aquaporin and stretch-activated channel, suggesting dystrophin involvement in signalling cascades (Mosqueira et al. 2013; Ehmsen, Poon, and Davies 2002). Dystrophin spectrin-like repeats 16 and 17 are also known to scaffold nNOS at the sarcolemma (Lai et al.2009).

Figure 1.6. The dystrophin associated complex



(Ehmsen, Poon, and Davies 2002)

Figure 1.6.
Schematic illustration of the dystrophin complex at the plasma membrane binding the extracellular matrix (laminin) and cytoskeleton F-actin.

1.6.2. Some molecular pathologies associated to the disease

Membrane tearing and increased fragility due to the lack of dystrophin and disrupted cytoskeleton-membrane-matrix connection is thought to induce several cellular responses which might be pathological or protective (Wallace and McNally 2009) in DMD muscle cells. Some of the main pathological characteristics of the disease will be discussed below. It is important to keep in mind that there are several other pathways and processes involved in the disease, however, they will not be discussed here.

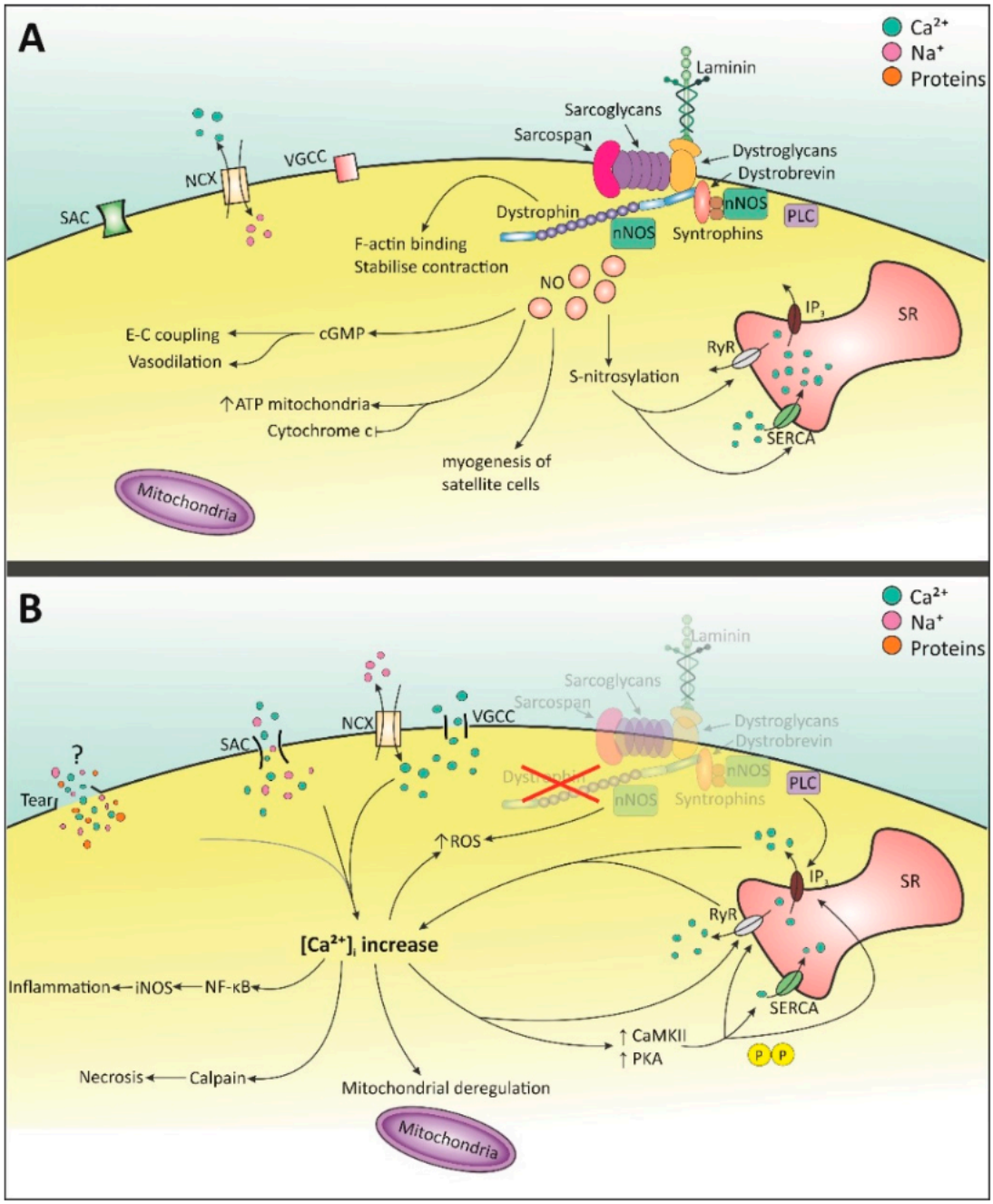
The dystrophin complex is also associated with the costameres, which are organised structures important in keeping the sarcolemma and contractile structures aligned, protect the sarcolemma against contraction-induced damage and to transmit contraction forces to the extracellular matrix. These structures were found to be substantially disorganised in the DMD muscle, resulting into increased sarcolemma fragility, and susceptibility to contraction-induced muscle injury and abnormal influx of Ca^{2+} (Mosqueira et al. 2013; Wallace and McNally 2009).

Elevated concentration of cytosolic calcium has been observed in DMD muscle fibres (Bodensteiner and Engel 1978; Turner et al. 1991), however, it is still unclear how this increase commences. There are many proposed mechanisms, such as the extracellular influx via microlesions in the sarcolemma, presence of calcium-permeable stretch-activated channels (Aguettaz et al. 2016; Turner et al. 1991), and up-regulation of calcium channels such as the calcium-permeable growth factor-regulated channel (TRPV2) which is found elevated in the mdx heart (Iwata et al. 2003). As calcium has crucial importance in heart physiology, in the excitation-contraction coupling and as a signalling molecule, elevated intracellular calcium in the heart may lead to several disturbances and defects in function. Although only two calcium binding proteins have been shown to be affected in the heart, calsequestrin and sarcalumenin, which are involved in sequestration and SERCA uptake (Lohan and Ohlendieck 2004), non-physiological calcium concentrations may activate inflammation and cell-death pathways (see Figure 1.7 for schematic) (van Westering, Betts, and Wood 2015).

The absence of dystrophin is also known to reduce the activity of the neuronal nitric oxide synthase (nNOS), as well as abolish its link to the plasma membrane, generating a clear

nNOS mislocalisation in skeletal muscle (Brenman et al. 1995). Defective nNOS activity and localisation directly affects the NO pathway and other NO-dependent pathways such as cGMP (Bia et al. 1999; Carnicer et al. 2017; Maya Khairallah et al. 2007).

Figure 1.7. Molecular pathways in heathy and dystrophic cells



(van Westering, Betts, and Wood 2015)

Figure 1.7
Molecular pathways involving calcium and NO signalling in healthy and dystrophic cell. (A) Heathy cell with functional dystrophin complex presenting physiological Ca^{2+} homeostasis and NO pathway, as well as normal E-C coupling process (B) Dystrophic cell where dystrophin is absent and complex is compromised. Several pathological processes are in place increasing intracellular calcium and activating pathological pathways. Abbreviations: SACs: stretched-activated channels; NCX: Na+-Ca2+ exchanger; VGCC: Voltage-gated Ca2+ channels; nNOS: neuronal nitric oxide synthase; SERCA: Sarcoplasmic/endoplasmic reticulum Ca2+-ATPase; RyR: ryanodine receptor; NO: nitric oxide; IP3: inositol 1,4,5-triphosphate; SR: sarcoplasmic reticulum; CaMKII: calmodulin-kinase II; PKA: protein kinase A.

1.6.3. DMD cardiomyopathy

The cardiomyopathy, a delayed symptom of DMD, manifests initially as left ventricle dilation and hypertrophy which progresses to dilated cardiomyopathy (Mazur et al. 2012; Mosqueira et al. 2013). Contractile abnormalities such as reduced fractional shortening and electrocardiogram abnormalities are also present and are associated with morphological changes of the myofilaments, fibrosis and defects in conductivity (Kirchmann et al. 2005; Wehling-Henricks et al. 2005; Sanyal and Johnson 1982). Mechanical stress vulnerability and workload-induced damage are also important components of cardiomyopathy in DMD (Nigro et al. 1990; Mosqueira et al. 2013). Cardiac function marked deteriorate as dystrophic hearts try to cope hypertrophy and suffer increased in fibrotic deposition (van Westering, Betts, and Wood 2015).

1.6.4. DMD animal models

The mdx mice, the most used animal model for DMD, has a point mutation in exon 23 of the dystrophin gene leading to a premature stop codon resulting in absence of dystrophin, as in humans (Bulfield et al. 1984). Although the mdx mouse presents with many aspects of DMD, the development and severity of the cardiac disease is milder compared to humans. Cardiomyopathy in mdx mice can already be detected at 3 months old (12 weeks) as increased right ventricle systolic volume and reduced ejection fraction (Stuckey

et al. 2012; Chu et al. 2002), as well as cardiac metabolic changes (Maya Khairallah et al. 2007).

Studies have been exploring the differences present in the mdx in order to generate an improved DMD animal model. Utrophin, an autosomal paralog of dystrophin, was already found up-regulated in the mice, contributing to the less severe phenotype (Tinsley et al. 1998). Many genetically engineered mice were generated in the attempt to increase the severity of the dystrophic phenotype, for example, mutations in utrophin, integrin α7, α-dystrobrevin, but none of these represent the human disease as all these genes are expressed in DMD (McGreevy et al. 2015; Chandrasekharan et al. 2010).

A recent study examined the contribution of cell surface glycans to the human-mouse differences in phenotype and generated the Mdx Cmah. This mouse model focuses on the Cmah gene, which is necessary for the biosynthesis of N-glycolylneuraminic acid (Neu5Gc), deletion. This gene is not present in human cells and it is almost undetectable in dogs, currently best available DMD animal model, but is present in skeletal and cardiac muscle cells of the mdx mice model. The Cmah-/-mdx shows accelerated dystrophic phenotype and mimic better the more severe aspects of the disease (Chandrasekharan et al. 2010)

1.7. AIM OF THIS THESIS

A better understanding of the functional role of dystrophin in the heart and the mechanism underpinning the cardiomyopathy in the disease are crucial for the development of more effective treatment strategies.

It has been hypothesised that defective nNOS-cGMP signalling within the cardiomyocytes may play a role in the pathogenesis of the cardiomyopathy associated

with dystrophin deficiency (more details about the literature available on Chapter 5). Studies have shown that cGMP increase, caused by the inhibition of PDE5, a phosphodiesterase that degrades cGMP, as well as overexpression of nNOS, show improved contractility, energy metabolism and promote cell integrity in these cells (M Khairallah et al. 2008; Bia et al. 1999; Adamo et al. 2010; M Khairallah et al. 2008). However, how the cGMP pathway, its regulation and compartmentalisation are affected in in the DMD pathogenesis has not been completely elucidated.

The aim of my project was to explore the hypothesis that altered cGMP dynamics are involved in the pathogenesis of the cardiac phenotype associated with DMD. To address this point, cGMP dynamics in cardiomyocytes from the mdx mouse model of DMD were monitored in different subcellular compartments using real time FRET imaging. As an interplay between cGMP and cAMP signalling has been established in cardiac myocytes and given the prominent role of cAMP in the regulation of heart function, as well as its involvement in the pathogenesis of heart failure, the dynamics of cAMP signals were also investigated in the mdx model using a similar imaging approach. Furthermore, analysis of mdx cardiomyocytes contractile properties was also performed in unloaded and loaded myocytes.

The specific aims of each chapters were as follows:

- Chapter 2) To give an overview of the methods and statistical analyses employed in this thesis.

- Chapter 3) To optimise a protocol to generate isolated cardiomyocytes that efficiently express the FRET-based sensors while maintaining and optimal contractile properties.
- Chapter 4) To design, generate and characterise FRET-based probes for cAMP and cGMP targeted to specific subcellular compartments.
- Chapter 5) To explore cAMP and cGMP dynamics in mdx cardiomyocytes from neonatal and adult mice in the bulk cytosol and at specific subcellular compartments using FRET, as well as determine the protein level and activity of PDEs, NOS and GC.
- Chapter 6) To assess the contractile response upon stimulation of beta adrenergic receptors, application of NO donors and PDE inhibition of adult mdx isolated cardiomyocytes either unloaded or under tension and on application of stretch.

1.8. REFERENCES

Adamo, Candace M, Dao-Fu Dai, Justin M Percival, Elina Minami, Monte S Willis, Enrico Patrucco, Stanley C Froehner, and Joseph A Beavo. 2010. “Sildenafil Reverses Cardiac Dysfunction in the Mdx Mouse Model of Duchenne Muscular Dystrophy.” *Proceedings of the National Academy of Sciences* 107 (44): 19079–83.

Aguettaz, E, JJ Lopez, A Krzesiak, L Lipskaia, S Adnot, RJ Hajjar, C Cognard, B Constantin, and S Sebille. 2016. “Axial Stretch-Dependent Cation Entry in Dystrophic Cardiomyopathy: Involvement of Several TRPs Channels.” *Cell Calcium* 59 (4): 145–55.

Ahmad, Faiyaz, Taku Murata, K Shimizu, Eva Degerman, Donald Maurice, and Vincent Manganiello. 2015. “Cyclic Nucleotide Phosphodiesterases: Important Signaling Modulators and Therapeutic Targets.” *Oral Diseases* 21 (1): e25–50.

Bachmann, Verena A., Johanna E. Mayrhofer, Ronit Ilouz, Philipp Tschaikner, Philipp Raffeiner, Ruth Röck, Mathieu Courcelles et al. "Gpr161 anchoring of PKA consolidates GPCR and cAMP signaling." *Proceedings of the National Academy of Sciences* (2016): 201608061.

Baillie, George S, Arvind Sood, Ian McPhee, Irene Gall, Stephen J Perry, Robert J Lefkowitz, and Miles D Houslay. 2003. “β-Arrestin-Mediated PDE4 cAMP Phosphodiesterase Recruitment Regulates β-Adrenoceptor Switching from Gs to Gi.” *Proceedings of the National Academy of Sciences* 100 (3): 940–45.

Bender, Andrew T, and Joseph A Beavo. 2006. “Cyclic Nucleotide Phosphodiesterases: Molecular Regulation to Clinical Use.” *Pharmacological Reviews* 58 (3): 488–520.

Bers, Donald M. 2002. “Cardiac Excitation–contraction Coupling.” *Nature* 415 (6868): 198–205.

Bia, Britta L, Paul J Cassidy, Martin E Young, Jill A Rafael, Brendan Leighton, Kay E Davies, George K Radda, and Kieran Clarke. 1999. “Decreased Myocardial nNOS, Increased iNOS and Abnormal ECGs in Mouse Models of Duchenne Muscular Dystrophy.” *Journal of Molecular and Cellular Cardiology* 31 (10): 1857–62.

Blake, Derek J, and Enca Martin-Rendon. 2002. “Intermediate Filaments and the Function of the Dystrophin–protein Complex.” *Trends in Cardiovascular Medicine* 12 (5): 224–28.

Bodensteiner, John B, and Andrew G Engel. 1978. “Intracellular Calcium Accumulation in Duchenne Dystrophy and Other Myopathies A Study of 567,000 Muscle Fibers in 114 Biopsies.” *Neurology* 28 (5): 439–439.

Boess, Frank G, Martin Hendrix, Franz-Josef van der Staay, Christina Erb, Rudy Schreiber, Wilma van Staveren, Jan de Vente, Jos Prickaerts, Arjan Blokland, and Gerhard Koenig. 2004. “Inhibition of Phosphodiesterase 2 Increases Neuronal cGMP, Synaptic Plasticity and Memory Performance.” *Neuropharmacology* 47 (7): 1081–92.

Brenman, Jay E, Daniel S Chao, Stephen H Gee, Aaron W McGee, Sarah E Craven, Daniel R Santillano, Ziqiang Wu, Fred Huang, Houhui Xia, and Matthew F Peters. 1996. "Interaction of Nitric Oxide Synthase with the Postsynaptic Density Protein PSD-95 and α1-Syntrophin Mediated by PDZ Domains." *Cell* 84 (5): 757–67.

Brenman, Jay E, Daniel S Chao, Houhui Xia, Ken Aldape, and David S Bredt. 1995. "Nitric Oxide Synthase Complexed with Dystrophin and Absent from Skeletal Muscle Sarcolemma in Duchenne Muscular Dystrophy." *Cell* 82 (5): 743–52.

Brescia, Marcella, and Manuela Zaccolo. 2016. "Modulation of Compartmentalised Cyclic Nucleotide Signalling via Local Inhibition of Phosphodiesterase Activity." *International Journal of Molecular Sciences* 17 (10): 1672.

Bulfield, Grahame, WG Siller, PA Wight, and Karen J Moore. 1984. "X Chromosome-Linked Muscular Dystrophy (Mdx) in the Mouse." *Proceedings of the National Academy of Sciences* 81 (4): 1189–92.

Burgin, Alex B, Olafur T Magnusson, Jasbir Singh, Pam Witte, Bart L Staker, Jon M Bjornsson, Margret Thorsteinsdottir, Sigrun Hrafnsdottir, Timothy Hagen, and Alex S Kiselyov. 2010. "Design of Phosphodiesterase 4D (PDE4D) Allosteric Modulators for Enhancing Cognition with Improved Safety." *Nature Biotechnology* 28 (1): 63–70.

Carnegie, Graeme K, Christopher K Means, and John D Scott. 2009. "A-kinase Anchoring Proteins: From Protein Complexes to Physiology and Disease." *IUBMB Life* 61 (4): 394–406.

Carnicer, Ricardo, Silvia Suffredini, Xing Liu, Svetlana Reilly, Jillian N Simon, Nicoletta C Surdo, Yin H Zhang, Craig A Lygate, Keith M Channon, and Barbara Casadei. 2017. "The Subcellular Localization of Neuronal Nitric Oxide Synthase Determines the Downstream Effects of NO on Myocardial Function." *Cardiovascular Research* 113 (3): 321–31.

Castro, Liliana RV, Ignacio Verde, Dermot MF Cooper, and Rodolphe Fischmeister. 2006. "Cyclic Guanosine Monophosphate Compartmentation in Rat Cardiac Myocytes." *Circulation* 113 (18): 2221–28.

Chandrasekharan, Kumaran, Jung Hae Yoon, Ying Xu, Marybeth Camboni, Paulus ML Janssen, Ajit Varki, and Paul T Martin. 2010. "A Human-Specific Deletion in Mouse Cmah Increases Disease Severity in the Mdx Model of Duchenne Muscular Dystrophy." *Science Translational Medicine* 2 (42): 42ra54-42ra54.

Chen, Jonathan, Lonny R Levin, and Jochen Buck. 2012. "Role of Soluble Adenylyl Cyclase in the Heart." *American Journal of Physiology-Heart and Circulatory Physiology* 302 (3): H538–43.

Chu, Victor, Jose M Otero, Orlando Lopez, Matthew F Sullivan, James P Morgan, Ivo Amende, and Thomas G Hampton. 2002. "Electrocardiographic Findings in Mdx Mice: A Cardiac Phenotype of Duchenne Muscular Dystrophy." *Muscle & Nerve* 26 (4): 513–19.

Conti, Marco, and Joseph Beavo. 2007. "Biochemistry and Physiology of Cyclic Nucleotide Phosphodiesterases: Essential Components in Cyclic Nucleotide Signaling." *Annu. Rev. Biochem.* 76: 481–511.

Conti, Marco, Delphine Mika, and Wito Richter. 2014. “Cyclic AMP Compartments and Signaling Specificity: Role of Cyclic Nucleotide Phosphodiesterases.” *The Journal of General Physiology* 143 (1): 29–38.

Derbyshire, Emily R, and Michael A Marletta. 2012. “Structure and Regulation of Soluble Guanylate Cyclase.” *Annual Review of Biochemistry* 81: 533–59.

Dodge, Kimberly L, Samone Khouangsathiene, Michael S Kapiloff, Robert Mouton, Elaine V Hill, Miles D Houslay, Lorene K Langeberg, and John D Scott. 2001. “mAKAP Assembles a Protein Kinase A/PDE4 Phosphodiesterase cAMP Signaling Module.” *The EMBO Journal* 20 (8): 1921–30.

Edwards, Helen V, Frank Christian, and George S Baillie. 2012. “cAMP: Novel Concepts in Compartmentalised Signalling.” In , 23:181–90. Elsevier.

Ehmsen, Jeffrey, Ellen Poon, and Kay Davies. 2002. “The Dystrophin-Associated Protein Complex.” *Journal of Cell Science* 115 (14): 2801–3.

Ervasti, James M, and Kevin P Campbell. 1991. “Membrane Organization of the Dystrophin-Glycoprotein Complex.” *Cell* 66 (6): 1121–31.

Ervasti, James M, Kay Ohlendieck, Steven D Kahl, Mitchell G Gaver, and Kevin P Campbell. 1990. “Deficiency of a Glycoprotein Component of the Dystrophin Complex in Dystrophic Muscle.” *Nature* 345 (6273): 315–19.

Florio, Vincent A, William K Sonnenburg, Richard Johnson, Keith S Kwak, Gregory S Jensen, Kenneth A Walsh, and Joseph A Beavo. 1994. “Phosphorylation of the 61-kDa Calmodulin-Stimulated Cyclic Nucleotide Phosphodiesterase at Serine 120 Reduces Its Affinity for Calmodulin.” *Biochemistry* 33 (30): 8948–54.

Francis, Sharron H, Mitsi A Blount, and Jackie D Corbin. 2011. “Mammalian Cyclic Nucleotide Phosphodiesterases: Molecular Mechanisms and Physiological Functions.” *Physiological Reviews* 91 (2): 651–90.

Francis, Sharron H, and Jackie D Corbin. 1994. “Structure and Function of Cyclic Nucleotide-Dependent Protein Kinases.” *Annual Review of Physiology* 56 (1): 237–72.

Gao, Tianyan, Atsuko Yatani, Mark L Dell’Acqua, Hidenori Sako, Stuart A Green, Nathan Dascal, John D Scott, and M Marlene Hosey. 1997. “cAMP-Dependent Regulation of Cardiac L-Type Ca 2+ Channels Requires Membrane Targeting of PKA and Phosphorylation of Channel Subunits.” *Neuron* 19 (1): 185–96.

Gilead Sciences, Gilead Science. n.d. “Study of Add-on Ambrisentan Therapy to Background Phosphodiesterase Type-5 Inhibitor (PDE5i) Therapy in Pulmonary Arterial Hypertension (ATHENA-1) (ATHENA-1) ClinicalTrials.gov Identifier: NCT00617305.” https://clinicaltrials.gov/ct2/show/results/NCT00617305?term=pde5&rank=13.

Griffith, Owen W, and Dennis J Stuehr. 1995. “Nitric Oxide Synthases: Properties and Catalytic Mechanism.” *Annual Review of Physiology* 57 (1): 707–34.

Guiraud, Simon, Annemieke Aartsma-Rus, Natassia M Vieira, Kay E Davies, Gert-Jan B van Ommen, and Louis M Kunkel. 2015. “The Pathogenesis and Therapy of Muscular Dystrophies.” *Annual Review of Genomics and Human Genetics* 16: 281–308.

Gurney, Mark E, Alex B Burgin, Olafur T Magnusson, and Lance J Stewart. 2011. "Small Molecule Allosteric Modulators of Phosphodiesterase 4." In *Phosphodiesterases as Drug Targets*, 167–92. Springer.

Hanoune, Jacques, and Nicole Defer. 2001. "Regulation and Role of Adenylyl Cyclase Isoforms." *Annual Review of Pharmacology and Toxicology* 41 (1): 145–74.

Hatzelmann, Armin, and Christian Schudt. 2001. "Anti-Inflammatory and Immunomodulatory Potential of the Novel PDE4 Inhibitor Roflumilast in Vitro." *Journal of Pharmacology and Experimental Therapeutics* 297 (1): 267–79.

Hayes, J Scott, Laurence L Brunton, Joan Heller Brown, James B Reese, and Steven E Mayer. 1979. "Hormonally Specific Expression of Cardiac Protein Kinase Activity." *Proceedings of the National Academy of Sciences* 76 (4): 1570–74.

Hayes, J Scott, Laurence L Brunton, and Steven E Mayer. 1980. "Selective Activation of Particulate cAMP-Dependent Protein Kinase by Isoproterenol and Prostaglandin E1." *Journal of Biological Chemistry* 255 (11): 5113–19.

Hoffman, Eric P, Robert H Brown, and Louis M Kunkel. 1987. "Dystrophin: The Protein Product of the Duchenne Muscular Dystrophy Locus." *Cell* 51 (6): 919–28.

Honda, Akira, Stephen R Adams, Carolyn L Sawyer, Varda Lev-Ram, Roger Y Tsien, and Wolfgang RG Dostmann. 2001. "Spatiotemporal Dynamics of Guanosine 3′, 5′-Cyclic Monophosphate Revealed by a Genetically Encoded, Fluorescent Indicator." *Proceedings of the National Academy of Sciences* 98 (5): 2437–42.

Huang, Zheng, Yves Ducharme, Dwight Macdonald, and Annette Robichaud. 2001. "The next Generation of PDE4 Inhibitors." *Current Opinion in Chemical Biology* 5 (4): 432–38.

Isidori, Andrea M. n.d. "Endocrine Cardiomyopathy: Response to Cyclic GMP PDE5 Inhibitors in Acromegaly Cardiomyopathy (SUM) ClinicalTrials.gov Identifier: NCT02611336." https://clinicaltrials.gov/ct2/show/NCT02611336?term=pde5&rank=40.

Iwata, Yuko, Yuki Katanosaka, Yuji Arai, Kazuo Komamura, Kunio Miyatake, and Munekazu Shigekawa. 2003. "A Novel Mechanism of Myocyte Degeneration Involving the Ca 2+-Permeable Growth Factor–regulated Channel." *The Journal of Cell Biology* 161 (5): 957–67.

Keravis, Thérèse, and Claire Lugnier. 2012. "Cyclic Nucleotide Phosphodiesterase (PDE) Isozymes as Targets of the Intracellular Signalling Network: Benefits of PDE Inhibitors in Various Diseases and Perspectives for Future Therapeutic Developments." *British Journal of Pharmacology* 165 (5): 1288–1305.

Khairallah, M, RJ Khairallah, ME Young, BG Allen, MA Gillis, G Danialou, CF Deschepper, BJ Petrof, and C Des Rosiers. 2008. "Sildenafil and Cardiomyocyte-Specific cGMP Signaling Prevent Cardiomyopathic Changes Associated with Dystrophin Deficiency." *Proceedings of the National Academy of Sciences* 105 (19): 7028–33.

Khairallah, Maya, Ramzi Khairallah, Martin E Young, Jason RB Dyck, Basil J Petrof, and Christine Des Rosiers. 2007. "Metabolic and Signaling Alterations in

Dystrophin-Deficient Hearts Precede Overt Cardiomyopathy." *Journal of Molecular and Cellular Cardiology* 43 (2): 119–29.

Kirchmann, C, D Kececioglu, R Korinthenberg, and S Dittrich. 2005. "Echocardiographic and Electrocardiographic Findings of Cardiomyopathy in Duchenne and Becker–Kiener Muscular Dystrophies." *Pediatric Cardiology* 26 (1): 66–72.

Klussmann, Enno. 2016. "Protein–protein Interactions of PDE4 Family members—Functions, Interactions and Therapeutic Value." *Cellular Signalling* 28 (7): 713–18.

Knowles, Richard G, and Salvador Moncada. 1994. "Nitric Oxide Synthases in Mammals." *Biochemical Journal* 298 (Pt 2): 249.

Kobayashi, Yvonne M, Erik P Rader, Robert W Crawford, Nikhil K Iyengar, Daniel R Thedens, John A Faulkner, Swapnesh V Parikh, Robert M Weiss, Jeffrey S Chamberlain, and Steven A Moore. 2008. "Sarcolemma-Localized nNOS Is Required to Maintain Activity after Mild Exercise." *Nature* 456 (7221): 511.

Kritzer, Michael D, Jinliang Li, Kimberly Dodge-Kafka, and Michael S Kapiloff. 2012. "AKAPs: The Architectural Underpinnings of Local cAMP Signaling." *Journal of Molecular and Cellular Cardiology* 52 (2): 351–58.

Kuhn, Michaela. 2003. "Structure, Regulation, and Function of Mammalian Membrane Guanylyl Cyclase Receptors, with a Focus on Guanylyl Cyclase-A." *Circulation Research* 93 (8): 700–709.

Lai, Yi, Gail D. Thomas, Yongping Yue, Hsiao T. Yang, Dejia Li, Chun Long, Luke Judge et al. "Dystrophins carrying spectrin-like repeats 16 and 17 anchor nNOS to the sarcolemma and enhance exercise performance in a mouse model of muscular dystrophy." *The Journal of clinical investigation* 119, no. 3 (2009): 624.

Lee, Dong I, Guangshuo Zhu, Takashi Sasaki, Gun-Sik Cho, Nazha Hamdani, Ronald Holewinski, Su-Hyun Jo, Thomas Danner, Manling Zhang, and Peter P Rainer. 2015. "Phosphodiesterase 9A Controls Nitric-Oxide-Independent cGMP and Hypertrophic Heart Disease." *Nature* 519 (7544): 472–76.

Li, Xiang, George S Baillie, and Miles D Houslay. 2009. "Mdm2 Directs the Ubiquitination of β-Arrestin-Sequestered cAMP Phosphodiesterase-4D5." *Journal of Biological Chemistry* 284 (24): 16170–82.

Li, Zhe, Yinuo Wu, Ling-Jun Feng, Ruibo Wu, and Hai-Bin Luo. 2014. "Ab Initio QM/MM Study Shows a Highly Dissociated SN2 Hydrolysis Mechanism for the cGMP-Specific Phosphodiesterase-5." *Journal of Chemical Theory and Computation* 10 (12): 5448–57.

Lohan, James, and Kay Ohlendieck. 2004. "Drastic Reduction in the Luminal Ca 2+-Binding Proteins Calsequestrin and Sarcalumenin in Dystrophin-Deficient Cardiac Muscle." *Biochimica et Biophysica Acta (BBA)-Molecular Basis of Disease* 1689 (3): 252–58.

Lohmann, SM, R Fischmeister, and U Walter. 1991. "Signal Transduction by cGMP in Heart." *Basic Research in Cardiology* 86 (6): 503–14.

Lomas, Oliver, and Manuela Zaccolo. 2014. “Phosphodiesterases Maintain Signaling Fidelity via Compartmentalization of Cyclic Nucleotides.” *Physiology* 29 (2): 141–49.

Lugnier, Claire. 2006. “Cyclic Nucleotide Phosphodiesterase (PDE) Superfamily: A New Target for the Development of Specific Therapeutic Agents.” *Pharmacology & Therapeutics* 109 (3): 366–98.

Lygren, Birgitte, Cathrine Rein Carlson, Katja Santamaria, Valentina Lissandron, Theresa McSorley, Jessica Litzenberg, Dorothea Lorenz, Burkhard Wiesner, Walter Rosenthal, and Manuela Zaccolo. 2007. “AKAP Complex Regulates Ca2+ Re-uptake into Heart Sarcoplasmic Reticulum.” *EMBO Reports* 8 (11): 1061–67.

Lynch, Martin J, George S Baillie, Ahmed Mohamed, Xiang Li, Charlotte Maisonneuve, Enno Klussmann, Gino van Heeke, and Miles D Houslay. 2005. “RNA Silencing Identifies PDE4D5 as the Functionally Relevant cAMP Phosphodiesterase Interacting with Barrestin to Control the Protein Kinase A/AKAP79-Mediated Switching of the β2-Adrenergic Receptor to Activation of ERK in HEK293B2 Cells.” *Journal of Biological Chemistry* 280 (39): 33178–89.

Mazur, Wojciech, Kan N Hor, Joshua T Germann, Robert J Fleck, Hussein R Al-Khalidi, Janaka P Wansapura, Eugene S Chung, Michael D Taylor, John L Jefferies, and D Woodrow Benson. 2012. “Patterns of Left Ventricular Remodeling in Patients with Duchenne Muscular Dystrophy: A Cardiac MRI Study of Ventricular Geometry, Global Function, and Strain.” *The International Journal of Cardiovascular Imaging* 28 (1): 99–107.

McCahill, Angela, Theresa McSorley, Elaine Huston, Elaine V Hill, Martin J Lynch, Irene Gall, Guy Keryer, Birgitte Lygren, Kjetil Tasken, and Gino van Heeke. 2005. “In Resting COS1 Cells a Dominant Negative Approach Shows That Specific, Anchored PDE4 cAMP Phosphodiesterase Isoforms Gate the Activation, by Basal Cyclic AMP Production, of AKAP-Tethered Protein Kinase A Type II Located in the Centrosomal Region.” *Cellular Signalling* 17 (9): 1158–73.

McCormick, Kristie, and George S Baillie. 2014. “Compartmentalisation of Second Messenger Signalling Pathways.” *Current Opinion in Genetics & Development* 27: 20–25.

McGreevy, Joe W, Chady H Hakim, Mark A McIntosh, and Dongsheng Duan. 2015. “Animal Models of Duchenne Muscular Dystrophy: From Basic Mechanisms to Gene Therapy.” *Disease Models & Mechanisms* 8 (3): 195–213.

Mongillo, Marco, Theresa McSorley, Sandrine Evellin, Arvind Sood, Valentina Lissandron, Anna Terrin, Elaine Huston, Annette Hannawacker, Martin J Lohse, and Tullio Pozzan. 2004. “Fluorescence Resonance Energy Transfer–based Analysis of cAMP Dynamics in Live Neonatal Rat Cardiac Myocytes Reveals Distinct Functions of Compartmentalized Phosphodiesterases.” *Circulation Research* 95 (1): 67–75.

Mosqueira, Matias, Ulrike Zeiger, Moritz Förderer, Heinrich Brinkmeier, and Rainer HA Fink. 2013. “Cardiac and Respiratory Dysfunction in Duchenne Muscular

Dystrophy and the Role of Second Messengers." *Medicinal Research Reviews* 33 (5): 1174–1213.

Nigro, G, LI Comi, L Politano, and RJI Bain. 1990. "The Incidence and Evolution of Cardiomyopathy in Duchenne Muscular Dystrophy." *International Journal of Cardiology* 26 (3): 271–77.

Nikolaev, Viacheslav O, Moritz Bünemann, Lutz Hein, Annette Hannawacker, and Martin J Lohse. 2004. "Novel Single Chain cAMP Sensors for Receptor-Induced Signal Propagation." *Journal of Biological Chemistry* 279 (36): 37215–18.

Nikolaev, Viacheslav O, Stepan Gambaryan, and Martin J Lohse. 2006. "Fluorescent Sensors for Rapid Monitoring of Intracellular cGMP." *Nature Methods* 3 (1): 23–25.

Omori, Kenji, and Jun Kotera. 2007. "Overview of PDEs and Their Regulation." *Circulation Research* 100 (3): 309–27.

Pandit, Jayvardhan. 2014. "PDE4: New Structural Insights into the Regulatory Mechanism and Implications for the Design of Selective Inhibitors." *Phosphodiesterases and Their Inhibitors*, 29–44.

Pekkinen, Minna, Mikael EB Ahlström, Ulrike Riehle, Minna M Huttunen, and Christel JE Lamberg-Allardt. 2008. "Effects of Phosphodiesterase 7 Inhibition by RNA Interference on the Gene Expression and Differentiation of Human Mesenchymal Stem Cell-Derived Osteoblasts." *Bone* 43 (1): 84–91.

Piggott, Leslie A, Kathryn A Hassell, Zuzana Berkova, Andrew P Morris, Michael Silberbach, and Thomas C Rich. 2006. "Natriuretic Peptides and Nitric Oxide Stimulate cGMP Synthesis in Different Cellular Compartments." *The Journal of General Physiology* 128 (1): 3–14.

Ponsioen, Bas, Jun Zhao, Jurgen Riedl, Fried Zwartkruis, Gerard van der Krogt, Manuela Zaccolo, Wouter H Moolenaar, Johannes L Bos, and Kees Jalink. 2004. "Detecting cAMP-induced Epac Activation by Fluorescence Resonance Energy Transfer: Epac as a Novel cAMP Indicator." *EMBO Reports* 5 (12): 1176–80.

Raeymaekers, Luc, Ft Hofmann, and Rik Casteels. 1988. "Cyclic GMP-Dependent Protein Kinase Phosphorylates Phospholamban in Isolated Sarcoplasmic Reticulum from Cardiac and Smooth Muscle." *Biochemical Journal* 252 (1): 269–73.

Rando, Thomas A. 2001. "The Dystrophin–glycoprotein Complex, Cellular Signaling, and the Regulation of Cell Survival in the Muscular Dystrophies." *Muscle & Nerve* 24 (12): 1575–94.

Reuter, Harald. 1984. "Ion Channels in Cardiac Cell Membranes." *Annual Review of Physiology* 46 (1): 473–84.

Russwurm, Michael, Florian Mullershausen, Andreas Friebe, Ronald Jäger, Corina Russwurm, and Doris Koesling. 2007. "Design of Fluorescence Resonance Energy Transfer (FRET)-Based cGMP Indicators: A Systematic Approach." *Biochemical Journal* 407 (1): 69–77.

Sachs, Benjamin D, George S Baillie, Julianne R McCall, Melissa A Passino, Christian Schachtrup, Derek A Wallace, Allan J Dunlop, Kirsty F MacKenzie, Enno Klussmann, and Martin J Lynch. 2007. "p75 Neurotrophin Receptor Regulates Tissue Fibrosis through Inhibition of Plasminogen Activation via a PDE4/cAMP/PKA Pathway." *The Journal of Cell Biology* 177 (6): 1119–32.

Sanyal, Shyamal K, and Warren W Johnson. 1982. "Cardiac Conduction Abnormalities in Children with Duchenne9s Progressive Muscular Dystrophy: Electrocardiographic Features and Morphologic Correlates." *Circulation* 66 (4): 853–63.

Sato, Moritoshi, Naoki Hida, Takeaki Ozawa, and Yoshio Umezawa. 2000. "Fluorescent Indicators for Cyclic GMP Based on Cyclic GMP-Dependent Protein Kinase Iα and Green Fluorescent Proteins." *Analytical Chemistry* 72 (24): 5918–24.

Sharma, Vivek K, Pallavi Rungta, and Ashok K Prasad. 2014. "Nucleic Acid Therapeutics: Basic Concepts and Recent Developments." *RSC Advances* 4 (32): 16618–31.

Sin, YY, HV Edwards, X Li, JP Day, F Christian, AJ Dunlop, DR Adams, M Zaccolo, MD Houslay, and GS Baillie. 2011. "Disruption of the Cyclic AMP Phosphodiesterase-4 (PDE4)–HSP20 Complex Attenuates the β-Agonist Induced Hypertrophic Response in Cardiac Myocytes." *Journal of Molecular and Cellular Cardiology* 50 (5): 872–83.

Stangherlin, Alessandra, and Manuela Zaccolo. 2012. "Phosphodiesterases and Subcellular Compartmentalized cAMP Signaling in the Cardiovascular System." *American Journal of Physiology-Heart and Circulatory Physiology* 302 (2): H379–90.

Stefan, Eduard, Burkhard Wiesner, George S Baillie, Rustam Mollajew, Volker Henn, Dorothea Lorenz, Jens Furkert, Katja Santamaria, Pavel Nedvetsky, and Christian Hundsrucker. 2007. "Compartmentalization of cAMP-Dependent Signaling by Phosphodiesterase-4D Is Involved in the Regulation of Vasopressin-Mediated Water Reabsorption in Renal Principal Cells." *Journal of the American Society of Nephrology* 18 (1): 199–212.

Stuckey, Daniel J, Carolyn A Carr, Patrizia Camelliti, Damian J Tyler, Kay E Davies, and Kieran Clarke. 2012. "In Vivo MRI Characterization of Progressive Cardiac Dysfunction in the Mdx Mouse Model of Muscular Dystrophy." *PloS One* 7 (1): e28569.

Sutherland, Earl W, and G Alan Robison. 1966. "A. THE ROLE OF CYCLIC-3', 5'-AMP IN RESPONSES TO CATECHOLAMINES AND OTHER HORMONES." *Pharmacological Reviews* 18 (1): 145–61.

Takimoto, Eiki, Diego Belardi, Carlo G Tocchetti, Susan Vahebi, Gianfrancesco Cormaci, Elizabeth A Ketner, An L Moens, Hunter C Champion, and David A Kass. 2007. "Compartmentalization of Cardiac β-Adrenergic Inotropy Modulation by Phosphodiesterase Type 5." *Circulation* 115 (16): 2159–67.

Tasken, Kjetil, and Einar Martin Aandahl. 2004. "Localized Effects of cAMP Mediated by Distinct Routes of Protein Kinase A." *Physiological Reviews* 84 (1): 137–67.

Taskén, Kristin A, Philippe Collas, Wolfram A Kemmner, Oliwia Witczak, Marco Conti, and Kjetil Taskén. 2001. “Phosphodiesterase 4D and Protein Kinase a Type II Constitute a Signaling Unit in the Centrosomal Area.” *Journal of Biological Chemistry* 276 (25): 21999–2.

Taylor, Susan S, Choel Kim, Dominico Vigil, Nina M Haste, Jie Yang, Jian Wu, and Ganesh S Anand. 2005. “Dynamics of Signaling by PKA.” *Biochimica et Biophysica Acta (BBA)-Proteins and Proteomics* 1754 (1): 25–37.

Tinsley, Jonathon, Nicolas Deconinck, Rosie Fisher, David Kahn, Steve Phelps, Jean-Marie Gillis, and Kay Davies. 1998. “Expression of Full-Length Utrophin Prevents Muscular Dystrophy in Mdx Mice.” *Nature Medicine* 4 (12): 1441–44.

Tsai, Emily J, and David A Kass. 2009. “Cyclic GMP Signaling in Cardiovascular Pathophysiology and Therapeutics.” *Pharmacology & Therapeutics* 122 (3): 216–38.

Turner, Paul R, PY Fong, Wilfred F Denetclaw, and Richard A Steinhardt. 1991. “Increased Calcium Influx in Dystrophic Muscle.” *The Journal of Cell Biology* 115 (6): 1701–12.

Vo, Ngan K, Jessica M Gettemy, and Vincent M Coghlan. 1998. “Identification of cGMP-Dependent Protein Kinase Anchoring Proteins (GKAPs).” *Biochemical and Biophysical Research Communications* 246 (3): 831–35.

Wallace, Gregory Q, and Elizabeth M McNally. 2009. “Mechanisms of Muscle Degeneration, Regeneration, and Repair in the Muscular Dystrophies.” *Annual Review of Physiology* 71: 37–57.

Wehling-Henricks, Michelle, Maria C Jordan, Kenneth P Roos, Bo Deng, and James G Tidball. 2005. “Cardiomyopathy in Dystrophin-Deficient Hearts Is Prevented by Expression of a Neuronal Nitric Oxide Synthase Transgene in the Myocardium.” *Human Molecular Genetics* 14 (14): 1921–33.

Westering, Tirsa LE van, Corinne A Betts, and Matthew JA Wood. 2015. “Current Understanding of Molecular Pathology and Treatment of Cardiomyopathy in Duchenne Muscular Dystrophy.” *Molecules* 20 (5): 8823–55.

Wettschureck, Nina, and Stefan Offermanns. 2005. “Mammalian G Proteins and Their Cell Type Specific Functions.” *Physiological Reviews* 85 (4): 1159–1204.

Wilson, Lindsay S, George S Baillie, Lisa M Pritchard, Bibiana Umana, Anna Terrin, Manuela Zaccolo, Miles D Houslay, and Donald H Maurice. 2011. “A Phosphodiesterase 3B-Based Signaling Complex Integrates Exchange Protein Activated by cAMP 1 and Phosphatidylinositol 3-Kinase Signals in Human Arterial Endothelial Cells.” *Journal of Biological Chemistry* 286 (18): 16285–96.

Xu, Kai Y, David L Huso, Ted M Dawson, David S Bredt, and Lewis C Becker. 1999. “Nitric Oxide Synthase in Cardiac Sarcoplasmic Reticulum.” *Proceedings of the National Academy of Sciences* 96 (2): 657–62.

Zaccolo, Manuela. 2011. “Spatial Control of cAMP Signalling in Health and Disease.” *Current Opinion in Pharmacology* 11 (6): 649–55.

Zaccolo, Manuela, Francesca De Giorgi, Charles Y Cho, Luxin Feng, Tom Knapp, Paul A Negulescu, Susan S Taylor, Roger Y Tsien, and Tullio Pozzan. 2000. “A

Genetically Encoded, Fluorescent Indicator for Cyclic AMP in Living Cells." *Nature Cell Biology* 2 (1): 25–29.

Zaccolo, Manuela, and Tullio Pozzan. 2002. "Discrete Microdomains with High Concentration of cAMP in Stimulated Rat Neonatal Cardiac Myocytes." *Science* 295 (5560): 1711–15.

Zhang, Manling, and David A Kass. 2011. "Phosphodiesterases and Cardiac cGMP: Evolving Roles and Controversies." *Trends in Pharmacological Sciences* 32 (6): 360–65.

Zhang, Qian, Jarrod E Church, Davin Jagnandan, John D Catravas, William C Sessa, and David Fulton. 2006. "Functional Relevance of Golgi-and Plasma Membrane-Localized Endothelial NO Synthase in Reconstituted Endothelial Cells." *Arteriosclerosis, Thrombosis, and Vascular Biology* 26 (5): 1015–21.

Zoccarato, Anna, Nicoletta C Surdo, Jan M Aronsen, Laura A Fields, Luisa Mancuso, Giuliano Dodoni, Alessandra Stangherlin, Craig Livie, He Jiang, and Yuan Yan Sin. 2015. "Cardiac Hypertrophy Is Inhibited by a Local Pool of cAMP Regulated by Phosphodiesterase 2." *Circulation Research* 117 (8): 707–19.

Chapter 2. Methods

2.1. PREPARATION OF ISOLATED CARDIOMYOCYTES

2.1.1. Adult Mouse Left ventricular cardiomyocyte isolation

a) Excision of the whole heart

Cervical dislocation of 12-week-old male wild-type mouse mdx or C57/BL10 and mdx was performed by manual technique to avoid thoracic trauma and bleeding. Midline skin incision using scissors and larger forceps to were done to reveal sternum and 2x lateral thoracic / costal incisions - mid-axillary line 5. After clear visualisation of great vessels, suture was placed behind aorta using smaller of the forceps (under a magnifying microscope) and a single loose tied around the aorta. Using a straight scissors, a single incision onto the aorta was done, the cannula was inserted and the suture knot was tightened to keep cannula in place. By lifting both ends of the suture, the heart was removed by cutting surrounding tissue with scissors.

b) Langendorff Perfusion isolation of cardiomyocytes

Cannula and heart were placed on Langendorff apparatus (Figure 2.1) and plain Tyrode Buffer was perfused for about two minutes to ensure perfusion was adequate and no leak. Perfusion taps were switched to the digestion enzyme reservoir and the enzyme perfused the heart for approximately 7-10 minutes or until flow increases to a flow by 50% or: drop rate 0.5 drops / sec to 1 drop / sec. During heart perfusion, the enzyme was collected to use in further digestions.

Figure 2.1. Langendorff Perfusion Apparatus and perfused heart

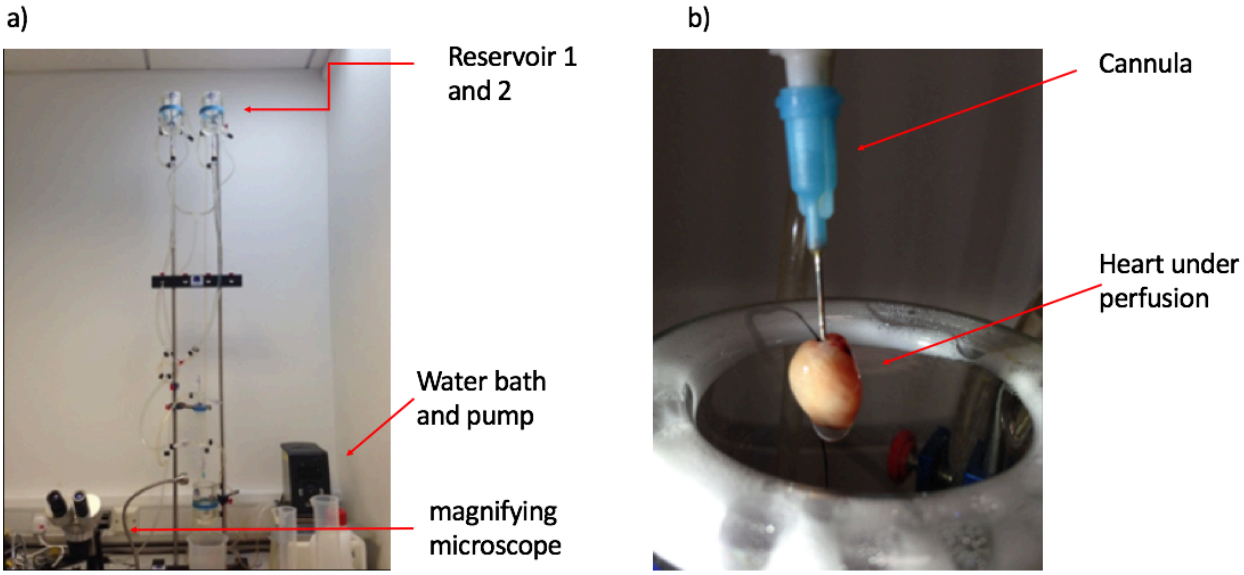


Figure 2.1
a) Image of the Langendorff Perfusion Apparatus, Reservoirs, water bath and pump, and magnifying microscope. Figure b is a close-up image of the perfused heart and cannula attached to the perfusion system.

c) Tissue Dissociation

After complete perfusion, the heart was placed in Petri dish with 5ml of enzyme solution and atria and RV were excised. The LV was then chopped with scissor, placed in a spare tube and triturated using a pipette in a 37^{o} bath for 30 seconds. Undigested tissue was filter through gauze and add 1% BSA was added to the cell suspension to terminate enzyme action. The remainder tissue (which was filtered with gauze) was placed in another test tube and triturated for 1 minute or until lumps disappear and solution cloudy. Both tubes were centrifuged at 500rpm for 3 minutes 1/1 (acc/dec). Supernatant was removed and discarded and both pellets were combined with Tyrode with 500µM Calcium (20ml buffer: 10µl 1M $CaCl_2$). After 10 minutes cells had precipitate and supernatant was again removed and replaced with Tyrode with 1mM Calcium (20ml buffer: 20µl 1M $CaCl_2$) for 30 minutes.

d) Cell culturing and adenovirus infection

After this second wash, supernatant was removed and replaced with MEM containing 2.5% FBS and plate on laminin-coated coverslips. After 2-3 Hours of cellular recovery, medium was gently removed and replaced with fresh MEM medium (no FBS). Infection of the cells with adenovirus encoding FRET based sensors was done using specific medium – Multiplicity of Infection (MOI) 1:100. For example: 1.2 $x10^6$ cells per mouse heart → 10^5 cells per 12 well plate therefore 1-2 μL of 10^{10} titre adenovirus. Cell was then incubated at 37°C in 5% CO_2 (Hank's solution with $NaHCO_3$) with expression within the next 24 hours.

2.1.2. Neonatal Mouse Left ventricular cardiomyocyte isolation

Day 1: ADS 1X from 10X stock (A) (about 150 mL), Medium 1st day (M1) and laminin-coated coverslips were prepared. Mice pups (P1 or P2) were sacrificed by cervical dislocation. Hearts were rapidly removed and placed in falcon with ice-cold buffer ADS (A). All hearts were placed in a first Petri dish and the atrium and aorta were cut and discarded. The LV was then minced into small pieces (about 1 mm^3) with scissors and collected with 5 ml pipette (collected in several steps, no more than 1 ml each as tissue might attach on the side of pipette) and put in a 50ml sterile tube. After tissues settled, 9 ml of the Collagenase buffer was added to the tube and incubated in the water-bath at 37 ºC for 5 min, constantly shaking. This first digestion step serves to get rid of most the pericardial collagen. Therefore, supernatant was discarded. 9 ml of the Collagenase buffer (B) were again added to the tube and incubate, under gentle shaking, at 37 ºC for 10 min. Supernatant was collected (cells are in the supernatant; the pellet contains undigested tissue) and 1 ml NCS was added to the supernatant. The tube was centrifuged at 1250 rpm, 5 min, and no brake. After discarding the supernatant, cells which are now in the pellet, were resuspended in 2 ml NCS and placed in the incubator. Lid was left loosen to let O_2/CO_2 in. These steps were repeated until all the tissue was digested (usually 4x). The content of all the tubes were then collected in one 50 ml tube and centrifuged at 1250 rpm, 5 min, and no brake. Cell pellet was resuspended in Medium 1st (M1) (10 ml every 5 hearts) and plated on 10 cm-cell culture dishes (one dish every 5 hearts) for 2 hours. This should make fibroblasts and endothelial cells attach to the dish and myocytes in suspension. After 2 hours supernatant from the dishes was collected and centrifuged at 1250 rpm, 5 min, and no brake. Pellet was than resuspended in Medium 1st day (M1), plated on laminin-coated coverslips and incubated at 37^o.

Day 2: Cells were washed with ADS (A) 3 times and medium M1 was changed to Medium 2nd day (M2). After 2 recovery hours in the incubator the cells can be infected or transfected.

Transfection or adenovirus infection of neonatal cardiomyocytes:

Cells were transfected using TransFectin™ Lipid Reagent (BIO-RAD 170-3351) transfection reagent and 1 µg DNA per well, or infected by adding 0.3µl of virus per coverslip (MOI 30) and incubate for 2 hours in incubator at 37º . After 2 hours, the medium was replaced with 1mL of fresh M2 media.

Preparation of Laminin-coated coverslips

(Laminin (mouse), 354232 BD Biosciences)

Laminin aliquots (100 µg/ml) were kept at – 80 ºC until the need to use. For neonatal cardiomyocytes, laminin stock was diluted in the ratio of 1/5 in PBS and for adult cardiomyocytes 1/1 in PBS. 250-300 µl were plated on each coverslip and incubate at 37 ºC for at least 1 hour before plating cells

2.2. IMAGING

2.2.1. FRET microscopy experiments

FRET-based microscopy experiments per performed using a setup comprising an inverted microscope (Olympus IX71) using a PlanApoN, 60X, NA 1.42 oil immersion objective, 0.17/FN 26.5 (Olympus, UK). The microscope was equipped with a coolSNAP HQ monochrome camera system (Photometrics, USA) and a beam-splitter optical device is required for the recording of dual wavelength emission of YFP and CFP (Dual-view simultaneous-imaging system, DV2 mag biosystem, Photometrics, USA). The FRET filter settings used throughout were: CFP excitation filter ET436/20x, dichroic mirror 455DCLP (Chroma Technology, Germany) in the microscope filter cube; dichroic mirror 505DCLP, YFP emission filter 545 nm, and CFP emission filter 480 nm (Chroma Technology, Germany) in the beam splitter. Images were acquired and processed using Meta imaging series 7.1, MetaFluor, (Molecular Devices, USA). FRET emission ratios were acquired every 10 seconds. FRET changes were measured as changes in the background-subtracted 480nm/545nm fluorescence emission intensity on excitation at 430 nm and expressed as R/R0, where R is the ratio at time t and R0 is the average ratio of the first 8 frames. Figure 2.2 illustrates MetaFluor frame analysis and FRET change traces calculated after background subtraction of CFP and YFP intensities.

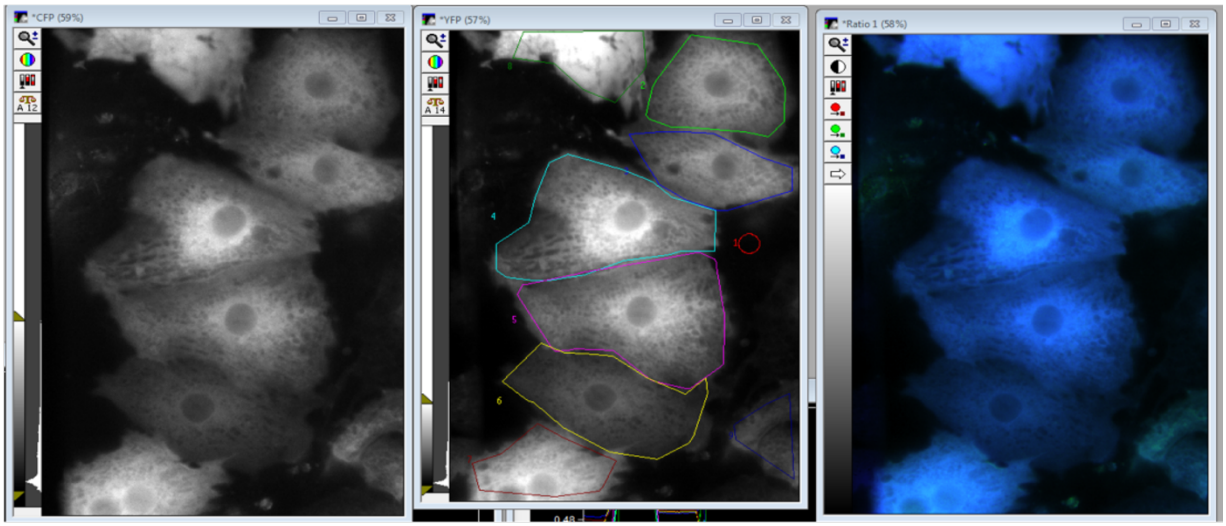
Cells were cultured on 15mm diameter sterilised borosilicate glass coverslips, which allow transfer to a perfusion chamber. The coverslips were held in place with a thin rim of silicone vacuum grease (18405 – Sigma-Aldrich, USA) in order to create a water-tight seal between the chamber and the coverslip. The chamber allowed the application of a stimulus to the bath of superfusate, as well as acute application of 10x concentrate stimuli.

During the experiment cells were maintained at room temperature in FRET saline solution (neonatal cells) or 1.4mM $CaCl_2$ Tyrode solution (adult cells).

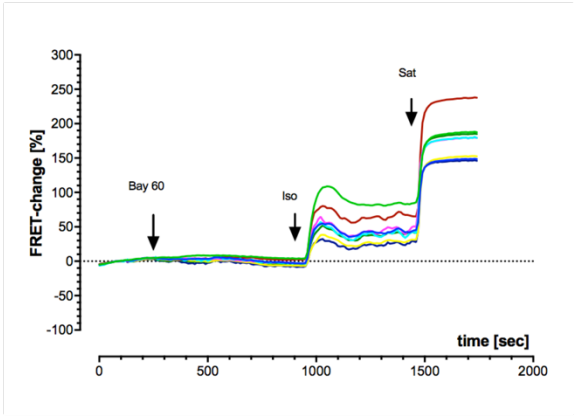
It was not possible to record FRET- changes in adult cardiomyocytes expressing cGMP sensors. Although the cells responded functionally to drugs, such as the NO donors, it was not possible to detect FRET- changes. This limitation might be due to the lack of sensitivity of the FRET sensors. The experiments in neonatal cardiomyocytes were successful, however, the variability of responses was very high specially in the sets where cGMP was being explored. Initially it was hypothesed that the variability was due to a high contamination of fibroblast or endothelial cells, however the high variability was still present even after controlling for this by selecting areas where all cells were contracting and presented clear structures of cardiomyocytes.

Figure 2.2. Analysis of FRET experiment

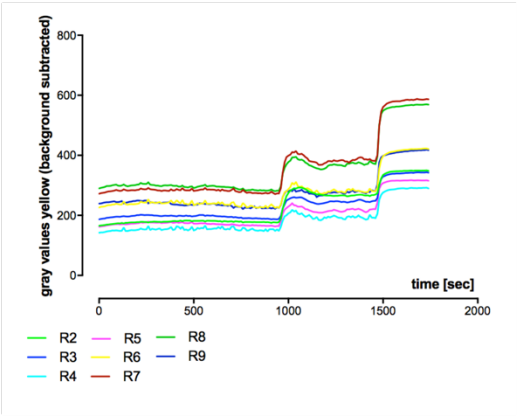
a)



b)



c)



d)

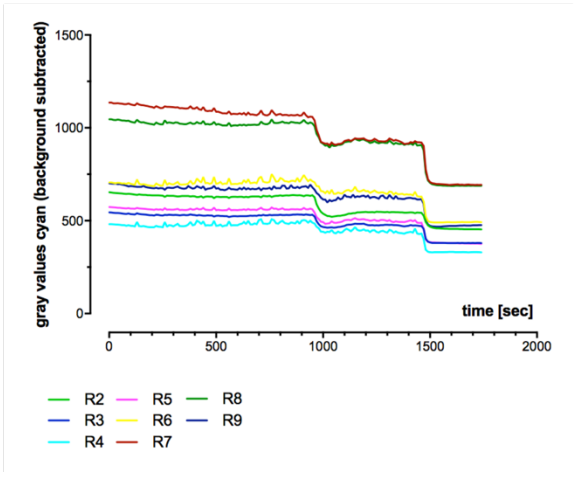


Figure 2.2
Analysis of FRET experiment. Panel a is a representative image (Screenshot) of the MetaFluor Software used to analyse each FRET frame where each individual channel is shown (CFP on the right, YFP in the middle, and ratio image on the left). The Regions of Interest (ROI) were drawn in the YFP image. ROI number 1 represents the background intensity which will then be subtracted by the intensity of each of the other ROI (cells) in each frame. Panel b represents the FRET-change trace of each individual ROI. This FRET-change is calculated by the ratio between the YFP intensity after background subtraction (c) and CFP intensity after background subtraction (d).

2.2.2. Immunofluorescence staining and confocal imaging

Twenty-four hours after infection or transfection with targeted-FRET based sensors, cardiomyocytes were fixed in paraformaldehyde 4% for 10 min, washed with PBS and permeabilised in 0.5% Triton X-100 for 10 min. After blocking with Abdil for 1 h, the cells were incubated with primary antibody against nNOS, eNOS, iNOS and dystophin (details available in Appendix I), at RT for 1h. Samples were then washed with PBS-0.1% Tween20 and incubated with relevant secondary antibody (detail available in Appendix I) for 60 min at room temperature. Cells were incubated with Wheat Germ Agglutinin, Alexa Fluor 594 Conjugate (5 μg ml^{-1}) (W11262, Thermo Fisher Scientific, MA, USA) for 10 min or 1:10.0000 MitoTracker red (M7512, Invitrogen) for 5 min at 37 °C before fixing the cells with formaldehyde 4%. The fixed cells were rinsed in PBS-0.1% Tween20 and mounted in Ibidi Mounting Medium (Thistle Scientific, UK). Images were acquired with an Inverted Olympus FV1000 confocal microscope.

2.2.3. FRET-based sensor calibration

a) In cell calibration procedure by microinfusion:

Microinfusion experiments were performed as described in detail in (Koschinski, Zaccolo 2015). CHO-cells expressing the FRET sensors were patch-clamped and simultaneously observed under FRET-excitation. After establishment of a tight seal between cell-membrane and patch-pipette ("Gigaseal") the membrane under the pipette-tip was ruptured and the whole-cell configuration was established. This configuration provides

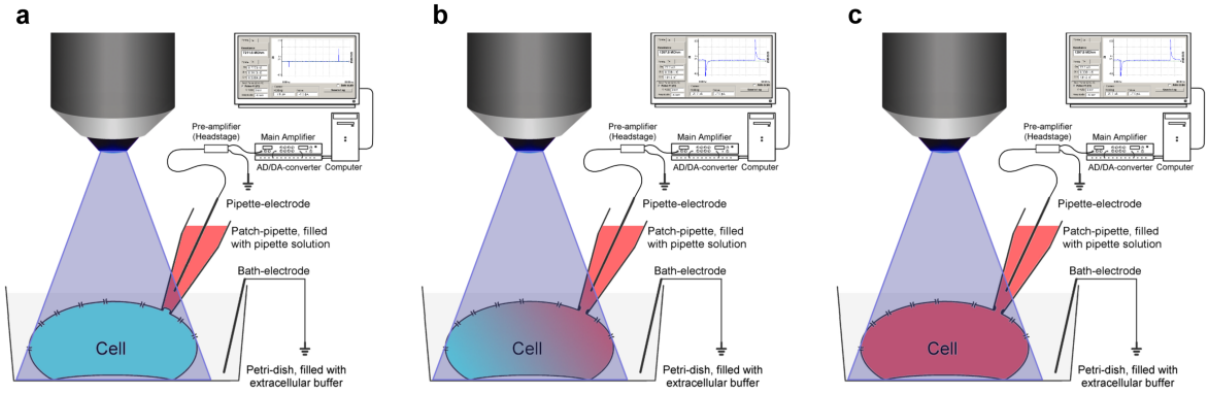
direct access from the pipette to the cytoplasm and cGMP / cAMP can either diffuse from the pipette into the cell or vice versa, depending on the respective cGMP / cAMP-concentration in the patch-pipette solution. FRET-ratio changes were monitored for different cAMP concentrations in the patch pipette and computed into concentration-dependency curves. Seal- and whole-cell resistances were monitored in parallel to ensure a permanently tight seal between pipette and cell-membrane. Seal procedure was performed under DIC illumination. Illumination was switched to fluorescence after a seal was successfully established. Holding potential was 0 mV, with a test-pulse of -10 mV. Pipettes were pulled from borosilicate glass (Hilgenberg) with a Sutter-Puller P-2000 (Sutter Instruments) and had a tip diameter of about 2 µm. Pipette resistance was in the range of 5-10 MΩ. Seal resistances typically were in the range of several Gigaohm, whole-cell resistances for CHO-cells were typically in between 0.5 to 1 Gigaohm. Pipette solutions ("intracellular buffer") contained 20 mM NaCl, 140 mM K-Glutamate, 2 mM $MgCl_2$, 0.00404 mM $CaCl_2$, 0.1 mM BAPTA (yielding a calculated free Ca^{2+}-concentration of 10 nM, low buffered) and 10 mM HEPES. All solutions were adjusted with KOH according to the measured intracellular pH of the cells (here pH 7.55) and supplemented with various cGMP / cAMP-Na-concentrations. The extracellular solution contained 140 mM NaCl, 3 mM KCl 3, 2 mM $MgCl_2$, 2 mM $CaCl_2$, 15 mM Glucose, 10 mM HEPES and was adjusted with NaOH to pH 7.2. Electrophysiological data were acquired with a Cairn Optopatch patch-clamp amplifier (Cairn Research) controlled by WinWCP software (John Dempster, University of Strathclyde).

FRET measurements were performed with a Nikon Eclipse FN-1, equipped with an Opto-LED fluorescent light source (Cairn-Research), a Dual-View beam splitter (Optical Insights) and a CoolSnap HQ^2 camera (Photometrix). All images were acquired with a

40x / 0.8 numerical aperture, long distance water dipping objective (Nikon). Excitation wavelength was 436 ± 25 nm, excitation / emission dichroic was 455 nm long pass. Emission light was split by a 505 nm longpass dichroic and filtered at 480 ± 15 nm for CFP emission and 535 ± 20 nm for YFP emission. Acquisition and analysis was performed using Optofluor (Cairn Research). All FRET measurements were background-subtracted and, if necessary, corrected for baseline drifts. FRET changes were determined at steady state indicated by a plateau of the ratio change.

As especially the YFP fluorophores are prone to quenching effects due to pH or Cl^-, for a correct determination of basal cAMP-values it was crucial to determine the intracellular pH and the influence of different ionic conditions on the FRET signal to correct for artificial shifts. For determination of the intracellular pH, cells expressing the FRET reporter were placed in a "high K^+" extracellular buffer (KCl: 140 mM, NaCl: 4 mM, $MgCl_2$: 2 mM, $CaCl_2$: 2 mM, Glucose: 15 mM, HEPES: 10 mM), adjusted to different pHs (range 6.8 to 8.0) with KOH or HCl. Nigericin (10 µM) and Valinomycin (5 µM) were added to permeabilize the membranes to $H^+$and K^+ and the change in FRET signal was recorded over time. pH-dependency curves were generated and a pH of 7.55 was identified as the pH value that did not affect the FRET signal, indicating that this pH reflects the mean intracellular pH of the CHO cell line. Method adapted from (Thomas et al. 1979). All intracellular buffers were subsequently matched to the pH of the cell clone under study.

Figure 2.3. Microinfusion technique - schematic of 'in cell' FRET sensor calibration



Koschinski, Andreas, and Manuela Zaccolo. "A novel approach combining real-time imaging and the patch-clamp technique to calibrate FRET-based reporters for cAMP in their cellular microenvironment." cAMP Signaling: Methods and Protocols (2015): 25-40.

Figure 2.3.
a) Cell is patched and a tight connection between the pipette and the cell membrane is stablished; b) Intracellular solution present inside the patch-pipette (volume is about 2 million times higher than cell volume) diffuses into the cell due to the cAMP concentration gradient; c) cAMP concentration equilibrates between cytosol and patch-pipette. The light coming from the objective represents the excitation of donor fluorophore. FRET is being recorded throughout the whole experiment.

b) Sensor calibration by saponin permeabilisation:

The saponin permeabilisation protocol was adapted from Yang et al 2014. In brief, the cells were placed into the same intracellular buffer as described above except for that BAPTA was replaced by 0.5 mM EGTA. The Ca^{2+}-concentration was 0.16 µM, yielding a nominal free Ca^{2+}-concentration of 10 nM, as calculated with MaxChelator (http://maxchelator.stanford.edu/). Imaging experiments were performed as described for the microinfusion experiments. After reaching a stable basal ratio, typically after about 3-5 minutes, saponin (from quillaja bark, Sigma, S4251, 8 µg/ml) and cGMP or cAMP (various concentrations) were applied and were permanently present. The resulting FRET change after saponin-induced membrane permeabilization was recorded, analyzed and computed into concentration-dependency curves as described for the microinfusion experiments (See Figure 2.4 for schematic).

All microinfusion, permeabilization and pH- experiments were carried out at 24-28°C. All mathematical corrections and analyses were performed with Excel™, Open Office and GraphPad Prism™. Best fit curves were generated using the built in fit function for sigmoidal dose response curves (variable slope, no constraints) of Graph Pad Prism™. All values are means ± SEM unless stated otherwise. Graphical editing / layout of figures and Western blot scans were performed with Micrografx Picture Publisher 8 and 10 (Micrografx Inc.). Where necessary, image processing was carried out according to the digital image integrity rules and standards.

Figure 2.4. Saponin calibration schematic

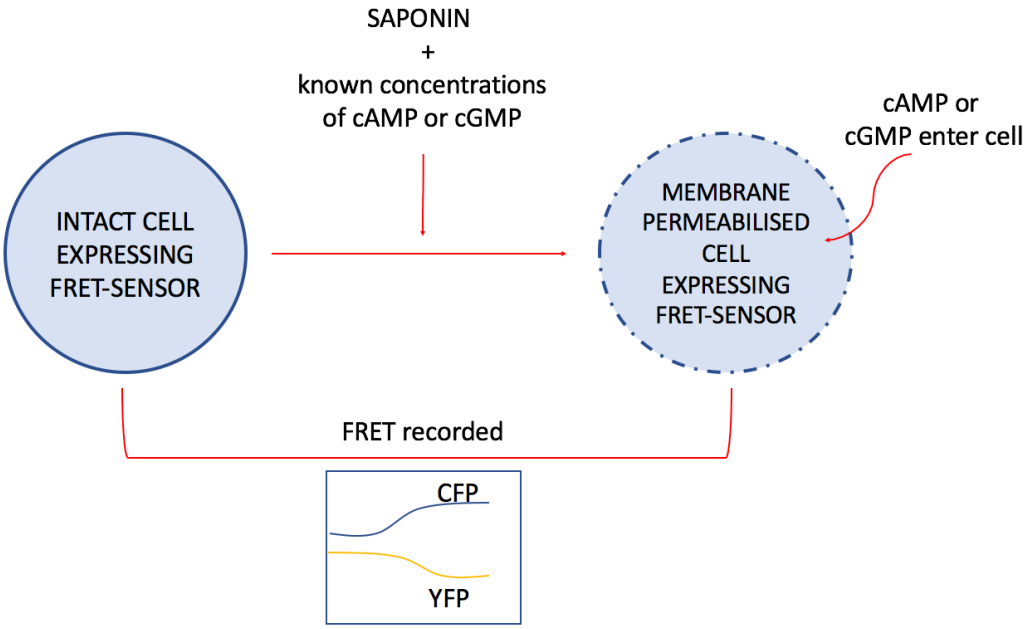


Figure 2.4
Schematic of Saponin calibration approach where cells expressing the FRET-sensor to be calibrated are permeabilised by Saponin. As cell membrane is permeabilised, known concentrations of cAMP or cGMP enter the cell. CFP and YFP intensities of the sensor are recorded during the whole duration of the experiment.

2.3. BIOCHEMISTRY

2.3.1. Western blotting

Isolated cardiomyocytes and LV tissues were lysed using ice-cold RIPA buffer or customised lysis buffer KHEM for dystrophin blot only (75 mM Tris-HCL-pH 6.8 + 10% SDS + 5% BME) supplemented with Complete EDTA-free protease inhibitor cocktail tablets on ice and gently agitated for 20 min. Protein concentrations were determined by Bradford assay. Samples equivalent to 40 µg proteins were separated on Bolt 4–12% Bis-Tris Plus Gels and blotted for nNOS, iNOS and eNOS. 3-8% Tris acetate gel from Invitrogen was used for the dystrophin western blot. After blocking with 5% milk for 1 h at room temperature membranes were incubated overnight at 4 °C with primary antibody for nNOS, eNOS and nNOS (table available in Appendix I). The blots were washed and incubated with appropriate horseradish peroxidase-conjugated secondary antibodies for 2 h at room temperature. Immunoreactive bands were visualized by ECL western blotting detection kit. Antibody dilutions and exposure times were adjusted to ensure that for each antibody the signal detected was within the linear range. Quantification of the band intensity was accomplished by densitometry using ImageJ software (http://rsbweb.nih.gov/ij/index.html). Densities measured are expressed as normalised to endogenous control.

2.3.2. Cell fractionation and western blotting

Cell fractionation was performed by following protocol described in Wieckowski (2009) with few modifications. Frozen LV tissues and frozen isolated cardiomyocyte pellet were lysed in Tris-HCL starting buffer (IB) constituted of 225-mM mannitol, 75-mM sucrose and 30-mM Tris–HCl (pH 7.4) by using homogeniser. Homogenate was transferred to a 15mL falcon tube and centrifuged at 740g for 5 min at 4^{o}C. Before centrifugation, 100µl of this homogenate was collected for whole cell lysate. Supernatant was collected and

centrifuged again at 740g at 4°C for further removal of unbroken cells. The supernatant was then centrifuged at 9000g for 10min at 4°C. The supernatant was further centrifuged at 20000g for 30min at 4°C. The pellet, containing the plasma membrane fraction was resuspended in 100µl of IB buffer. Further centrifugation of supernatant 100000g for 1h resulted in isolation of ER (pellet) which was resuspended in 50µl of IB buffer. The lysates were then quantified using Bradford assay and samples equivalent to 40 µg proteins were used for western blotting following the protocol described above. The final samples were not 100% pure and contained small contamination of other sub-fractions. This fact added difficulties in achieving high quality blots.

2.3.3. cAMP and cGMP ELISA

cAMP and cGMP total levels were measured by using the direct cAMP ELISA kit (Enzo Life Sciences) according the manufactures instructions. Samples equivalent to 8µg/µl of cell lysate derived from neonatal cardiomyocytes, adult cardiomyocytes and LV tissue from neonatal and adult hearts (the same lysate used for western blotting) were assayed in duplicate. The overnight-acetylated format was applied for cGMP detection.

2.3.4. sGC activity assay

sGC activity assay was adapted from Stasch et al 2006. Adult cardiomyocytes were lysed using ice-cold RIPA buffer supplemented with Complete EDTA-free protease inhibitor cocktail tablets. Protein concentration was quantified by using Bradford assay. Samples equivalent to 0.8µg/µl of cell lysate were incubated for 5 minutes in a reaction mixture containing 50mmol/L TRIS HCL 7.5, 4mmol/L $MgCl_2$, 100µM IBMX, 7.5mmol/L creatine phosphate, 0.2mmol/L creatine phosphokinase, 1mmol/L L-NAME and 1mmol/L GTP. Samples were then separated into different tubes and treated with NO

donor 50μM, NO donor 50μM + 5 μM Bay 41 22-72, NO donor 50μM + Cinaciguat, Bay 41 by itself and Cinaciguat by itself. cGMP was then measured by using direct cGMP ELISA kit (Enzo Life Sciences) non-acetylated format.

2.3.5. qPCR

RNA was extracted from isolated cardiomyocytes using TRIzol reagent (TRI Reagent T3934 Sigma) and from LV tissues by using RNeasy Fibrous Tissue Mini Kit from Qiagen. RNA was quantified using Nanodrop. Reverse transcription of total RNA was performed by using High-Capacity cDNA Reverse Transcription Kit from Applied Biosystems from 1μM RNA. 1/5 dilution of cDNA (reaching 25ng) was used in each qPCR reaction. Samples were plated in triplicate and qPCR reaction was performed by using Taqman probes for PDE2A (Mm01136644_m1), PDE3A (Mm00479581_m1), PDE3B (Mm00691635_m1), PDE4A (Mm01147149_m1), PDE4B (Mm00480174_m1), PDE4D (Mm00456879_m1), PDE5A (Mm00463177_m1), PDE9 (Mm00501039_m1), AC5 (Mm00674122_m1) and AC6 (Mm00475772_m1). Analysis were done manually as shown in Figure 2.5.

Figure 2.5. qPCR analysis

					technical	Biological			
Well	Sample Name	Target Name	CT	ΔCT	ΔCT Mean of triplicate	ΔCT Mean controls	ΔΔCT	fold change	Mean fold change
A1	Neo WT1	PDE4A	28.7750702	8.92567635	8.79593277	8.989922629	-0.1939899	1.14392293	1.0071378
A1	Neo WT1	GapDH	19.8493938						
A2	Neo WT1	PDE4A	28.3778381	8.74548531					
A2	Neo WT1	GapDH	19.6323528						
A3	Neo WT1	PDE4A	28.5779915	8.71663666					
A3	Neo WT1	GapDH	19.8613548						
B1	Neo WT2	PDE4A	27.2486172	9.06328201	8.957460403		-0.0324622	1.02275616	
B1	Neo WT2	GapDH	18.1853352						
B2	Neo WT2	PDE4A	26.6370716	8.87719917					
B2	Neo WT2	GapDH	17.7598724						
B3	Neo WT2	PDE4A	26.9106312	8.93190002					
B3	Neo WT2	GapDH	17.9787312						
C1	Neo WT3	PDE4A	28.4121075	9.4315815	9.216374715		0.22645209	0.85473429	
C1	Neo WT3	GapDH	18.980526						
C2	Neo WT3	PDE4A	27.8602848	9.31692505					
C2	Neo WT3	GapDH	18.5433598						
C3	Neo WT3	PDE4A	26.0871544	8.9006176					
C3	Neo WT3	GapDH	17.1865368						

					technical	Biological				
Well	Sample Nam	Target Name	CT	ΔCT	ΔCT Mean of triplicates	ΔCT Mean controls	ΔΔCT	fold change	Mean fold change	Mean fold change MDX/Mean fold change WT
D1	Neo mdx1	PDE4A	27.4694214	8.9459362	8.833411535	8.755484263	-0.1565111	1.11458844	1.178248161	1.16989767
D1	Neo mdx1	GapDH	18.5234852							
D2	Neo mdx1	PDE4A	27.6397114	8.93503571						
D2	Neo mdx1	GapDH	18.7046757							
D3	Neo mdx1	PDE4A	25.9417305	8.6192627						
D3	Neo mdx1	GapDH	17.3224678							
E1	Neo mdx2	PDE4A	28.4814129	8.90851021	8.646509806		-0.3434128	1.2687544		
E1	Neo mdx2	GapDH	19.5729027							
E2	Neo mdx2	PDE4A	26.005991	8.35872841						
E2	Neo mdx2	GapDH	17.6472626							
E3	Neo mdx2	PDE4A	26.9459667	8.6722908						
E3	Neo mdx2	GapDH	18.2736759							
F1	Neo mdx3	PDE4A	27.8762493	8.93346214	8.786531448		-0.2033912	1.15140165		
F1	Neo mdx3	GapDH	18.9427872							
F2	Neo mdx3	PDE4A	26.9466019	8.80395699						
F2	Neo mdx3	GapDH	18.1426449							
F3	Neo mdx3	PDE4A	26.2212391	8.62217522						
F3	Neo mdx3	GapDH	17.5990639							

Figure 2.5
Representative Excel sheet of qPCR analysis where the ΔΔCT is the difference between the ΔCT of the technical replicates and the biological replicates. The fold change is calculated as POWER(2,- ΔΔCT). The mean fold change was then normalised by the mean fold change of the WT. Therefore, WT equals 1 and the mdx value is relative to WT. Top panel illustrates WT raw values and calculations and bottom panel the mdx.

2.4. CONSTRUCTION OF TARGETED FRET-BASED SENSORS

A DNA fragment encompassing the short peptide corresponding to the N-terminal targeting signal from Lyn Kinase, a posttranslationally myristoylated and palmitoylated sequence, which targets the protein to the plasma membrane and peptides of yeast translocase outer mitochondria membrane (OMM) protein TOM 70 (yTOM70) were extracted from existing constructs by using specific restriction enzymes. PCR-amplified and inserted the fragment in between the specific restriction sites upstream the first fluorophore of the sensor at the N-terminus of the cytosolic version of the sensor to be targeted. The constructs were generated in DUAL + vector and adenovirus was generated

by Vector Biolabs. Figure 2.6 displays the amino acid sequence of the targeting sequences in frame after insertion.

Figure 2.6. Targeted FRET-based sensor - Cloning strategy

Plasma membrane cAMP

AAGCTTGCTAGCATGGGCTGCATCAAGAGCAAGCGCAAGGAC
AACCTGAACGACGACGGCGTGGACATGAAGACCGCTAGCAA
GCTTGCCGCCACCATGGCGGCCGCAATGGTGAGCAAGGGCGAGG
AGCTGTTCACCGGGGTGGTGCCCATCCTGGTCGAGCTGGACGGCGA
CGTAAACGGCCACAAGTTCAGCGTGTCCGGCGAGGGCGAGGGCGA
TGCCACCTACGGCAAGCTGACCCTGAAGTTCATCTGCACCACCGGCA
AGCTGCCCGTGCCCTGGCCCACCCTCGTGACCACCCTGTCCTGGGG
CGTGCAGTGCTTCGCCCGCTACCCCGACCACATGAAGCAGCACGAC
TTCTTCAAGTCCGCCATGCCCGAAGGCTACGTCCAGGAGCGCACCAT
CTTCTTCAAGGACGACGGCAACTACAAGACCCGCGCCGAGGTGAA
GTTCGAGGGCGACACCCTGGTGAACCGCATCGAGCTGAAGGGCAT
CGACTTCAAGGAGGACGGCAACATCCTGGGGCACAAGCTGGAGTA
CAACTACTTTAGCGACAACGTCTATATCACCGCCGACAAGCAGAAGA
ACGGCATCAAGGCCAACTTCAAGATCCGCCACAACATCGAGGACGG
CGGCGTGCAGCTCGCCGACCACTACCAGCAGAACACCCCCATCGGC
GACGGCCCCGTGCTGCTGCCCGACAACCACTACCTGAGCACCCAGT
CCAAGCTGAGCAAAGACCCCAACGAGAAGCGCGATCACATGGTCCT
GCTGGAGTTCGTGACCGCCGCCcGATATCgcccgtgggaactcatgagatgg
aggaggagttggccgaagctgtggccctgctctcccagcgggggcctgacgccctgctc
actgtggcacttcgaaagccccaggtcagcgcacggatgaagagctggacctcatcttt
gaggagctgctgcacatcaaggctgtggcccacctctccaactcggtgaagcgagaatta
gcgg

Plasma membrane cGMP

AGGCCGCTAGCATGGGCTGCATCAAGAGCAAGCGCAAGGACA
ACCTGAACGACGACGGCGTGGACATGAAGACCGCTAGCCCTA
GGGAGCTCTCTGGCTAACTAGAGAACCCACTGCTTACTGGCTTATCG
AAATTAATACGACTCACTATAGGGAGACCCAAGCTGCCACCATGGTG
AGCAAGGGCGAGGAGCTGTTCACCGGGGTGGTGCCCATCCTGGTC
GAGCTGGACGGCGACGTAAACGGCCACAAGTTCAGCGTGTCCGGC
GAGGGCGAGGGCGATGCCACCTACGGCAAGCTGACCCTGAAGTTC
ATCTGCACCACCGGCAAGCTGCCCGTGCCCTGGCCCACCCTCGTGAC
CACCCTGACCTGGGGCGTGCAGTGCTTCAGCCGCTACCCCGACCAC
ATGAAGCAGCACGACTTCTTCAAGTCCGCCATGCCCGAAGGCTACG
TCCAGGAGCGCACCATCTTCTTCAAGGACGACGGCAACTACAAGAC
CCGCGCCGAGGTGAAGTTCGAGGGCGACACCCTGGTGAACCGCAT
CGAGCTGAAGGGCATCGACTTCAAGGAGGACGGCAACATCCTGGG
GCACAAGCTGGAGTACAACTACATCAGCCACAACGTCTATATCACCG
CCGACAAGCAGAAGAACGGCATCAAGGCCAACTTCAAGATCCGCCA
CAACATCGAGGACGGCAGCGTGCAGCTCGCCGACCACTACCAGCAG
AACACCCCCATCGGCGACGGCCCCGTGCTGCTGCCCGACAACCACT
ACCTGAGCACCCAGTCCGCCCTGAGCAAAGACCCCAACGAGAAGC
GCGATCACATGGTCCTGCTGGAGTTCGTGACCGCCGCCCAGGCATTC
CGGAAGTTCACCAAATCCGAAAGGTCCAAGGATCTCATAAAGGAGG
CCATCCTTGACAATGACTTTATGAAGAACTTGGAGCTGTCACAGATC
CAAGAGATTGTGGATTGTATGTACCCAGTGGAGTACGGCAAAGACA
GCTGCATCATC

Outer Mitochondria membrane cGMP

CCGGATCCGAATTCACCATGAAGAGCTTCATTACAAGGAACAAGACAGCCATTTTGGCAACCG
TTGCTGCTACAGGTACTGCCATCGGTGCCTACTATTATTACAACGAATTCGATCTCTGGCTAA
CTAGAGAACCCACTGCTTACTGGCTTATCGAAATTAATACGACTCACT
ATAGGGAGACCCAAGCTGCCACCATGGTGAGCAAGGGCGAGGAGC
TGTTCACCGGGGTGGTGCCCATCCTGGTCGAGCTGGACGGCGACGT
AAACGGCCACAAGTTCAGCGTGTCCGGCGAGGGCGAGGGCGATGC
CACCTACGGCAAGCTGACCCTGAAGTTCATCTGCACCACCGGCAAG
CTGCCCGTGCCCTGGCCCACCCTCGTGACCACCCTGACCTGGGGCG
TGCAGTGCTTCAGCCGCTACCCCGACCACATGAAGCAGCACGACTTC
TTCAAGTCCGCCATGCCCGAAGGCTACGTCCAGGAGCGCACCATCTT
CTTCAAGGACGACGGCAACTACAAGACCCGCGCCGAGGTGAAGTT
CGAGGGCGACACCCTGGTGAACCGCATCGAGCTGAAGGGCATCGA
CTTCAAGGAGGACGGCAACATCCTGGGGCACAAGCTGGAGTACAA
CTACATCAGCCACAACGTCTATATCACCGCCGACAAGCAGAAGAACG
GCATCAAGGCCAACTTCAAGATCCGCCACAACATCGAGGACGGCAG
CGTGCAGCTCGCCGACCACTACCAGCAGAACACCCCCATCGGCGAC
GGCCCCGTGCTGCTGCCCGACAACCACTACCTGAGCACCCAGTCCG
CCCTGAGCAAAGACCCCAACGAGAAGCGCGATCACATGGTCCTGCT
GGAGTTCGTGACCGCCGCCCAGGCATTCCGGAAGTTCACCAAATCC
GAAAGGTCCAAGGATCTCATAAAGGAGGCCATCCTTGACAATGACTT
TATGAAGAACTTGGAGCTGTCACAGATCCAAGAGATTGTGGATTGTA
TGTACCCAGTGGAGTACGGCAAAGACAGCTGCATCATCAAAGAAGG
AGATGTGGGGTCACTGGTGTATGTCATGGAAGATGGTAAGGTTGAA
GTTACAAAAGAAGG

Figure 2.6
Fragment of aa sequence of targeted FRET-based sensors where sequence in blue and orange represent the restriction sites, the sequence in red correspond to the targeting sequence, the sequence in green represents the first fluorophore of the specific FRET-based probe and sequence in black represent linker and/or initial sequence of the cyclic nucleotide binding domain.

2.5. SARCOMERE SHORTENING AND FORCE MEASUREMENTS

a) Sarcomere shortening

AMVMs with resting sarcomere lengths between 1.50 and 1.80 μm were examined for shortening dynamics. Experiments were performed using an inverted microscope (Olympus IX71) with a PlanApoN, 40X, NA 1.30 oil immersion objective. Myocytes were imaged by using the transillumination light path equipped with an additional red filter and recorded by a MyoCam-S CCD video camera (IonOptix Milton, MA). Cells were electrically stimulated at 5 Hz with 2ms pulse duration in the presence of 1.4 mM Ca^{2+} at 37 °C ± 1 °C. Sarcomere shortening was measured using the video-based sarcomere detection system by IonOptix Myocyte Contractility Recording System, (IonOptix Milton, MA). The Sarcomere acquisition module collected real-time sarcomere length at 250Hz. The amplitude and velocity of shortening/relengthening were analysed using the IonWizard software (IonWizard's analysis function to monotonic transients). Parameters from 10 contractions were averaged to minimizes beat-to-beat variation and obtain mean values at baseline (control), and in response to stimulus (Figure 2.7).

Analysis steps: (1) Select area to be analysed (10 single contractility transients), (2) select average events, (3) Add an event mark to the averaged transient curve starting before the pacing mark and finishing after complete recovery, (4) press monotonic transient analysis (M), (5) export averaged transient curve and monotonic analysis parameters (the parameters compared in this thesis are available at Table 2.1) to an Excel sheet.

Table 2.1. Monotonic Analysis Parameters used for analysis

Parameter	Details
bl.	The baseline (bl) is the y-axis value at t0. For example, bl for sarcomere length. detection will be the relaxed sarcomere length

dep v.	The departure velocity (dep v) is a value that characterizes the speed with which the cell contracts. It is the maximal rate of change during the contraction.
peak.	The peak is the maximal displacement from baseline.
peak h.	The peak height (peak h) is the difference between the peak and baseline values.
bl%peak h.	The baseline as a percentage of peak height is the percent change during the transient.
ret v.	The return velocity (ret v) is the maximal rate of the return phase of the transient. It's the same as "dep v" except that it describes the recovery phase of the transient. The speed of cardiomyocyte relaxation/re-lengthening.
t to bl xx%.	The time to xx percentage of the baseline is a characterization of cellular relaxation
sin exp tau.	The single exponential tau (sin exp tau) is the exponential decay time constant of the function. This is commonly used as a means of characterizing the speed of recovery (relaxation or calcium reuptake). Tau's units are in time (seconds) and a greater tau value equates to a longer recovery or return to baseline.

Information extracted from IonOptix.com (IonOptix 2017)

Figure 2.7. Unloaded Cardiomyocyte Contractility

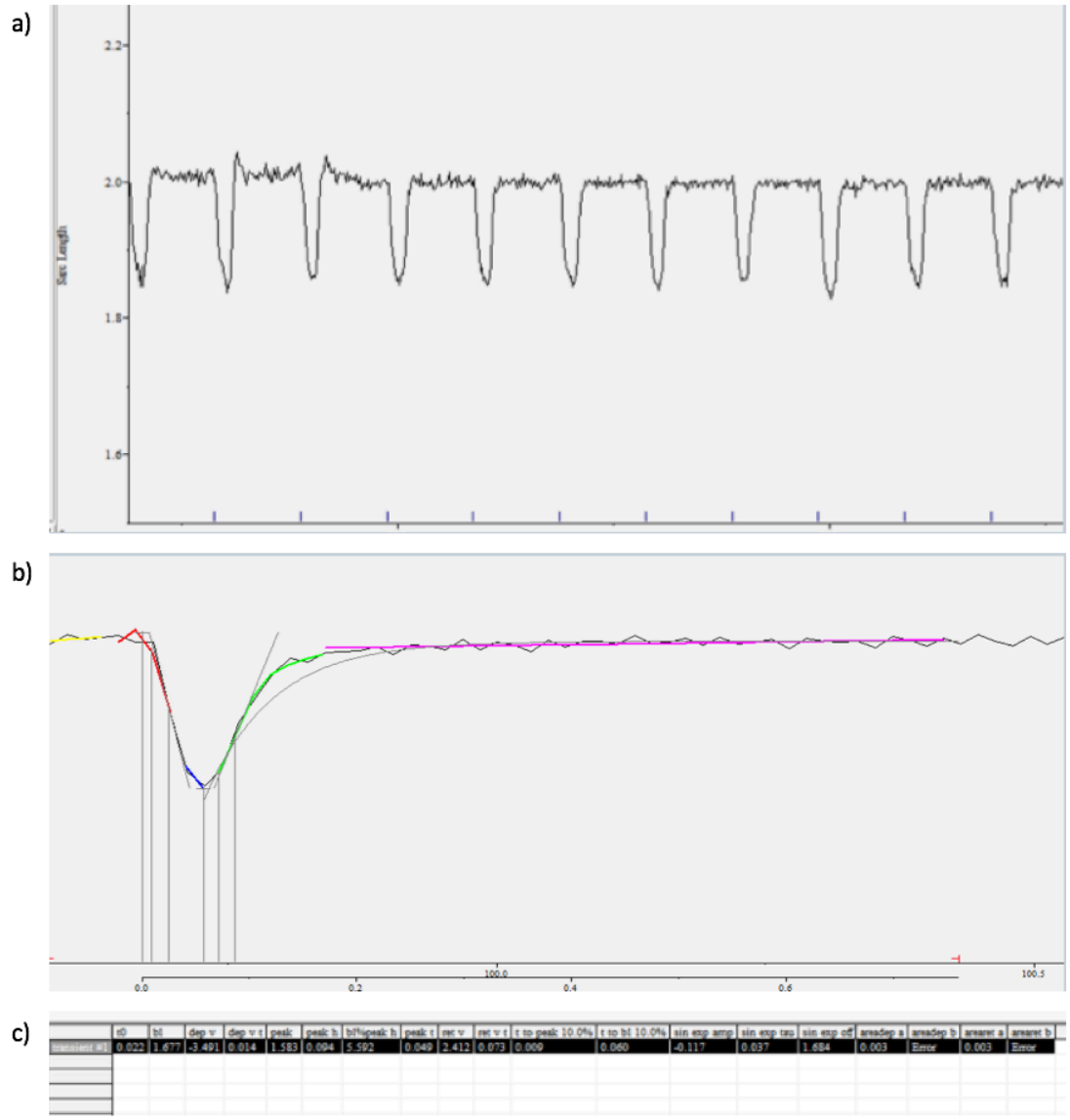


Figure 2.7
Print Screen of the monotonic transient analysis of the unloaded isolated cardiomyocytes contractility. a) Single contractility curves from selected experiment to be averaged for analysis. Graph (b) is the averaged transient curve; c) The Monotonic Transient Analysis parameters analysed.

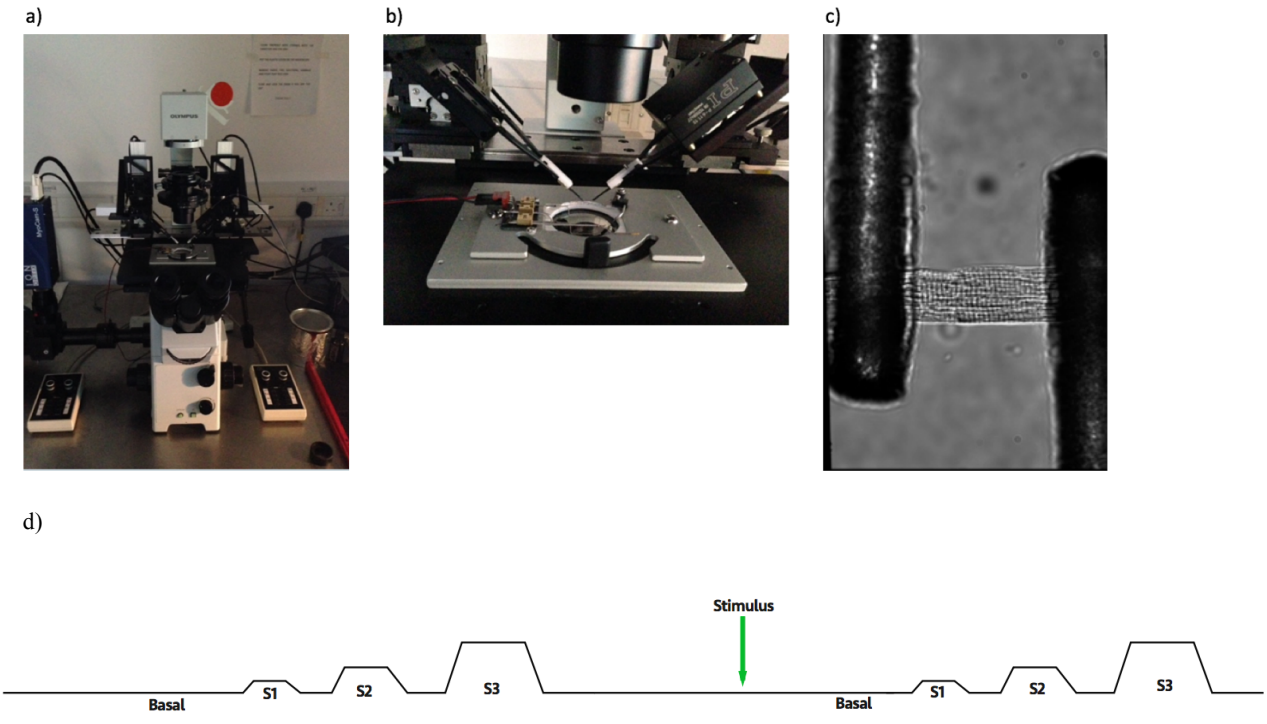
b) Force measurement

Freshly isolated AMVM force of contraction was recorded by the OptiForce software from IonOptix under the same experimental conditions described above (sarcomere shortening). The OptiForce works by using laser light to interrogate a reflective cantilever arm attached to one edge of the cardiomyocyte. Contractile forces bend the cantilever and

produce changes in the light path length. Light reflected from the cantilever combines with light reflected from the tip of the optical fibre. When the combined light waves are in-phase, the intensity of light returning to the recorder increases; out-of-phase, the intensity diminishes, creating an exquisitely sensitive transducer. On the other edge of the cell, a stiff glass fibre is attached. The stiffness of the force transducer used was 2.1N/V. The glass rod and the force transducer fibre was coated with MyoTak glue. After introduced into the solution, the force transducer was automatic calibrated by the OptiForce software. After attachment, the cell was lifted from the coverslip and force of contraction started to be recorded. After 5 minutes (basal/ un-stretched), the force was recorded at different sarcomere length by applying stretch to the cells. The stretches were driven by a programmable piezo motor (MyoStretcher from IonOptix) connected to the glass rod. A series of three increasing stretching steps were applied to the cell, each step had the same speed and the cell was shank back to the original length between each step. The steps were programmed as following: (1) Δ+0.5v, - 0.5v in 0.2 seconds, (2) Δ+0.5v +0.5v, -0.5v -0.5v in 0.2 + 0.2 seconds and (3) Δ+0.5v +0.5v+0.5v, -0.5v -0.5v-0.5v in 0.2 +0.2+0.2 seconds (Figure 2.8). The cell was hold at each stretch step for 5 seconds (delay) before being put back at start sarcomere length. These series of stretches had previously been programmed and saved into the software as Eppoch 1, therefore, the same programme was applied to all the cell. After the cell reached maximum stretch and was set back to the original length, a stimulus was added to the cell (Isoproterenol or IBMX), and the same series of stretches were repeated. To reduce data variability, the raw force generated was normalised by the cross-sectional area of each cell. The cross-sectional area of the cardiomyocyte was calculated by using the mathematical formula of an elliptic. Analysis were done similarly as for the sarcomere length where parameters from 10 contractions were averaged to minimizes beat-to-beat variation and obtain mean

values at baseline (control), and in response to stimulus to each stretching point (Figure 2.8). It is important to note that this technique is extremely challenging. The fragility of the probes, force transducer and cells add great limitations to system. Additionally, the analysis of the generated forces is not simple. As each cell has a different length, thickness and depth, it is necessary to normalise the forces and stretches to each cell. In this thesis, this normalisation was done by measuring the cross-sectional area of each cell. Although this is a method used by several labs, it does not take in account the length of the cell. It was also important to compare the effect of each stretching step in the sarcomere length as the mdx cells are known to have different stiffness when compared to control cells. Another limitation of this system is the inability to measure reliable diastolic forces.

Figure 2.8. Analysis of sarcomere shortening and force of contraction



e)

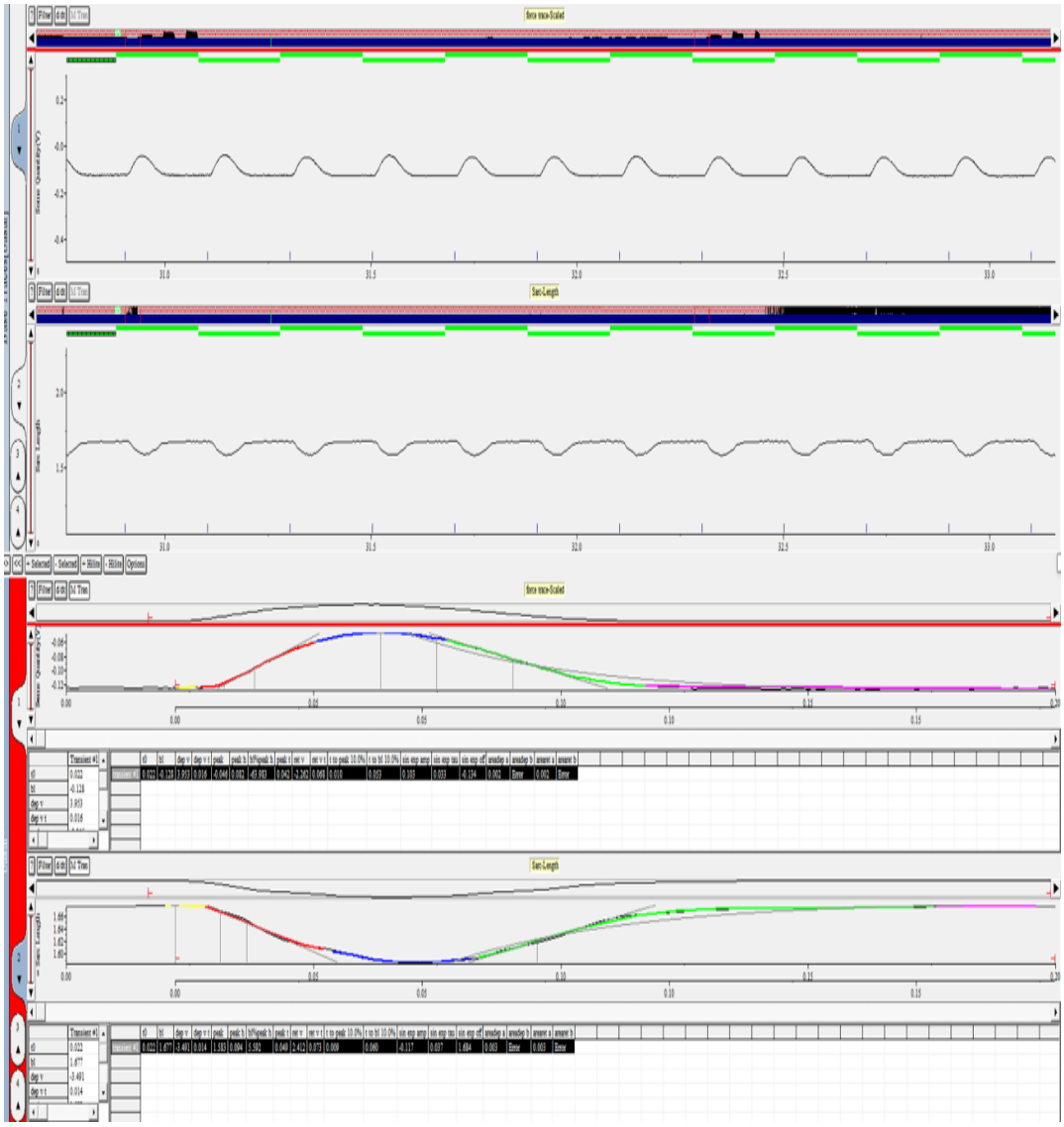


Figure 2.8
a) Image of microscope and Myo Stretching equipment; b) Image of chamber and bath where the cells and Myo Pacing electrodes were inserted. Above the chamber is located both rods, one being the force transducer and the other the stiff glass fibre. The Piezo motor is located on the right-side arm (small black squared box); c) Magnified image of both rods attached to the edges of a single isolated cardiomyocyte. It is possible to visualise the MyoTak glue coating in both rods; d) Eppoch stretching protocol where s1, s2 and s3 mean stretching step 1,2 and 3 e) Print screen of the IonOptix analysis software where force and sarcomere shortening single transients (top panel) were averaged (lower panel) for analysis. The transients forming peaks are related to the force measurements whereas the ones forming deeps to the sarcomere length measurements.

2.6. STATISTICS

Sample size:

According to previous studies in our laboratory and power calculations taking in consideration the variability of the data, effect size (20% or more FRET change difference) and significance level (0.05), it was stablished n>20 as the number of cells to be analysed for each condition and n>3 for biological replicates.

Data normality:

The normality of the data was analysed by applying the D'Agostino-Pearson normality test using the GraphPad Prism 7 software. This test computes the skewness and kurtosis in order to quantify how far the distribution is from the Gaussian asymmetry and shape (Figure 2.9).

Statistical tests:

The statistical tests were applied as the following:

1) Two-away ANOVA with multiple comparisons, where the animal was set as strain a factor and the interventions as repeated measurements, was applied to compare all the FRET experiments described on Chapter 5 (assuming that the data follows a Gaussian distribution after applying the analysis described above).
2) Student T-tests were applied when comparing 2 sets of responses only, for example when comparing each contractility parameter between both strains individually (Chapter .2 and 6) (assuming that the data follows a Gaussian distribution after applying the analysis described above).
3) For experimental data performed with 3 replicates only and where it was not possible to assume normal distribution, the Mann-Whitney U test was applied (Western blotting on Chapter 5).

Data are presented as means ± standard error of the mean. Graph Pad Prism 5 software was used for all statistical analyses. The significance level was set at $p<0.05$ and the following annotation has been used: * = $0.05<p<0.01$, ** = $0.01<p<0.001$, ***= $0.001<p<0.0001$, **** = $p<0.0001$. Sample sizes, biological and technical replicate numbers, are stated in each figure.

2.7. REFERENCES

IonOptix, IonOptix. 2017. “Monotonic Transient Analysis Parameters.” August 22. http://www.ionoptix.com/wp-content/uploads/2014/07/Monotonic-Transient-Analysis-Defined.pdf.

Koschinski, Andreas, and Manuela Zaccolo. "A novel approach combining real-time imaging and the patch-clamp technique to calibrate FRET-based reporters for cAMP in their cellular microenvironment." *cAMP Signaling: Methods and Protocols* (2015): 25-40.

Stasch, Johannes-Peter, Peter M. Schmidt, Pavel I. Nedvetsky, Tatiana Y. Nedvetskaya, Arun Kumar Hs, Sabine Meurer, Martin Deile et al. "Targeting the heme-oxidized nitric oxide receptor for selective vasodilatation of diseased blood vessels." *Journal of Clinical Investigation* 116, no. 9 (2006): 2552.

Thomas, J.A., Buchsbaum, R.N., Zimniak, A. and Racker, E., 1979. Intracellular pH measurements in Ehrlich ascites tumor cells utilizing spectroscopic probes generated in situ. *Biochemistry*, *18*(11), pp.2210-2218.

Wieckowski, Mariusz R., Carlotta Giorgi, Magdalena Lebiedzinska, Jerzy Duszynski, and Paolo Pinton. "Isolation of mitochondria-associated membranes and mitochondria from animal tissues and cells." *Nature protocols* 4, no. 11 (2009): 1582-1590.

Yang, Yi, Tao Guo, Tetsuro Oda, Asima Chakraborty, Le Chen, Hitoshi Uchinoumi, Anne A. Knowlton et al. "Cardiac Myocyte Z-Line Calmodulin Is Mainly RyR2-Bound, and Reduction Is Arrhythmogenic and Occurs in Heart FailureNovelty and Significance." *Circulation research* 114, no. 2 (2014): 295-306.

Chapter 3: Optimisation of adult mice cardiomyocytes isolation and infection

Parts of this chapter have been published in: Lomas, Oliver, Marcella Brescia, Ricardo Carnicer, Stefania Monterisi, Nicoletta C. Surdo, and Manuela Zaccolo. "Adenoviral transduction of FRET-based biosensors for cAMP in primary adult mouse cardiomyocytes." cAMP Signaling: Methods and Protocols (2015): 103-115.).

3.1. INTRODUCTION

The development of an effective protocol to isolate and express FRET-biosensors in adult murine primary cells gained great importance with the emergence of transgenic mouse models (Lomas et al. 2015; Zhou et al. 2000). In the specific context of this thesis, this development became a priority due to the necessity to perform experiments on isolated ventricular cardiomyocytes from the mutant Dmd^{mdx}, a model for DMD, and WT cells expressing FRET-based biosensors.

Freshly isolated adult mouse myocytes are able to maintain their functional properties for up to 8 hours after isolation without being cultured (Zhou et al. 2000). Non-cultured cells are suitable for Ca^{2+} measurements, cell contractility, western blotting and other acute experiments (Shan, Marchase, and Chatham 2008; Takeishi et al. 1998; Nakayama et al. 2006). However, for the purpose of this project, adult myocytes are required to be viable for at least 24 hours in culture in order to express the transgene – transduced FRET-biosensors.

Transgenic mice expressing FRET-based biosensors have been successfully generated (Nikolaev et al. 2006). However, although efficient, this approach requires extra time for

the development of the transgenic animal, which adds significant limitation to the use of a high number of different and novel sensor constructs generated for this project. Adult murine cardiomyocytes are not only difficult to subject to gene transduction, whether using plasmid or adenoviral vectors. They also present a significant challenge to maintain in culture features of freshly isolated cells long enough to allow expression of the desired fluorescent protein. It has been estimated that the rate of loss of contractile function in rodent cardiomyocytes is species-dependent, with up to 50% of mouse cardiomyocytes losing the ability to contract after 24 hours in culture, whereas >75% of rat cardiomyocytes can contract after 48 hours of culture (Pavlović, McLatchie, and Shattock 2010). Additionally, the cardiomyocytes present with autofluorescence originated from mitochondrial NADH, FAD and other compounds (Eng, Lynch, and Balaban 1989), which can pose a problem with FRET biosensors as the excitation spectrum of these compounds significantly overlaps with that of YFP-Venus (a common fluorophore used in FRET biosensors).

Other studies have also recognized the difficulty to stablish a successful method to isolate and culture high-quality cardiomyocytes, as well as its importance in achieving reproducibility and relevance of experimental results (Powell and Twist 1976; Pinz et al. 2011; Jian et al. 2016) . Several methods have been published (Powell and Twist 1976; Pinz et al. 2011; Wolska and Solaro 1996), however in our hands it was not possible to generate high yields and high quality cardiomyocytes expressing FRET-based sensors by simply following these protocols. For this reason, improvements (described in this chapter) were made to obtain a method for effective transduction of genetically encoded FRET biosensors by adenoviral vectors of sufficient quality to allow the investigation of cAMP/cGMP signalling in viable adult murine cardiomyocytes after 24 hours of culture.

3.2. INITIAL PROTOCOL

The initial isolation, culture, and infection protocols available in the laboratory and routinely used for the isolation of rat cardiac myocytes, yielded a cell viability of ~80% when applied to mouse hearts; yet were found unsatisfactory for three reasons. First, merely 10% of the cells were viable after culture and ~50% of them showed the desired well-defined non-rounded extremities. Second, only ~20% of cells contracted on application of 1Hz field stimulation. Lastly, the infection efficiency was only about 10%. In addition, the infected cells showed a weak fluorescence, only about 3-4 folds higher than cell autofluorescence. The inefficient infection complicated the discrimination and identification of infected from autofluorescent cells. In an attempt to improve this, measurements of CFP and YPF intensities of non-infected cardiomyocytes were recorder under different treatments in order to assess the interference of solutions/media in the autofluorescence levels. Conditions tested included two different culture media: Medium 199, as suggested in the original protocol available in the lab (SchlUter and Schreiber 1997), and MEM (Minimum Essential Medium) as an alternative medium. The first rationale for the use of MEM-based culture medium is based upon observations reported in a study in which the expression of the Coxsackie adenovirus receptor (CAR), responsible for allowing entry of the adenovirus into the cardiomyocyte, was found to be enhanced compared to other media such as the M-199 (Li et al. 2003). The second reason to select the MEM-based culture medium is based on evidence available in another study where a sequence of MEM + 2.5% FBS for 1 hour, followed by MEM without FBS was successfully employed to culture cardiomyocytes and avoid the growth of other cell types, such as fibroblasts (Zhou et al. 2000). Furthermore, alternative storage solutions with low (0.2 mM) and high (1 mM) Ca^{2+} concentration were also tested. The impact of using a BSA rinsing step, as suggested in the original protocol, was also assessed. None of the

above conditions reduced the autofluorescent signal significantly. Although the signal of potentially infected cells resulted to be significantly higher than the autofluorescence signal (Figure 3.1), the ratio of signal to noise was not optimal.

Figure 3.1. Cardiomyocytes autofluorescence under different conditions

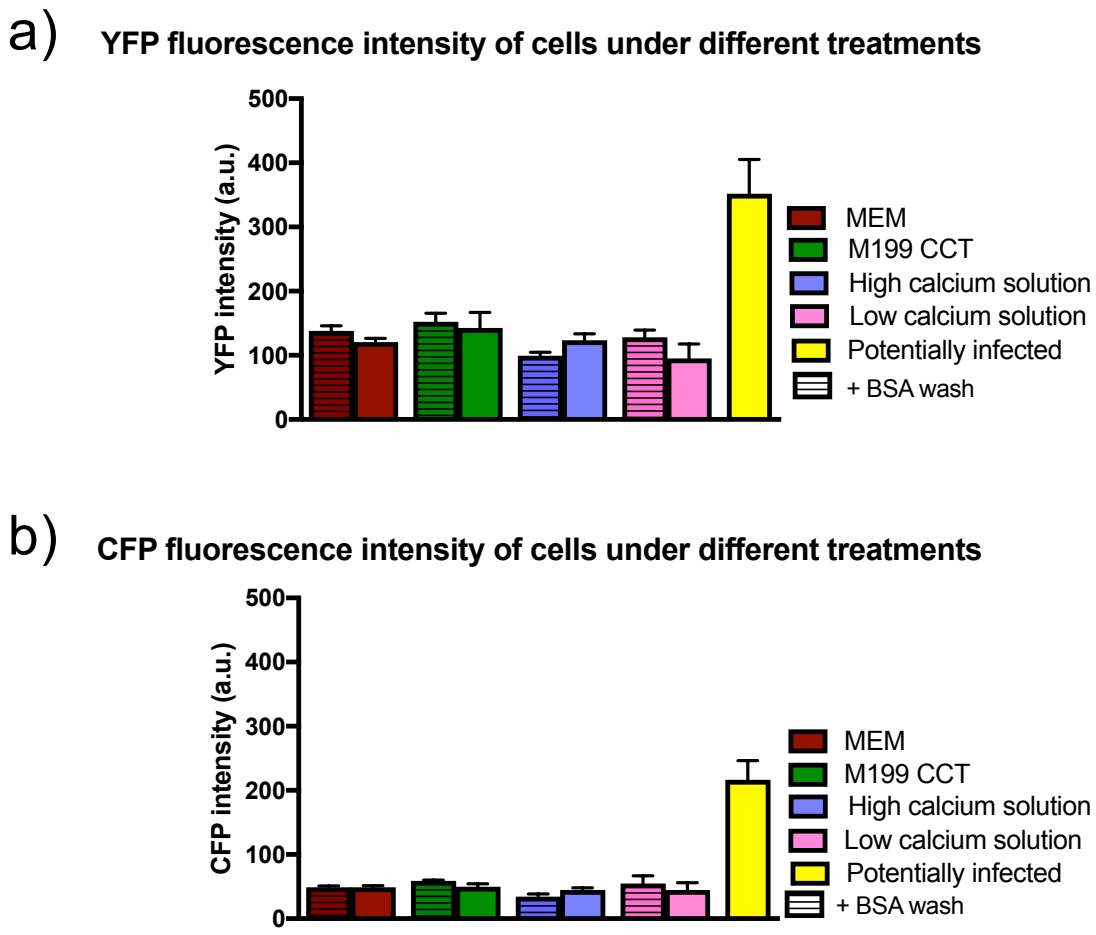


Figure 3.1.
A, B) CFP and YFP intensities of non-infected adult mice cardiomyocytes cultured over-night under the different treatments. For comparison, the emission intensities of infected myocytes cultured in M199 are also shown.

3.2.1. Characterisation of Isolated cardiomyocytes - Initial protocol

A) Comparison between fresh and cultured myocytes with and without virus infection

Contractility was verified using the Ionoptix contractility system in order to examine the effects of maintaining the cells in culture over a period of 20-24 hours and to verify whether infection of myocytes would further compromise cell contractility. It was found that presence of adenoviral infection does not contribute to the reduced ability of the myocytes to contract; rather, the initial yield of quality cells influences such decrease. Thus, it is important to be fastidious with the isolation of adult cardiomyocytes as the initial yield influences the quantity and quality of cells obtained after culture (Figure 3.2).

Figure 3.2. Influence of adenovirus infection on the number of contractile cells

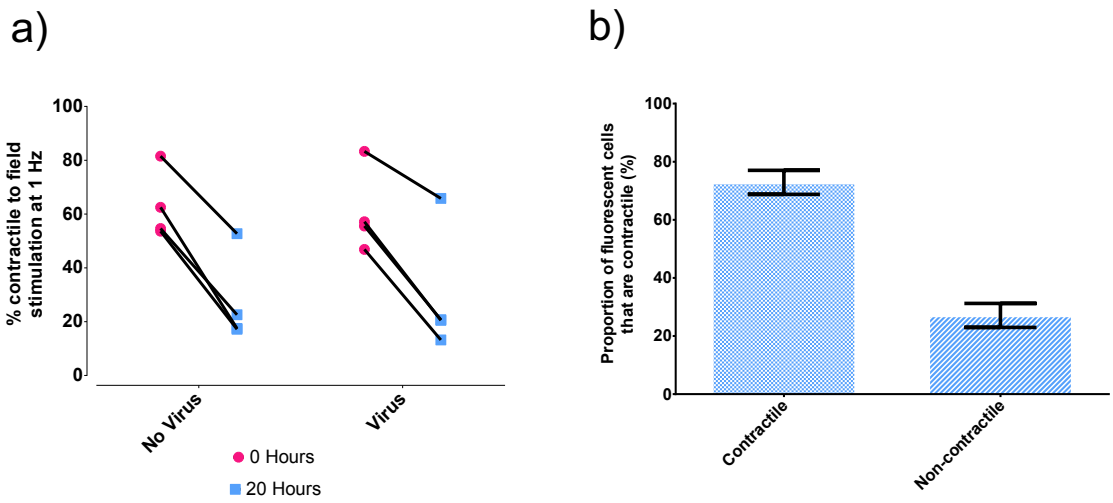


Figure 3.2.
A) Effect of 20 hours of culture on overall number of contractile cells. B) Proportion of contractile cells when only considering those expressing the sensor after 20 hours in culture, where ~ 80% were contractile. All data n=3 animals (~30 cells per group). Means + 95% C.I.). Work conducted in collaboration with Oliver Lomas.

B) Fractional shortening

To examine the impact of cell culture on fractional shortening, field-stimulated mouse adult cardiomyocytes were monitored either directly after isolation or after 20 hours in culture. Figure 3.3 shows these results: the cultured cells presented significantly shorter sarcomere length and delay in relaxation phase compared to freshly isolated ones. Similar results were described by Zhou et al where cultured cells presented with 46% increase in relaxation phase when compared to freshly isolated cardiomyocytes (Zhou et al. 2000).

Figure 3.3. Fractional shortening comparison of fresh and cultured cardiomyocytes (initial protocol)

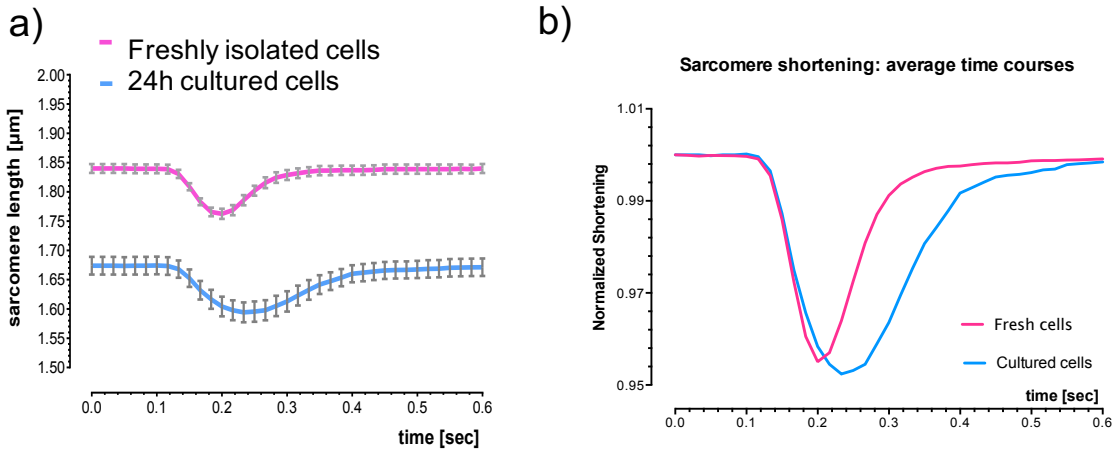


Figure 3.3.
a) Average of cardiomyocytes fractional shortening (~ 20 cells per group). b) Curves shown in A after normalization with respect to initial sarcomere length. Work conducted in collaboration with Oliver Lomas.

3.3. IMPROVED PROTOCOL

An improved protocol to isolate, culture and efficiently infect the adult mouse cardiomyocytes was developed (the full protocol is described in Chapter 2). The main changes introduced to the protocol were as follows.

3.3.1. Culture medium and addition of Cytochalasin D

A cell viability assay using SYTOX Green nucleic acid stain as an indicator of cell death was performed to assess the influence of the different culture media on the viability of the cells after 24h of culture. SYTOX green is a cationic unsymmetrical dye that upon binding to cellular nucleic acids results in a > 500-fold enhancement in fluorescence. This dye does not penetrate living cells, however, it makes dead cells and cells with compromised membranes bright green (absorption and emission maxima at 502 and 523nm, respectively) (Roth et al. 1997).

The addition of Cytochalasin D, which in sub-micromolar concentrations has been found to preserve structural integrity and contractile function in adult rat cardiomyocytes (Tian et al. 2012) was also assessed as a supplement to the overnight media. The main mechanism of action of this compound is thought to be via actions on the cytoskeleton that prevents the loss of T-tubules, a deterioration of the mature phenotype that has been observed in cultures rodent ventricular cardiomyocytes (Pavlović, McLatchie, and Shattock 2010).

To perform this assay, freshly isolated adult WT cardiomyocytes were plated on laminin coated coverslips under 4 different culturing conditions: (1) M-199 culturing media, (2) M-199 culturing media + 0.5µ Cytochalasin D, (3) MEM culturing media and (4) MEM culturing media + 0.5µ Cytochalasin D. Cells were cultured for 24 hours. After the culturing period, 2µl of SYTOX green was added to the media 5 minutes before imaging the cells. 10 phase-contrast and correspondent fluorescent images were acquired for each condition. All images were analysed by counting the number of live cells in the phase-contrast image and in the correspondent fluorescent image, where only dead or damaged

cells were visible (Figure 3.4). As a control, the assay was also performed in freshly isolated cells plated on laminin for 2 hours. The counting of the cells was done both manually and by using ImageJ. The data are represented as % of viable cells (as number of viable cells / total number of cells). As displayed in Figure 3.5, the culturing media MEM was substantially better in keeping the cells viable after 24 hours of culture. The addition of Cytochalasin D to either of the culturing media did not show any significant improvement.

Figure 3.4. SYTOX green cell viability assay- M199 vs. MEM

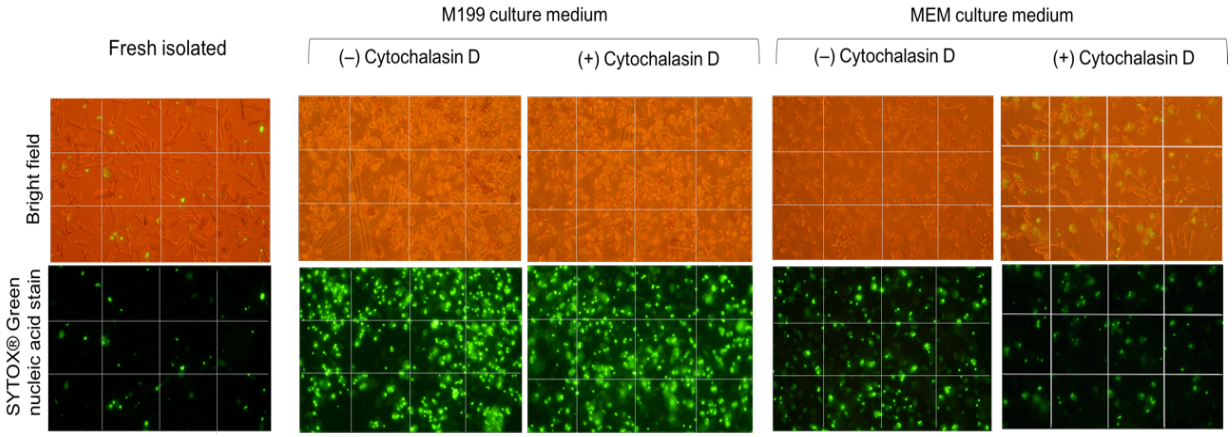


Figure 3.4.
Representative phase-contrast (top panel) of the cells and correspondent fluorescent images of the cells expressing SYTOX green fluorescence (lower panel). Grid was used to facilitate the analysis and the quantification of the data. All images were acquired on a Nikon Eclipse TS 100 microscope equipped with a Nikon D 5100 camera. Excitation was 500 nm, emission was 535 LP.

Figure 3.5. SYTOX green cell viability assay quantification and comparison.

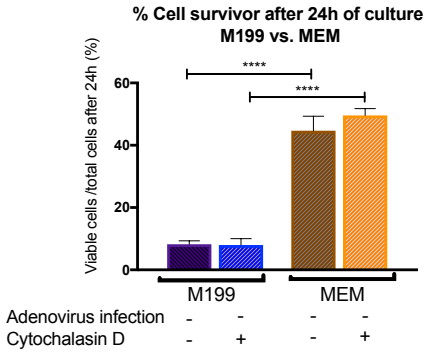


Figure 3.5.
Comparison between the effect of M-199 and MEM culturing media with and without Cytochalasin-D on adult mouse cardiomyocytes survival after 24h in culture. Data represented as number of viable cells over number of total cells from SYTOX green assay. (Graph show means of 10 areas per condition per animal; 3 WT animals. Error bars represent SEM; One-way ANOVA, * = 0.05<p<0.01, ** = 0.01<p<0.001, ***= 0.001<p<0.0001, **** = p<0.0001).

3.3.2. Adenovirus infection

The adenoviral transduction is highly dependent on the culture medium. As mentioned earlier, studies have shown that cardiomyocytes cultured in MEM develop higher expression of Adenovirus binding receptors, consequently are more effectively transduced then in M199 (90% versus 5% in M199 medium) (Li et al. 2003). To assess whether this was also true in our cells, an assay similar to the one described above was performed. Isolated cardiomyocytes were plated on laminin coated coverslips under 4 different culturing conditions: (1) 1mL of M-199 culturing media + 1µL H187 FRET-based sensor adenovirus; (2) 1mL of M-199 culturing media + 0.5µM Cytochalasin D 1µL H187 FRET- based sensor adenovirus (3) 1mL of MEM culturing media +1µL H187 FRET- based sensor adenovirus and (4) 1mL of MEM culturing media + 0.5µM Cytochalasin D + 1µL H187 FRET- based sensor adenovirus.

To drive expression of the large proteins that constitute the FRET biosensors, a high ratio of viral particle to cardiomyocyte (Multiplicity of Infection or MOI) of 100 was required. For example, 1µl of a viral preparation with a titer of 10^{10} viral particles per ml is applied to culture of 100,000 (10^5) cells; i.e. a ratio of 10^7 viral particles to 10^5 cells. Adenovirus-directed gene expression in adult mouse has been reported to be highly efficient. According to Zhou et al, a uniform expression was reached in all cardiomyocytes at MOI>30 (Zhou et al. 2000).

The media containing the adenovirus was removed after 2 hours and replaced by fresh media in all the samples. After 24 hours 10 phase-contrast and correspondent fluorescent images were acquired for each condition (Figure 3.6). All images were analysed by counting the number of live cells in the phase-contrast image and in the corresponding fluorescent image where only cells expressing the FRET-based sensor were visible. Cells counting was done both manually and by using ImageJ. The data were represented as % fluorescent cells (number of fluorescent cells / total number of live cells).

Although the quantitative analysis of this assay does not show significant differences between the infection efficiency under the use of different media, when analysed in combination with the cell viability assay (Figure 3.5), leads to the conclusion that culturing these cells with MEM is more beneficial then with using M-199. The lack of significance between the infection efficiency assay can be explained by the significant lower number of live cells under M-199 when compared with the high number of live cells cultured with MEM. The use of Cytochalasin D did not make any difference to the infection efficiency of the cardiomyocytes.

Figure 3.6. Adenovirus infection efficiency under M199 and MEM

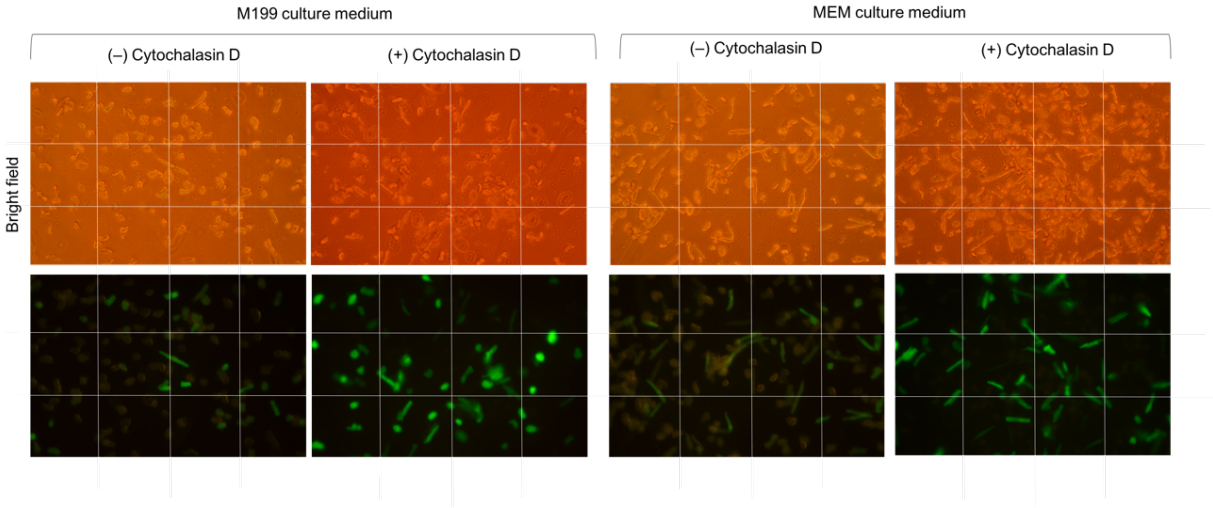


Figure 3.6.
Representative phase-contrast (top panel) and correspondent fluorescent images (lower panel) of the cells. Grid was used to facilitate the analysis and the quantification of the data. All images were acquired on a Nikon Eclipse TS 100 microscope equipped with a Nikon D 5100 camera. Excitation was 500 nm, emission was 535 LP.

Figure 3.7. Adenovirus infection efficiency assay quantification and comparison

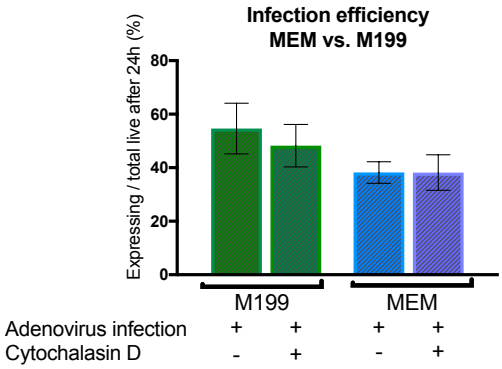


Figure 3.7.
Comparison between the effect of M-199 and MEM culturing media with and without Cytochalasin-D on the adenovirus infection efficiency. Data represented as number of fluorescent cells over number of total live cells. (Graph show means from 10 areas per condition per animal; 3 WT animals. Error bars represent SEM).

3.3.3. Heart extraction

Based on observations, keeping the overall extraction procedure duration to a maximum of 5 minutes increases the amount of viable and high-quality cells after culture. Prolonged extractions can either damage the isolated heart (e.g. as a consequence of hypoxia) or induce stress pathways (Bell, Mocanu, and Yellon 2011). It is necessary to be fastidious with the isolation of adult cardiomyocytes as the better the initial yield of cells, the greater the number and quality of cells obtained, ultimately improving the reliability of the subsequent fluoroscopic experiments.

Figures 3.8 and 3.9 show images of cardiomyocytes isolated from the different protocols highlighting the improvements obtained in cell morphology, infection and initial yield after the changes described above were applied.

Figure 3.8. Improvement in cardiomyocytes' morphology under different isolation protocols

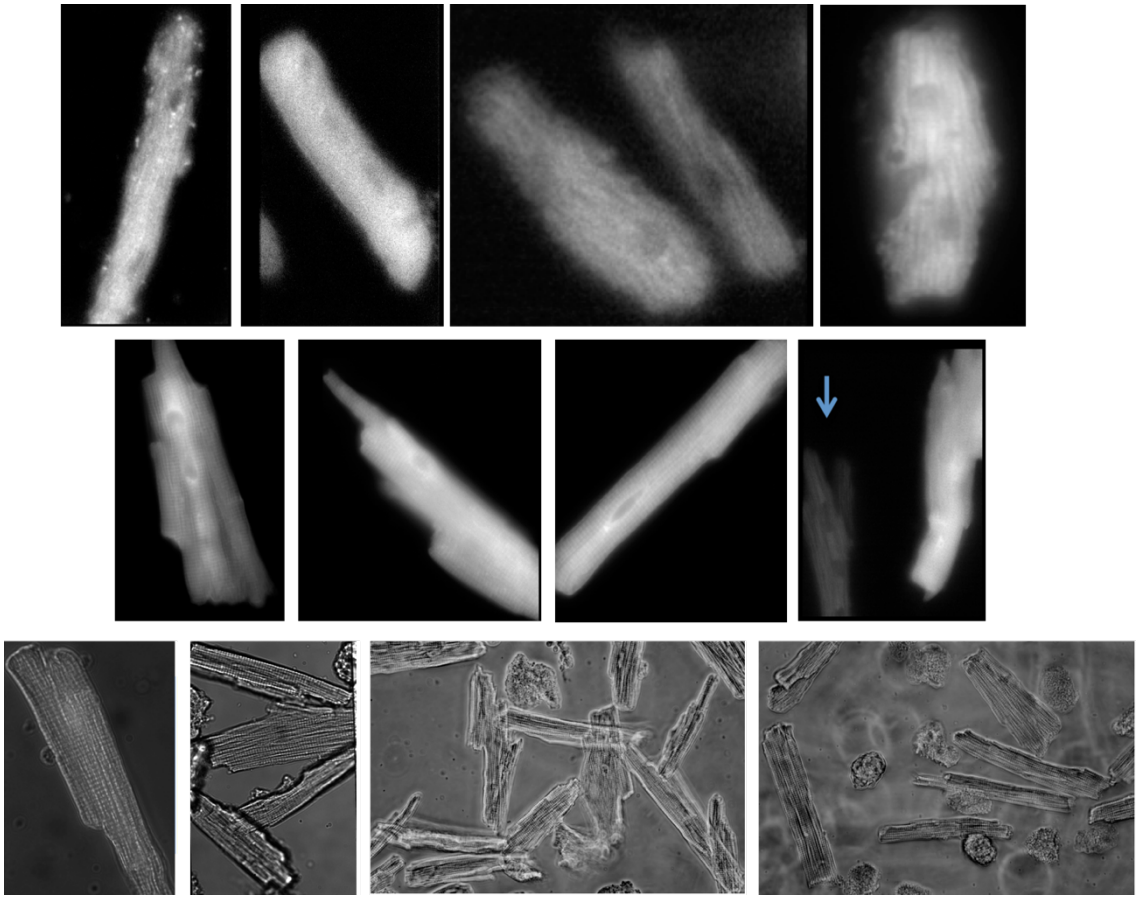


Figure 3.8.
60X Single wavelength images of myocytes acquired at 500nm excitation and collected at 535nm (200ms exposure time) infected with the FRET-based sensor Cygnet.
A, B) Myocyte expressing the sensor Cygnet after 20h of culture showing rounded extremities and no clear image of cellsted with the FRET-based sensor Cygnet.lls obtained, ultimately improving the reliabilitautofluorescence compatible with mitochondria (possibly NADH dependent), longitudinal striations.
D) Potentially infected cardiomyocyte (5% of the cells only) exhibiting higher fluorescence intensity than in C) yet still presenting the autofluorescence longitudinal pattern.
E, F, G) High quality cells showing the improvements in shape, structure and level of expression of the sensor (improved protocol).
H) Comparison between autofluorescent cell (arrow) and infected cell. I), J) Bright field images of cells infected and cultured for 20 hours using the improved protocol. L), M) 20X bright field phase contrast image of fresh and cultured cardiomyocytes, respectively from improved protocol.

Figure 3.9. Improvement in the initial yield of cells from the different isolation protocols

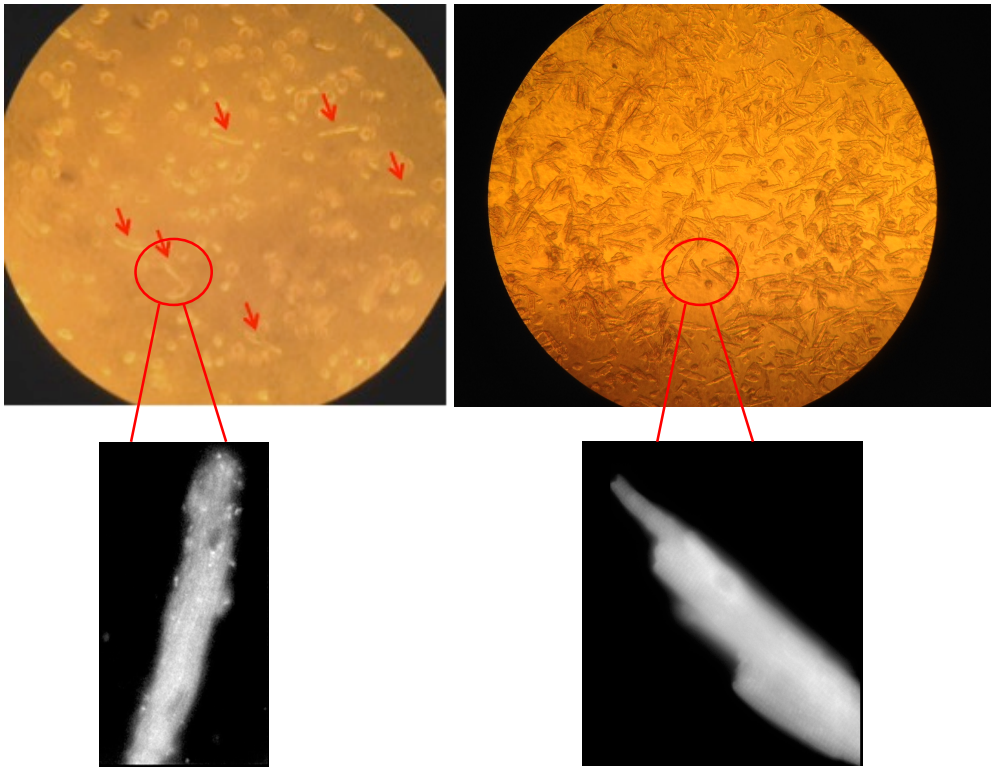


Figure 3.9.
A) Field image of cultured cardiomyocytes from initial protocol. B) Field image of cultured cardiomyocytes from improved protocol. Arrows indicate live cells.

3.3.4. Contractility

To examine the impact of the improved protocol on cell contractility, the sarcomere shortening in single, 1Hz field-stimulated mouse adult cardiomyocytes was analysed. As shown in Figure 3.10, cells cultured for 24 hours and obtained with the improved protocol show similar contractile properties as the freshly isolated ones. Figure 3.10 (panel C) shows that the relaxation phase, which was significantly affected under the initial culturing conditions, is significantly improved under the new culturing conditions (compare to Figure 3.3). These data are represented as single exponential tau (exponential decay time constant of the function). A high tau relates to longer recovery being commonly used to characterise the speed of recovery (relaxation or calcium reuptake) of

the cells (Givvimani et al. 2015) (IonOptix 2017) (Surdo et al. 2017). Although other parameters, such as the return velocity, can also be used to describe the return phase of the contraction, tau was the best parameter to demonstrate the significance of this specific set of data (Givvimani et al. 2015; Turdi et al. 2010; IonOptix 2017).

Figure 3.10. Fractional shortening comparison of fresh and cultured cardiomyocytes (improved protocol)

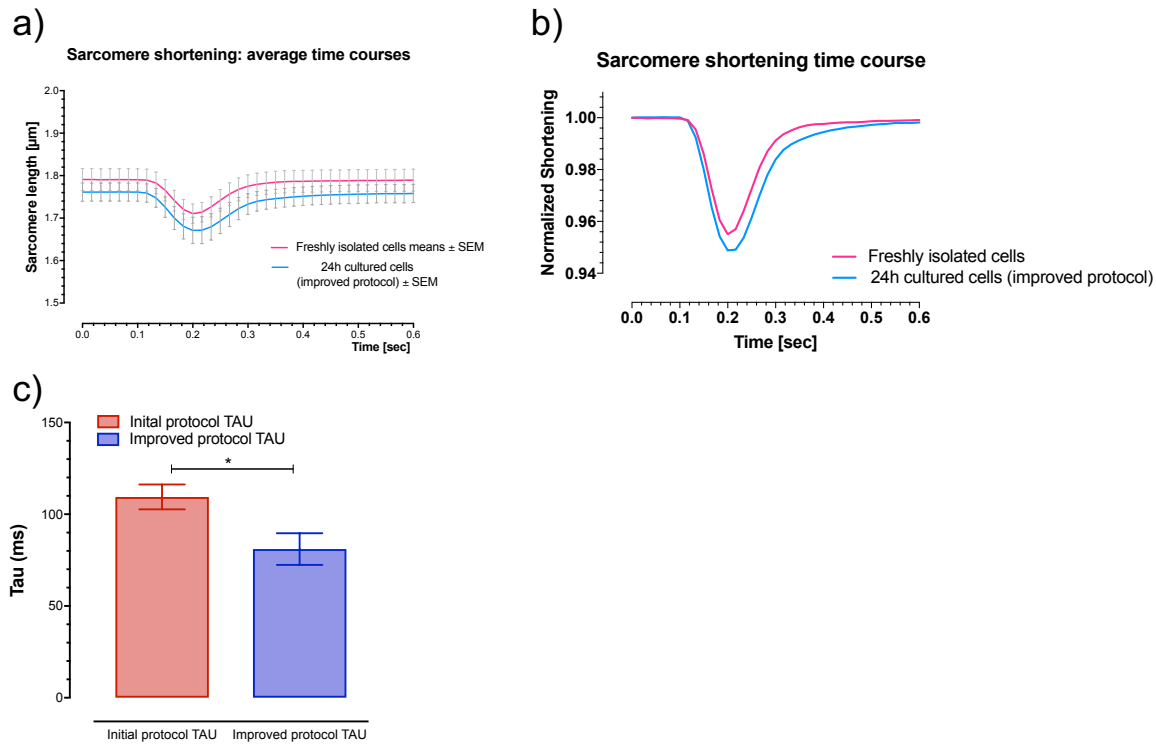
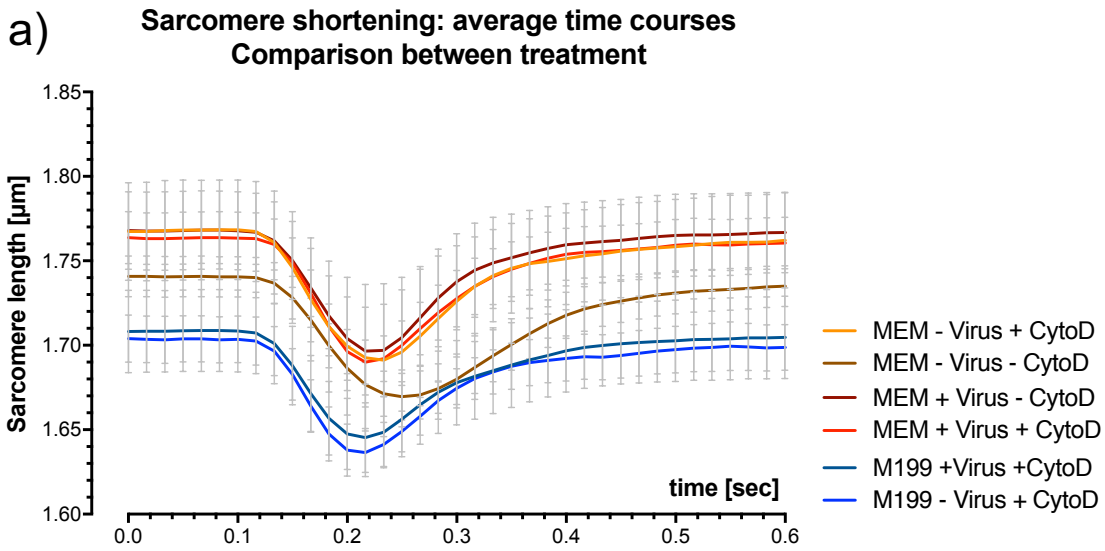


Figure 3.10.
a) Sarcomere length fractional shortening (~20 cells per group). b) Curves shown in A after normalization with respect to initial sarcomere length. c) Comparison between single exponential tau for initial and improved protocols. (Graphs show means of 30 cells per condition per animal; 3 WT animals. Error bars represent SEM; T-test, * = 0.05<p<0.01, ** = 0.01<p<0.001, ***= 0.001<p<0.0001, **** = p<0.0001.)

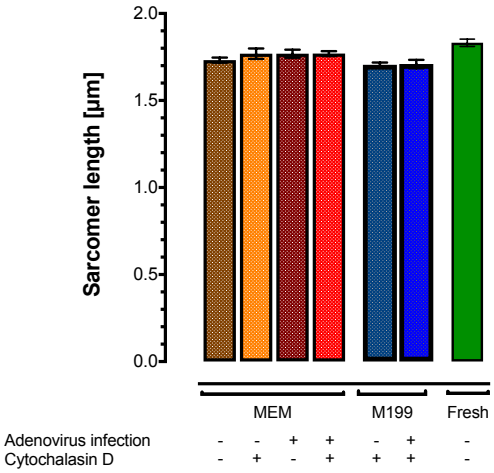
The effect of the different culturing media (M-199 vs. MEM with and without Cytochalasin D) on contractility was also assessed. However, it was not possible to obtain a comparison between all the conditions as there were not enough viable and contractile

cells cultured under M-199. Figure 3.11 shows a comparison between the contractile parameters of freshly isolated cells and the different culturing conditions. Cardiomyocytes cultured with M-199 showed to have a significant overall poor performance when compared to cell cultures with MEM. The use of Cytochalasin D as supplement to the MEM has showed to be the best culturing condition as the contractile parameters of these cells were closer to the freshly isolated ones and significantly better than cardiomyocytes cultured without Cytochalasin D. Although these cells performed better in all the parameters analysed, the Cytochalasin D contribution was especially visible in the relaxation phase, represented here as return velocity and time to 50% return to baseline. This last parameter refers to the first half of the relaxation phase whereas the return velocity is calculated based on the return phase as a whole. These data suggest that the Cytochalasin D has significant effect on the first half of the relaxation phase.

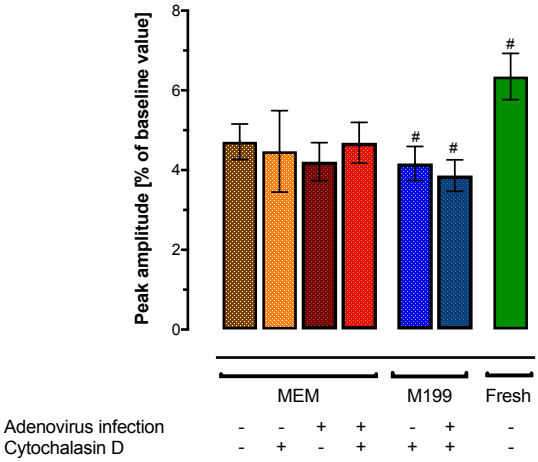
Figure 3.11. Fractional shortening comparison between different culturing conditions



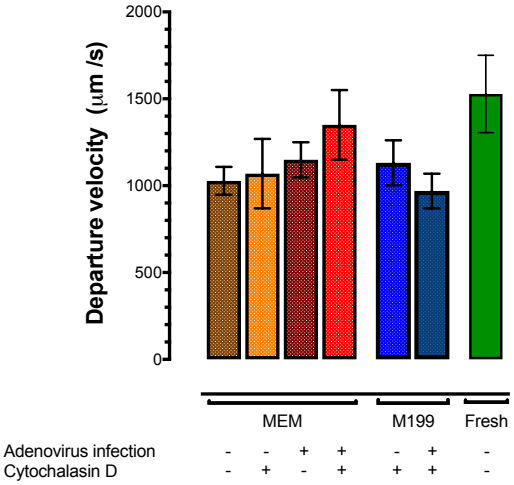
b)


Sarcomer length [µm]
2.0
1.5
1.0
0.5
0.0
MEM
M199
Fresh
Adenovirus infection - - + + - + -
Cytochalasin D - + - + + + -

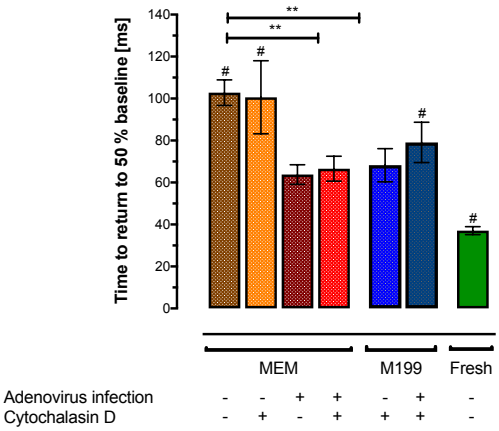
c)


Peak amplitude [% of baseline value]
8
6
4
2
0
#
MEM
M199
Fresh
Adenovirus infection - - + + - + -
Cytochalasin D - + - + + + -

d)


Departure velocity (µm /s)
2000
1500
1000
500
0
MEM
M199
Fresh
Adenovirus infection - - + + - + -
Cytochalasin D - + - + + + -

e)


Time to return to 50 % baseline [ms]
140
120
100
80
60
40
20
0
**
**
#
MEM
M199
Fresh
Adenovirus infection - - + + - + -
Cytochalasin D - + - + + + -

f)

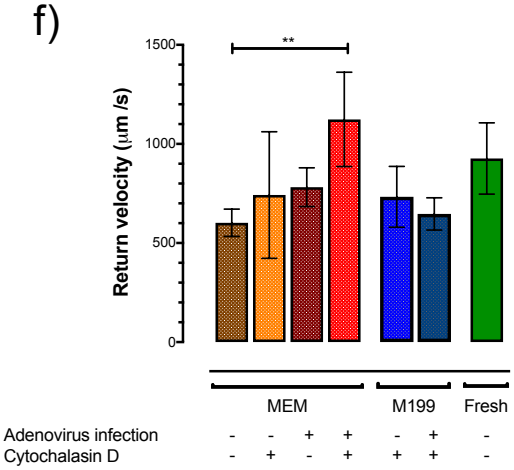

Return velocity (µm /s)
1500
1000
500
0
**
MEM
M199
Fresh
Adenovirus infection - - + + - + -
Cytochalasin D - + - + + + -

Figure 3.11.
a) Sarcomere length fractional shortening (~20 cells per group) for each condition. b) Basal sarcomere length; c) Peak amplitude; d) Departure velocity; e) Time to 50% return baseline; f) Return velocity comparison of WT cardiomyocytes cultured for 24h under the different culturing conditions and freshly isolated cells. (Graphs show means of 20 cells per condition per animal; 3 WT animals. Error bars represent SEM; T-test, * = 0.05<p<0.01, ** = 0.01<p<0.001, ***= 0.001<p<0.0001, **** = p<0.0001.)

3.4. CHARACTERIZATION OF ISOLATED MDX CARDIOMYOCYTES

After reaching a successful protocol to isolated and culture WT cardiac myocytes it was necessary to assess whether the MDX cardiomyocytes could be isolated and cultured by using the same protocol or if it any changes were still required as other genetic modified mouse cardiomyocytes have been described to be more fragile and not to perform as well after isolation procedures (Jian et al. 2016). As shown in Figure 3.12, the cardiomyocytes from MDX mice are successfully isolated, cultured and infected under the same optimal protocol conditions established for WT cells (Figure 3.13). The cell viability assay and infection efficiency assay were not repeated in full on MDX cells as the optimal condition had already been stablished using WT cells. SYTOX green was used to assess whether the cell viability of MDX cells was different when compared to WT cells under the improved conditions. The adenovirus infection efficiency was also assessed (Figures 3.12 and 3.13).

Figure 3.12. Adenovirus infection and cell viability assay in MDX cardiomyocytes

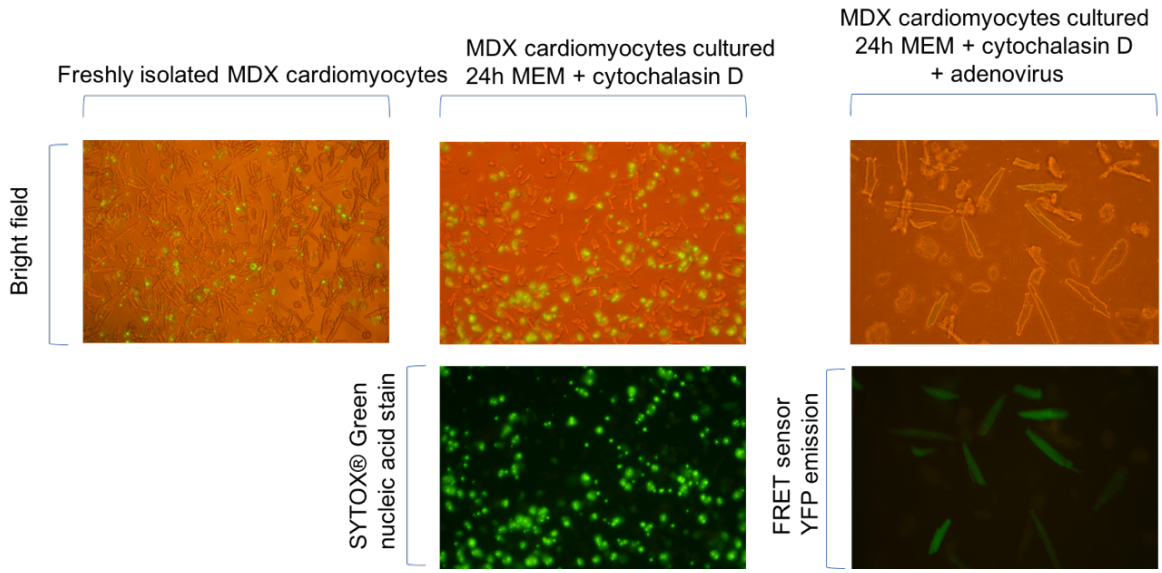


Figure 3.12.
Representative phase-contrast (top panel) and correspondent fluorescent images (lower panel) of the cells. Right panel represents yield of fresh isolated cells. Image shows phase contrast and SYTOX green fluorescence merged. Middle panel represents MDX cells after 24h under MEM + CytoD culture. Left panel represents infection efficiency of MDX cardiomyocytes. All images were acquired on a Nikon Eclipse TS 100 microscope equipped with a Nikon D 5100 camera. Excitation was 500 nm, emission was 535 LP.

Figure 3.13. MDX adenovirus infection and cell viability assay quantification and comparison.

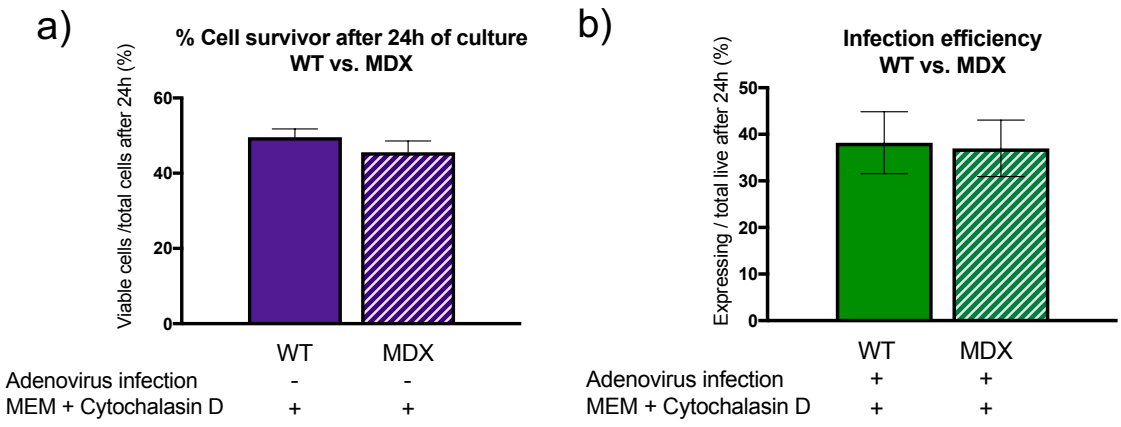


Figure 3.13.
a) Comparison between the WT and MDX cardiomyocytes under MEM + Cytochalasin D culturing media on cell viability. Data represented as number of live cells over number of total cells. b) Comparison between the WT and MDX cardiomyocytes under MEM + Cytochalasin D

culturing media on the adenovirus infection efficiency. Data represented as number of fluorescent cells over number of total cells live cells. (Graph show means of 10 areas per condition per animal; 3 WT animals. Error bars represent SEM).

To verify the contractile performance of isolated MDX myocytes, fractional shortening of cultured and freshly isolated cells was recorded and analysed. The results showed significant differences between the cultured MDX cells and the freshly isolated ones in all the parameters analysed: basal sarcomere length, peak amplitude, departure and return velocities were significantly reduced in cultured MDX cardiomyocytes (Figure 3.14). However, the contractility of freshly isolated MDX cardiomyocytes does not differ from freshly isolated WT cells (Figure 3.15). This data suggests that MDX cells can withstand isolation but are particularly sensitive to culture conditions. Although not enough data was collected to establish statistical significance, changes in the protocol such as higher concentration of Cytochalasin D, longer recovery culturing media (MEM + FSB) and lower concentration of Liberase enzyme for digestion were tested in the attempt to improve the quality of MDX cultured cardiomyocytes but did not show any improvement.

Figure 3.14. Fractional shortening comparison of fresh and cultured MDX cardiomyocytes.

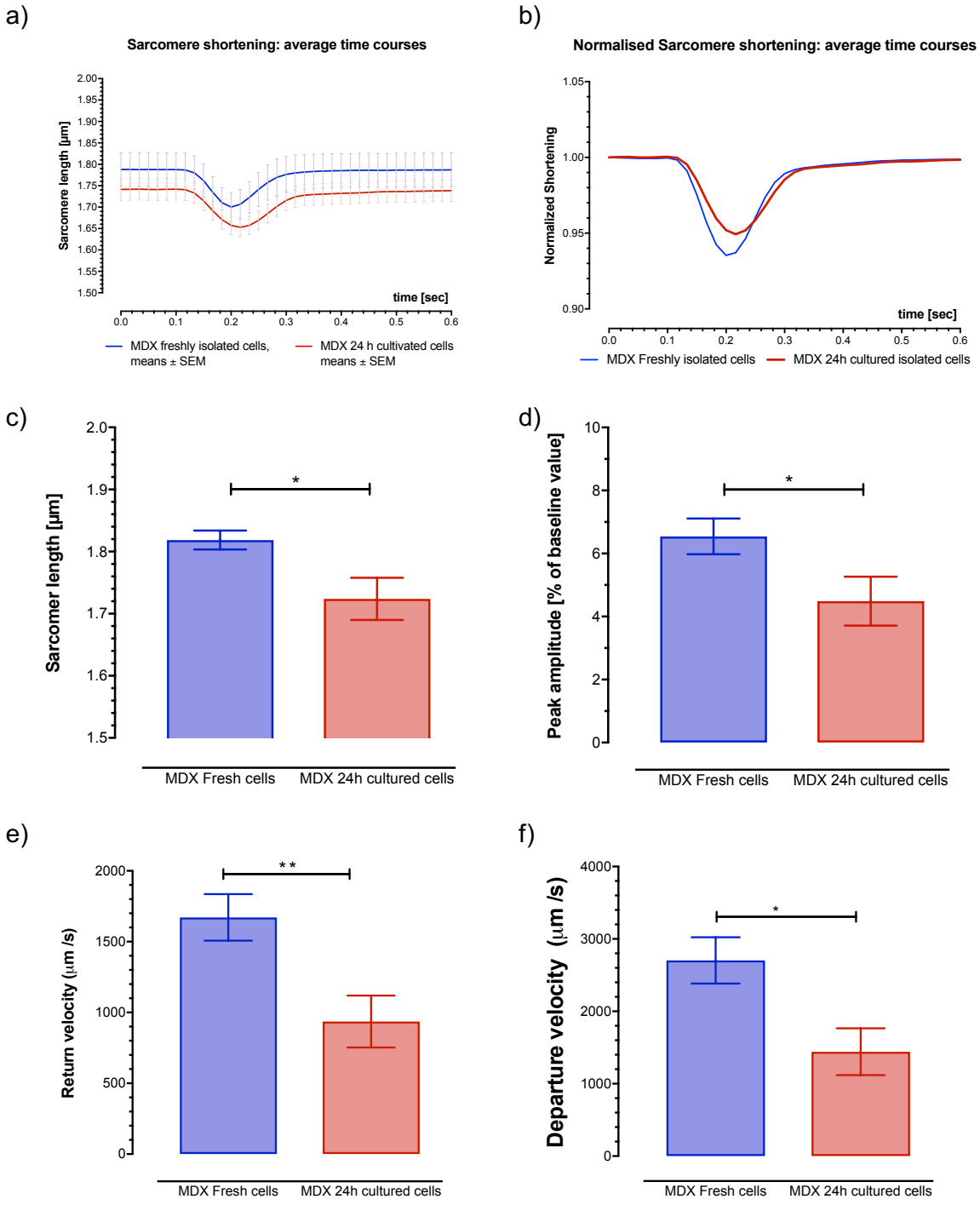


Figure 3.14.
A) Sarcomere fractional shortening (~12 cells per group). B) Curves shown in A after normalization to initial sarcomere length. C), D), E) and F) Sarcomere length, peak amplitude, return velocity and departure velocity, respectively. (Freshly isolated MDX cells vs. cultured). T-test, * = 0.05<p<0.01, ** = 0.01<p<0.001. G) Sarcomere fractional shortening (Freshly isolated from WT and MDX).

Figure 3.15. Fractional shortening comparison of fresh and cultured cardiomyocytes – WT vs. MDX

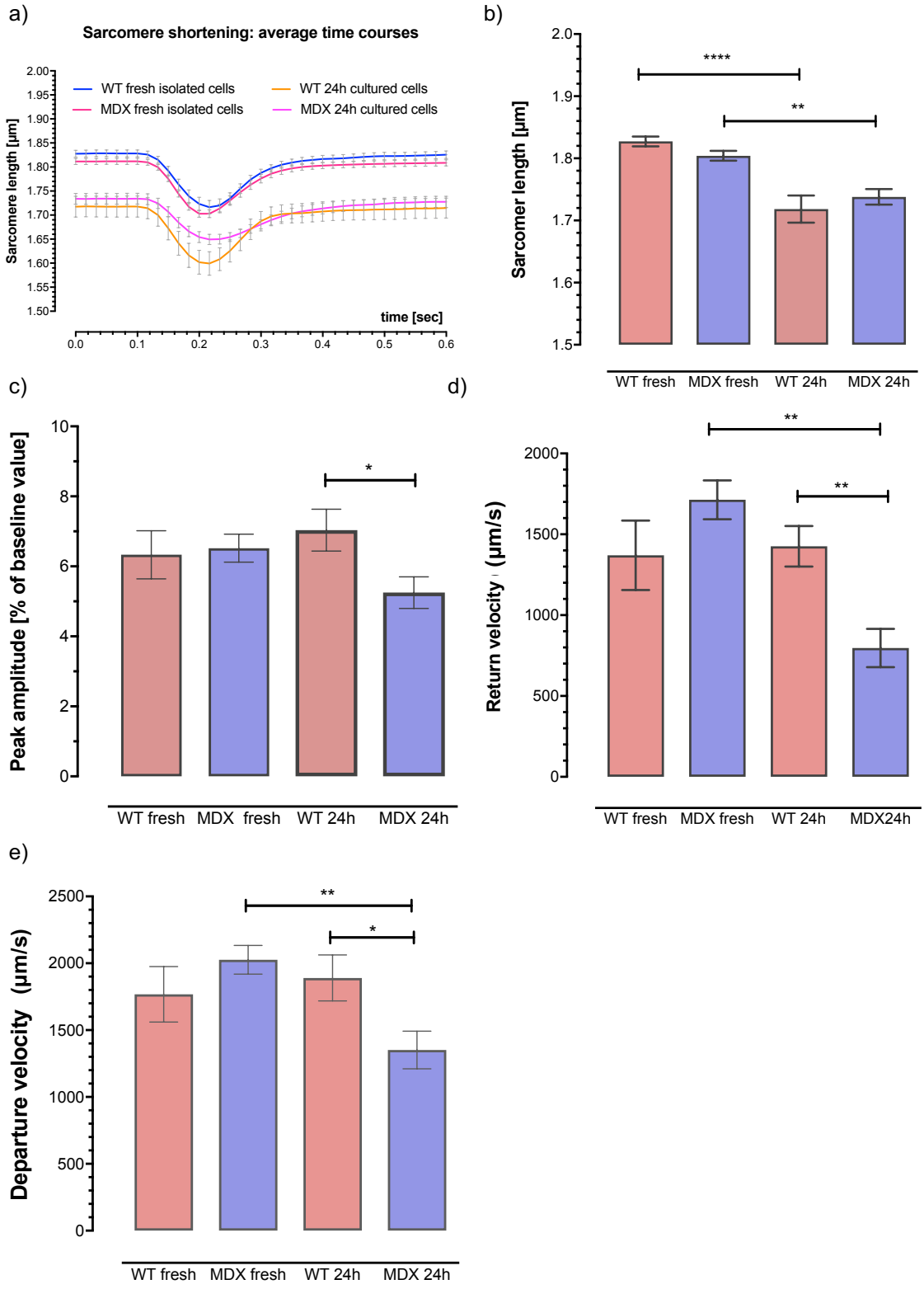


Figure 3.15.
A) Sarcomere fractional shortening (~12 cells per group). B) Curves shown in A after normalization to initial sarcomere length. C), D), E) and F) Sarcomere length, peak amplitude,

return velocity and departure velocity, respectively. (Freshly isolated MDX cells vs. cultured). T-test, * = 0.05<p<0.01, ** = 0.01<p<0.001. G) Sarcomere fractional shortening (Freshly isolated from WT and MDX).

3.5. DISCUSSION AND CONCLUSION

Most studies using cultured adult cardiomyocytes utilise cells from rats or other large animals as these are robust, less fragile and resist better to culture conditions and infection compared to mouse cells (Zhou et al. 2000)(Jian et al. 2016)(Hirsch, Borton, and Metzger 2003)(Pinz et al. 2011).

The focus of my project is on cyclic nucleotide signalling in the MDX mouse model of Duchenne muscular dystrophy; therefore, I faced the challenge of isolating, infecting and culturing adult mice cardiomyocytes in order to perform FRET experiments in these cells. As presented in this chapter, an improved protocol yielding high quality cardiomyocytes expressing adequate levels of FRET-based sensors was generated. Additionally, the cardiomyocytes generated by using this novel protocol presented the best contractile characteristics after culture and infection compared to the other methods already published.

A summary of improvements reached after protocol optimisation can be found at the table below.

Table 3.1. Summary of improvements on isolating cardiomyocytes

	Initial protocol	Improved protocol	Main contributor to improvement
Cell viability after 24h in culture	10%	50%	-Expertise in isolation technique -MEM culturing media
Well-defined-non rounded extremities cells	50%	80%	-Expertise in isolation technique -MEM culturing media -Cytochalasin D
Contracting cells after 24h in culture	20%	70%	-Expertise in isolation technique -MEM culturing media -Higher number of healthy and viable cells
Contracting kinetics	Slower relaxation phase	Similar to freshly isolated cells	-Expertise in isolation technique -MEM culturing media -Higher number of healthy and viable cells -Cytochalasin D
Infection efficiency	5 – 10%	60%	-MEM -Higher MOI
CFP signal/autofluorescence	3	7	-Expertise in isolation technique -Improved infection efficiency
YFP signal/autofluorescence	4	10	-Expertise in isolation technique -Improved infection efficiency

Table 3.1.
Summary of improvements and changes applied for successful development of protocol.

Cell viability assay showed that culturing the cell with MEM significantly maintained the number of viable cells after 24h in culture. The combination of these data and the infection efficiency assay resulted in selecting MEM as the ideal media for the proposed experiments once the % of viable and expressing FRET-based sensor cells were optimal under these culturing conditions. Contractile characteristics were used as a parameter to assess cell quality after culture. Several parameters such as basal sarcomere length, peak

amplitude, return velocity and departure velocity were analysed to compare the quality of cells isolated and cultured under different conditions.

Cytochalasin D supplementation showed to be significantly beneficial for the cardiomyocytes in maintaining high quality contractile characteristics after culture. In particular, this compound showed to be important in maintaining contractile characteristics related to the relaxation phase after culture. The return phase (relaxation phase) had been the most affected parameter under non-optimal culturing and isolation conditions. This specific characteristic was analysed in three different way throughout this chapter: as Tau, Time to 50% return of baseline and return velocity. WT cells were found to maintain their ability to contract without significant loss when compared to freshly isolated cells despite being cultured for 24 hours (after protocol improvement). In contrast, the contractile properties of dystrophic cardiomyocytes resulted to be somewhat compromised after cell culture.

The MDX freshly isolated cardiomyocytes present similar contractile performance when compared to WT cells, however, their performance after culture suggests that the dystrophic cells are more prone to deterioration under culturing conditions. This finding is not surprising as the DMD muscle cells are known to have unstable membranes due to the lack of dystrophin and exhibit increased susceptibility to contraction-induced sarcolemmal damage (Petrof et al. 1993). Jian et al suggested that isolation method using *in vivo* cannulation of the carotid artery instead of the aorta (as performed in this chapter), minimize myocardial ischemia favouring high quality isolation of cardiomyocytes prone to damage, such as from heart disease and some genetically-modified models. Aortic cannulation was performed in WT mice or other strains less vulnerable to ischemic

damage (Jian et al. 2016). The same study suggested that the MDX mice does not benefit from the carotid artery cannulation method, therefore this approach was not explored in this thesis.

In conclusion, the protocol discussed in this chapter, is a reliable method to isolate and culture cardiomyocytes after adenoviral infection. The limitation encountered on the contractile performance of the MDX cardiomyocytes were taken in consideration on the planning and execution of the further experimental data described in this thesis.

3.6. REFERENCES

Bell, Robert M, Mihaela M Mocanu, and Derek M Yellon. 2011. "Retrograde Heart Perfusion: The Langendorff Technique of Isolated Heart Perfusion." *Journal of Molecular and Cellular Cardiology* 50 (6): 940–50.

Eng, John, Ronald M Lynch, and Robert S Balaban. 1989. "Nicotinamide Adenine Dinucleotide Fluorescence Spectroscopy and Imaging of Isolated Cardiac Myocytes." *Biophysical Journal* 55 (4): 621–30.

Givvimani, S, SB Pushpakumar, N Metreveli, S Veeranki, S Kundu, and SC Tyagi. 2015. "Role of Mitochondrial Fission and Fusion in Cardiomyocyte Contractility." *International Journal of Cardiology* 187: 325–33.

Hirsch, Jennifer C, Andrea R Borton, and Joseph M Metzger. 2003. "Isolation, Culture, and Gene Transfer of Adult Canine Cardiac Myocytes." *Cardiac Cell and Gene Transfer: Principles, Protocols, and Applications*, 145–57.

IonOptix, IonOptix. 2017. "Monotonic Transient Analysis Parameters." August 22. http://www.ionoptix.com/wp-content/uploads/2014/07/Monotonic-Transient-Analysis-Defined.pdf.

Jian, Zhong, Yi-Je Chen, Rafael Shimkunas, Yuwen Jian, Mark Jaradeh, Karen Chavez, Nipavan Chiamvimonvat, Jil C Tardiff, Leighton T Izu, and Robert S Ross. 2016. "In Vivo Cannulation Methods for Cardiomyocytes Isolation from Heart Disease Models." *PloS One* 11 (8): e0160605.

Li, Zhenbo, Ram V Sharma, Dongsheng Duan, and Robin L Davisson. 2003. "Adenovirus-mediated Gene Transfer to Adult Mouse Cardiomyocytes Is Selectively Influenced by Culture Medium." *The Journal of Gene Medicine* 5 (9): 765–72.

Lomas, Oliver, Marcella Brescia, Ricardo Carnicer, Stefania Monterisi, Nicoletta C Surdo, and Manuela Zaccolo. 2015. "Adenoviral Transduction of FRET-Based Biosensors for cAMP in Primary Adult Mouse Cardiomyocytes." *cAMP Signaling: Methods and Protocols*, 103–15.

Nakayama, Hiroyuki, Benjamin J Wilkin, Ilona Bodi, and Jeffery D Molkentin. 2006. "Calcineurin-Dependent Cardiomyopathy Is Activated by TRPC in the Adult Mouse Heart." *The FASEB Journal* 20 (10): 1660–70.

Nikolaev, Viacheslav O, Moritz Bünemann, Eva Schmitteckert, Martin J Lohse, and Stefan Engelhardt. 2006. "Cyclic AMP Imaging in Adult Cardiac Myocytes Reveals Far-Reaching β1-Adrenergic but Locally Confined β2-Adrenergic Receptor–mediated Signaling." *Circulation Research* 99 (10): 1084–91.

Pavlović, Davor, Linda M McLatchie, and Michael J Shattock. 2010. "The Rate of Loss of T-tubules in Cultured Adult Ventricular Myocytes Is Species Dependent." *Experimental Physiology* 95 (4): 518–27.

Petrof, Basil J, Joseph B Shrager, Hansell H Stedman, Alan M Kelly, and H Lee Sweeney. 1993. "Dystrophin Protects the Sarcolemma from Stresses Developed during Muscle Contraction." *Proceedings of the National Academy of Sciences* 90 (8): 3710–14.

Pinz, Ilka, Ming Zhu, Ulrike Mende, and Joanne S Ingwall. 2011. "An Improved Isolation Procedure for Adult Mouse Cardiomyocytes." *Cell Biochemistry and Biophysics* 61 (1): 93–101.

Powell, T, and VW Twist. 1976. "A Rapid Technique for the Isolation and Purification of Adult Cardiac Muscle Cells Having Respiratory Control and a Tolerance to Calcium." *Biochemical and Biophysical Research Communications* 72 (1): 327–33.

Roth, Bruce L, Martin Poot, Stephen T Yue, and Paul J Millard. 1997. "Bacterial Viability and Antibiotic Susceptibility Testing with SYTOX Green Nucleic Acid Stain." *Applied and Environmental Microbiology* 63 (6): 2421–31.

SchlUter, Klaus-Dieter, and Daniela Schreiber. 1997. "Adult Ventricular Cardiomyocytes."

Shan, Dan, Richard B Marchase, and John C Chatham. 2008. "Overexpression of TRPC3 Increases Apoptosis but Not Necrosis in Response to Ischemia-Reperfusion in Adult Mouse Cardiomyocytes." *American Journal of Physiology-Cell Physiology* 294 (3): C833–41.

Surdo, Nicoletta C, Marco Berrera, Andreas Koschinski, Marcella Brescia, Matias R Machado, Carolyn Carr, Peter Wright, Julia Gorelik, Stefano Morotti, and Eleonora Grandi. 2017. "FRET Biosensor Uncovers cAMP Nano-Domains at β-Adrenergic Targets That Dictate Precise Tuning of Cardiac Contractility." *Nature Communications* 8.

Takeishi, Yasuchika, Guoxiang Chu, Darryl M Kirkpatrick, Zhenling Li, Hisao Wakasaki, Evangelia G Kranias, George L King, and Richard A Walsh. 1998. "In Vivo Phosphorylation of Cardiac Troponin I by Protein Kinase Cbeta2 Decreases Cardiomyocyte Calcium Responsiveness and Contractility in Transgenic Mouse Hearts." *Journal of Clinical Investigation* 102 (1): 72.

Tian, Qinghai, Sara Pahlavan, Katharina Oleinikow, Jennifer Jung, Sandra Ruppenthal, Anke Scholz, Christian Schumann, Annette Kraegeloh, Martin Oberhofer, and Peter Lipp. 2012. "Functional and Morphological Preservation of Adult Ventricular Myocytes in Culture by Sub-Micromolar Cytochalasin D Supplement." *Journal of Molecular and Cellular Cardiology* 52 (1): 113–24.

Turdi, Subat, Xiujuan Fan, Ji Li, Junxing Zhao, Anna F Huff, Min Du, and Jun Ren. 2010. "AMP-activated Protein Kinase Deficiency Exacerbates Aging-induced Myocardial Contractile Dysfunction." *Aging Cell* 9 (4): 592–606.

Wolska, Beata M, and R John Solaro. 1996. "Method for Isolation of Adult Mouse Cardiac Myocytes for Studies of Contraction and Microfluorimetry." *American Journal of Physiology-Heart and Circulatory Physiology* 271 (3): H1250–55.

Zhou, Ying-Ying, Shi-Qiang Wang, Wei-Zhong Zhu, Andrej Chruscinski, Brian K Kobilka, Bruce Ziman, Su Wang, Edward G Lakatta, Heping Cheng, and Rui-Ping Xiao. 2000. "Culture and Adenoviral Infection of Adult Mouse Cardiac Myocytes: Methods for Cellular Genetic Physiology." *American Journal of Physiology-Heart and Circulatory Physiology* 279 (1): H429–36.

Chapter 4. Construction and characterization of FRET-based sensors

4.1. INTRODUCTION

4.1.1. Detection of cyclic nucleotides in living cells

cAMP signalling has been intensely studied since its discovery in 1953 by the use of several different techniques (Brescia and Zaccolo 2016). Biochemical methods, such as the radioimmunoassays (RIAs), have been reliable tools to quantify total concentrations of cyclic nucleotides in cells and tissues (Gesellchen et al. 2011). This technique is based on the competition between endogenous cAMP/cGMP from the samples of interest and exogenous ^{125}I-labelled cyclic nucleotide for binding to immobilised anti-cAMP or cGMP antibodies (Brooker et al. 1979; Sprenger and Nikolaev 2013). This approach has been gradually substituted by non-radioactive methods which exploit similar biochemical properties of non-radioactive substrate competition and antibody-based detection with several different technologies ranging from fluorescence polarization (FP) (Prystay et al. 2001) to enzymatic approaches (Williams 2004). Although these methods are reliable and highly sensitive, they present limitations which unable their use to analyse real-time dynamics of cyclic nucleotides in living cells at different subcellular localisations and under different conditions. These limitations include: (1) the necessity of disrupting/lysing the cells, (2) poor time resolution, as the concentrations are detected in steady state and cannot resolve the fast dynamics of the signalling, (3) detection of total, rather than free cyclic nucleotide (4) measure of accumulation over time rather than dynamic events within the cells and (5) the inability to analyse compartmentalised and localised intracellular events (no spatial resolution) (Stangherlin 2010; Sprenger and Nikolaev 2013; Gesellchen et al. 2011).

Technologies to monitor cyclic nucleotides dynamics and fluctuations in single intact living cells with high temporal and spatial resolution were created to overcome these limitations. The two main methods rely on the expression of biosensors which detect the signalling differences in real time and in living cells by using (1) biosensors based on cyclic nucleotide gated ion channels (Finn, Grunwald, and Yau 1996), or (2) sensors based on the phenomenon of Fluorescence Resonance Energy Transfer (FRET), discussed in detail below (Sprenger and Nikolaev 2013).

4.1.2. FRET

Föster (or fluorescence) Resonance Energy Transfer (FRET) is a direct way to measure cAMP or cGMP in single living cells with high spatial and time resolution. This has been the method of choice to explore cAMP and GMP signalling in cardiomyocytes from DMD in this thesis. Details of the technique are discussed below.

FRET is a distance-dependent physicochemical phenomenon that takes advantage of a process in which non-radiative energy is transferred from a donor to an acceptor fluorophore (often these are spectral variants of the green fluorescent protein, GFP) bound to a detector molecule, in this case, a cyclic nucleotide binding domain (CNBD). Being a dipole-dipole interaction, the energy transfer efficiency (E) is highly dependent on the distance between donor-acceptor (R) and the relative orientation (angle) of the dipole moments of the fluorophores (K^2). Therefore, FRET can be modulated by changes in the conformation of the protein to which the fluorophores are bound, if this change affects the distance and orientation between the two fluorophores.

The energy transfer efficiency (E), as described in equation 1 (Figure 4.1), varies as the sixth power of the distance between the fluorophores and become negligible as they are separated by more than 10nm (Machado and Pantano 2015; Piston and Kremers 2007). The Föster radius (R_0) can be defined based on equation 2 (Figure 4.1) where R_0 is dependent of the quantum yield (Q_d) of the donor fluorophore, the refractive index of the medium (n) which is generally taken as 1.4 in aqueous solutions, and the integral (J) of the emission spectrum overlap, which changes according to the fluorophore pair used in FRET- sensor (Machado and Pantano 2015; Wu and Brand 1994).

The emission spectrum overlaps integral J, described in equation 3 (Figure 4.1), represents the degree of overlap between the spectrum of donor fluorescence emission ($F_D(\lambda)$), and the acceptor excitation spectrum, ($E_A(\lambda)$). A high quantum yield donor, as well as a high absorbing acceptor and significant overlap in the fluorophores spectra (at least 30%), are requirements to achieve a robust FRET signal (Piston and Kremers 2007; Stangherlin 2010).

Figure 4.1. FRET equations

Equation 1 $$E=\left[1+\left(\frac{R}{R_0}\right)^6\right]^{-1}$$

Equation 2 $$R_0= 9.78 \cdot 10^3 \cdot (Q_d K^2 n^{-4} J)^{1/6}$$

Equation 3 $$J(\lambda) = \int F_D(\lambda) \cdot E_A(\lambda) \cdot \lambda^4 \, d\lambda$$

Figure 4.1.
Equation 1) FRET efficiency; Equation 2) Föster radius equation; 3) Emission spectrum overlap integral (J) equation.

As the FRET efficiency highly depends on the donor-acceptor distance, FRET- based sensors must include a binding domain which acts as a transducer by undergoing a

conformational transition in respond to a specific molecular event, such as the CNBD on binding of a cyclic nucleotide, as well as an appropriate pair of spectral variants of GFP, that act as the donor-acceptor FRET fluorophores, fused to the CNBD, or (Machado and Pantano 2015). With this configuration, binding of the cyclic nucleotide leads to a change in protein conformation, which affects the distance between the GFPs and modulates the degree of FRET. From this the cAMP/cGMP concentration can be inferred.

Figure 4.2. FRET sensor

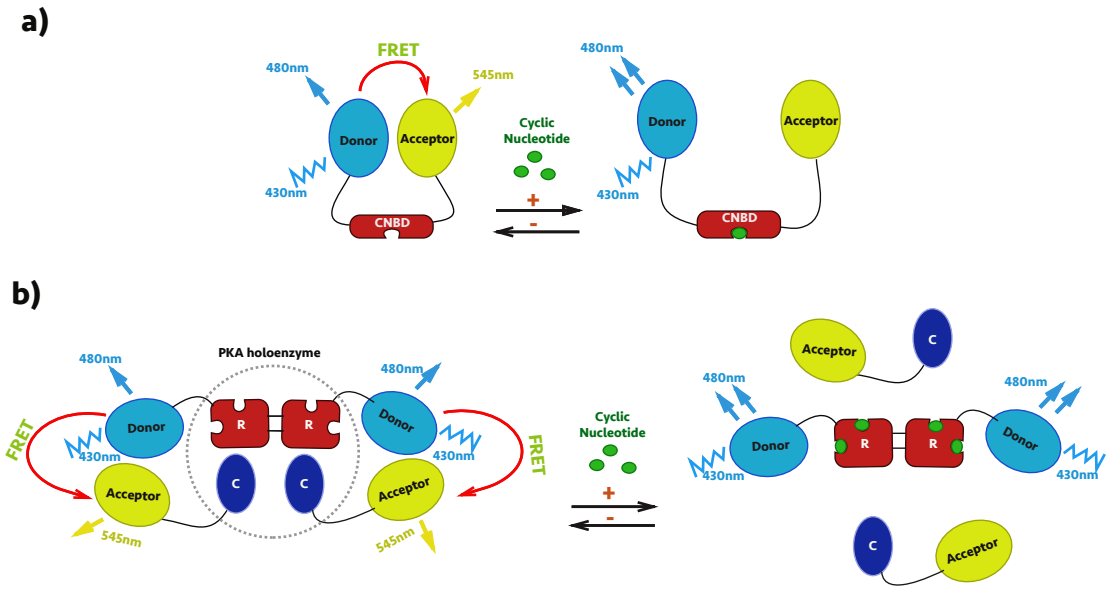


Figure 4.2.
a) Schematic of the structure and mechanism of action of unimolecular FRET-based sensor; b) Schematic of the structure and mechanism of action of multimolecular (PKA-based) FRET sensor. In the absence of cyclic nucleotide, the conformation of the sensor allows donor and acceptor to be in close proximity and FRET occurs. Upon excitation at 430nm (CFP excitation peak), part of the excited energy of the donor is transferred by resonance to the acceptor, which becomes excited. Both emissions (480nm for CFP and 535nm for YFP) can be recorded. With the increase of cyclic nucleotide and consequent binding to the cyclic nucleotide binding domain (CNBD), a conformational change moves the two fluorophores apart and FRET can no longer occur. Abbreviations: CNBD: cyclic nucleotide binding domain; FRET: Fluorescent resonance energy transfer; R: PKA regulatory subunit; C: PKA catalytic subunit.

4.1.3. FRET- based sensors

A number of genetically encoded sensors based on FRET have been developed to detect changes in cyclic nucleotides. Some of them will be discussed below.

a) cAMP FRET-based sensors

cAMP FRET-based methods have been generated since 1991 when Adams and colleagues developed the first sensor named FICRhR. This sensor is based on PKA and the on *in vitro* labelling of the PKA regulatory subunit (R) with rhodamine, and the catalytic subunit (C) with fluoresceine (Adams and Harootunian 1991). FRET occurs in the absence of cAMP, as the subunits are associated into a tetramer (R_2C_2) and the dyes are in close proximity. However, when cAMP is present, it binds to the regulatory subunits dissociating the tetramer structure, consequently separating the labelled subunits and impeding FRET to happen. Although this method was used in several studies (Bacskai et al. 1993; DeBernardi and Brooker 1996; Goaillard, Vincent, and Fischmeister 2001), limitations and technical difficulties such as the need to microinject micromolar concentrations of the purified labelled proteins into living cells, restricted its use for wider applications (Sprenger and Nikolaev 2013; Goaillard, Vincent, and Fischmeister 2001).

In 2000, Zaccolo et al. developed the first genetically encoded cAMP FRET probe based on PKA and green fluorescent protein (GFP) mutants where the RII subunit of PKA (regulatory subunit of the PKA type II) was fused with ECFP and the catalytic subunit to EYFP (R-CFP/C-YFP sensor) (Zaccolo et al. 2000). By using this sensor, it was possible to detect, for the first time, cAMP at microdomains in rat neonatal cardiac myocytes (NRCMs). PKA RII subunits bind to endogenous AKAPs located in proximity of the Z-lines, therefore, this sensor is targeted, showing a striated pattern in the cell, and allows monitoring of cAMP in this specific intracellular location. Additionally, experiments

using this sensor showed the role of specific PDE isoforms, in particular PDE3 and PDE4, in shaping intracellular cAMP signalling (Zaccolo et al. 2000; Mongillo et al. 2004). Despite the substantial improvement when compared to the FICRhR, the R-CFP/C-YFP sensor still presented limitations which had to be resolved. These were: First, the labelled C and R subunits were expressed in cells after co-transfection with two distinct plasmids. This technical step added difficulty to assure that equal concentrations of both subunits were expressed in the cells. Second, the kinetics of the sensor could be slower than the real cAMP kinetics as the cAMP-dependent dissociation of R and C subunits happens via a cooperative mechanism (Taylor et al. 2005). Lastly, the active catalytic subunit is able to phosphorylate PDEs, ACs and other downstream targets, potentially affecting cAMP levels (Stangherlin 2010). Variations of this PKA-based sensor have been developed with the aim to improve its dynamic range (Lissandron et al. 2005) and affinity (Zawadzki and Taylor 2004). However, due to the limitations listed above, subsequent work led to the development of unimolecular probes based on the protein exchange factor directly activated by cAMP (EPAC).

The structure of EPAC, a guanine nucleotide exchange factor (GEF) for the small GTPase proteins Rap1 and Rap2, contains a cyclic nucleotide binding domain and a regulatory domain (*Ras exchange motif*, REM) which is self-inhibitory. EPAC folds itself in an inactive form when cAMP levels are low, preventing the binding of Rap to the GEF domain at the C-terminus, and unfolds itself with the binding of cAMP to the binding domain (Gesellchen et al. 2011). A number of different sensors exploiting the cAMP – EPAC binding properties were generated in 2004 (Nikolaev et al. 2004; Ponsioen et al. 2004; DiPilato, Cheng, and Zhang 2004). The CFP-Epac-YFP sensor (Ponsioen et al. 2004) and the ICUE (*Indicator of cAMP using EPAC*) (DiPilato, Cheng, and Zhang 2004)

were designed by sandwiching the full length EPAC1 between CFP and YFP. The H30 sensor was developed by introducing mutations to the CFP-EPAC-YFP to make it catalytic inactive. Deletion of the EPAC DEP domain was also introduced to achieve a cytosolic version of the sensor (Ponsioen et al. 2004; Terrin et al. 2006). This probe presents faster activation kinetics and higher dynamic range than the PKA based sensors, however it displays lower affinity for cAMP.

Nikolaev et al. developed the first simplified class of unimolecular sensors based on the fusion of a single cAMP binding domain from either EPAC1 (EPAC1-camps), EPAC2 (EPAC2-camps) or PKA (PKA-camps) to CFP and YFP (Nikolaev et al. 2004). These sensors have the advantage of not containing catalytic and regulatory subunits, avoiding the possible interference of these with intracellular processes and displaying high temporal resolutions (Stangherlin 2010).

For the past decade, studies have been trying to improve and optimise FRET-based sensor for cAMP. Photophysics properties of the sensor, such as the photostability, sensitivity to microenviromental conditions, as the pH, Cl^- and UV light, and the folding efficiency at 37^oC are some of the primary considerations when designing a new sensor. Biological properties, such as the inert characteristic of the sensors, the lack of interference with cellular and protein function are also taken in consideration (van der Krogt et al. 2008).

The enhanced YFP has shown to be pH and Cl^- dependent (Jayaraman et al. 2000), therefore, substituting it with a more stable fluorophore was one of the rationales to further improve FRET-based sensors. Other improvements included: (1) minimise the

spectral overlap between donor and acceptor excitation, aiming to maximise FRET span, and (2) substitute the CFP for a brighter donor.

Jalink and colleagues tested several different combinations of fluorophores pairs in sandwich with the full length EPAC, including distinct dipole orientation mutants and duplicate acceptors (tandem) trying to achieve the above improvements.

After systematic comparison, a EPAC construct displaying a shorter linker between donor and acceptor and a tandem of the 173 venus circular permuted (cp^{173} Venus) as donor, yielded the largest improvement in the sensor dynamic range (van der Krogt et al. 2008). This sensor is described as CFP-EPAC-cp^{173}Venus-Venus.

Venus is a YFP variant with significant lower pKa, less pH sensitive and UV resistant (Nagai et al. 2002). Additionally, it increased the brightness of the acceptor channel by 10% and significantly improved the FRET efficiency compared to the initial sensor. The removal of 16 aa between donor and acceptor, not only brought both fluorophores closer together, but also diminished their rotational freedom (Evers et al. 2006; van der Krogt et al. 2008).

The addition of a circular permuted (cp) strongly affects the dipole orientation of the fluorophores as amino- and carboxyl termini of the acceptor is relocated to alternative locations on the surface of the FP barrel. In the case of the cp^{173}, the N-terminus is on the opposing side of the barrel (Nagai et al. 2004; Baird, Zacharias, and Tsien 1999). The final improvement step was done by adding a cp^{173} Venus tandem as the donor. The rationale was to increase the possibility of presenting acceptors at a favourable angle and increase FRET efficiency (van der Krogt et al. 2008).

In 2011, Jalink and colleagues developed the third-generation EPAC-based FRET sensors, mTurq-EPAC-cp^{173}Venus-Venus, also called ^{T}EPAC^{VV}(J. B. Klarenbeek et al. 2011). The substitution of the donor CFP fluorophore with mTurquoise substantially improved the FRET dynamic range, signal-to-noise ratio and photo stability of the CFP-EPAC-cp^{173}Venus-Venus sensor. This result is due to the doubled quantum efficiency of mTurquoise when compared to CFP and its single-exponential fluorescence decay (J. B. Klarenbeek et al. 2011).

A fourth-generation of EPAC-based sensors was developed in 2015 (J. Klarenbeek et al. 2015), where mTurquoise2 (Goedhart et al. 2012) was incorporated in pair with the tandem of the circular permutated version Venus. Additionally, a point mutation was added to EPAC, increasing its affinity for cAMP by 2 to 3-fold. Several combinations were tested and developed, however, the ^{T}EPAC^{VV,} or EPAC-S^{H188} (new nomenclature), continued to present the best performance, as well as its mutated version for high affinity, EPAC-S^{H187} (J. Klarenbeek et al. 2015).

In addition to directly detect levels of cAMP by using the FRET sensors mentioned above, the catalytic activity of PKA can also be investigated with temporal and spatial resolution by the use of the A-kinase activity reporter (AKAR) FRET sensors. There are four versions of AKAR sensors developed to date (AKAR1-4) (Zhang et al. 2001; Allen and Zhang 2006; Zhang et al. 2005; Depry, Allen, and Zhang 2011). Their structure contains a peptide that is a PKA substrate sequence and a phosphate-binding acceptor domain sandwiched between donor and acceptor fluorophores. The main difference between the AKARs is the donor and acceptor fluorophores pair which vary from eCFP or cerulean as donor, and YFP or venus as acceptor. The latest and improved version, AKAR4, uses

cerulean, a brighter version of CFP, and cpVenus as the FPs (Depry, Allen, and Zhang 2011).

Figure 4.3. cAMP FRET sensors

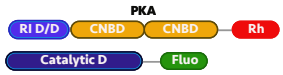
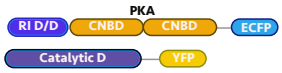
Sensor	Schematic structure	Sensor	Schematic structure
FICRhR		PKA-camps	
R-CFP/C-YFP		CFP-EPAC (ΔDEP-CD)- td cp173 Venus	
CFP-EPAC-YFP ICUE		mTurq-EPAC (ΔDEP-CD)- td cp173 Venus	
H30 CPF-EPAC (ΔDEP-CD)- YFP		H188 mTurq2Δ-EPAC (ΔDEP-CD)- td cp173 Venus	
EPAC-camps		H187 mTurq2Δ-EPAC (ΔDEP-CD-Q270E)- td cp173 Venus	

Figure 4.3.
cAMP FRET-based sensors. Name and schematic structure of the sensor design. Abbreviations: RI D/D: dimerization/ docking domain of PKA regulatory subunit type I; RII D/D: dimerization/ docking domain of PKA regulatory subunit II; Catalytic D: PKA catalytic domain; CNBD: cyclic nucleotide binding domain; Rh: rhodamine; Fluo: fluorescein; CFP: cyan fluorescent protein; YFP: yellow fluorescent protein; td cp^{173} venus: tandem of two circular permuted venus fluorescent protein; mTurq: monomeric Turquoise fluorescent protein; ΔDEP: deletion of the DEP domain to prevent membrane targeting; CD: catalytically dead mutant (T781A and F782A aa of Epac1 WT protein); Q270E: Q270E mutant for high cAMP affinity.

4.1.4. Measuring intracellular cGMP in live cells

Real time detection of cGMP occurred for the first time in 1998 with the use of genetically encoded cyclic nucleotide gate channels (CNGCs) (Trivedi and Kramer 1998). These channels contain a C-terminal cyclic nucleotide binding domain which is involved in regulation of the channel gating. For analysis of cGMP dynamics, these channels were genetically modified to be sensitive and selective for cGMP only (Goulding, Tibbs, and Siegelbaum 1994). After expressing this construct in cells, concentrations of cyclic

nucleotides can be inferred by monitoring the activity of the channel using real-time patch clamp techniques (Rich et al. 2000).

In 2008, Nausch and colleagues generated a range of non-FRET cGMP sensors called fluorescent indicators of cGMP, or FlincGs (Nausch et al. 2008). These sensors display a tandem PKG-I derived cGMP binding (cGKI) site fused to a single circular permuted GFP (cpGFP). Binding of cGMP to the cGMP binding domain, causes a conformational change on the GFP fluorophore changing its emission intensity. Different truncated PKG-I variants were used to generate three distinct versions of FlincG presenting different dynamic ranges, dissociation constant and selectivity (Stangherlin 2010; Nausch et al. 2008).

a) cGMP FRET sensors

Several cGMP FRET-based sensors have been generated to date. Most of them display one or two cGMP binding site sandwiched between CFP and YFP. Differently from the cAMP FRE-based sensors, where substantial work has been done to improve the efficiency of the sensors by modifying the donor – acceptor fluorophore pair, the main difference between the available cGMP sensors is the choice of binding domain (derived from PDEs or PKG).

The first successful cGMP FRET sensor, called CGY-Del 1, was developed in 2000 (Sato et al. 2000). This sensor displayed PKG Iα - Δ1-47, in which both cGMP binding domains (a and b) were present and the dimerization domain was deleted, sandwiched between ECFP and EYFP. Although this sensor showed an increase in FRET upon cGMP binding,

its use was limited as they presented low specificity to cGMP (Stangherlin 2010; Honda et al. 2001).

The Cygnet sensors (Honda et al. 2001), another set of cGMP FRET sensors based on PKG, were developed shortly after CGY-Del 1 became available. After testing several mutants of full length PKGIα, a construct displaying a N-terminus deletion (Δ1-77) and both binding domains, sandwiched between ECFP and EYFP successfully responded to increase in cGMP. This sensor was called Cygnet-1 (cGMP indicator using energy transfer). An improved version, Cygnet – 2, was generated by introducing a mutation, T516A, to make the construct catalytically inactive. This sensor was further modified by substituting EYFP for citrine, a pH insensitive version of YFP, and it was called Cygnet 2.1(Honda et al. 2001). Due to the small dynamic range and temporal resolution of these sensors, other groups attempted to generate improved versions by developing shorter cGMP sensors.

Nikolaev and colleagues generated the cGES series of cGMP sensors by sandwiching only one cGMP binding domain between CFP and YFP. cGES-GKI uses the cGMP binding domain B from PKG (cGKIB), whereas cGES-DE2 the GAF B domain from PDE2A and cGES-DE5, the regulatory GAF A domain from PDE5A (Nikolaev, Gambaryan, and Lohse 2006). From these three sensors generated, the one displaying the GAF A domain from PDE5A stood out by presenting high selectivity and time resolution (Sprenger and Nikolaev 2013). Later this sensor was modified by exchanging the YFP and CFP for T-Sapphire and Dimer 2 and generating a red version of the cGES-DE5 (Niino, Hotta, and Oka 2009). This approach led to an ~ 40-fold increase in the affinity

for cGMP and was used in the generation of a transgenic mouse model with cardiomyocyte- specific expression of cGMP-FRET (K. Götz et al. 2014).

Russwurm and colleagues generated three constructs that contain the tandem cGMP binding domain (a and b) from cGKI sandwiched between CFP and YFP (Russwurm et al. 2007). These sensors, called cGI-500, cGI-3000 and cGI-6000, cover a range of different $EC_{50,}$ 500nM, 3000nM and 6000nM, respectively. This difference is based on the different tandem cGMP binding domains. All three FRET-sensors showed to be successful in measuring intracellular cGMP dynamics due to their high selectivity, fast kinetics and greater dynamic range when compared to the other available sensors (Thunemann, Fomin, et al. 2013). The cGi500 sensor was later used to generate a mouse model expressing the sensor in cardiovascular tissue (Thunemann, Wen, et al. 2013).

Figure 4.4. cGMP FRET sensors

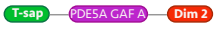
Sensor	Schematic structure	Sensor	Schematic structure
CGY-Del1		cGES-DE5	
Cygnet 1		red cGES-DE5	
Cygnet 2		cGi 500	
Cygnet 2.1		cGi 3000	
cGES-GKI		cGi 6000	
cGES-DE2		FlincG	

Figure 4.4.
cGMP FRET-based sensors. Name and schematic structure of the sensor design.
Abbreviations: cGKI BD: cGMP binding domain of cGMP-dependent protein kinase type I; CFP: cyan fluorescent protein; YFP: yellow fluorescent protein; cp GFP: circular permuted of green

fluorescent protein; T-sap: T-sapphire fluorescent protein; Dim 2: Dimer 2 fluorescent protein; T516A: mutation for catalytic inhibition; PDE2 GAF B: cGMP binding GAF B domain of phosphodiesterase 2; PDE5 GAF A: cGMP binding GAF A domain of phosphodiesterase 5; the number above the cGKI represent the first and last aa.

4.1.5. Targeted FRET-based sensors

As discussed in detail in the Introduction chapter, cyclic nucleotide signalling is compartmentalised and non-uniform within the cell. Both cAMP and cGMP present different dynamics, concentration and regulation at different subcellular locations or compartments. To explore such local fluctuations, targeting domains were added to many of the probes discussed above, localising the sensor to the specific cell compartment of interest. The first cAMP targeted sensors were generated by fusing sequences that target the plasma membrane, mitochondria or nucleus to the ICUE (N- or C-terminus) (DiPilato, Cheng, and Zhang 2004). The use of these sensors demonstrated different cAMP dynamics in the cytosol and plasma membrane upon β- adrenergic stimulation. Later, several other groups used a similar approach to target other sensors. For example, the plasma membrane and nucleus targeted H30 (Terrin et al. 2006), PKA type I and PKA type II (RI_EPAC and RII_EPAC, respectively) and targeted EPAC1-camps (Di Benedetto et al. 2008).

EPAC-camps sensors have been the main probe used for targeted analysis of cAMP signalling. It has also been targeted to PDE3/4 (Herget, Lohse, and Nikolaev 2008), Hsp20 (Sin et al. 2011), subsarcolemmal caveolae and associated with AC8 (Wachten et al. 2010). Data from these studies illustrated the contiguous domains of cAMP and the contribution of PDEs in the regulation of such compartmentalisation. However, the fusion of targeting domains to a FRET-based probe can substantially affect the characteristics of the sensor (Di Benedetto et al. 2008; Gesellchen et al. 2011), limiting the possibility to directly compare responses of sensors targeted to different subcellular compartments in the same cell (Surdo et al. 2017).

To overcome such drawback, Surdo et al. generated a novel set of FRET-based probes called CUTIe (cAMP Universal Tag for imaging experiments), which can potentially be targeted to any protein of interest without affecting the properties of the sensor. This probe was designed based on a novel topology: The YFP was moved from the N-terminus of the sensor and added within loop 4 -5 of the CNBD. In this way, insertion of a targeting domain to the N-terminus does not interfere with the FRET module and problems of steric hindrance are minimised (Surdo et al. 2017).

Figure 4.5. Structure of the different targeting strategies

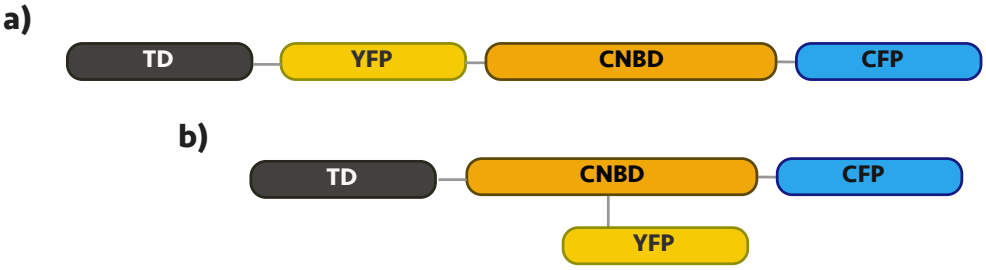


Figure 4.5.
a) Structure of traditional FRET-based sensor and targeting strategy; b) Structure of novel FRET- based sensor, CUTIe, and targeting strategy.

Although a large amount of work has been done to develop novel and improved tools to study compartmentalised cAMP signalling, not much has been developed for targeted cGMP signalling. Apart from some attempts, such as the targeting cGES-DE2 sensor to PDE5, most of the details on compartmentalised cGMP are inferred from cAMP-cGMP cross-talk experiments (Mongillo et al. 2006) or pharmacological approaches targeting different components of the pathway, such as NO-GC, NP receptors, and PDEs (K. Götz et al. 2014; Nagendran et al. 2007; Takimoto et al. 2005; Lee et al. 2015).

4.1.6 Calibration of FRET sensors

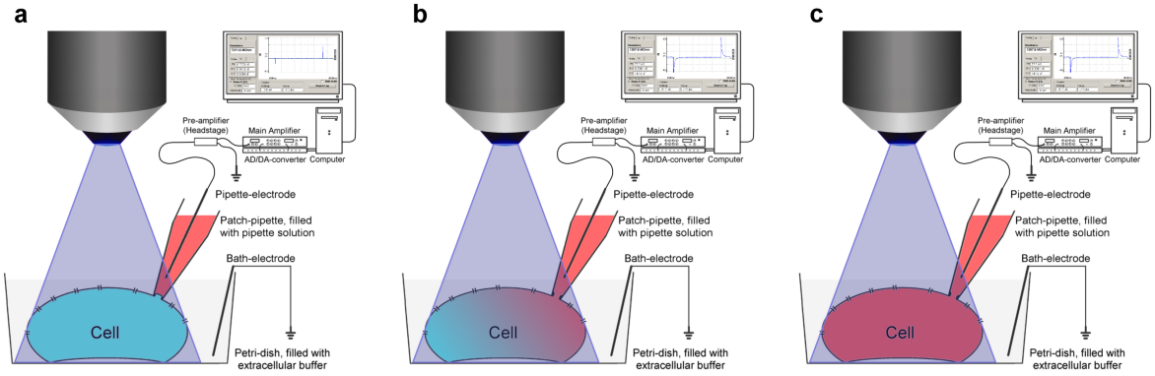
The ability to directly compare FRET responses between two or more different FRET probes (e.g. Cytosolic vs. targeted sensor) is crucial for appropriate analysis of compartmentalised signalling. As modifications implemented to target the probes often lead to a change on the sensor's performance, especially on the dynamic range and affinity, the direct comparison of responses achieved by each sensor can be challenging, and represent a substantive limitations for such studies (Sprenger et al. 2015; Di Benedetto et al. 2008; Surdo et al. 2017a). To overcome such issue, two different approaches have been taken. The first approach consists in the normalisation of the responses to the maximal response achieved at saturation, as for example obtained by high concentrations of Forskolin and IBMX. This is an effective approach if used to compare sensors presenting similar dose-response curves, affinity for the signal molecule and saturation levels. However, it should not be implemented otherwise as the results obtained might be misleading (Koschinski and Zaccolo 2015a). Another limitation of this approach is the difficulty to reach sensor saturation for the cGMP sensors, especially in cardiomyocytes. Reliable cGMP measurements in these cells have shown to be challenging due to the low cGMP concentrations and low sensitivity to most of available drugs and permeable cGMP analogues (K. R. Götz and Nikolaev 2013; K. Götz et al. 2014). The second approach is the construction of accurate dose-response calibration curves for each individual FRET-based sensor. Calibration of the sensors has shown to be a more robust method to compare responses between different probes as it allows the translation of percent of FRET-change into real cyclic nucleotide concentrations.

While in most published protocols such calibration is performed *in vitro* with known concentrations of cyclic nucleotide (Violin et al. 2008; Nikolaev et al. 2004; Russwurm

et al. 2007), Dr. Andreas Koschinski, a postdoctoral fellow in the Zaccolo group, developed an approach to calibrate the sensors 'in cell' (Koschinski and Zaccolo 2015b; Stangherlin et al. 2014; Surdo et al. 2017b), abolishing the limitations of the non-physiological *in vitro* methods which have been shown to significantly influence the performance of the sensor (Koschinski and Zaccolo 2015b).

Koschinski's method is based on a microinfusion technique where a combination of FRET-imaging and whole-cell patch-clamp is employed. CHO cells expressing the sensor are patched with a glass pipette filled with pH-matched intracellular solution containing known concentrations of cAMP or cGMP. After stablishing a tight connection between the pipette and the cell membrane, a direct flow between the cytosol and the intracellular solution in the pipette is achieved. The FRET sensor expressed in the patched cells responds to the specific concentration of cyclic nucleotide of the infused solution. The FRET change is recorded in real time throughout the whole duration of the experiment. An accurate calibration curve is constructed based on the data acquired from several cells and cyclic nucleotide concentrations. Apart from being the most physiological approach available to date, this approach has other advantages: It allows the measurement of total dynamic range of the sensor as it is possible to have a readout below the basal concentration of the cells by depleting the cytosol of cyclic nucleotide by infusing a solution with no cAMP or cGMP. Additionally, as mentioned before, this method can be applied to any type of sensor or signalling molecule (Koschinski and Zaccolo 2015b) and has been successfully applied in the characterisation of the novel CUTIe sensors (Surdo et al. 2017a).

Figure 4.6. Microinfusion technique - schematic of 'in cell' FRET sensor calibration



Koschinski, Andreas, and Manuela Zaccolo. "A novel approach combining real-time imaging and the patch-clamp technique to calibrate FRET-based reporters for cAMP in their cellular microenvironment." cAMP Signaling: Methods and Protocols (2015): 25-40.

Figure 4.6.
a) Cell is patched and a tight connection between the pipette and the cell membrane is stablished; b) Intracellular solution present inside the patch-pipette (volume is about 2 million times higher than cell volume) diffuses into the cell due to the cAMP concentration gradient; c) cAMP concentration equilibrates between cytosol and patch-pipette. The light coming from the objective represents the excitation of donor fluorophore. FRET is being recorded throughout the whole experiment.

4.2. AIMS OF THIS CHAPTER

The cyclic nucleotides signalling is known to be highly compartmentalised (Zaccolo 2011; McCormick and Baillie 2014) within the cardiac myocytes. Disruption of this compartmentalisation might lead to defective signalling and cell function (Zaccolo 2011). As the main aim of this thesis is to explore the dynamics of cAMP and cGMP in isolated cardiomyocytes of the mdx mice by using FRET, it was necessary to first construct the appropriate FRET-based probes. Therefore, the specific aim of this chapter is to demonstrate the development and strategy to construct cAMP and cGMP FRET-based probes targeted to the plasma membrane and to the outer mitochondria membrane. Furthermore, this chapter demonstrate an attempt in generating an improved version of the cGI500 sensor for measurement of cytosolic cGMP in cardiomyocytes and the characterisation and validation of these sensors.

Most of the microinfusion experiments and calibrations performed in this chapter were done in CHO cells. These cells are not as complex as cardiomyocytes, are easily cultured and transfected. Additionally, they present low basal levels of PDE activity, which reduces possible artefacts in the calibration measurements that may derive from partial hydrolysis of microinfused cyclic nucleotides (Koschinski and Zaccolo 2015b).

4.3. AN ATTEMPT TO FURTHER IMPROVE THE cGI500 FRET-BASED SENSOR

Initial FRET experiments in my project were performed using the cGMP sensor Cygnet 2.1, as this sensor was available in the lab and used previously by colleagues. However, this sensor did not show satisfactory performance as presented low dynamic range, quick saturation (shown in Figure 4.7) and pH sensitivity. The performance of Cygnet 2.1 in cardiomyocytes was assessed by performing experiments to evaluate the response of the sensor to cGMP and its dynamic range. Therefore, cardiomyocytes were treated with a membrane permeable cGMP analogue. As adult cardiomyocytes did not show consistent reactions to this treatment, the performance of the sensor was initially analysed in cultured neonatal rat cardiomyocytes. Figures 4.7a and 4.7b show representative recordings of these experiments. 20μM 8-Bromo-cGMP-AM was sufficient to reliably induce a FRET-change of about 18.6 ± 2.0% (n=6, SEM) (Figure 4.7c). As the addition of the PDE-inhibitor IBMX (100 μM) was unable to further increase the FRET change (19.5 ± 2.8%, n=6, SEM, p = 0.7, t-test) (Figure 4.7b and c) it was concluded that 20μM 8-Bromo-cGMP-AM is sufficient to saturate this sensor. Based on these experiments a maximal dynamic range of about 20% for the Cygnet 2.1 sensor could be defined.

As bath application of 8-Bromo-cGMP AM did not reliably induce FRET changes in adult mice cardiomyocytes expressing Cygnet, experiments in which these cells were

microinfused with known amounts of cGMP were performed (microinfusion technique described above). The mean FRET change upon 1 mM cGMP was 15.2 ± 2.2% (n=3, SEM). To evaluate that this change was due to the application of cGMP and not to nonspecific effects due to the technique we also performed control experiments with no cGMP in the pipette solution. As expected, the sensor showed a negative response, as in this case the basal intracellular cGMP diffuses out of the cell into the pipette and leads to a decreased intracellular concentration (Figures 4.7g and h).

Figure 4.7. Analysis of Cygnet 2.1 performance in cardiomyocytes

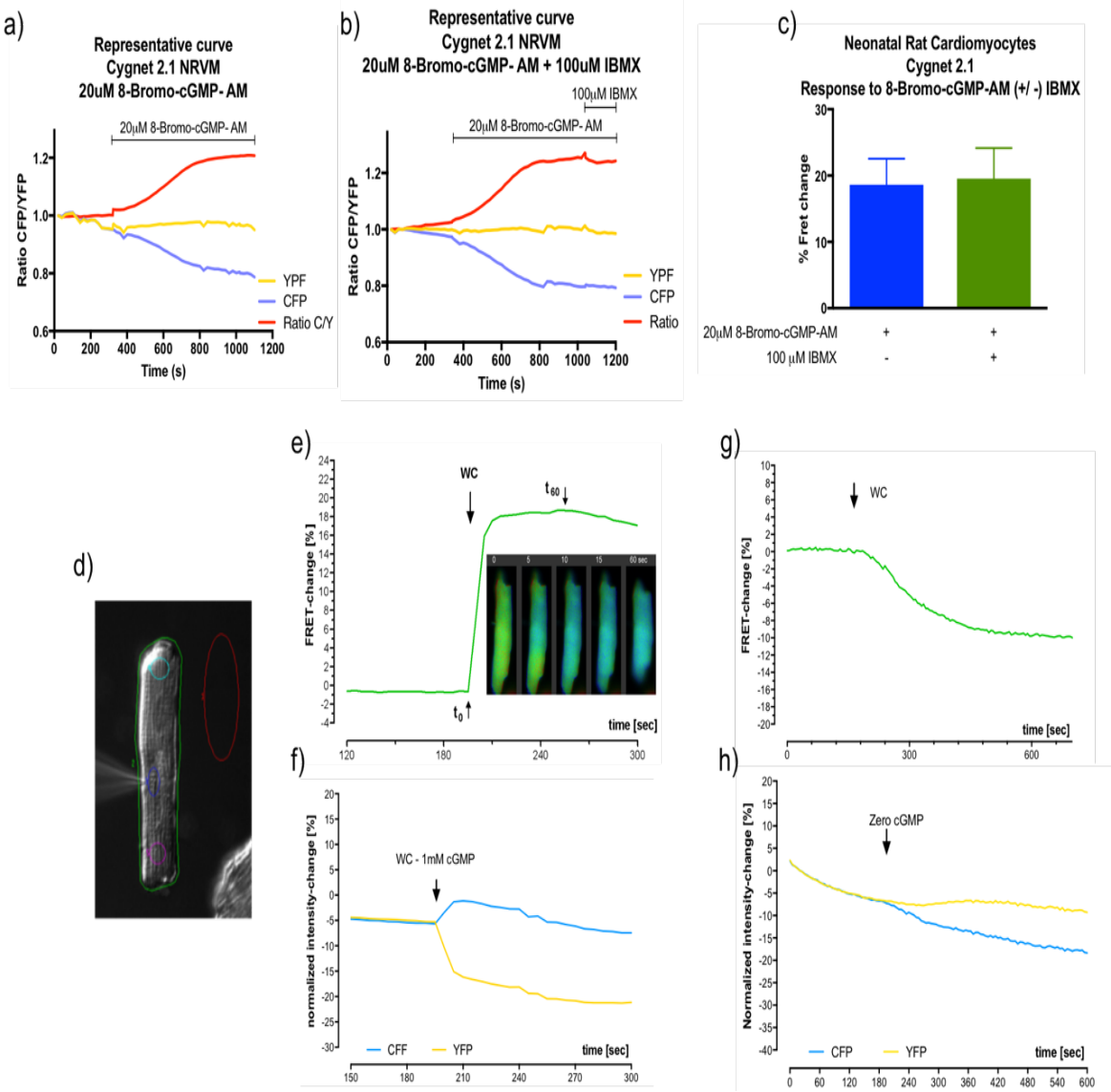


Figure 4.7.
a, b) Representative curves of response to 20μM 8-Bromo-cGMP-AM; b) with subsequent addition of 100 μM IBMX; c) Analysis of the effect of 20 μM 8-Bromo-cGMP-AM with and without IBMX. T-test, p= 0.7; d) Differential interference contrast (DIC) image of a patched cardiomyocyte; e) Representative FRET change curve (CFP/YPF) upon microinfusion with 1 mM cGMP. The insert shows a sequence of intensity modulated false colour images of this experiment, with green indicating a low, and blue a high cGMP concentration. The indicated time points t_0 and t_{60} correspond to the times the images of the sequence were acquired; f) Normalized YFP and CFP emission intensities of the same experiment; g) Representative FRET change curve (CFP/YFP) upon zero cGMP microinfusion; h) Normalized YFP and CFP emission intensities of the same experiment. "WC" indicates the establishment of the direct access to the cytosol and the start of the microinfusion.

Although this sensor shows a reasonable dynamic range, the difficulty to use it in reliably in adult cardiac myocytes was a clear limitation. As more recent versions of cGMP FRET reporters had become available (cGi500) and new designs for high-performing cyclic nucleotide sensors had been described (H187) it was decided to take advantage of these recent advances and attempt to generate an improved version of the cGMP reporter to use in my studies. Therefore, a new version of the cGi500 sensor was generated using the backbone of H187 EPAC sensor, which contains a mTurquoise2 and tandem circular permuted Venus (J. B. Klarenbeek et al. 2011). As this combination of fluorophores is significantly less pH sensitive, presents higher fluorescence intensities, dynamic range and has significantly improved the performance of the CFP-EPAC-YFP sensor, the rationale for the new sensor was to exchange the EPAC sequence for the cGMP binding domain tandem from cGKI present in the cGI500 sensor (Figure 4.8a), maintaining the fluorophore pair as in H187.

As shown in Figure 4.8b, the new sensor did not meet the expectations and showed reduced maximal FRET change when compared to the original cGi500. A possible explanation for this decrease in FRET efficiency is the change in distance and angle between donor and acceptor fluorophore. As the cGMP binding domain of cGI500 is substantially smaller than the full length EPAC present in the H187, the distance and

reciprocal orientation of the fluorophores may result sub-optimal in my engineered version. Possible solutions to this problem are the addition of linkers between the fluorophores and the binding domain, as well as the removal of one of the Venus moieties. However, as the outcome of these further modification was unpredictable and the fixed time was available for completion of my theses, alternative venues were not explored. The cGI500 was therefore chosen to continue the development of the project.

Figure 4.8. An attempt to further improve the cGI 500 sensor

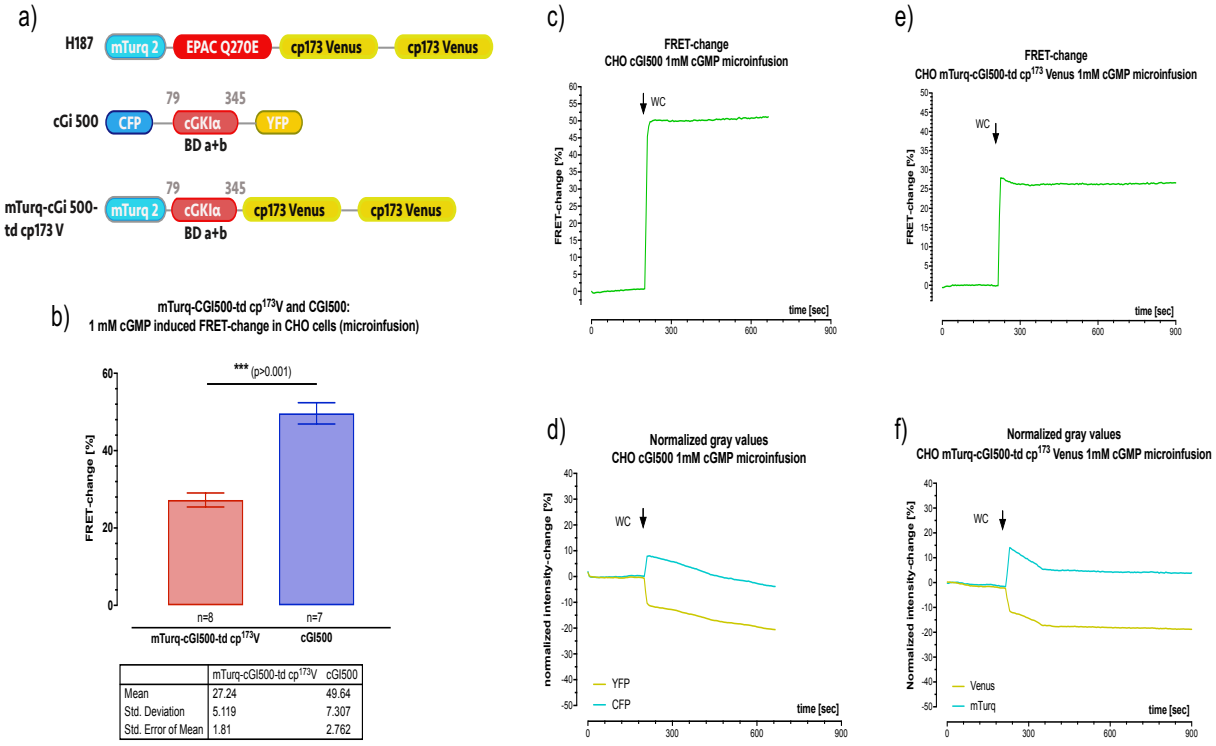


Figure 4.8.
a) Structure of the sensors H187 and cGI500 used for the generation of the mTurq-cGI500-td cp^{173} venus; b) Analysis of the effect of 1mM cGMP microinfused into CHO cells expressing either the original cGI500 or the novel version. Graph show means of 7 to 8 cells per condition per animal; Error bars represent SEM; T-test, * = 0.05<p<0.01, ** = 0.01<p<0.001, ***= 0.001<p<0.0001, **** = p<0.0001; c) Representative FRET change curve achieved with 1mM cGMP microinfused into CHO cells expressing cGI500; d) Normalised gray values of YFP and CFP emission intensities related to the FRET change on c; e) Representative FRET change curve achieved with 1mM cGMP microinfused into CHO cells expressing mTurq-cGI500-td cp^{173} V; f) Normalised gray values of YFP and CFP emission intensities related to the FRET change on graph e. "WC" indicates the establishment of the direct access to the cytosol and the start of the microinfusion.

4.4. GENERATION OF TARGETED cGMP AND cAMP FRET-BASED SENSORS

The main aim of this thesis is to explore cGMP and cAMP signalling in the cytosol and subcellular compartments of cardiomyocytes derived from the MDX model. Due to the pathophysiology of the disease, two subcellular compartments, the plasma membrane and the outer mitochondria membrane, were selected for analysis. There are two reasons for this: First, mitochondria dysfunction has long been considered to be involved in the pathogenesis of the disease (Wrogemann and Pena 1976). Studies have shown that mitochondria from MDX mouse muscle present significant uncoupling of oxidative phosphorylation (reduction of P/O ratio), reduced maximal ATP synthesis capacity and 50% decreased activity of all respiratory chain-linked enzymes (Kuznetsov et al. 1998; Percival et al. 2012). Additionally, dystrophic muscle presents reduced density of the subsarcolemmal mitochondrial (SSM) pool as well as mislocalization, and diminished ATP availability which promotes cell death (Percival et al. 2012), and calcium-dependent necrosis through mitochondrial-dependent pathway (Millay et al. 2008). These data are evidence for the mitochondria dysfunction in the dystrophic muscle.

Most of these studies were performed in skeletal muscle and suggested that such dysfunction results from Ca^{2+} overload. However, nNOS-cGMP has emerged as a relevant pathway in DMD as there is evidence suggesting that it is disturbed in the absence of dystrophin (Brenman et al. 1995) and plays a role in mitochondrial biogenesis and function (Oldenburg et al. 2004; Miyashita et al. 2009; Nisoli et al. 2003). In addition, cAMP is also involved in the regulation of mitochondrial function, including oxidative phosphorylation and ATP synthesis (REF). Therefore, exploring cGMP and cAMP local signalling at the mitochondria in the MDX model could be a promising and interesting area of study.

Second, sarcolemma-associated nNOS is reduced in the absence of dystrophin. As discussed earlier, an important role of nNOS-derived NO is to stimulate sGC and generate cGMP. As cyclic nucleotide signalling is highly compartmentalised, one aim of my project was to understand whether the absence of dystrophin causes any disruption on the plasmalemma localised cGMP signalling, and how this could affect the pathway in other compartments of the cell, such as the cytosol. In addition, given the PDE-mediated interplay between cAMP and cGMP, analysis of cAMP dynamics at these sites was also pursued.

For the above-mentioned reasons, plasma membrane (PM) and outer mitochondria membrane (OMM) targeted FRET-based sensors were generated.

4.4.1. Cloning strategy

a) Plasma membrane cGMP and cAMP probes

The plasma membrane version of cGI500 was generated by fusing a short peptide corresponding to the N-terminal targeting signal from Lyn Kinase (Resh 1999) to the N terminus of the cGI500 sensor. This corresponds to a posttranslationally myristoylated and palmitoylated sequence which targets the protein to the plasma membrane. This peptide was already available in the lab and it was removed from other plasma membrane targeted sensors already available. The same approach was applied to generate the plasma membrane-targeted H187 and the localisation of both sensors was validated using confocal imaging and line fluorescence intensity with a plasma membrane marker (Figure 4.9).

Figure 4.9. Plasma membrane targeted FRET-based sensors

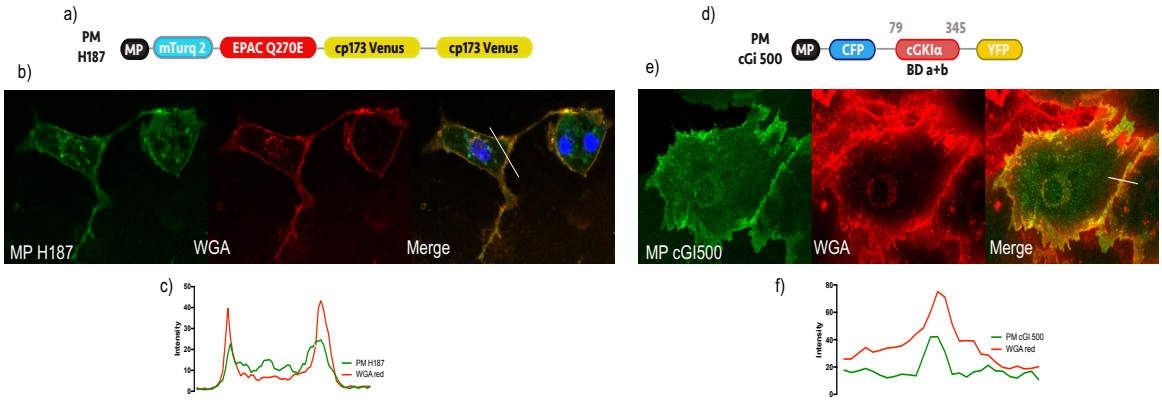


Figure 4.9.
a) Structure of PM H187 sensor; b) Confocal imaging of fixed neonatal cardiac myocytes expressing PM H187 (right panel), Wheat Germ Agglutinin (WGA) Alexa Fluor 594 for membrane staining (middle panel) and merge (left panel) showing the co-localization; c) Plot profile of PM H187 and WGA intensities at the location indicated by the white line on the merged image; d) Structure of PM cGi500 sensor; b) Confocal imaging of fixed neonatal cardiac myocytes expressing PM cGI500 (right panel), Wheat Germ Agglutinin (WGA) Alexa Fluor 594 for membrane staining (middle panel) and merge (left panel) showing the co-localization; c) Plot profile of PM cGI500 and WGA intensities at the location indicated by the white line on the merged image. MP is the abbreviation for MyrPalm.

b) Outer mitochondria membrane cGMP and cAMP probes

The outer mitochondria membrane version of the H187 had already been generated by a lab colleague, Dr. Kostantinos Lefkimmiatis (unpublished data) by fusing a mitochondria targeting peptide from the yeast translocase outer mitochondria membrane (OMM) protein TOM 70 (yTOM70) (Suzuki, Maeda, and Mihara 2002). This peptide will target the sensor to the outer mitochondria membrane facing the cytosol. As the OMM H187 sensor presents satisfactory localization and performance, the same sequence was fused to the N-terminus of the cGI500 and also mTurq-cGI500-td cp^{173}V (in short, ^{T}cGI^{VV}). The development of these constructs was done simultaneously with the experiments comparing the performance of both cytosolic sensors (discussed above – Figure 8). Even though the maximal FRET change was smaller in ^{T}cGI^{VV}, the fusion of the yTOM70 to this sensor displayed better localization and healthier mitochondria than the same fusion to the N-terminus of the traditional cGI500. As shown in Figures 4.10 d and f, the

expression of the OMM cGI500 sensor in CHO cells was well localized (co-localized with MitoTracker), however, resulted in damaged mitochondria (rounded and fragmented) whereas the expression the OMM ^{T}cGI^{VV} in CHO cells resulted in normal mitochondria morphology (typical elongated mitochondria). The localization of construct OMM ^{T}cGI^{VV} was also assessed in neonatal mouse cardiomyocytes (Figures 4.10 g and h). As the mitochondria in these cells are larger than in CHO cells, the expression of OMM ^{T}cGI^{VV} in combination with MitoTracker red staining shows clearly the localisation of the FRET sensor at the OMM compared to the dye in the matrix where MitoTracker binds to proteins by reacting with thiol groups and cysteine residues (Presley, Fuller, and Arriaga 2003) (Figures 4.10 g-i). .

Figure 4.10. Outer membrane mitochondria targeted FRET-based sensors

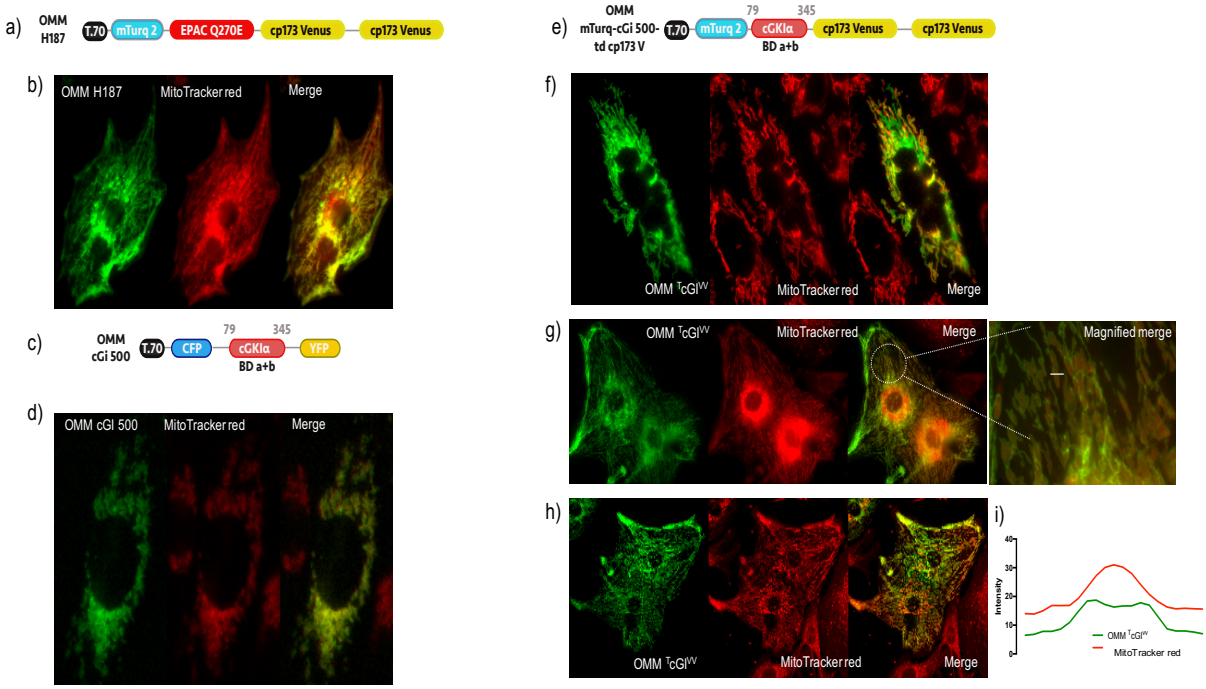


Figure 4.10.
a) Structure of OMM H187 sensor kindly provided by Dr. Kostantinos Lefkimmiatis; b) Imaging of live neonatal cardiac myocytes expressing OMM H187 (right panel), MitoTracker red for mitochondria matrix staining (middle panel) and merge (left panel) showing the co-localization; c) Structure of OMM cGI500 sensor; d) Imaging of live CHO cells expressing OMM cGI500 (right panel), MitoTracker red for mitochondria matrix staining (middle panel) and merge (left panel) showing the co-localization; e) Structure of OMM ^{T}cGI^{VV} sensor; f) Imaging of live CHO cells expressing OMM ^{T}cGI^{VV} (right panel), MitoTracker red for mitochondria matrix staining

(middle panel) and merge (left panel) showing the co-localization; g) Imaging of live neonatal cardiomyocytes expressing OMM ^{T}cGI^{VV} (right panel), MitoTracker red for mitochondria matrix staining (middle right panel) and merge (middle left panel) showing the co-localization, and magnified merge (left panel); h) Confocal imaging of fix neonatal cardiomyocyte expressing OMM ^{T}cGI^{VV} (right panel), MitoTracker red for mitochondria matrix staining (middle panel) and merge (left panel) showing the co-localization MP; i) Plot profile of OMM ^{T}cGI^{VV} and MitoTracker red intensities at the location indicated by the white line on the merged image. T.70 is the abbreviation for yeast TOM70, and OMM for outer mitochondria membrane.

4.5. CHARACTERIZATION OF THE NEW SENSORS

a) pH sensitivity

pH-measurements were performed in order to assess the pH sensitivity of the fluorophores constituting the newly developed FRET sensors. YFP is well known to be pH sensitive and the YFP variant named Venus is supposed to be less affected by the pH, as previously discussed. The experiments were performed by adding extracellular solutions at different pH to CHO cells expressing the FRET sensor and recording the FRET change after creating pores on the cells to equilibrate the intra and extra cellular pH. The pores were generated by addition of Nigericin and Valimomycin, as shown in Figure 4.11. Nigericin is an antiporter and builds up a new gradient for Potassium, as for every H+, one K+ is imported or exported from the cell. This gradient will build up contrary to the pH-gradient preventing more H+ to come in (or diffuse out) as there are very few active channels in CHO cells. Therefore Valinomycin, a potassium pore-forming reagent, is used to equalize and dissipate any potassium gradient.

The cGi500 FRET- reporter showed to be significantly pH sensitive, especially at pH < 7.2 (Figure 4.11b, c) whereas the OMM cGi500 H187 resulted to be less affected by the pH (Figure 4.11e). This data is not only relevant to the characterization of the new generated sensors but also to determine the intracellular pH of the cells by observing which pH did not cause a FRET- change as shown in Figure 11d. The intracellular pH of the cells is an important parameter to take in consideration when calibrating the sensors

using the microinfusion technique as the pH of the patch-pipet solution must perfectly match with the intracellular pH of the cells.

Figure 4.11. pH sensitivity the of sensors

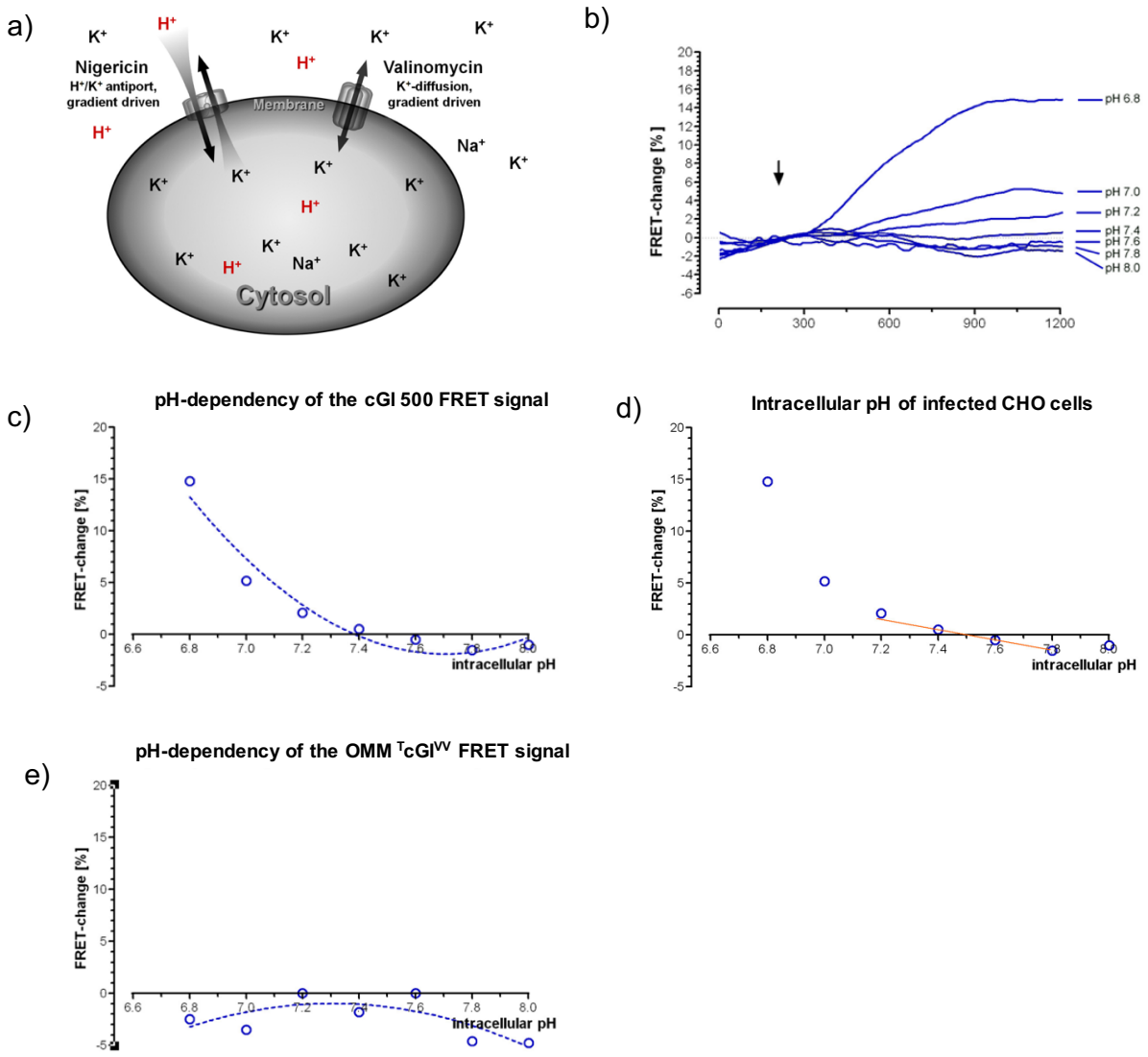


Figure 4.11.
a) Schematic of the role of Nigericin and Valinomycin on the pH dependency experiments. Image kindly provided by Dr. Andreas Koschinski; b) Single FRET-change curves of CHO cells expressing the cGi500 sensor related to each intracellular pH; c) Best fit curve of cGi500 FRET-sensor pH dependency; d) Measurement of CHO cells intracellular pH determination curve (orange line) by best fit curve crossing axis;.This panel shows the same curve presented in panel c, but highlights the X crossing point which refers to the intracellular pH e) Best fit curve of OMM ^{T}cGi500^{VV} FRET-sensor pH dependency.

b) Calibration curve

As previously discussed in this thesis, the calibration of FRET-sensors is a crucial part of the characterization of FRET reporters. The data allow the determination of the sensors EC50, Hill coefficient, sensitivity range and provide a calibration curve on the basis of which it is possible to assign FRET changes to actual concentrations of cyclic nucleotide. Although the microinfusion technique is the most physiological method to calibrate the sensors, it is very time consuming and technically demanding. For this reason, the calibration of these sensors was done only partially by microinfusion and partially by using a modified Saponin approach from Yang et al. (Yang et al. 2014).

Saponins, which derive their name from the Latin *sapone* or soap, are a group of natural compounds widely present in plants. they have the ability to precipitate cholesterol due to their lipophilic and hydrophilic portion (de Paula Barbosa 2014). Due to this lytic property, when applied in sufficient concentration, saponins create holes with variable sizes on the cell membrane (Glauert, Dingle, and Lucy 1962), providing a useful approach to achieve cell permeabilisation (Seeman 1967; Yang et al. 2014). For FRET-sensor calibration, CHO cells expressing the FRET probe under analysis were placed into a bath solution containing known amounts of cAMP or cGMP. Saponin was added to permeabilize the membrane allowing the entry of the cyclic nucleotide. FRET was recorded in real-time and for several different concentrations of cyclic nucleotide, enabling the construction of a concentration-dependency curve.

The main advantage of the Saponin calibration approach is the possibility to record several cells at the same time and generate the concentration-dependency curve relatively fast. By contrast, the microinfusion experiment allows analysis of a single cell at a time.

For the saponin method it is also necessary to systematically test for the optimal extracellular solution conditions, including its components and pH, as well as establish the appropriate concentration of saponin, as the commercially available substance does not contain a well-defined amount of saponins. Additionally, this approach might not be ideal for calibration of sensors targeted to the plasma membrane, as the action of saponins on the lipid bilayer of the membrane might affect the sensor.

Figure 4.12 demonstrate initial calibration data of the targeted sensors. CHO cells expressing the targeted probes (Figure 4.12a) were used to explore the dynamic range of the sensors and whether fusion of the targeting sequence affected the properties of the cytosolic version (Figure 4.12b and c). Although the calibration of these sensors was initiated by using the microinfusion approach (Figure 4.12d and e), it was finalised by using the saponin approach due to time restrictions. The saponin curves are presented in for the cytosolic cGI500 and plasma membrane cGI500 are available in Figure 4.12e.

Figure 4.12. Calibration of FRET-based sensors

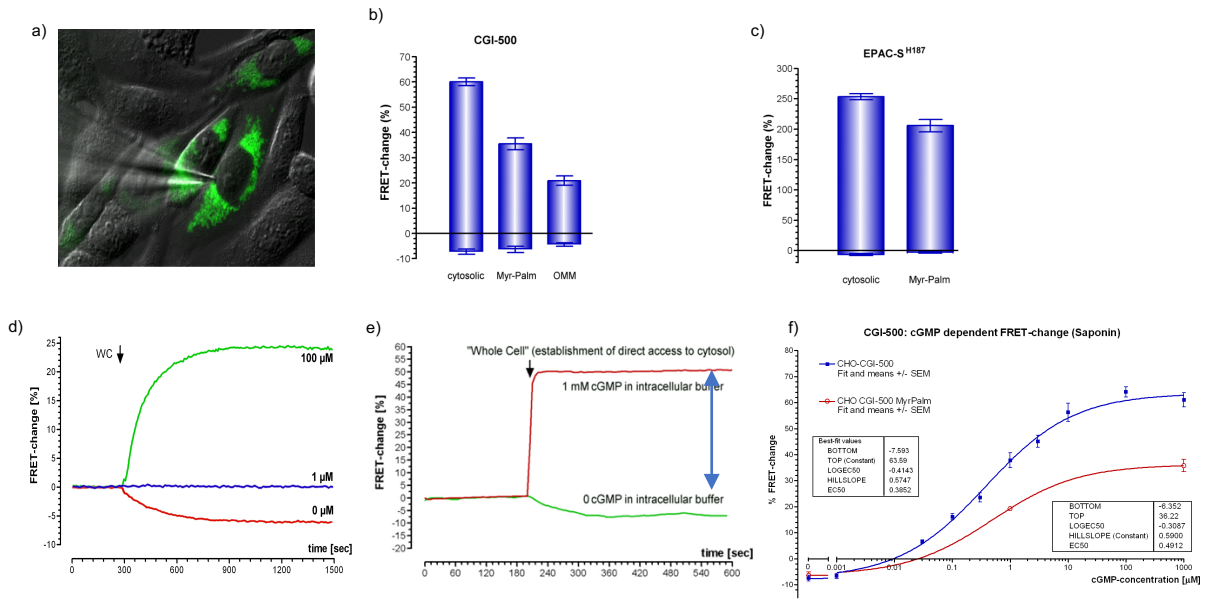


Figure 4.12.
a) Fluorescence image of patched CHO cell expressing OMM ^{T}cGi^{VV}; b) Dynamic range of cytosolic and targeted versions of cGI500 and (c) of the cytosolic H187 and targeted version. Data regarding the OMM H187 sensor is not available in this thesis as the experiments were performed by Dr. Lefkimmiatis. Dynamic range was calculated by adding the mean value of the negative FRET-change at permeabilization (CGI500 cytosolic) or microinfusion (all other sensors) of 0 cGMP / cAMP to the mean value of FRET-change at saturating conditions (1mM cGMP / cAMP). According to the rules of error propagation, the errors of the respective means were added. d) Representative FRET response curves to different concentrations of cGMP illustrating how concentration dependency curve, or calibration curve is constructed; e) Representative FRET- curve in response to maximum stimulation, 1mM cGMP (red curve) and zero cGMP (green curve). Blue arrow represents the dynamic range of the sensor. f) Final concentration dependency calibration curve of cGI 500 and MP cGI 500- sensor illustrating the correlation of FRET-change and real cGMP concentration, and characterization of sensor. Construction of calibration curve was conducted in collaboration with Dr. Andreas Koschinski.

4.6. DISCUSSION AND CONCLUSIONS

Development of Föster resonance energy transfer (FRET) significantly improved the study of cyclic nucleotides signalling in living cells. To date, there is a vast range of FRET-based biosensors available for cAMP and cGMP detection in the cytosol as well as in subcellular compartments, allowing the analysis of the signalling path with high spatial and temporal resolution. A number of laboratories have been working on the generation of improved FRET-based sensors, especially for cAMP. The development of CUTIe (Surdo et al. 2017a) and the 4th generation EPAC sensors (J. Klarenbeek et al. 2015) are some of the most recent accomplishments in the field. Although several cGMP FRET probes have been developed, no targeted versions had been developed so far.

This chapter presented the results of the attempt to further improve the cGI 500 probe by changing its fluorophores. There is a large body of evidence indicating that donor-acceptor pair choice may significantly impact the performance of these sensors, by improving, and in some cases by reducing, FRET efficiency (Niino, Hotta, and Oka 2009; van der Krogt et al. 2008; J. B. Klarenbeek et al. 2011). Here, a simple approach was taken to implement the backbone of H187 (mTurquoise and td cp^{173} Venus) in the cGI 500 sensor. As shown here, this approach was not successful, supporting the fact that a

more systematic study, including the use of different joining linkers, will be required in order to improve performance.

The calibration of the FRET sensors is crucial for the direct comparison between responses achieved by two or more different sensors. As this thesis aims to compare the CN dynamics by using FRET- based sensors between two cell types, and not between two different sensors, the calibration of the sensors is not required to achieved reliable comparison. Nonetheless, it was important to characterize the new sensors developed to have a readout of the maximal FRET-change achieved by each of them. This is especially relevant for the cGMP sensors as it is difficult to reach maximal FRET changes with the available drugs in cardiomyocytes as there is no reliable saturating drug, such as the cocktail of Forskolin and IBMX, for cGMP. Furthermore, when completes, these calibration curves can be used to transform FRET-changes into real cyclic nucleotides concentration. Furthermore, this chapter presents a complete 'in cell' calibration curve for the cGI500 sensor, which was never published before. It is important to note that although this calibration curve presents similar maximal FRET-change to the reported value (Russwurm et al. 2007), the EC50 achieved by 'in cell' calibration was about half of the reported *in vitro*.

This chapter also demonstrated the successful targeting of cGMP and cAMP sensors to the plasma membrane and the outer mitochondria membrane. Although the fusion of the targeting domain significantly reduced the FRET efficiency and dynamic range, these sensors reliably detected cGMP at the specific compartments. FRET data using the targeted sensors, as well as the H187 and cGI500, in a comparison between WT and mdx cardiomyocytes will be presented in the next chapter.

4.7. REFERENCES

Adams, Stephen R, and Alec T Harootunian. 1991. “Fluorescence Ratio Imaging of Cyclic AMP in Single Cells.” *Nature* 349 (6311): 694.

Allen, Michael D, and Jin Zhang. 2006. “Subcellular Dynamics of Protein Kinase A Activity Visualized by FRET-Based Reporters.” *Biochemical and Biophysical Research Communications* 348 (2): 716–21.

Bacskai, Brian J, Binyamin Hochner, Martyn Mahaut-Smith, Stephen R Adams, Bong-Kiun Kaang, Eric R Kandel, and Roger Y Tsien. 1993. “Spatially Resolved Dynamics of cAMP and Protein Kinase A Subunits in Aplysia Sensory Neurons.” *SCIENCE-NEW YORK THEN WASHINGTON*- 260: 222–222.

Baird, Geoffrey S, David A Zacharias, and Roger Y Tsien. 1999. “Circular Permutation and Receptor Insertion within Green Fluorescent Proteins.” *Proceedings of the National Academy of Sciences* 96 (20): 11241–46.

Brenman, Jay E, Daniel S Chao, Houhui Xia, Ken Aldape, and David S Bredt. 1995. “Nitric Oxide Synthase Complexed with Dystrophin and Absent from Skeletal Muscle Sarcolemma in Duchenne Muscular Dystrophy.” *Cell* 82 (5): 743–52.

Brescia, Marcella, and Manuela Zaccolo. 2016. “Modulation of Compartmentalised Cyclic Nucleotide Signalling via Local Inhibition of Phosphodiesterase Activity.” *International Journal of Molecular Sciences* 17 (10): 1672.

Brooker, Gary, JF Harper, WL Terasaki, and RD Moylan. 1979. “Radioimmunoassay of Cyclic AMP and Cyclic GMP.” *Advances in Cyclic Nucleotide Research* 10: 1–33.

DeBernardi, Maria A, and Gary Brooker. 1996. “Single Cell Ca2+/cAMP Cross-Talk Monitored by Simultaneous Ca2+/cAMP Fluorescence Ratio Imaging.” *Proceedings of the National Academy of Sciences* 93 (10): 4577–82.

Depry, Charlene, Michael D Allen, and Jin Zhang. 2011. “Visualization of PKA Activity in Plasma Membrane Microdomains.” *Molecular bioSystems* 7 (1): 52–58.

Di Benedetto, Giulietta, Anna Zoccarato, Valentina Lissandron, Anna Terrin, Xiang Li, Miles D Houslay, George S Baillie, and Manuela Zaccolo. 2008. “Protein Kinase A Type I and Type II Define Distinct Intracellular Signaling Compartments.” *Circulation Research* 103 (8): 836–44.

DiPilato, Lisa M, Xiaodong Cheng, and Jin Zhang. 2004. “Fluorescent Indicators of cAMP and Epac Activation Reveal Differential Dynamics of cAMP Signaling within Discrete Subcellular Compartments.” *Proceedings of the National Academy of Sciences of the United States of America* 101 (47): 16513–18.

Evers, Toon H, Elisabeth MWM van Dongen, Alex C Faesen, EW Meijer, and Maarten Merkx. 2006. “Quantitative Understanding of the Energy Transfer between Fluorescent Proteins Connected via Flexible Peptide Linkers.” *Biochemistry* 45 (44): 13183–92.

Finn, John T, Maria E Grunwald, and King-Wai Yau. 1996. “Cyclic Nucleotide-Gated Ion Channels: An Extended Family with Diverse Functions.” *Annual Review of Physiology* 58 (1): 395–426.

Gesellchen, Frank, Alessandra Stangherlin, Nicoletta Surdo, Anna Terrin, Anna Zoccarato, and Manuela Zaccolo. 2011. “Measuring Spatiotemporal Dynamics of Cyclic AMP Signaling in Real-Time Using FRET-Based Biosensors.” *Receptor Signal Transduction Protocols: Third Edition*, 297–316.

Glauert, Audrey M, JT Dingle, and JA Lucy. 1962. “Action of Saponin on Biological Cell Membranes.” *Nature* 196 (4858): 953–55.

Goaillard, Jean-Marc, Pierre Vincent, and Rodolphe Fischmeister. 2001. “Simultaneous Measurements of Intracellular cAMP and L-type Ca2+ Current in Single Frog Ventricular Myocytes.” *The Journal of Physiology* 530 (1): 79–91.

Goedhart, Joachim, David Von Stetten, Marjolaine Noirclerc-Savoye, Mickaël Lelimousin, Linda Joosen, Mark A Hink, Laura Van Weeren, Theodorus WJ Gadella Jr, and Antoine Royant. 2012. “Structure-Guided Evolution of Cyan Fluorescent Proteins towards a Quantum Yield of 93%.” *Nature Communications* 3: 751.

Götz, Konrad R, and Viacheslav O Nikolaev. 2013. “Advances and Techniques to Measure cGMP in Intact Cardiomyocytes.” *Guanylate Cyclase and Cyclic GMP: Methods and Protocols*, 121–29.

Götz, Konrad, Julia Sprenger, Ruwan K Perera, Julia H Steinbrecher, Stephan E Lehnart, Michaela Kuhn, Julia Gorelik, Jean-Luc Balligand, and Viacheslav O Nikolaev. 2014. “Transgenic Mice for Real Time Visualization of cGMP in Intact Adult Cardiomyocytes.” *Circulation Research*, CIRCRESAHA-113.

Goulding, Evan H, Gareth R Tibbs, and Steven A Siegelbaum. 1994. “Molecular Mechanism of Cyclic-Nucleotide-Gated Channel Activation.” *Nature* 372 (6504): 369–74.

Herget, Sabine, Martin J Lohse, and Viacheslav O Nikolaev. 2008. “Real-Time Monitoring of Phosphodiesterase Inhibition in Intact Cells.” *Cellular Signalling* 20 (8): 1423–31.

Honda, Akira, Stephen R Adams, Carolyn L Sawyer, Varda Lev-Ram, Roger Y Tsien, and Wolfgang RG Dostmann. 2001. “Spatiotemporal Dynamics of Guanosine 3′, 5′-Cyclic Monophosphate Revealed by a Genetically Encoded, Fluorescent Indicator.” *Proceedings of the National Academy of Sciences* 98 (5): 2437–42.

Jayaraman, Sujatha, Peter Haggie, Rebekka M Wachter, S James Remington, and AS Verkman. 2000. “Mechanism and Cellular Applications of a Green Fluorescent Protein-Based Halide Sensor.” *Journal of Biological Chemistry* 275 (9): 6047–50.

Klarenbeek, Jeffrey B, Joachim Goedhart, Mark A Hink, Theodorus WJ Gadella, and Kees Jalink. 2011. “A mTurquoise-Based cAMP Sensor for Both FLIM and Ratiometric Read-out Has Improved Dynamic Range.” *PloS One* 6 (4): e19170.

Klarenbeek, Jeffrey, Joachim Goedhart, Aernoud van Batenburg, Daniella Groenewald, and Kees Jalink. 2015. “Fourth-Generation Epac-Based FRET Sensors for cAMP Feature Exceptional Brightness, Photostability and Dynamic Range: Characterization of Dedicated Sensors for FLIM, for Ratiometry and with High Affinity.” *PloS One* 10 (4): e0122513.

Koschinski, Andreas, and Manuela Zaccolo. 2015a. “A Novel Approach Combining Real-Time Imaging and the Patch-Clamp Technique to Calibrate FRET-Based

Reporters for cAMP in Their Cellular Microenvironment." *cAMP Signaling: Methods and Protocols*, 25–40.

———. 2015b. "A Novel Approach Combining Real-Time Imaging and the Patch-Clamp Technique to Calibrate FRET-Based Reporters for cAMP in Their Cellular Microenvironment." *cAMP Signaling: Methods and Protocols*, 25–40.

Krogt, Gerard NM van der, Janneke Ogink, Bas Ponsioen, and Kees Jalink. 2008. "A Comparison of Donor-Acceptor Pairs for Genetically Encoded FRET Sensors: Application to the Epac cAMP Sensor as an Example." *PloS One* 3 (4): e1916.

Kuznetsov, Andrey V, Kirstin Winkler, Falk Wiedemann, Peter von Bossanyi, Knut Dietzmann, and Wolfram S Kunz. 1998. "Impaired Mitochondrial Oxidative Phosphorylation in Skeletal Muscle of the Dystrophin-Deficient Mdx Mouse." *Molecular and Cellular Biochemistry* 183 (1–2): 87–96.

Lee, Dong I, Guangshuo Zhu, Takashi Sasaki, Gun-Sik Cho, Nazha Hamdani, Ronald Holewinski, Su-Hyun Jo, Thomas Danner, Manling Zhang, and Peter P Rainer. 2015. "Phosphodiesterase 9A Controls Nitric-Oxide-Independent cGMP and Hypertrophic Heart Disease." *Nature* 519 (7544): 472–76.

Lissandron, Valentina, Anna Terrin, Maddalena Collini, Laura D'alfonso, Giuseppe Chirico, Sergio Pantano, and Manuela Zaccolo. 2005. "Improvement of a FRET-Based Indicator for cAMP by Linker Design and Stabilization of Donor–acceptor Interaction." *Journal of Molecular Biology* 354 (3): 546–55.

Machado, Matías, and Sergio Pantano. 2015. "Structure-Based, In Silico Approaches for the Development of Novel cAMP FRET Reporters." *cAMP Signaling: Methods and Protocols*, 41–58.

McCormick, Kristie, and George S Baillie. 2014. "Compartmentalisation of Second Messenger Signalling Pathways." *Current Opinion in Genetics & Development* 27: 20–25.

Millay, Douglas P, Michelle A Sargent, Hanna Osinska, Christopher P Baines, Elisabeth R Barton, Grégoire Vuagniaux, H Lee Sweeney, Jeffrey Robbins, and Jeffery D Molkentin. 2008. "Genetic and Pharmacologic Inhibition of Mitochondrial-Dependent Necrosis Attenuates Muscular Dystrophy." *Nature Medicine* 14 (4): 442.

Miyashita, Kazutoshi, Hiroshi Itoh, Hirokazu Tsujimoto, Naohisa Tamura, Yasutomo Fukunaga, Masakatsu Sone, Kenichi Yamahara, Daisuke Taura, Megumi Inuzuka, and Takuhiro Sonoyama. 2009. "Natriuretic Peptides/cGMP/cGMP-Dependent Protein Kinase Cascades Promote Muscle Mitochondrial Biogenesis and Prevent Obesity." *Diabetes* 58 (12): 2880–92.

Mongillo, Marco, Theresa McSorley, Sandrine Evellin, Arvind Sood, Valentina Lissandron, Anna Terrin, Elaine Huston, Annette Hannawacker, Martin J Lohse, and Tullio Pozzan. 2004. "Fluorescence Resonance Energy Transfer–based Analysis of cAMP Dynamics in Live Neonatal Rat Cardiac Myocytes Reveals Distinct Functions of Compartmentalized Phosphodiesterases." *Circulation Research* 95 (1): 67–75.

Mongillo, Marco, Carlo G Tocchetti, Anna Terrin, Valentina Lissandron, York-Fong Cheung, Wolfgang R Dostmann, Tullio Pozzan, David A Kass, Nazareno Paolocci, and Miles D Houslay. 2006. "Compartmentalized Phosphodiesterase-2

Activity Blunts β-Adrenergic Cardiac Inotropy via an NO/cGMP-Dependent Pathway." *Circulation Research* 98 (2): 226–34.

Nagai, Takeharu, Keiji Ibata, Eun Sun Park, Mie Kubota, Katsuhiko Mikoshiba, and Atsushi Miyawaki. 2002. "A Variant of Yellow Fluorescent Protein with Fast and Efficient Maturation for Cell-Biological Applications." *Nature Biotechnology* 20 (1): 87–90.

Nagai, Takeharu, Shuichi Yamada, Takashi Tominaga, Michinori Ichikawa, and Atsushi Miyawaki. 2004. "Expanded Dynamic Range of Fluorescent Indicators for Ca2+ by Circularly Permuted Yellow Fluorescent Proteins." *Proceedings of the National Academy of Sciences of the United States of America* 101 (29): 10554–59.

Nagendran, Jayan, Stephen L Archer, Daniel Soliman, Vikram Gurtu, Rohit Moudgil, Alois Haromy, Chantal St Aubin, Linda Webster, Ivan M Rebeyka, and David B Ross. 2007. "Phosphodiesterase Type 5 Is Highly Expressed in the Hypertrophied Human Right Ventricle, and Acute Inhibition of Phosphodiesterase Type 5 Improves Contractility." *Circulation* 116 (3): 238–48.

Nausch, Lydia WM, Jonathan Ledoux, Adrian D Bonev, Mark T Nelson, and Wolfgang R Dostmann. 2008. "Differential Patterning of cGMP in Vascular Smooth Muscle Cells Revealed by Single GFP-Linked Biosensors." *Proceedings of the National Academy of Sciences* 105 (1): 365–70.

Niino, Yusuke, Kohji Hotta, and Kotaro Oka. 2009. "Simultaneous Live Cell Imaging Using Dual FRET Sensors with a Single Excitation Light." *PloS One* 4 (6): e6036.

Nikolaev, Viacheslav O, Moritz Bünemann, Lutz Hein, Annette Hannawacker, and Martin J Lohse. 2004. "Novel Single Chain cAMP Sensors for Receptor-Induced Signal Propagation." *Journal of Biological Chemistry* 279 (36): 37215–18.

Nikolaev, Viacheslav O, Stepan Gambaryan, and Martin J Lohse. 2006. "Fluorescent Sensors for Rapid Monitoring of Intracellular cGMP." *Nature Methods* 3 (1): 23–25.

Nisoli, Enzo, Emilio Clementi, Clara Paolucci, Valeria Cozzi, Cristina Tonello, Clara Sciorati, Renata Bracale, Alessandra Valerio, Maura Francolini, and Salvador Moncada. 2003. "Mitochondrial Biogenesis in Mammals: The Role of Endogenous Nitric Oxide." *Science* 299 (5608): 896–99.

Oldenburg, Olaf, Qining Qin, Thomas Krieg, Xi-Ming Yang, Sebastian Philipp, Stuart D Critz, Michael V Cohen, and James M Downey. 2004. "Bradykinin Induces Mitochondrial ROS Generation via NO, cGMP, PKG, and mitoK ATP Channel Opening and Leads to Cardioprotection." *American Journal of Physiology-Heart and Circulatory Physiology* 286 (1): H468–76.

Paula Barbosa, Antony de. 2014. "Saponins as Immunoadjuvant Agent: A Review." *African Journal of Pharmacy and Pharmacology* 8 (41): 1049–57.

Percival, Justin M, Michael P Siegel, Gary Knowels, and David J Marcinek. 2012. "Defects in Mitochondrial Localization and ATP Synthesis in the Mdx Mouse Model of Duchenne Muscular Dystrophy Are Not Alleviated by PDE5 Inhibition." *Human Molecular Genetics* 22 (1): 153–67.

Piston, David W, and Gert-Jan Kremers. 2007. “Fluorescent Protein FRET: The Good, the Bad and the Ugly.” *Trends in Biochemical Sciences* 32 (9): 407–14.

Ponsioen, Bas, Jun Zhao, Jurgen Riedl, Fried Zwartkruis, Gerard van der Krogt, Manuela Zaccolo, Wouter H Moolenaar, Johannes L Bos, and Kees Jalink. 2004. “Detecting cAMP-induced Epac Activation by Fluorescence Resonance Energy Transfer: Epac as a Novel cAMP Indicator.” *EMBO Reports* 5 (12): 1176–80.

Presley, Andrew D, Kathryn M Fuller, and Edgar A Arriaga. 2003. “MitoTracker Green Labeling of Mitochondrial Proteins and Their Subsequent Analysis by Capillary Electrophoresis with Laser-Induced Fluorescence Detection.” *Journal of Chromatography B* 793 (1): 141–50.

Prystay, Linda, Annie Gagne, Patricia Kasila, Li-An Yeh, and Peter Banks. 2001. “Homogeneous Cell-Based Fluorescence Polarization Assay for the Direct Detection of cAMP.” *Journal of Biomolecular Screening* 6 (2): 75–82.

Resh, Marilyn D. 1999. “Fatty Acylation of Proteins: New Insights into Membrane Targeting of Myristoylated and Palmitoylated Proteins.” *Biochimica et Biophysica Acta (BBA)-Molecular Cell Research* 1451 (1): 1–16.

Rich, Thomas C, Kent A Fagan, Hiroko Nakata, Jerome Schaack, Dermot MF Cooper, and Jeffrey W Karpen. 2000. “Cyclic Nucleotide–gated Channels Colocalize with Adenylyl Cyclase in Regions of Restricted cAMP Diffusion.” *The Journal of General Physiology* 116 (2): 147–62.

Russwurm, Michael, Florian Mullershausen, Andreas Friebe, Ronald Jäger, Corina Russwurm, and Doris Koesling. 2007. “Design of Fluorescence Resonance Energy Transfer (FRET)-Based cGMP Indicators: A Systematic Approach.” *Biochemical Journal* 407 (1): 69–77.

Sato, Moritoshi, Naoki Hida, Takeaki Ozawa, and Yoshio Umezawa. 2000. “Fluorescent Indicators for Cyclic GMP Based on Cyclic GMP-Dependent Protein Kinase Iα and Green Fluorescent Proteins.” *Analytical Chemistry* 72 (24): 5918–24.

Seeman, Philip. 1967. “Transient Holes in the Erythrocyte Membrane during Hypotonic Hemolysis and Stable Holes in the Membrane after Lysis by Saponin and Lysolecithin.” *The Journal of Cell Biology* 32 (1): 55–70.

Sin, YY, HV Edwards, X Li, JP Day, F Christian, AJ Dunlop, DR Adams, M Zaccolo, MD Houslay, and GS Baillie. 2011. “Disruption of the Cyclic AMP Phosphodiesterase-4 (PDE4)–HSP20 Complex Attenuates the β-Agonist Induced Hypertrophic Response in Cardiac Myocytes.” *Journal of Molecular and Cellular Cardiology* 50 (5): 872–83.

Sprenger, Julia U, and Viacheslav O Nikolaev. 2013. “Biophysical Techniques for Detection of cAMP and cGMP in Living Cells.” *International Journal of Molecular Sciences* 14 (4): 8025–46.

Sprenger, Julia U, Ruwan K Perera, Julia H Steinbrecher, Stephan E Lehnart, Lars S Maier, Gerd Hasenfuss, and Viacheslav O Nikolaev. 2015. “In Vivo Model with Targeted cAMP Biosensor Reveals Changes in Receptor-Microdomain Communication in Cardiac Disease.” *Nature Communications* 6: 6965.

Stangherlin, Alessandra. 2010. “Cyclic Nucleotide Signalling Interplay in Rat Neonatal Cardiac Myocytes: FRET-Based Targeted Biosensors Reveal Compartment-Specific Modulation of cAMP Levels by cGMP.”

Stangherlin, Alessandra, Andreas Koschinski, Anna Terrin, Anna Zoccarato, He Jiang, Laura Ashley Fields, and Manuela Zaccolo. 2014. “Analysis of Compartmentalized cAMP: A Method to Compare Signals from Differently Targeted FRET Reporters.” *Fluorescent Protein-Based Biosensors: Methods and Protocols*, 59–71.

Surdo, Nicoletta C, Marco Berrera, Andreas Koschinski, Marcella Brescia, Matias R Machado, Carolyn Carr, Peter Wright, Julia Gorelik, Stefano Morotti, and Eleonora Grandi. 2017a. “FRET Biosensor Uncovers cAMP Nano-Domains at β-Adrenergic Targets That Dictate Precise Tuning of Cardiac Contractility.” *Nature Communications* 8.

———. 2017b. “FRET Biosensor Uncovers cAMP Nano-Domains at β-Adrenergic Targets That Dictate Precise Tuning of Cardiac Contractility.” *Nature Communications* 8.

Suzuki, Hiroyuki, Maki Maeda, and Katsuyoshi Mihara. 2002. “Characterization of Rat TOM70 as a Receptor of the Preprotein Translocase of the Mitochondrial Outer Membrane.” *Journal of Cell Science* 115 (9): 1895–1905.

Takimoto, Eiki, Hunter C Champion, Diego Belardi, Javid Moslehi, Marco Mongillo, Evanthia Mergia, David C Montrose, Takayoshi Isoda, Kate Aufiero, and Manuela Zaccolo. 2005. “cGMP Catabolism by Phosphodiesterase 5A Regulates Cardiac Adrenergic Stimulation by NOS3-Dependent Mechanism.” *Circulation Research* 96 (1): 100–109.

Taylor, Susan S, Choel Kim, Dominico Vigil, Nina M Haste, Jie Yang, Jian Wu, and Ganesh S Anand. 2005. “Dynamics of Signaling by PKA.” *Biochimica et Biophysica Acta (BBA)-Proteins and Proteomics* 1754 (1): 25–37.

Terrin, Anna, Giulietta Di Benedetto, Vanessa Pertegato, York-Fong Cheung, George Baillie, Martin J Lynch, Nicola Elvassore, Anke Prinz, Friedrich W Herberg, and Miles D Houslay. 2006. “PGE1 Stimulation of HEK293 Cells Generates Multiple Contiguous Domains with Different [cAMP]: Role of Compartmentalized Phosphodiesterases.” *The Journal of Cell Biology* 175 (3): 441–51.

Thunemann, Martin, Natalie Fomin, Christian Krawutschke, Michael Russwurm, and Robert Feil. 2013. “Visualization of cGMP with cGi Biosensors.” *Guanylate Cyclase and Cyclic GMP: Methods and Protocols*, 89–120.

Thunemann, Martin, Lai Wen, Matthias Hillenbrand, Ioannis-Angelos Vachaviolos, Susanne Feil, Thomas Ott, Xiaoxing Han, Dai Fukumura, Rakesh K Jain, and Michael Russwurm. 2013. “Transgenic Mice for cGMP Imaging.” *Circulation Research*, CIRCRESAHA-113.

Trivedi, Bhavya, and Richard H Kramer. 1998. “Real-Time Patch-Cram Detection of Intracellular cGMP Reveals Long-Term Suppression of Responses to NO and Muscarinic Agonists.” *Neuron* 21 (4): 895–906.

Violin, Jonathan D, Lisa M DiPilato, Necmettin Yildirim, Timothy C Elston, Jin Zhang, and Robert J Lefkowitz. 2008. “β2-Adrenergic Receptor Signaling and

Desensitization Elucidated by Quantitative Modeling of Real Time cAMP Dynamics." *Journal of Biological Chemistry* 283 (5): 2949–61.

Wachten, Sebastian, Nanako Masada, Laura-Jo Ayling, Antonio Ciruela, Viacheslav O Nikolaev, Martin J Lohse, and Dermot MF Cooper. 2010. "Distinct Pools of cAMP Centre on Different Isoforms of Adenylyl Cyclase in Pituitary-Derived GH3B6 Cells." *J Cell Sci* 123 (1): 95–106.

Williams, Christine. 2004. "cAMP Detection Methods in HTS: Selecting the Best from the Rest." *Nature Reviews. Drug Discovery* 3 (2): 125.

Wrogemann, K, and SDJ Pena. 1976. "Mitochondrial Calcium Overload: A General Mechanism for Cell-Necrosis in Muscle Diseases." *The Lancet* 307 (7961): 672–74.

Wu, PG, and Ludwig Brand. 1994. "Resonance Energy Transfer: Methods and Applications." *Analytical Biochemistry* 218 (1): 1–13.

Yang, Yi, Tao Guo, Tetsuro Oda, Asima Chakraborty, Le Chen, Hitoshi Uchinoumi, Anne A Knowlton, Bradley R Fruen, Razvan L Cornea, and Gerhard Meissner. 2014. "Cardiac Myocyte Z-Line Calmodulin Is Mainly RyR2-Bound, and Reduction Is Arrhythmogenic and Occurs in Heart FailureNovelty and Significance." *Circulation Research* 114 (2): 295–306.

Zaccolo, Manuela. 2011. "Spatial Control of cAMP Signalling in Health and Disease." *Current Opinion in Pharmacology* 11 (6): 649–55.

Zaccolo, Manuela, Francesca De Giorgi, Charles Y Cho, Luxin Feng, Tom Knapp, Paul A Negulescu, Susan S Taylor, Roger Y Tsien, and Tullio Pozzan. 2000. "A Genetically Encoded, Fluorescent Indicator for Cyclic AMP in Living Cells." *Nature Cell Biology* 2 (1): 25–29.

Zawadzki, Kerri M, and Susan S Taylor. 2004. "cAMP-Dependent Protein Kinase Regulatory Subunit Type IIβ ACTIVE SITE MUTATIONS DEFINE AN ISOFORM-SPECIFIC NETWORK FOR ALLOSTERIC SIGNALING BY cAMP." *Journal of Biological Chemistry* 279 (8): 7029–36.

Zhang, Jin, Christopher J Hupfeld, Susan S Taylor, Jerrold M Olefsky, and Roger Y Tsien. 2005. "Insulin Disrupts [Beta]-Adrenergic Signalling to Protein Kinase A in Adipocytes." *Nature* 437 (7058): 569.

Zhang, Jin, Yuliang Ma, Susan S Taylor, and Roger Y Tsien. 2001. "Genetically Encoded Reporters of Protein Kinase A Activity Reveal Impact of Substrate Tethering." *Proceedings of the National Academy of Sciences* 98 (26): 14997–2.

Chapter 5. Analysis of compartmentalised cAMP and cGMP signalling in dystrophic cardiac myocytes

5.1. INTRODUCTION ON CYCLIC NUCLEOTIDES AND DUCHENNE MUSCULAR DYSTROPHY

5.1.1. cAMP and Duchenne Muscular Dystrophy

Far before the NO-cGMP pathway emerged as possible pharmacological target for DMD, groups started exploring changes on the cAMP-PKA pathway in human dystrophic muscle samples and other dystrophic cell types. This interest became greater shortly after studies suggested the involvement of plasma membrane defects in the pathogenesis of the disease.

Mawatari et al. observed in 1974 that adenylyl cyclase in human skeletal DMD muscle samples generated significantly less cAMP upon epinephrine and sodium fluoride than healthy muscle homogenates, however, did not show reduced basal activity. Interestingly, cAMP was found to be altered in most of the muscle diseases studied, however, in different ways. Duchenne muscular dystrophy skeletal muscles presented significant lower basal levels of adenylyl cyclase (AC), as well as lower fluoride-activated ACs and lower levels of phosphodiesterases (Canal, Frattola, and Smirne 1975). As the activity of lipase was found to be low in human DMD muscle, a study investigated whether low levels of cAMP could be an explanation as this second messenger is involved in the activation of lipase. The results were in agreement with the studies mentioned above, showing that the activity of AC was considerably reduced in Duchenne dystrophic muscle as the amount of cAMP produced upon stimulation was significant lower when compared to health muscle (Susheela et al. 1975).

At that time, apart from muscle cells, several experiments were done using erythrocyte. This cell type also presented biochemical abnormalities which were thought to be similar to the ones of symptomatic tissues (Mawatari, Schonberg, and Olarte 1976). Abnormalities in protein phosphorylation by PKA were found in membranes from DMD red blood cells and other muscular dystrophy diseases, such as the myotonic muscular dystrophy (MyD). While MyD samples showed reduced phosphorylation levels, the same proteins were found highly phosphorylated in samples from DMD patients and DMD carriers (Roses, Herbstreith, and Appel 1975). However, Fisher at el. did not confirm these result when performing a similar study a few years later, where they found that the phosphorylation levels of plasma membrane proteins from DMD erythrocytes were not differently from healthy patients (Fischer et al. 1978). In addition, while Mawatari et al. found that basal and stimulated AC activity levels were two to three times higher in erythrocyte membranes from DMD patients than controls (Mawatari, Schonberg, and Olarte 1976), in agreement with Roses et al. findings, no difference was found between the membranes from normal and DMD for adenylyl cyclase in Fisher's experiments (Fischer et al. 1978). The adenylyl cyclase activity again found was significantly higher in erythrocyte from dystrophic boys in another study (Wacholtz et al. 1979), which also reported that basal levels of the AC enzyme were different between adults and children patients. This is an important point as it suggests that controls and samples need to be age matched, and also that the signalling pathway is dynamic and undergoes changes from childhood to adulthood. However, others reported that the abnormalities found in muscle cells and erythrocytes were not present in DMD fibroblast. The crude homogenate, as well as the membrane- enriched fraction of these cells presented normal basal enzyme activity and normal response to catecholamines (Cerri, Willner, and Miranda 1982).

In spite of these somewhat contradictory findings, the majority of these studies concluded that endogenous protein kinase activity might be involved in the pathogenesis of DMD disease and in the membrane alterations observed. It was also suggested that the reason for the discrepancies found in the different cell type may be due to the difference in AC isoforms expressed in each tissue (Cerri, Willner, and Miranda 1982).

5.1.2. NO - cGMP and Duchenne Muscular Dystrophy

The link between the cGMP pathway and Duchenne Muscular Dystrophy was not established as a follow up to the experiments exploring the involvement of the cAMP pathway (discussed above). Although several groups continued to work towards gaining further understanding on the pathophysiology of the disease, the specific stream of research exploring cAMP signalling in dystrophic muscle seems to have suffered a deceleration after the mid 80s, as very few publications can be found since then.

No suggestions had been made regarding the possible involvement of cGMP until 1995 when Brenman et al. demonstrated that sarcolemmal nNOS is complexed with dystrophin in skeletal muscle, and, in the absence of dystrophin, it accumulates in the cytosol of human mdx skeletal muscle cells (Brenman et al. 1995). Even though the experimental data shows that nNOS accumulates in the cytosol, it was also demonstrated that overall levels of nNOS were significantly reduced in DMD tissues compared with normal human muscle, suggesting a decreased stability of nNOS in the cytosol (Brenman et al. 1995). A follow up study showed that nNOS localisation to the sarcolemma is mediated by direct binding of the enzyme to α-syntrophin, a protein that is part of the dystrophin complex, via a PDZ motif interaction (Brenman et al. 1996). The PDZ domain is a unique motif in the N-terminus of nNOS which binds to PDZ repeats in postsynaptic density 95 (Cho, Hunt, and Kennedy 1992), of α-syntrophin. Other proteins containing PDZ domains

might also be recruited to the dystrophin complex via association with the syntrophins, therefore the complex is likely to be different depending on the muscle type. Furthermore, in order to allow interactions with other PDZ proteins, a smaller fraction of α-syntrophin may be associated with nNOS in other muscle types (Brenman et al. 1996). The association of nNOS and eNOS to the plasma membrane happens through different mechanisms: nNOS, interacts via α-syntrophin as explained above, and eNOS via a myristoylation sequence present in its N-terminus in addition to posttranslational palmitoylation regulated by a specific agonist, bradykinin (Brenman et al. 1995).

Another study developed at a similar time, confirmed the absence of nNOS at the plasma membrane and low activity level of nNOS in DMD muscle, however it did not demonstrate the accumulation of the enzyme in the cytosol (Chang et al. 1996). As the study showed reduced levels of nNOS mRNA in DMD, the authors suggested that nNOS does not get redistributed from the sarcolemma to the cytosol and that the low nNOS levels are not simply due to the disturbed dystrophin complex, but also due to a defect on expression levels related to the disease (Chang et al. 1996). This evidence suggested a potential role for nNOS – NO signalling in the pathogenesis of Duchenne Muscular Dystrophy.

The localisation of NOS enzymes within the cell is crucial for their function. NO is a short-lived free radical, which is quickly oxidised, and presents limited diffusion in certain cell types. For example, the diffusion is cardiomyocytes is limited as these cells present high concentrations of myoglobin, which has affinity for NO and therefore can act as an effective scavenger for NO. In addition cardiac myocytes have high levels of superoxide anions (in disease states), which can react with NO limiting its bioavailability (Seddon, Shah, and Casadei 2007). Therefore, the close proximity of NOS to their

respective pool of effectors is necessary for achieving their specific effect within the cell (Zhang and Casadei 2012).

Although the association of nNOSμ, a muscle specific splice variant of nNOS (Silvagno, Xia, and Bredt 1996), with the dystrophin complex and sarcolemmal localisation is well established in skeletal muscle, in healthy heart nNOS localises mainly to the sarcoplasmic reticulum (SR) in co-localisation with the ryanodine receptor (RyR2), whereas only a small proportion is localised at the sarcolemmal membrane. However, eNOS and nNOS can translocate to different cellular compartment in certain disease states or in response to stimuli (Zhang and Casadei 2012). Sarcolemmal nNOS has been shown to be increased in a rat model of post-infarction LV remodelling (Damy et al. 2003), in failing human hearts (Damy et al. 2004) and in ischemia/reperfusion under β-adrenergic stimulation (Bendall et al. 2004). This increase has been suggested to protect the myocardium against excessive sympathetic stimulation by reducing phospholamban phosphorylation and impairing LV diastolic function (Carnicer et al. 2017).

As described in detail in the introduction chapter, nNOS, via generation of NO, activates the soluble guanylyl cyclase (sGC) to synthesise cGMP (Figure 5.1). Therefore, the defect found in nNOS levels and localisation in DMD could potentially affect the activity and compartmentalisation of its downstream effectors, such as the sGC, cGMP level, as well as the cGMP effectors and their intracellular role.

Several groups have been exploring the involvement of the NO-cGMP pathway in the cardiomyopathy of DMD, even though strong experimental data in support of nNOS in association with the dystrophin complex in the heart is lacking.

It has been demonstrated, however, that nNOS is in complex with α1-syntrophin and the sarcolemma Ca^{2+} / calmodulin-dependent ATPase (PMCA) in the heart (J. C. Williams et al. 2006) and also to be targeted to the sarcolemma by dystrophin spectrin-like repeats 16 and 17 scaffold for nNOS in skeletal muscle (Lai et al. 2009) . Controversially, a proteomics analysis published 6 years later did not find similar results. nNOS was not found in association with full length dystrophin and did not show co-localisation with dystrophin by immunostaining in cardiomyocytes, even though alpha-syntrophin was detected in the dystrophin IP experiment (Johnson et al. 2012; Ramachandran et al. 2013). This data supports the notion that the localisation of nNOS in cardiomyocytes is not primarily dependent on the association with α1-syntrophin at the dystrophin complex as it is the case in skeletal muscle. As discussed above, the main localisation of nNOS in cardiomyocytes is found at the SR (Xu et al. 1999). Others have also demonstrated nNOS association with mitochondria (Kanai et al. 2001).

In 1999, a study comparing the activity of each NOS isoform in the heart of mdx mice against age paired controls at 2, 6 and 12 months old, demonstrated that nNOS activity is significantly decreased in the mdx heart since earlier age, whereas eNOS activity is unchanged and iNOS activity was significantly increased in older mdx heart (Bia et al. 1999). The increase of iNOS activity is likely to be linked with the increase in intracellular Ca^{2+}, macrophage infiltration and inflammation, which are typical consequences of the remodelling associated with the cardiomyopathy (Bridges 1986; Bia et al. 1999). The same study also reported ECG abnormalities in MDX from 6 months onwards similar to abnormalities found in human patients (Bia et al. 1999). The overexpression of nNOS in dystrophin-deficient hearts has been shown to bring positive effects, especially in preventing fibrosis (Wehling-Henricks et al. 2005). The reduction in fibrosis

consequently resulted in other improvements related to cardiac function, such as the disappearance of the polyphasic R-waves previously observed in ECG, and the reduction of myocardial macrophage concentrations, suggesting that manipulation of cardiac NO production or pathway may provide therapeutic strategies to ameliorate the cardiomyopathy associated with DMD (Wehling-Henricks et al. 2005).

Additional supporting data on the mdx cardiomyopathy and the defect of the NO/cGMP pathway became available in 2007 when M. Khairallah et al. demonstrated significant metabolic, contractile and regulatory pathways alterations in perfused *ex vivo* hearts from 10-12 weeks old mdx mice (Maya Khairallah et al. 2007). Apart from reporting (I) a major shift in substrate selection from fatty acid to carbohydrate associated with higher oxygen consumption, (II) alterations in the mitochondrial citric acid cycle (CAC), (III) compromised cardiac contractile performance and efficiency and (IV) reduced cellular integrity, the work demonstrated that mdx hearts present increased expression of the atrial natriuretic peptide (ANP) gene as well as increased expression of the α1 subunit of the soluble guanylyl cyclase. Although overexpression of the ANP gene is a known marker of cardiac remodelling, the authors suggested that in this case the increase in DMD hearts might be a compensatory mechanism for the defective NO/cGMP signalling pathway as other study reported cardioprotective roles for natriuretic peptides under altered NO signalling (Woods 2004). The alterations found in CAC enzymes alone were not sufficient to explain the defects reported in this study; therefore, a defective NO pathway, which is known to play a crucial role in metabolism-contraction coupling (Recchia 2002), was thought to be partly responsible for the metabolic alterations in the mdx heart (Maya Khairallah et al. 2007).

A follow up work from the same authors used genetic and pharmacological approaches to test the hypothesis that defective on NO/cGMP pathway is involved in the early metabolic alterations, preceding overt cardiomyopathy, in mdx heart and whether the stimulation of cGMP production, downstream of NO generation, improves the contractile performance, energy metabolism, and sarcolemmal integrity (M Khairallah et al. 2008). Perfused ex vivo hearts from a genetic modified mdx mice overexpressing cardiomyocyte-specific guanylyl cyclase (mdx/$GC^{+/0}$) and consequent up-regulation of cGMP, presented similar values for several contractile parameters, such as left ventricular end-diastolic pressure, cardiac power and rate-pressure product; however, the authors found a remarkable ability to maintain contractile performance with age (from 12 to 20 weeks) when compared to the clear deterioration of mdx hearts. Furthermore, mdx/$GC^{+/0}$, presented significant lower levels of lactate dehydrogenase (LDH) release, which indicates reduced cardiomyocyte damage, and lower levels of cardiomyocyte sarcolemmal injury (determinate by Evans blue dye uptake), when compared to mdx. The pharmacological treatment of mdx hearts with the PDE5 inhibitor Sildenafil resulted in improved ability to sustain elevated heart rate in response to isoproterenol for longer period of time, while showing significantly less cardiomyocyte sarcolemma injury. Furthermore, Sildenafil treated mdx hearts presented significant lower levels of ANP mRNA, as well as lower levels of α1 subunit of soluble guanylyl cyclase when compared to untreated hearts (M Khairallah et al. 2008).

The impact of long-term administration of sildenafil on improving mdx cardiac dysfunction was further analysed by using echocardiography in young mice, before the development of cardiomyopathy, and in older mdx mice, after cardiomyopathy has developed. Results showed that young mdx chronically treated with sildenafil were able

to maintain a relatively normal myocardial performance index (MPI) with age, which is a sensitive measure of left ventricular systole and diastolic performance, suggesting that sildenafil can attenuate cardiomyopathy in mdx especially improving the diastolic dysfunction observed in mdx mice as early as 8 weeks old (Adamo et al. 2010). Additionally, sildenafil was also efficient in reversing left ventricular diastolic dysfunction in older animals which had already developed cardiomyopathy. Remarkably, the MPI improvement upon PDE5 inhibition was significant within three days of treatment and progressively deteriorated 10 days after sildenafil removal, suggesting that the positive effect achieved upon sildenafil is independent of long-term cardiac remodelling. These beneficial effects of chronic sildenafil treatment could be explained by the increased PKG protein expression and enhanced PKG-dependent phosphorylation of GSK-3B observed in the mdx hearts (Adamo et al. 2010). This PKG-dependent phosphorylation has been associated with benefits of sildenafil treatment in ischemia/reperfusion models of cardiac damage and decreased apoptosis, fibrosis and increased contractility. Furthermore, sildenafil was also found to prevent excessive mitochondrial permeability transition pore (PTP), mitochondrial oxidative stress and activation of cell death signalling present in young mdx hearts (Ascah et al. 2011).

A comparison between two months old mdx and mdx:utrophin$^{-/-}$ (double knockout for dystrophin and utrophin) hearts, showed that although the activity of nNOS was markedly decreased in both models, the expression of nNOS was only lower in mdx:utrophin-/- cardiomyocytes, suggesting that utrophin might have a role in maintaining the normal expression levels of nNOS but not its function (Ramachandran et al. 2013). This study also reported normal values of sGC protein and activity in both types of cardiomyocytes and suggested that the defective NO pathway found in mdx hearts does not affect the

downstream effectors but only upstream components, such as the L-arginine transporter (cationic amino acid transporters – CATs) which expression was found to be significantly increased (Ramachandran et al. 2013). These data, however, appear in contradiction with the studies mentioned above where the manipulation of cGMP levels significantly improved cardiac function in mdx. A possible explanation for such discrepancy is the fact that Ramachandran et al. measured the sGC expression and activity using tissue homogenates derived from the apices of the heart only and not from the whole ventricles. Furthermore, the nNOS data presented was acquired from isolated cardiomyocytes, however, it was not specified from which part of the heart these were originated from.

The vast majority of the data presented above provide strong evidence to support a disruption of the NO-cGMP pathway in mdx heart and importantly, that enhanced cGMP signalling results into significant cardiac function improvement. As it is a priority in the muscular dystrophy community to discover and optimise therapies for the associated cardiomyopathy, a clinical trial where sildenafil was administrated to DMD patients was established. Unfortunately, the results did not confirm the preclinical studies mentioned above. Even though the clinical trial was based on a very small sample size (6 patients only) and presented very high variability, extrapolated data suggest that significant positive result would not have been found even with a larger number of participants (Leung et al. 2014). A possible explanation for such result is that sildenafil might be able to inhibit other PDEs, such as PDE1. PDE1 hydrolyses cGMP and also cAMP, which may produce off-target side effects. This limitation of sildenafil was also discussed by others: as PDE1C is highly expressed in cardiomyocytes and vascular smooth muscle, its partial inhibition could have contributed to some of the cardioprotective effects of sildenafil described above (Adamo et al. 2010; M Khairallah et al. 2008).

A substantial limitation of most of these studies is the lack of data regarding other cGMP pathway regulatory mechanisms, such as the influence of the other cGMP hydrolysing PDEs and the compartmentalisation of the signalling. None of the studies explored the pathway at the cellular level. As the experiments were performed either in whole tissue lysates or perfused hearts, it is not clear whether defective NO-cGMP signalling is present in cardiomyocytes or other cell types present in the heart (Figure 5.2). The same is true for the sildenafil treatment applied to the heart: it is not possible to identify which cell type is mostly affected by the treatment and the mechanism responsible for the beneficial effects.

Figure 5.1. Schematic of cyclic nucleotide signalling in healthy cardiomyocyte

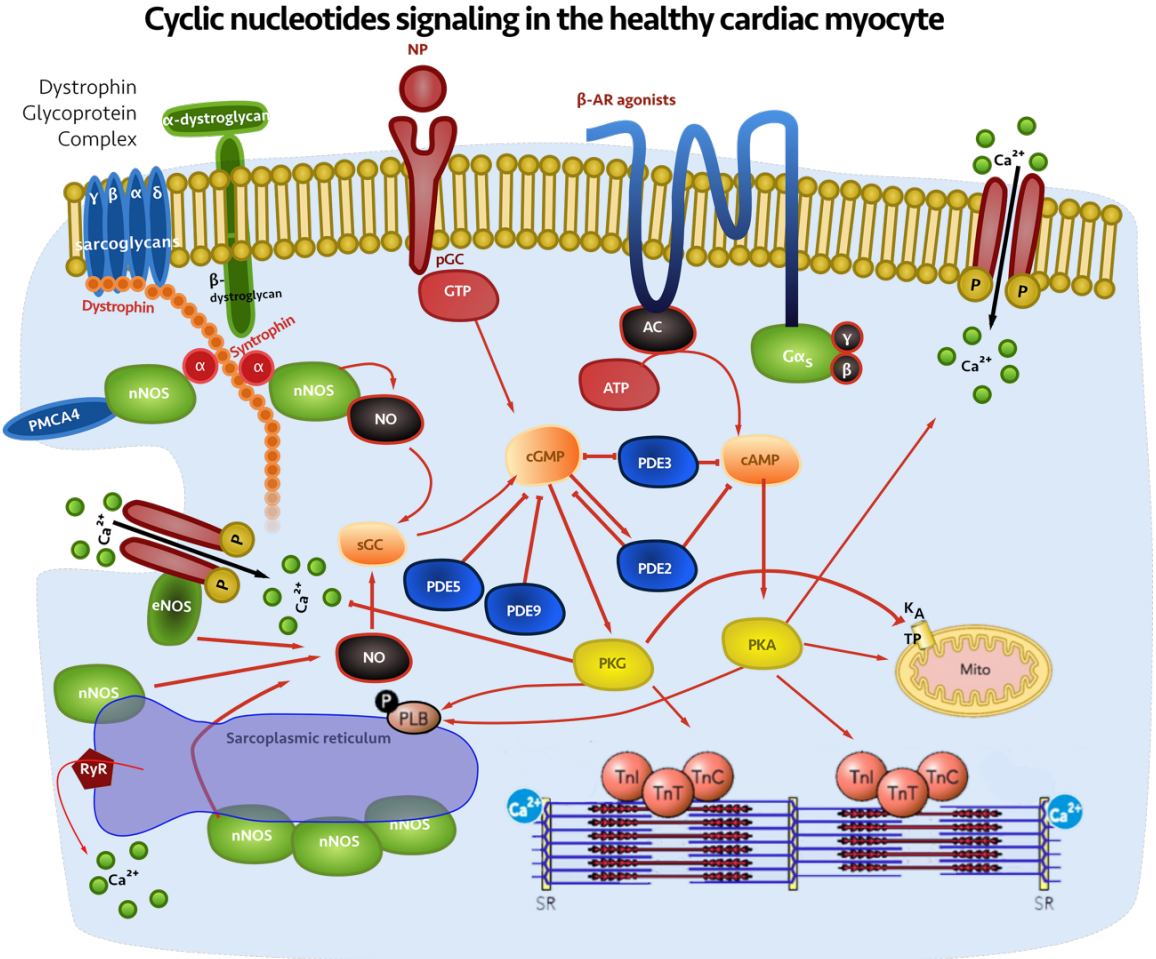


Figure 5.1.
Simplified schematic of cGMP and cAMP in cardiomyocytes in relationship with the dystrophin complex in healthy cardiomyocytes.

5.2. SPECIFIC AIMS

There is a clear need to elucidate the details of NO-cGMP signalling in DMD hearts, especially at the single cell level. Given the prominent role of cAMP in the regulation of heart function and its involvement in the pathogenesis of heart failure, the close connection with the cGMP pathway via a crosstalk system (Zaccolo and Movsesian 2007), and the initial work exploring cAMP-PKA signalling in DMD, the dynamics of cAMP signalling in the mdx model are also of relevance.

Compartmentalisation of cyclic nucleotide signalling is a well described phenomenon (detailed in the introduction chapter), that exists to ensure the appropriate interaction of second messenger molecules (cAMP and cGMP) with the appropriate effector proteins. Such functionality provides the cells with the ability to transform an extracellular stimulus into specific downstream events that lead to unique physiological outcomes. Compartmentalisation of cyclic nucleotide has been particularly dissected in the heart and its disruption is involved in cardiac dysfunction (McCormick and Baillie 2014; Conti, Mika, and Richter 2014; Brescia and Zaccolo 2016). Several studies have been trying to understand the spatial and temporal regulation and the organization of such compartments; however, details remain to be defined, especially regarding the cGMP signalling (Brescia and Zaccolo 2016). Imaging of cyclic nucleotides with FRET-based biosensors allows us to understand their levels and dynamics in living cells.

Figure 5.2. Hypothetical scenario of cGMP and cAMP signalling disruption in dystrophic cardiomyocytes

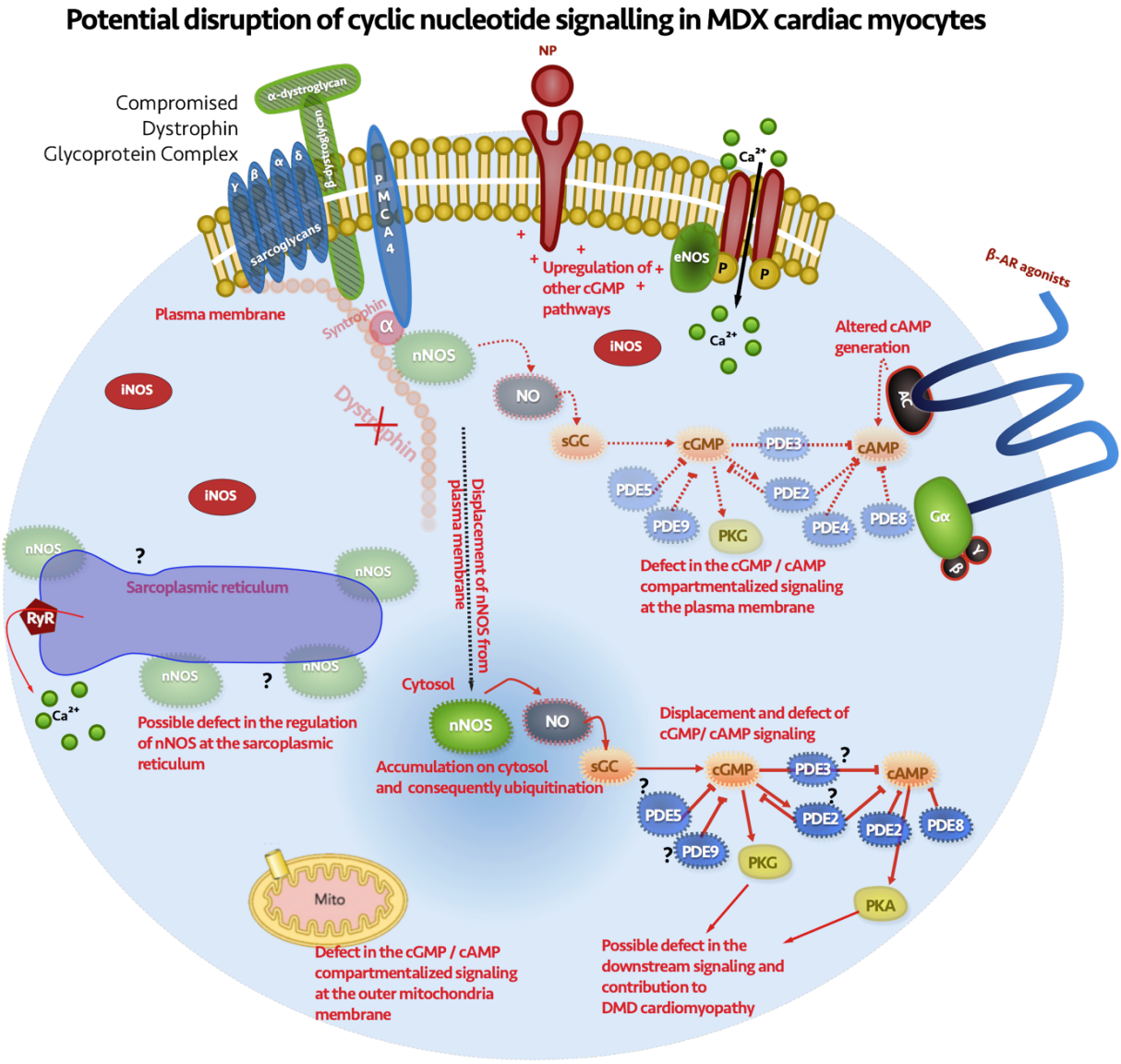


Figure 5.2.
Schematic of possible cAMP and cGMP scenario present in dystrophic cardiomyocytes where cGMP and cAMP regulation, as well as generation is affected at different subcellular compartments due to plasma membrane displacement and/or defects in regulatory mechanism and PDE activity.

Therefore, the main aims of these chapter are:

1) To explore local cGMP dynamics in cardiomyocytes from WT mice (C57BL/10ScSn) and MDX with the use of FRET technique and FRET-based sensors targeted to the

cytosol, plasma membrane and outer mitochondria membrane (discussed in detail in chapter 4).

2) To explore cGMP and cAMP interplay in these compartments and the role of PDEs in its regulation.

3) Explore other relevant components of the pathway, such as the different NOS isoforms, activity of sGC and redox state using biochemical approaches.

4) To establish whether there are age-related differences in the above.

5.3. RESULTS

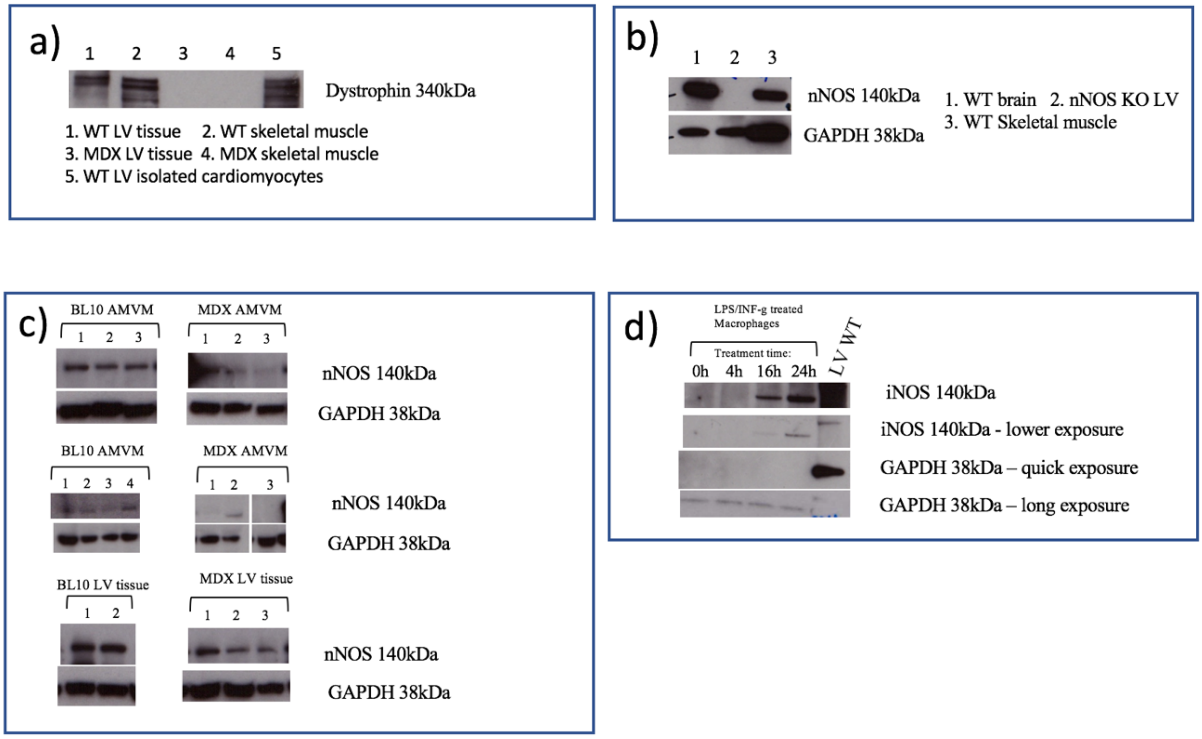
5.3.1. nNOS, eNOS and iNOS expression levels in specific cardiomyocyte compartments change with age

Although several studies have already reported the expression levels of the different NOS isoforms in mdx heart (as discussed earlier in this chapter) (Bia et al. 1999; Wehling-Henricks et al. 2005), most of these data derived from adult mice tissue homogenates. As the aim of this chapter is to analyse cGMP and cAMP signalling in different cellular compartments of isolated neonatal cardiomyocytes and adults (12 weeks old) it became important to stablish the level of expression of each NOS isoform in these cells and in the relevant sub cellular compartments. Available reports of such analysis were not found in the literature. Therefore, the protein expression of nNOS, eNOS and iNOS were determined by western blotting analysis in lysates of isolated cardiomyocytes, left ventricle (LV) tissue homogenates, as well as in the plasma membrane and sarcoplasmic reticulum fractions of cardiac myocytes from adult and neonatal hearts.

As shown in Figures 5.3 and 5.4, the results found in isolated cardiomyocytes from adult heart were in agreement with the majority of previous studies where nNOS expression was found to be significant lower in the mdx cardiomyocytes, whereas eNOS was

unchanged and iNOS was significantly higher. However, even though nNOS and iNOS presented similar trend, the statistical significance was lost when LV tissue homogenates were analysed. Surprisingly, the expression of eNOS was found to be significant lower in the mdx LV tissue compared to control suggesting the possibility that this difference might be due to increased expression of eNOS in other cell types present in the LV tissue, such as fibroblasts or endothelial cells.

Figure 5.3. nNOS, eNOS and iNOS Western blotting



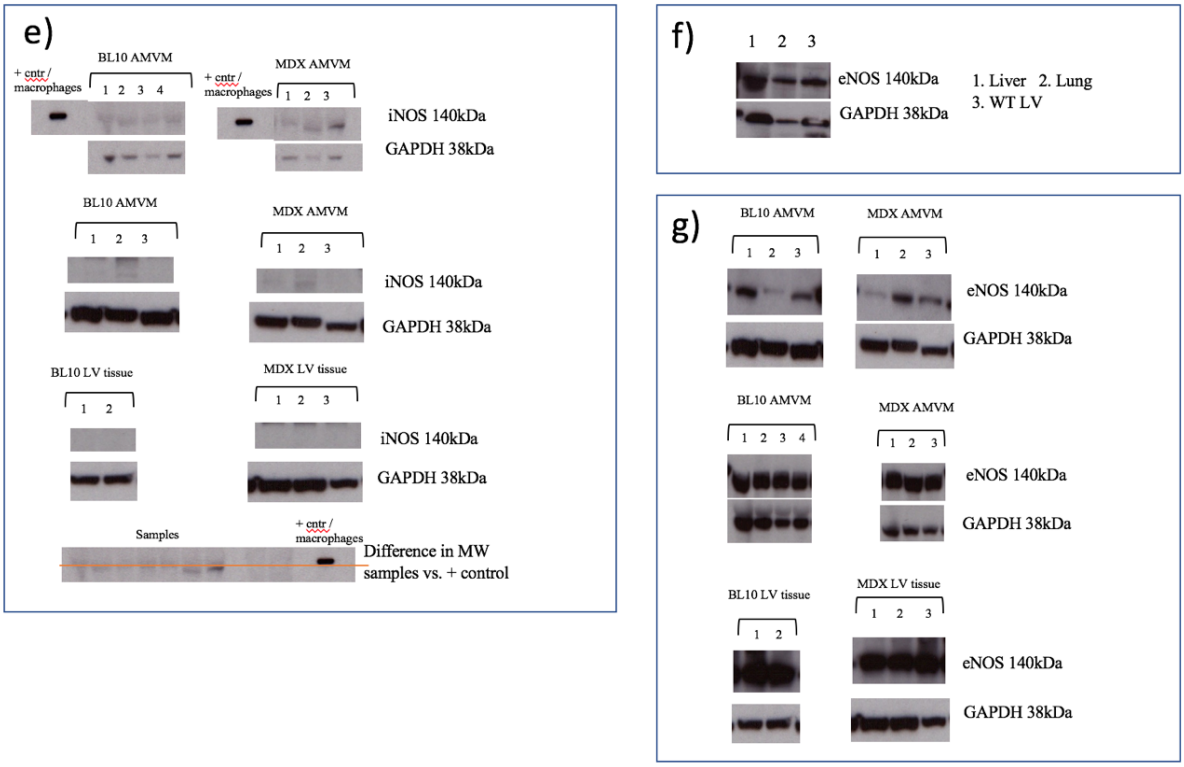


Figure 5.3.
Western blotting analysis of cell lysates obtained from isolated cardiomyocytes and tissues. Membranes were probed for dystrophin (a), nNOS (b and c), iNOS (d and e) and eNOS (f and g). Panel g shows two strips for GAPDH with different exposure times. GAPDH signal was very high in LV sample but very low on macrophages samples. An extremely long exposure was necessary to detect GAPDH bands on macrophages. LV GAPDH band lost its signal by long exposure. Membranes a, b, d and f represent control western blotting to validate antibodies. Membranes c, e and g are representative western blotting where the expression of nNOS, eNOS and iNOS is compared in isolated cardiomyocytes and left ventricle tissue from 12 weeks old mdx and age-matched control C57BL/10ScSn mice. One gel was run for each NOS isoform and included the control and mdx samples, as presented side-by-side, in the same gel. 24 hours LPS/INF-g treated microphages were used as positive control for iNOS. These was kindly provided the lab of Professor David Greaves at the Sir William Dunn School of Pathology University of Oxford. Data from these membranes were quantified and are available in figure 5.4.

Unfortunately, it was not possible to perform similar experiments in neonatal isolated cardiomyocytes. As the heart of the two days old mice are significant smaller than the 12 weeks old animals, the number of cells obtained after isolation was also significant lower. It would be possible to perform such experiment by pulling the heart of several pups together to reach sufficient protein concentrations. Although many attempts were made, it was very challenging to obtain the large number of pups required as it was almost

impossible to coordinate several females to litter at the same time. Nonetheless, fractionation experiments were performed with hearts of neonatal pups and adult mice.

Figure 5.4. Comparison between nNOS, eNOS and iNOS expression in isolated cardiomyocytes and left ventricle tissue of mdx and BL10 mice

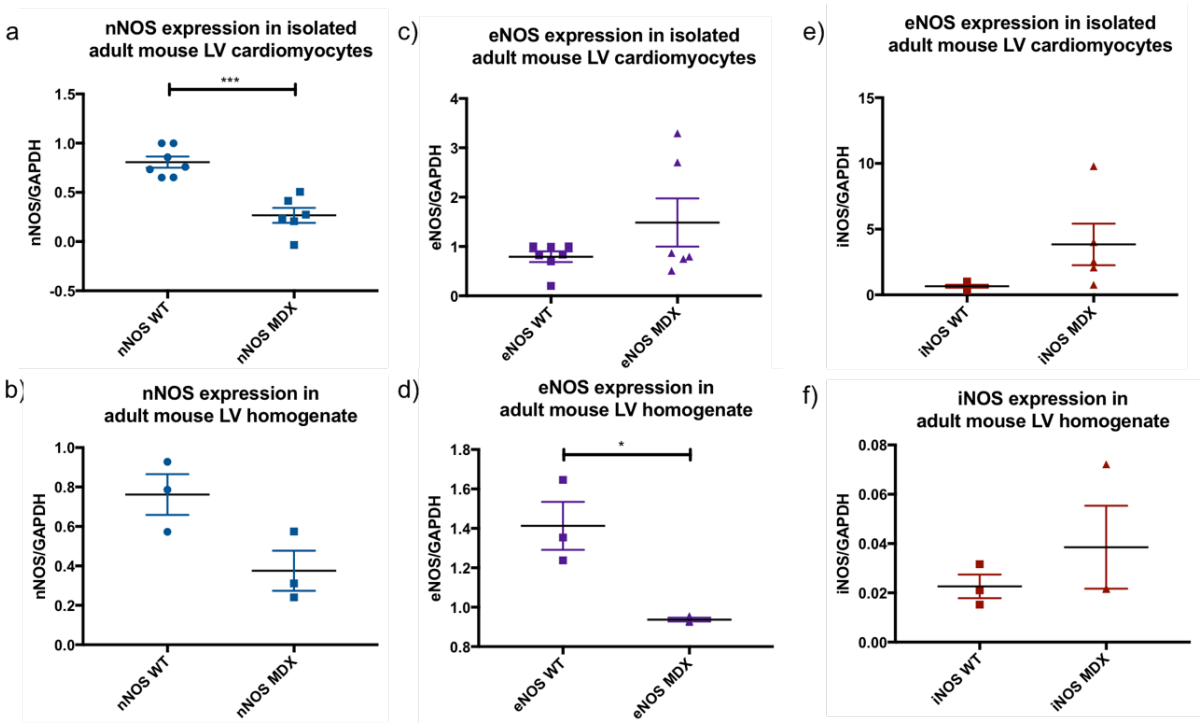


Figure 5.4.
Quantification and analysis of Western blotting of isolated cardiomyocytes lysate (a, c and e) and left ventricle homogenates (b, d and f) from 12 weeks old mdx and C57BL/10ScSn mice. Graphs show densitometry analysis and present the ratio value of total nNOS (a and b), eNOS (c and d) and iNOS (e and f) protein after normalisation to the endogenous control GAPDH. Values are means ± SEM. N = 6 for a, c and e (isolated cardiomyocytes) and N=3 for b, d and f (LV tissue homogenate. Unpaired t-test applied for comparison between both animals in the isolated cardiomyocytes sets (N=6) and Mann- Whitney test for LV homogenate sets (N=3). * = 0.05<p<0.01, ** = 0.01<p<0.001, ***= 0.001<p<0.0001. Data are plotted as aligned dot plot.

It is well known that nNOS localises mostly at the sarcoplasmic reticulum of cardiomyocytes and only a small proportion is located at the plasmalemma (Carnicer et al. 2017; Xu et al. 1999). Even though there are sufficient reports indicating the lower expression of nNOS and disturbed NO-cGMP pathway in the absence of dystrophin, there is no strong evidence supporting the existence of a complex between nNOS and

dystrophin in the heart. In order to understand the distribution and expression of the different NOS isoforms in subcellular compartments, the plasma membrane (PM) fraction and the sarcoplasmic reticulum (SR) fraction of neonatal and adult mdx hearts were blotted for nNOS, eNOS and iNOS. It is important to note that the sub-fractionation and blots quality is not optimal. Due to technical limitations, it was not possible to achieve clean plasma membrane and sarcoplasmic reticulum sub-fraction samples without contamination of other cellular compartments. However, it was possible to achieved enriched samples for these specific subcellular compartments.

As shown in Figures 5.5 – 5.8, nNOS expression at the plasma membrane enriched sample is significantly different in neonatal and adult hearts. In two days old mice, cardiac myocyte PM nNOS expression in mdx is significant higher than in wt, however, the expression of nNOS at the PM of adult mdx cardiac myocytes is substantially lower (does not reach statistical significance) than in controls. Although not statically significant, there is a trend for higher eNOS level and significant higher iNOS at the plasma membrane of neonatal mdx cardiac myocytes. The trend in adults shows a reduction in all isoforms.

Figure 5.5. Plasma membrane and Sarcoplasmic Reticulum fractions nNOS, eNOS and iNOS Western blotting

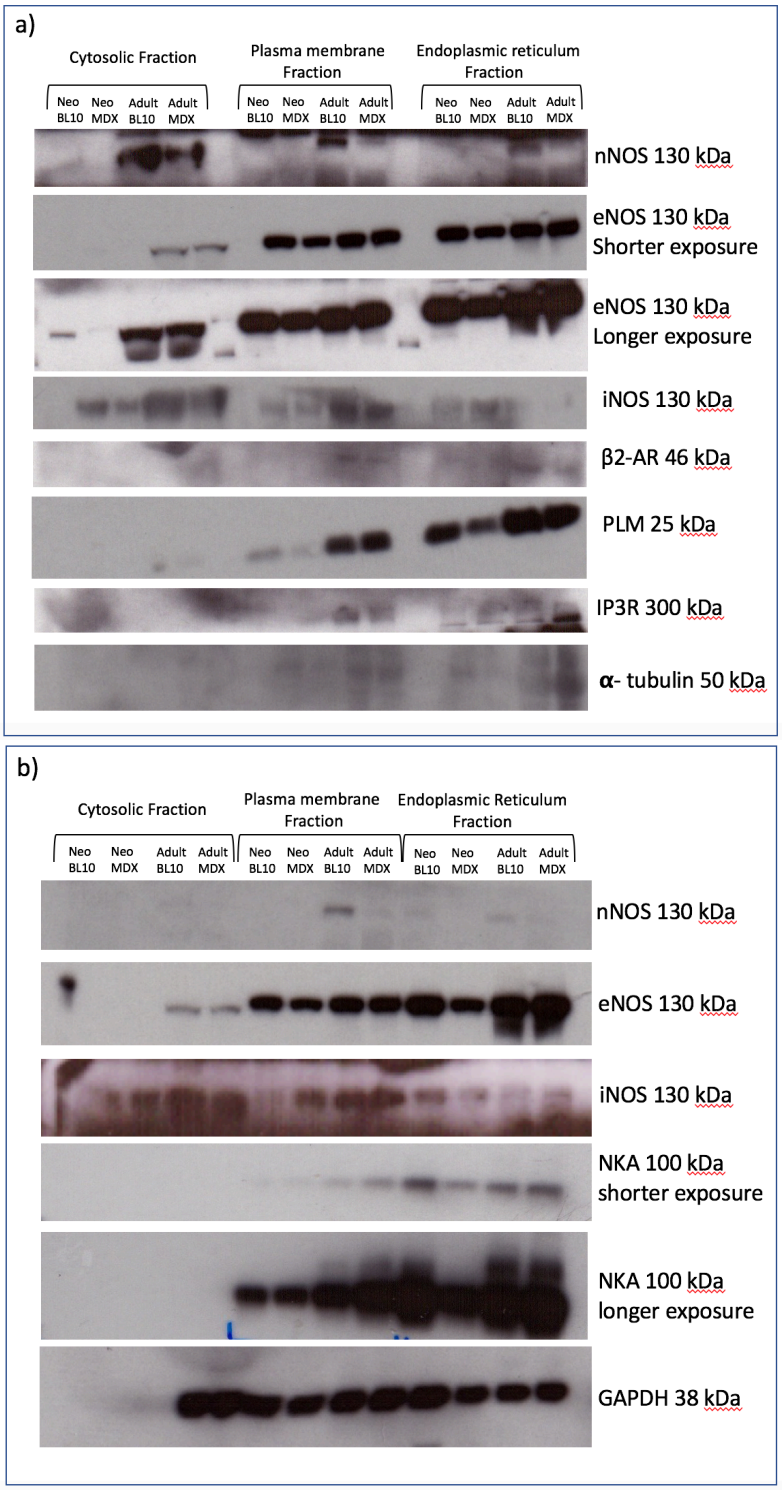


Figure 5.5.
Western blotting analysis of the plasma membrane and sarcoplasmic reticulum fractions obtained from neonatal and adult (12 weeks old) left ventricle tissue. Membranes were probed for nNOS, iNOS, eNOS, PLM, NKA and B2-AR (controls for plasma membrane fraction), IP3R

(control for sarcoplasmic reticulum), alpha-tubulin and GAPDH (endogenous control). Data from these membranes were quantified and are available in figure 5.6 and 5.7.

The amount of nNOS at the enriched SR sub-fraction (Figure 5.6) was also found to be substantially lower in the adult mdx heart when compared to the control. Although not significant due to the high variability and low N number, the expression of nNOS was also lower at the SR of neonatal mdx hearts. These data suggest that the nNOS levels get altered since early age at the SR, but this affects the expression of the enzyme at the plasma membrane only at a later stage. eNOS levels remain unchanged, whereas iNOS levels were substantially, but not significantly, higher at the mdx SR.

Figure 5.6. Comparison between nNOS, eNOS and iNOS expression at the plasma membrane of cardiac myocytes from mdx and BL10 mice

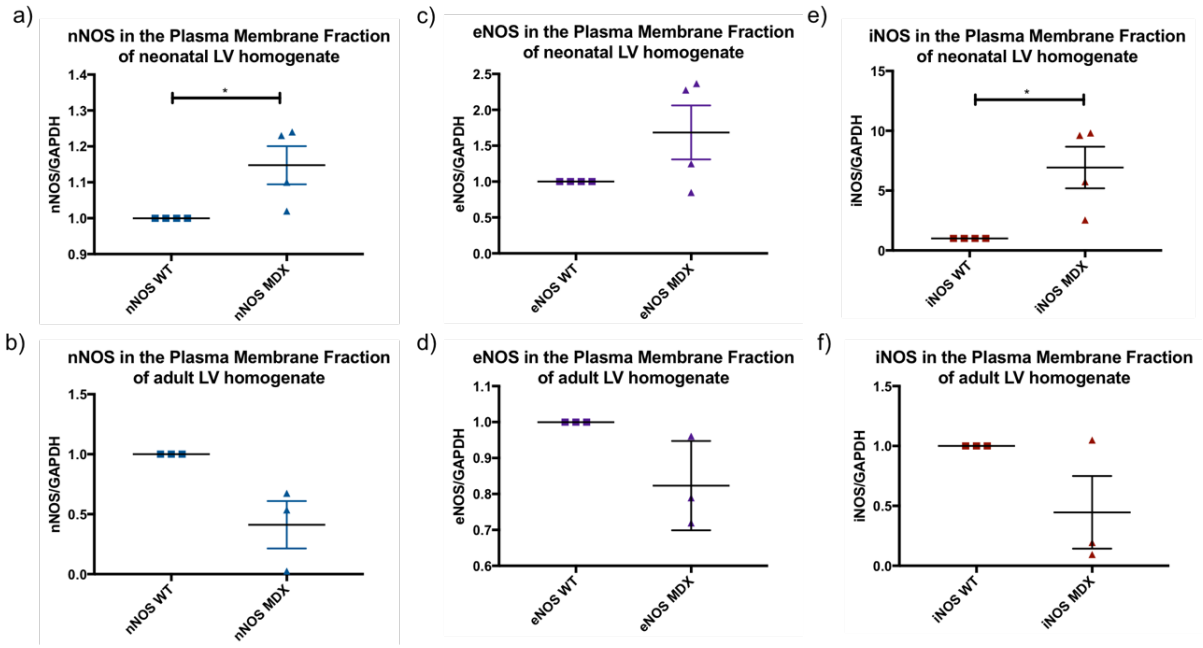


Figure 5.6.
Quantification and analysis of Western blotting of plasma membrane fraction of neonatal (a, c and e) and adult (b, d and f) mdx and C57BL/10ScSn mice left ventricular myocytes. Graphs show densitometry analysis and present the ratio value of total nNOS (a and b), eNOS (c and d) and iNOS (e and f) protein after normalisation to the endogenous control GAPDH and to WT levels (taken as 100%). Values are means ± SEM. N ≥ 3. Mann- Whitney test was applied as statistical test where * = 0.05<p<0.01. Data are plotted as scattered dot plot

iNOS expression is known to be upregulated as part of the immune responses triggered in cardiomyocytes suffering septic shock, myocarditis and other cardiomyopathies and is not expected to be found in healthy heart (Mungrue et al. 2002). However, it was possible to detect this isoform at the SR of neonatal BL10 mice, but not in adults, and not at the plasma membrane. It is important to keep in mind that the molecular weight (MW) of the band detected by the iNOS-specific antibody on the samples was lower than the band detected on the positive control (Figure 5.4e). It was not possible to establish whether the bands found in the samples were due to unspecific binding or due to MW differences from the iNOS present in cardiac tissue and the protein induced in the macrophages used as a positive control. Although in the densitometry analysis care was taken to exclude the lower bands and separate gels were run for each NOS isoform, it is necessary to consider

these discrepancies when drawing conclusions. Representative western blotting membranes and controls are available in Figure 5.5.

Figure 5.7. Comparison between nNOS, eNOS and iNOS expression at the sarcoplasmic reticulum fraction of mdx and BL10 cardiac myocytes

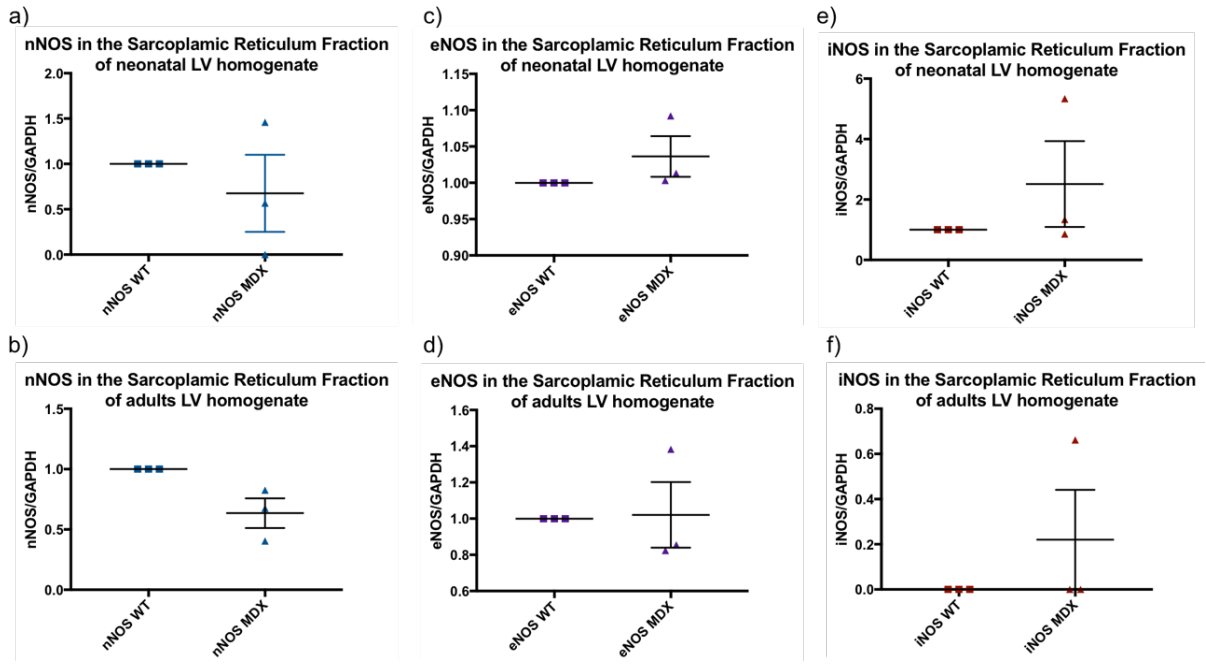


Figure 5.7.
Quantification and analysis of Western blotting of the sarcoplasmic reticulum fraction of neonatal (a, c and e) and adult (b, d and f) left ventricular myocytes from mdx and C57BL/10ScSn mice. Graphs show densitometry analysis and present the ratio value of total nNOS (a and b), eNOS (c and d) and iNOS (e and f) protein after normalisation to the endogenous control GAPDH and to WT levels (taken as 100%). Values are means ± SEM. N = 3. Mann- Whitney test was applied as statistical test. Data are plotted as scattered dot plot.

As seen in Figure 5.7, the cytosolic fraction of wt and mdx neonatal and adult cardiac myocytes were also blotted for nNOS, eNOS and iNOS. However, for reasons not yet understood, it was not possible to detect endogenous control bands in these fractions. Due to this limitation, these bands were not analysed. Proteins known to localise to the plasma membrane, such as the Na+ K+ ATPase (NKA), phospholemman (PLM) and β2 adrenergic receptor (β2 AR), were used as controls for the plasma membrane fraction. The inositol trisphosphate receptor (IP3R) was blotted as control for the sarcoplasmic

reticulum.

As nNOS expression was detected at the plasma membrane of cardiomyocytes by western blotting, immunofluorescence (IF) experiments were performed in neonatal and adult cardiomyocytes in an attempt to visualise its localisation in these cells (Figure 5.8 -5.9). As other groups had already reported (Ramachandran et al. 2013), it was not possible to successfully detect endogenous nNOS at the plasma membrane of wt adult cardiomyocytes. This might be explained by the very low levels of nNOS expression detected at the plasmalemma of cardiomyocytes, as well as in the cytosol. Yet, it was possible to detect a general, likely non-specific, nNOS signal in neonatal cells. Intensity profile analysis indicate that there is a small degree of endogenous nNOS co-localisation with WGA and dystrophin, however, this might be an artefact as the nNOS signal is spread all over the cytosol of the neonatal cardiomyocytes (Figure 5.8).

Carnicer et al., showed that the overexpression of GFP-tagged nNOS using a nNOS.eGFP adenovirus injection into the heart of nNOS knockout mice resulted in significant increased NOS activity and localisation at the sarcolemmal and t-tubular membranes, as well as demonstrable immunoprecipitation of nNOS with syntrophin (Carnicer et al. 2017). In agreement with those findings, infection of isolated neonatal and adult BL10 cardiomyocytes with nNOS.eGFP adenovirus resulted in similar results. A strong signal was detected at the plasma membrane, and co-localisation with WGA and dystrophin could be shown in neonatal and adult cardiomyocytes (Figure 5.8a, b and c). As shown in Figure 5.8a and 5.8b-c, these cells also presented nNOS signal localised to another cellular structure which resembles t-tubules.

Figure 5.8. nNOS detection in intact wt neonatal and adult cardiomyocytes

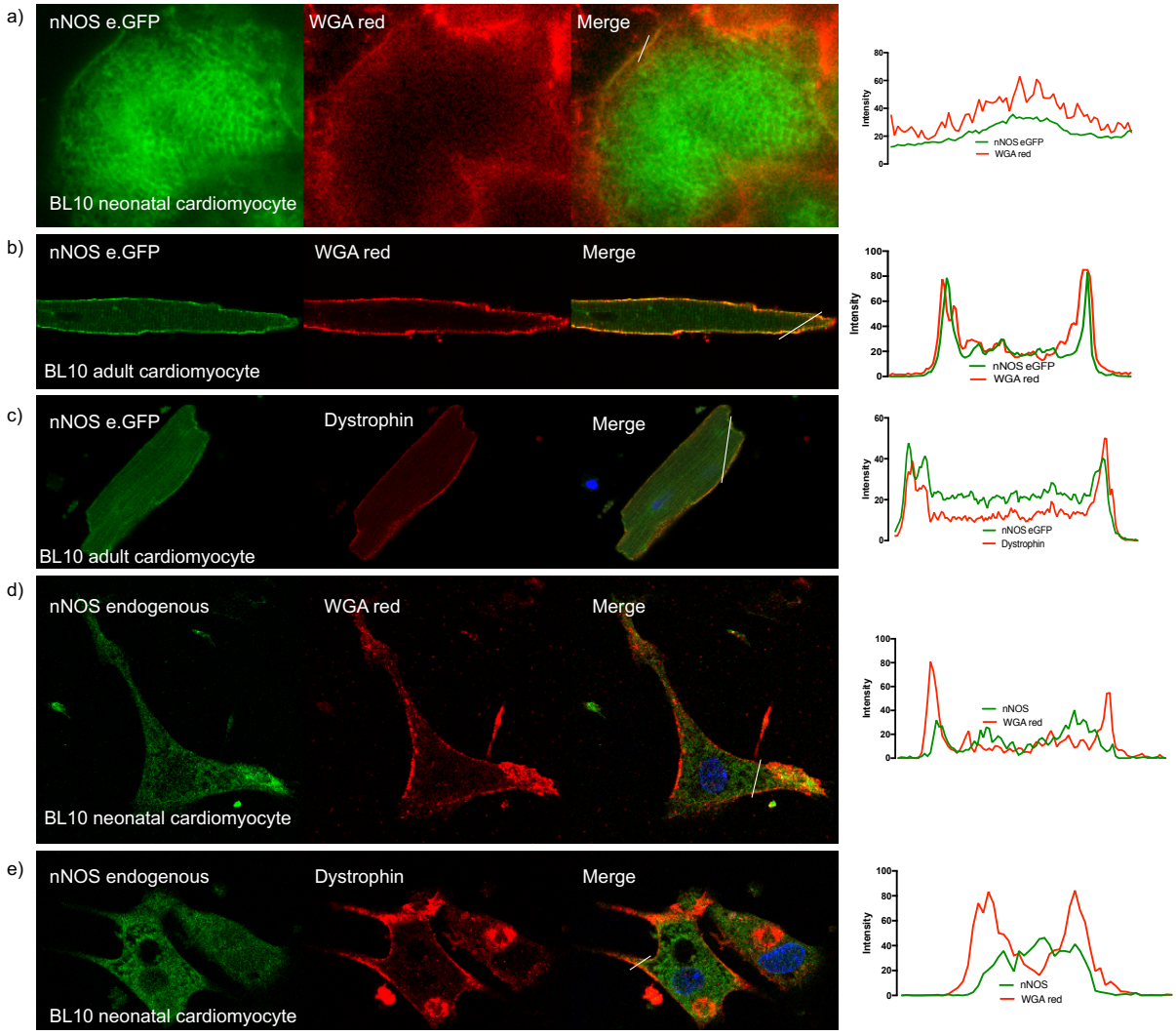


Figure 5.8.
Confocal imaging of fixed neonatal or adult wt (C57BL/10ScSn) cardiomyocyte expressing nNOS.eGFP adenovirus and wheat Germ Agglutinin staining (a and b); nNOS.eGFP adenovirus and dystrophin immunostaining (c); nNOS immunostaining and wheat Germ Agglutinin red staining (d) and nNOS and dystrophin immunostaining. The graphs on the left represent the intensity profile of green and red channels at the plasma membrane calculated along the line indicated in the merged image.

The overexpression of nNOS.eGFP also resulted in sarcolemmal localisation in adult mdx cardiomyocytes, however, the striated pattern observed in adult wt cardiomyocytes was not found in these cells (Figure 5.9a). Neonatal mdx cardiomyocytes showed overexpression pattern of nNOS.eGFP similar to that observed in wt neonatals (Figure 5.9b). The signal generated by endogenous nNOS and dystrophin antibody was low and

non-specific in both neonatal and adult mdx cardiomyocytes (Figure 5.9a – 5.9c). As shown in Figure 5.9 WGA staining was not as successful as in wt cardiomyocytes, limiting the co-localisation analysis. The intensity profile traces beside the IF images on Figure 5.9 b, c and e illustrate the low and noisy signal generated by endogenous nNOS staining. Dystrophin immunostaining was not expected to give a signal in mdx cardiomyocytes as these cells do not express dystrophin (shown in Figure 5.9d), however non-specific fluorescence was detected. A possible explanation for this immunostaining observed is the fact that the primary antibody used was developed in mouse, which can generate unspecific binding to other mouse Ig as the sample derives from the same animal species where the antibody was generated.

Figure 5.9. nNOS detection in intact mdx neonatal and adult cardiomyocytes

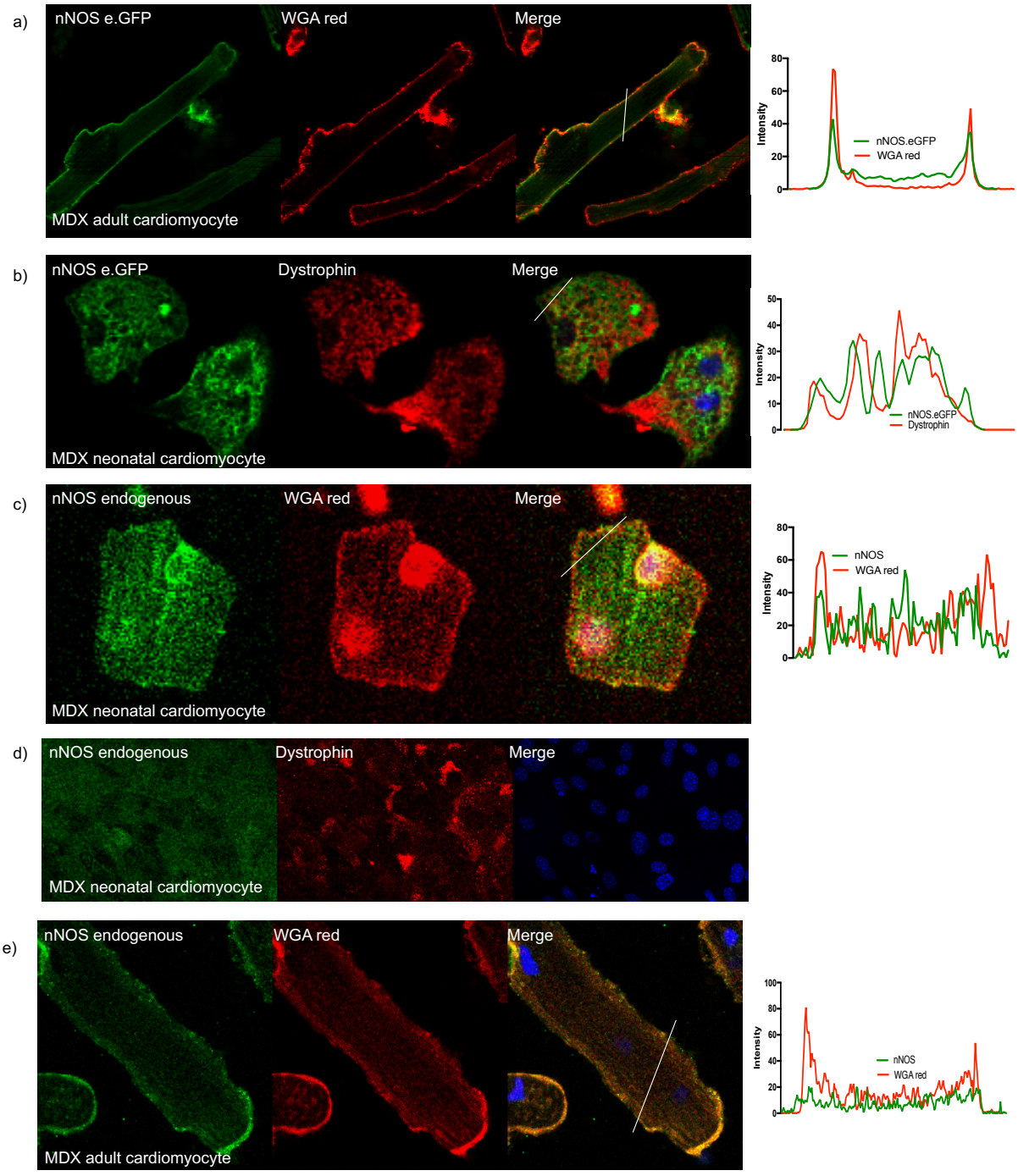


Figure 5.9.

Confocal imaging of fixed neonatal or adult mdx cardiomyocyte expressing nNOS and dystrophin immunostaining (a); nNOS immunostaining and wheat Germ Agglutinin staining (b and d); and nNOS.eGFP adenovirus expression and wheat Germ Agglutinin staining (c and e). The graphs on the left represent the intensity profile of both channels at the plasma membrane calculated at the area indicated by the white line on the merged image.

5.3.2. mdx cardiomyocytes show significant differences in basal cyclic nucleotide levels

In a first set of experiments, cyclic nucleotides (CN) levels in mdx cardiomyocytes were analysed to compare the basal cGMP and cAMP in cultured cardiac myocytes from mdx vs. BL10 controls. For these experiments, the basal FRET ratios generated by cytosolic probes expressed in cardiomyocytes were recorded. The FRET signal is very reliable when measuring relative dynamic changes in CN but is less robust when used to determined steady state levels due to the large cell-to-cell variability in the FRET signal which makes it difficult to detect a difference, particularly when the difference is small or the sample size is limited. Therefore, it was decided that basal CN would also be measured by performing cGMP and cAMP ELISA assays in cell and tissue homogenates. It is important to keep in mind that the ELISA assay measures total levels of CN within the cell, whereas the FRET approach detects only the free CN in the cytosol. This is an advantage of the FRET technique as it allows monitoring of CNs that are available to deliver a signal.

As shown in Figure 5.10, basal levels of free cGMP in the bulk cytosol of neonatal mdx cardiomyocytes resulted to be significantly lower than in wt (Figure 5.10a -5.10b). Statistical significance was not found in total levels detected by the ELISA approach in isolated neonatal cardiomyocytes or LV tissue homogenate (Figure 5.10c).

On the other hand, free cAMP levels are significantly higher in the cytosol of neonatal mdx cardiomyocytes (Figure 5.10d). Statistical significance was also not reproduced by the ELISA approach. Total cAMP levels were found to be similar in mdx and BL10 isolated cardiomyocytes, however, the neonatal LV homogenate data present significantly lower total cAMP levels in the mdx (Figure 5.10f). These data suggest that

although cAMP levels in neonatal cardiomyocytes is higher, other heart cells might present significant lower levels.

Figure 5.10. Basal cGMP and cAMP levels in neonatal mdx heart

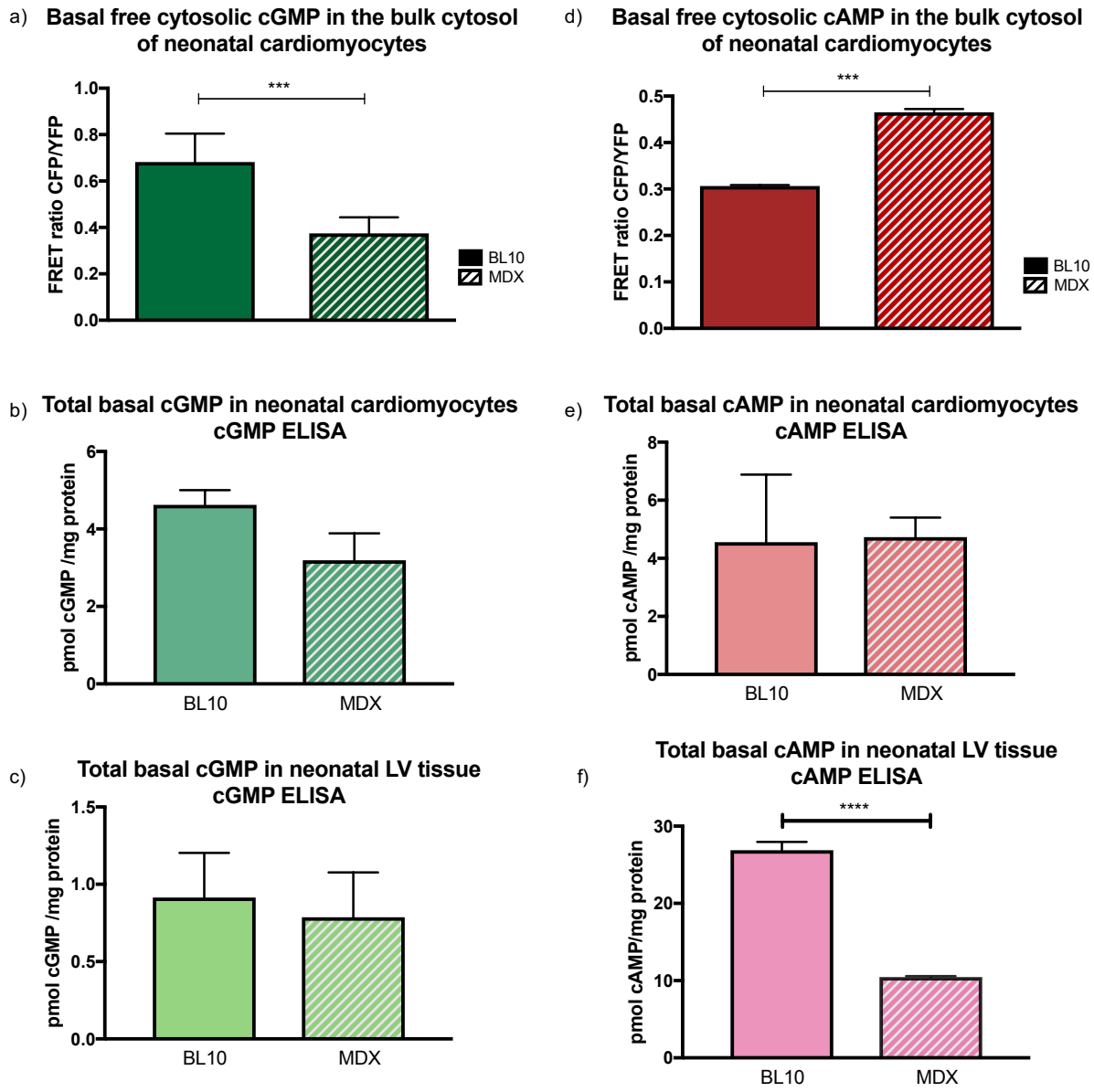


Figure 5.10.
Measurement of cytosolic free cGMP in isolated neonatal cardiomyocytes by using basal FRET ratios (a); Measurement of cytosolic free cAMP in isolated neonatal cardiomyocytes by using basal FRET ratios (d); Measurement of total cGMP by ELISA in isolated neonatal cardiomyocytes (b) and left ventricle (LV) tissue homogenate (c); Measurement of total cAMP by ELISA in isolated neonatal cardiomyocytes (e) and left ventricle (LV) tissue homogenate (f). Graphs show means basal rations of $\geq$ 20 cells per condition (a and d) and 3 biological replicates for ELISA measurements; Error bars represent SEM; T-test, * = 0.05<p<0.01, ** = 0.01<p<0.001, ***= 0.001<p<0.0001, **** = p<0.0001.

Surprisingly, as shown in Figure 5.11, measurement of basal CN levels in adult isolated cardiomyocytes and LV tissue show opposite results than the ones discussed above. Free cytosolic cGMP is significantly higher in isolated mdx cardiomyocytes compared to control cells (Figure 5.11a). ELISA measurements confirm significantly higher total cGMP levels in mdx adult cardiomyocytes (Figure 5.11b), indicating that the not only cytosolic cGMP is altered. ELISA data in LV homogenate did not display significant differences between mdx and BL10 (Figure 5.11c), suggesting that the other cell types present in the heart might compensate for the excess of cGMP in dystrophic cardiomyocytes. cAMP levels, both basal free and total, did not show significant different levels when compared to WT (Figures 5.11d and 5.11f). Although there is trend for higher total cAMP in mdx isolated cardiomyocytes and LV tissue, no statistical significance was found.

Figure 5.11. Basal cGMP and cAMP levels in adult mdx heart

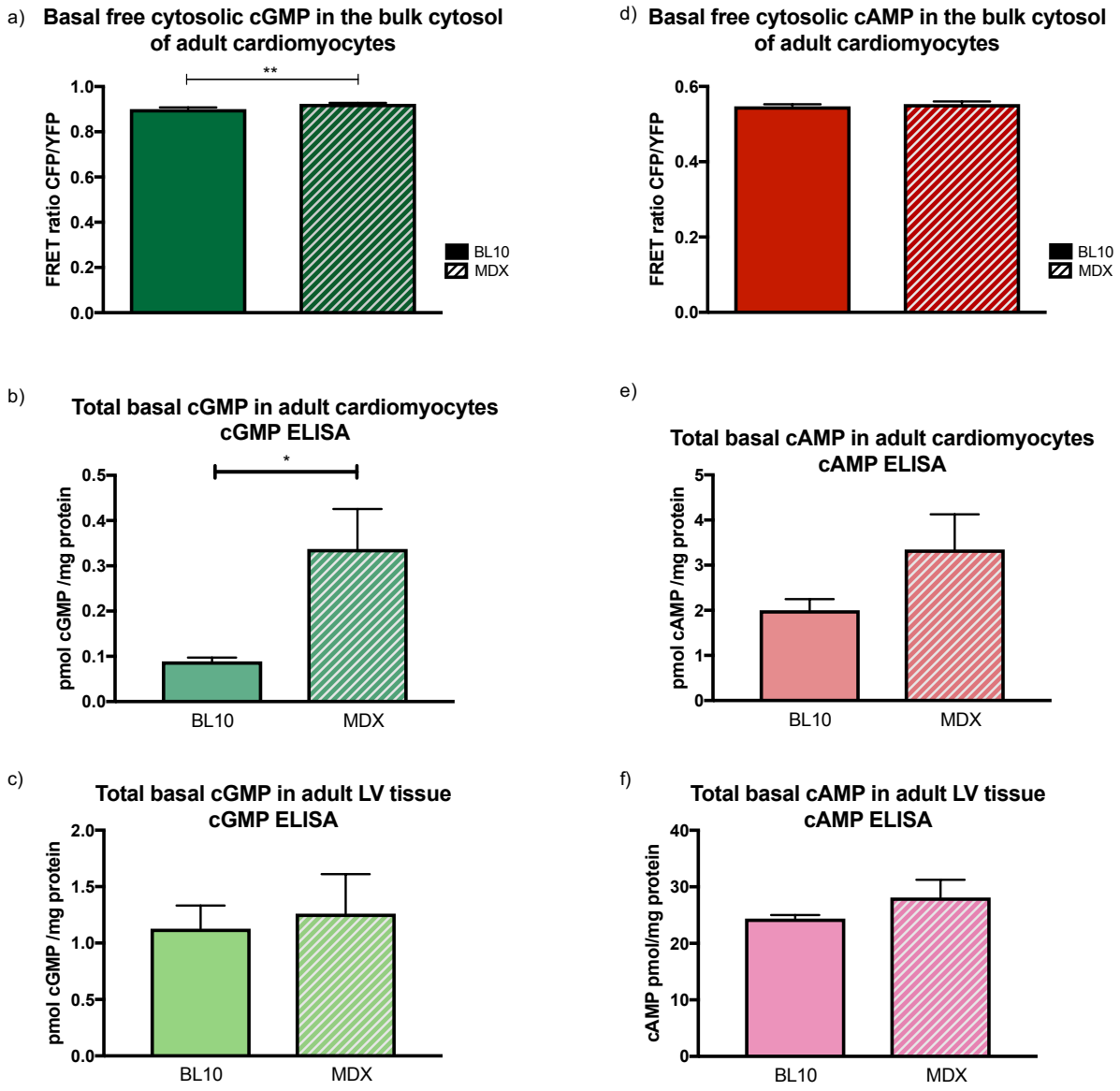


Figure 5.11.
Measurement of cytosolic free cGMP in isolated adult cardiomyocytes by using basal FRET ratios (a); Measurement of cytosolic free cAMP in isolated adult cardiomyocytes by using basal FRET ratios (d); Measurement of total cGMP by ELISA in isolated adult cardiomyocytes (b) and left ventricle (LV) tissue homogenate (c); Measurement of total cAMP by ELISA in isolated adult cardiomyocytes (e) and left ventricle (LV) tissue homogenate (f). Graphs show means basal ratios of ≥ 20 cells per condition (a and d) and 3 biological replicates for ELISA measurements; Error bars represent SEM; T-test, * = 0.05<p<0.01, ** = 0.01<p<0.001, ***= 0.001<p<0.0001, **** = p<0.0001.

These data suggest that cAMP and cGMP signalling and regulation change with age and compensatory mechanisms might be activated over time to increase cGMP levels in cardiomyocytes. Table 5.1 confirms that total and free concentration of CN change with

age in the heart of healthy animals. While total cAMP levels decrease with age in isolated cardiomyocytes and left ventricle tissue, free cAMP seems to increase in wt isolated cardiomyocytes. cGMP levels in isolated cardiomyocytes showed similar profile with age, as total cGMP levels increased while free cGMP concentration decreased. However, total cGMP concentrations in LV tissue seems to increase with age, suggesting that other heart cells might present different fluctuations with age. Total cAMP levels decrease with age in cardiomyocytes from both animal models, yet, free levels suffer slight increase. However, total cAMP in mdx LV tissue present high increase while cAMP levels go on the opposite direction in wt LV tissue. The table below shows the same data from Figure 5.10 and 5.11 differently organised to facilitate comparison between CN levels at the different ages.

Table 5.1. Basal cyclic nucleotide fluctuations with age

	[cAMP] neonatal	[cAMP] adult	[cGMP] neonatal	[cGMP] adult
MDX isolated cells	**Total cAMP:** 4.727 ± 0.6735 pmol cAMP/mg protein **Free cAMP:** 0.465 ± 0.0074 FRET change	**Total cAMP:** 3.348 ± 0.7813 pmol cAMP/mg protein **Free cAMP:** 0.5535 ± 0.0070 FRET change	**Total cGMP:** 3.195 ± 0.6908 pmol cGMP/mg protein **Free cGMP:** 0.3745 ± 0.0052 FRET change	**Total cGMP:** 0.3372 ± 0.08839 pmol cGMP/mg protein **Free cGMP:** 0.924 ± 0.0039 FRET change
BL10 isolated cells	**Total cAMP:** 4.556 ± 2.331 pmol cAMP/mg protein **Free cAMP:** 0.3064 ± 0.002 FRET change	**Total cAMP:** 2.004 ± 0.2424 pmol cAMP/mg protein **Free cAMP:** 0.5473 ± 0.0052 FRET change	**Total cGMP:** 4.622 ± 0.3788 pmol cGMP/mg protein **Free cGMP:** 0.6821 ± 0.0085 FRET change	**Total cGMP:** 0.089 ± 0.0083 pmol cGMP/mg protein **Free cGMP:** 0.9 ± 0.0078 FRET change
MDX LV tissue	**Total cAMP:** 10.46 ± 0.129 pmol cAMP/mg protein	**Total cAMP:** 28.13 ± 1.804 pmol cAMP/mg protein	**Total cGMP:** 0.7871 ± 0.1671 pmol cGMP/mg protein	**Total cGMP:** 1.261 ± 0.2013 pmol cGMP/mg protein
BL10 LV tissue	**Total cAMP:** 26.88 ± 1.083 pmol cAMP/mg protein	**Total cAMP:** 24.38 ± 0.3608 pmol cAMP/mg protein	**Total cGMP:** 0.9149 ± 0.1664 pmol cGMP/mg protein	**Total cGMP:** 1.127 ± 0.1191 pmol cGMP/mg protein

Table 5.1.
Summary of basal cyclic nucleotides in isolated cardiomyocytes and left ventricle tissue from at wt (C57BL/10ScSn) and mdx mice at two different time points, neonatal (two days old) and adult (12 weeks old). Table shows the same data acquired with two different approaches: cAMP

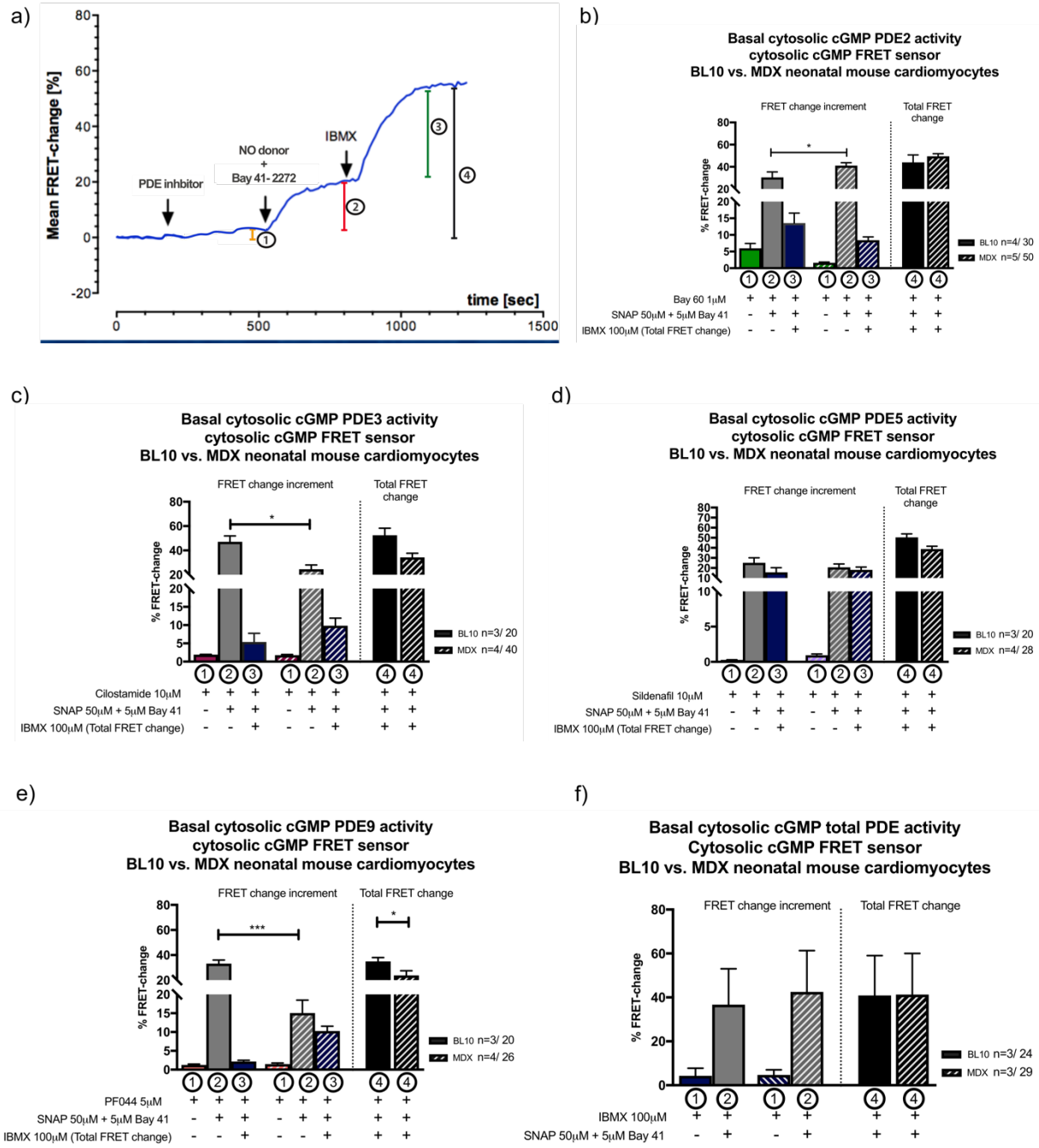
and cGMP ELISA for total cAMP and cGMP and basal FRET ratio analysis of isolated cardiomyocytes expressing cytosolic FRET-probes for cAMP (H187) and cGMP (cGI 500) for free cAMP and cGMP. Data show Mean ± SEM.

5.3.3. PDE levels are altered in the cytosol of mdx cardiomyocytes

To test the contribution of individual PDEs to the regulation of basal cGMP and cAMP levels in the bulk cytosol, BL10 and MDX cardiomyocytes expressing either the cytosolic cGMP FRET-probe (cGI 500) or the cytosolic cAMP FRET-probe (H187) were treated with specific inhibitors of individual PDE families that are known to be expressed in the heart. Figure 5.12 display these FRET results where Figure 5.12a illustrate a FRET-change trace with experimental protocol and analysis. Figures 5.12b – 5.12f represents each experimental set separately, whereas Figure 5.12g displays a summary of the single experimental sets to facilitate comparison.

As shown in Figure 5.12b (summary panel), detection of FRET changes on inhibitor application indicate that in mdx cardiac myocytes PDE2 contributes substantially less and PDE5 contributes substantially more to the regulation of the basal level of cGMP as compared to control cardiomyocytes. The activity of the other cGMP-degrading PDE tested (PDE3 and PDE9), as well as the total PDE activity (assessed by applying IBMX), were not significantly different in the two cell types, however, the generation of cGMP upon NO donor after inhibition of PDE2, PDE3 and PDE9 were significantly altered suggesting that these PDEs might differently regulate the GC in the mdx mice.

Figure 5.12. Basal cGMP PDE activity in neonatal cardiomyocytes



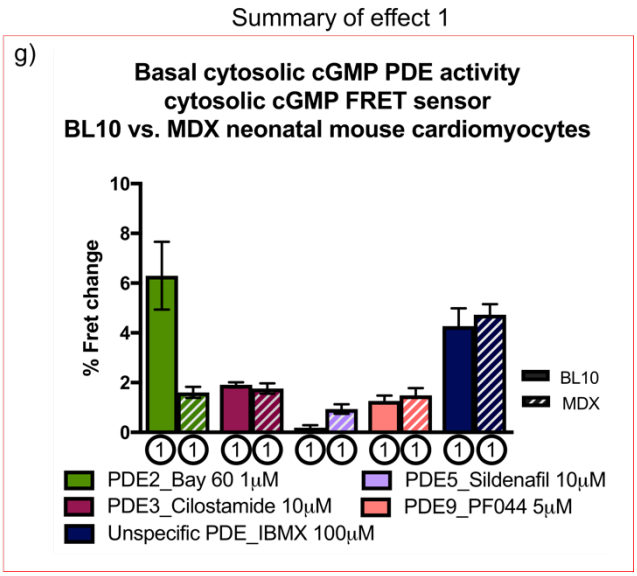


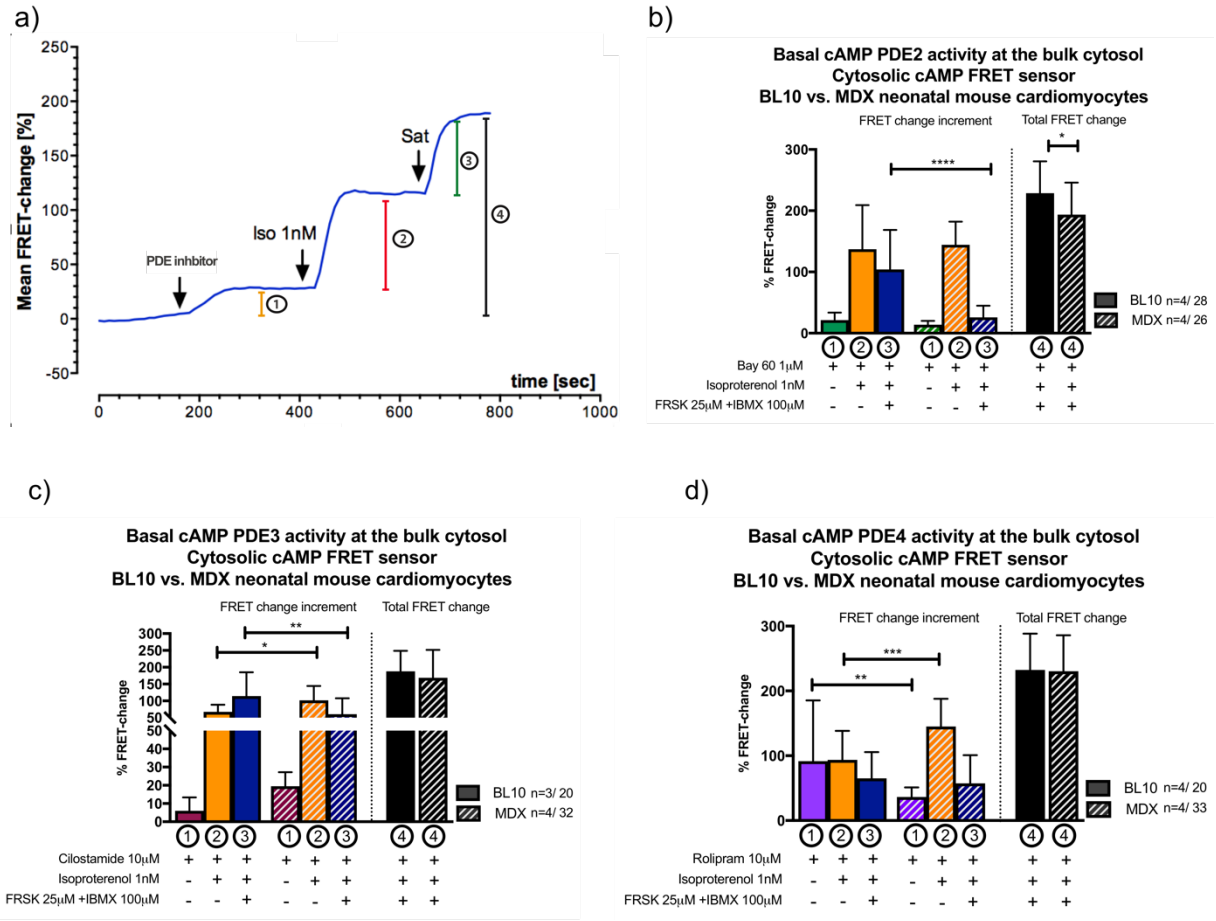
Figure 5.12.
FRET change data recorded in mdx and C57BL/10ScSn individually expressing cytosolic cGMP FRET-based sensor, cGI 500, in response to bath application of 1μM Bay 60 (b), 10μM Cilostamide (c), 10μM Sildenafil (d), 5μM PF-04447943 (e) and 100μM 3-isobutyl-1-methylxanthine (IBMX) (f) followed by 50μM of the NO donor S-Nitroso-N-Acetyl-D,L-Penicillamine (SNAP) in combination of 5 μM of soluble guanylyl cyclase stimulator BAY 41-2272 and 100μM 3-isobutyl-1-methylxanthine (IBMX). The FRET-change trace in graph (a) represents experimental protocol and analysis protocol. The numbers and arrows below the trace indicates how the analysis was performed and which areas of the trace are being represented in the bar graphs. The same number legend is used below each bar graph to facilitate understanding of the data. Graphs (b), (c), (d), (e) and (f) represent each experimental set separately, whereas graph (g) displays a summary of the relevant data from the individual sets. N number is indicated in each individual set as n= biological replicates/ individual cells. Error bars represent SEM; Two-way ANOVA, * = 0.05<p<0.01, ** = 0.01<p<0.001, ***= 0.001<p<0.0001.

Figure 5.13 displays the basal cAMP activity in neonatal cardiomyocytes and is constructed using the same structure as the figure discussed above.

As shown in Figure 5.13, the basal activity of cAMP-degrading PDEs was also found to be significantly different in the cytosol of neonatal mdx cardiomyocytes when compared to the BL10 control. The summary graph (Figure 5.13g) or each individual set (Figure 5.13b – 5.13f) show that PDE2 and PDE8 activities are substantially and PDE4 activity is significantly lower in mdx whereas PDE3 activity is higher. The total PDE activity assessed by treating the cells with IBMX was not different in dystrophic vs control cells. As the activity of most of the PDEs is lower in the mdx neonatal cardiomyocytes, it was

expected that total PDE levels were also lower. It is important to keep in mind that IBMX is a non-selective pan-PDE inhibitor, however, it does not inhibit PDE8. Therefore, the lack of difference upon IBMX treatment might be due to the over activity of PDE3, which might compensate for the lower PDE2 and PDE4 activity and by the fact that PDE8 is not inhibited. It is also important to note that the response to isoproterenol is significantly altered in the mdx after the inhibition of each individual PDE, suggesting different PDE regulation of the ACs.

Figure 5.13. Basal cAMP PDE activity in neonatal cardiomyocytes



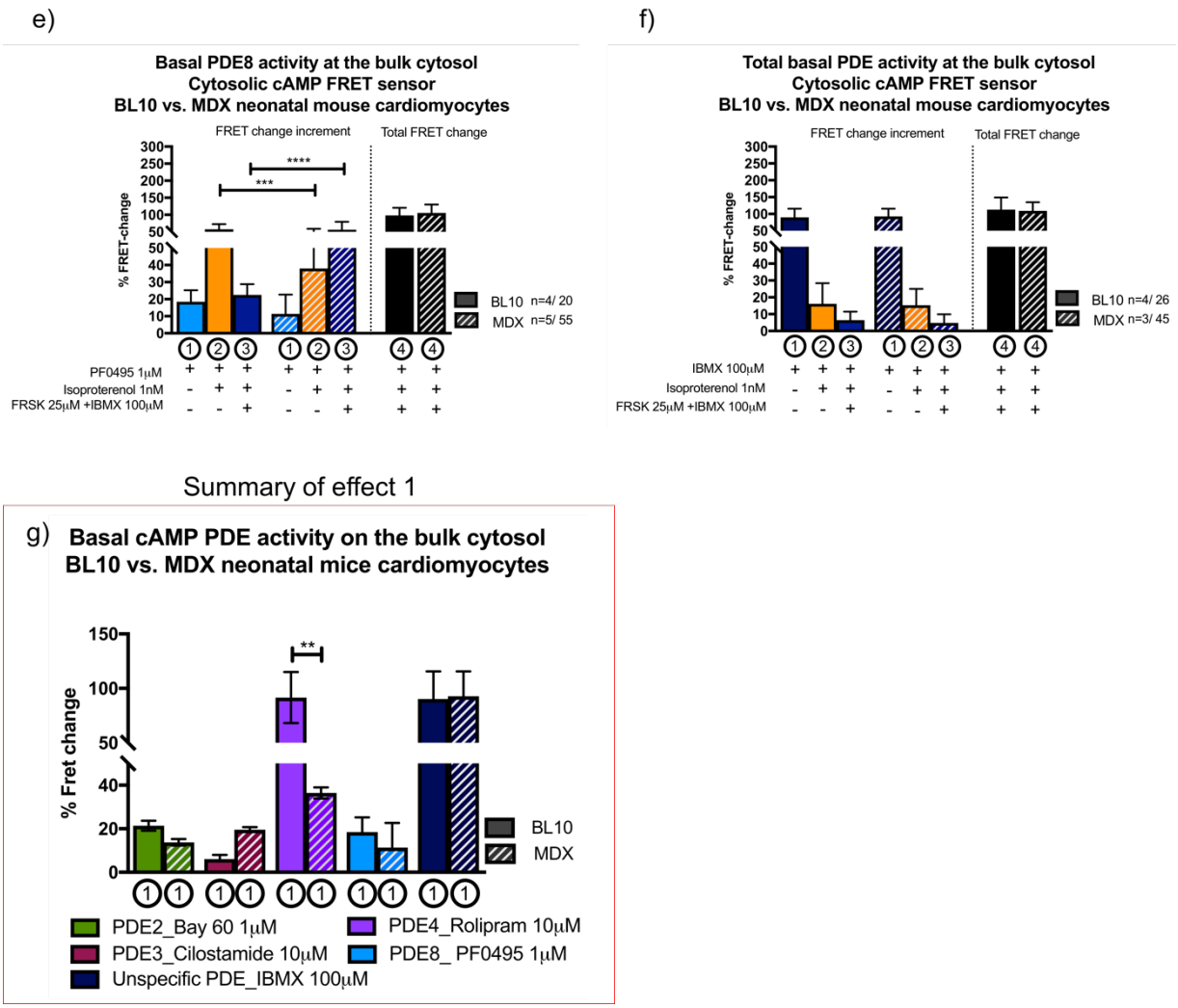


Figure 5.13.
Summary of FRET change recorded in mdx and C57BL/10ScSn individually expressing cytosolic cAMP FRET-based sensor, H187, in response to bath application of 1μM Bay 60 (b), 100μM 3-isobutyl-1-methylxanthine (IBMX) (c), 1 μM PF-04957325 (d), 10μM Cilostamide (e), and 10 μM Rolipram (f) followed by 1nM Isoproterenol and 25μM of the adenylyl cyclase stimulator Forskolin (FRSK) in combination with 100μM 3-isobutyl-1-methylxanthine (IBMX). The FRET-change trace in graph (a) represents experimental protocol and analysis protocol. The numbers and arrows below the trace indicates how the analysis was performed and which areas of the trace are being represented in the bar graphs. The same number legend is used below each bar graph to facilitate understanding of the data. Graphs (b), (c), (d), (e) and (f) represent each experimental set separately, whereas graph (g) displays a summary of the relevant data from the individual sets. N number is indicated in each individual set as n= biological replicates/ individual cells. Error bars represent SEM; Two-way ANOVA, * = 0.05<p<0.01, ** = 0.01<p<0.001, ***= 0.001<p<0.0001, **** = p<0.0001.

Reliable cyclic nucleotides measurements, especially cGMP, in adult isolated cardiomyocytes are known to be challenging (K. Götz et al. 2014; K. R. Götz and Nikolaev 2013). Basal levels of cGMP are significant lower than cAMP, therefore, sensors have failed to robustly report cGMP in adult cardiomyocytes. In our hands, it has been impossible to detect FRET signals induced by NO donors in adult cardiomyocytes expressing the cGI 500 sensor. There is a general consensus (both in published literature and from personal communications at conferences) that this is the case. Götz (K. Götz et al. 2014) for example, reported that upon SNAP and other fast kinetic NO-donors such as DEA/NOno cGMP increase was not detected in cells expressing FRET-based sensors for cGMP. Therefore, in order to understand the expression levels of PDEs in adult cardiomyocytes, qPCR for mRNA levels of the different PDE were performed. To compare whether PDE mRNA change with age, the same experiment was performed in neonatal cardiomyocytes.

As shown in Figure 5.14a, mRNA levels of each individual PDE was not found to be significantly different in mdx neonatal cardiomyocytes when comparted to controls. These data indicate that, at the neonatal stage, the differences encountered are mostly due to post-transcriptional regulation of PDEs levels. However, the mRNA of all the PDE tested were significantly higher in adult mdx cardiomyocytes when compared to control (Figure 5.14b). cGMP specific PDEs, PDE5 and PDE9, presented mRNA levels 3 to 4 folds higher than wt, whereas cAMP PDEs presented 1 to 2-fold increase. This increase in cGMP PDE mRNA levels could be an attempt of the cell to compensate for the significantly higher cGMP levels found in the adult mdx heart.

Figure 5.14. PDE mRNA levels in neonatal and adult mdx heart

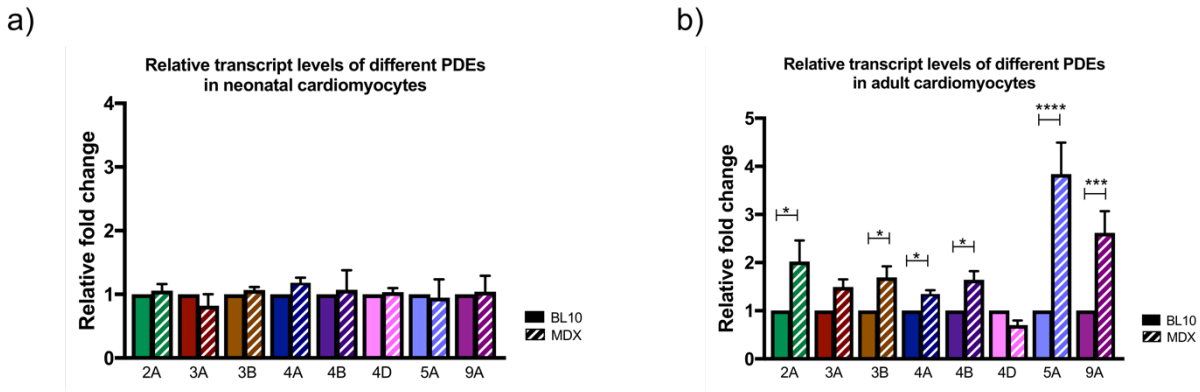
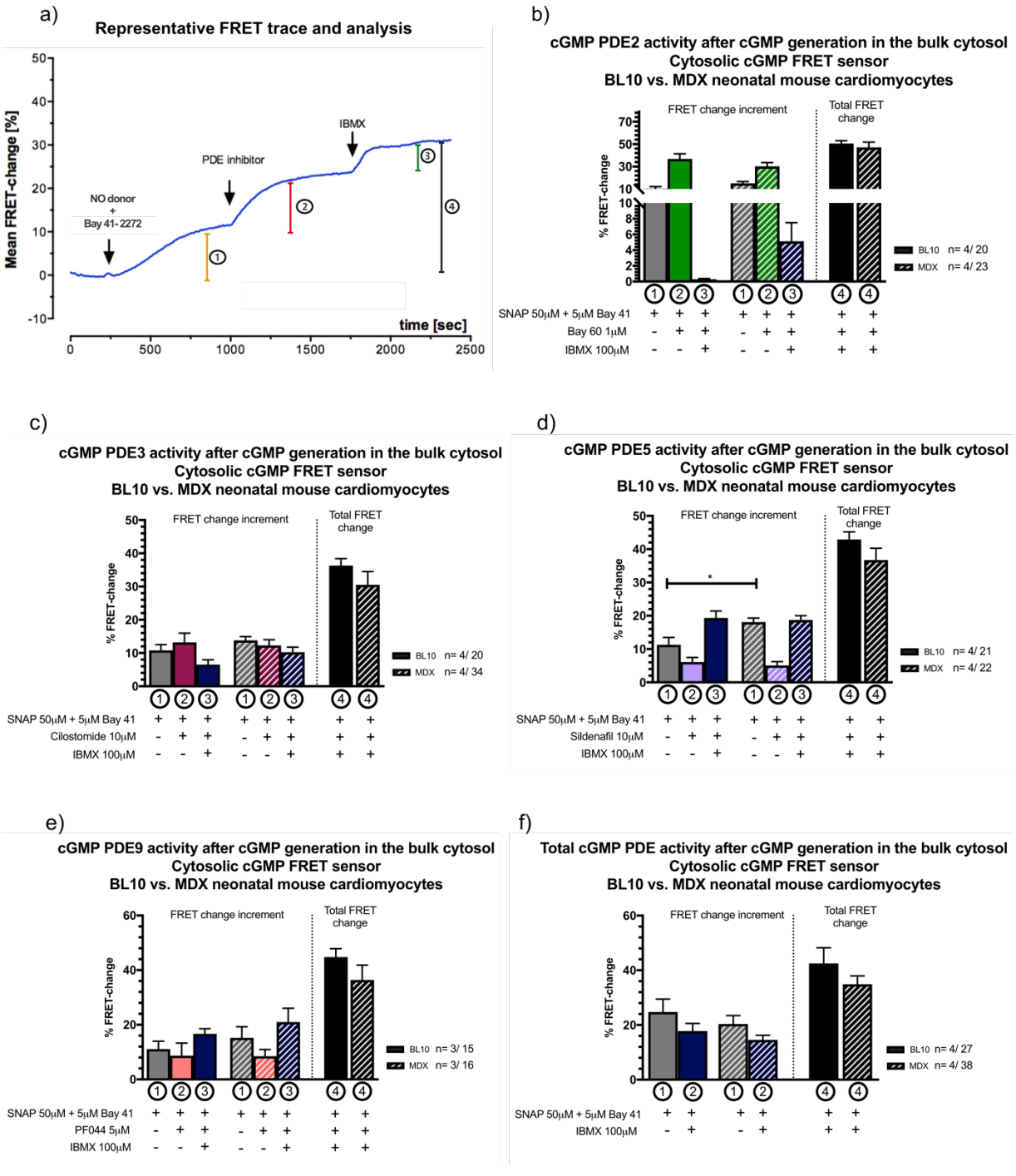


Figure 5.14.
Individual PDE mRNA analysis of isolated cardiomyocytes from neonatal (a) and adult (b) mice. Graphs show means of 3 biological replicates measurements in triplicate normalised related to wt levels; Error bars represent SEM; Two-way ANOVA, * = 0.05<p<0.01, **** = p<0.0001.

5.3.4. mdx cardiomyocytes show compromised ability to generate cAMP and present different levels of PDE activity

The activity of each PDE in the bulk cytosol was also assessed after the generation of cyclic nucleotide upon Isoproterenol or NO donor and sGC stimulator. As shown in Figure 5.15, mdx and wt neonatal cardiomyocytes have similar abilities to generate cGMP upon NO donor and sGC stimulator (as seen in each individual set or summary panel g). Also, the activity of cGMP PDEs in the cytosol after generation of cGMP was similar in mdx and wt cells. These data suggest that neonatal cardiomyocytes have similar levels of NO sensitive sGC in the cytosol and PDEs with similar hydrolysing capacities. This finding could be in agreement with the lack of difference between wt and mdx mRNA levels of PDEs in neonatal cardiomyocytes shown above.

Figure 5.15. cGMP PDE activity after cGMP generation in neonatal cardiomyocytes



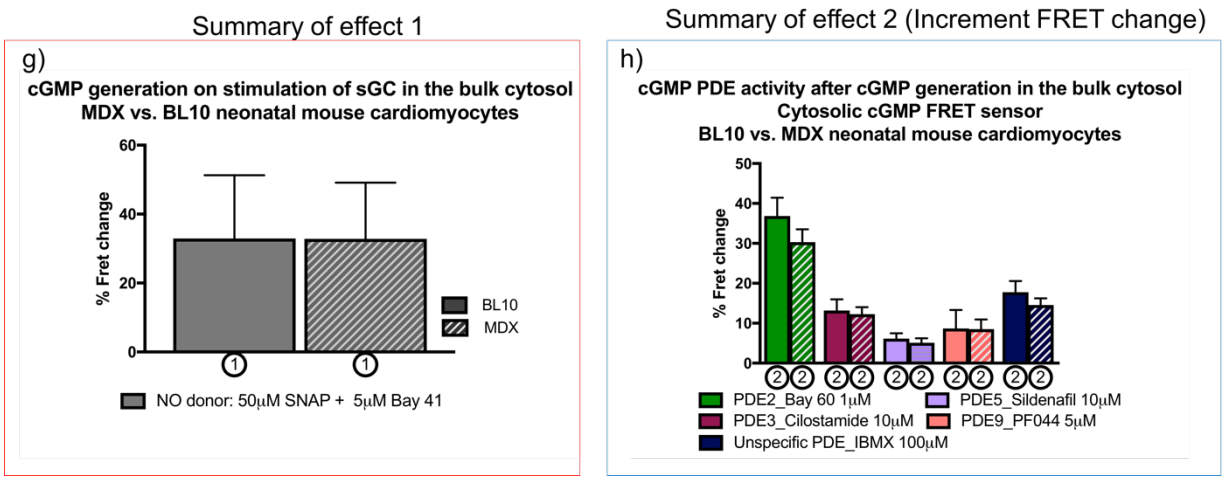


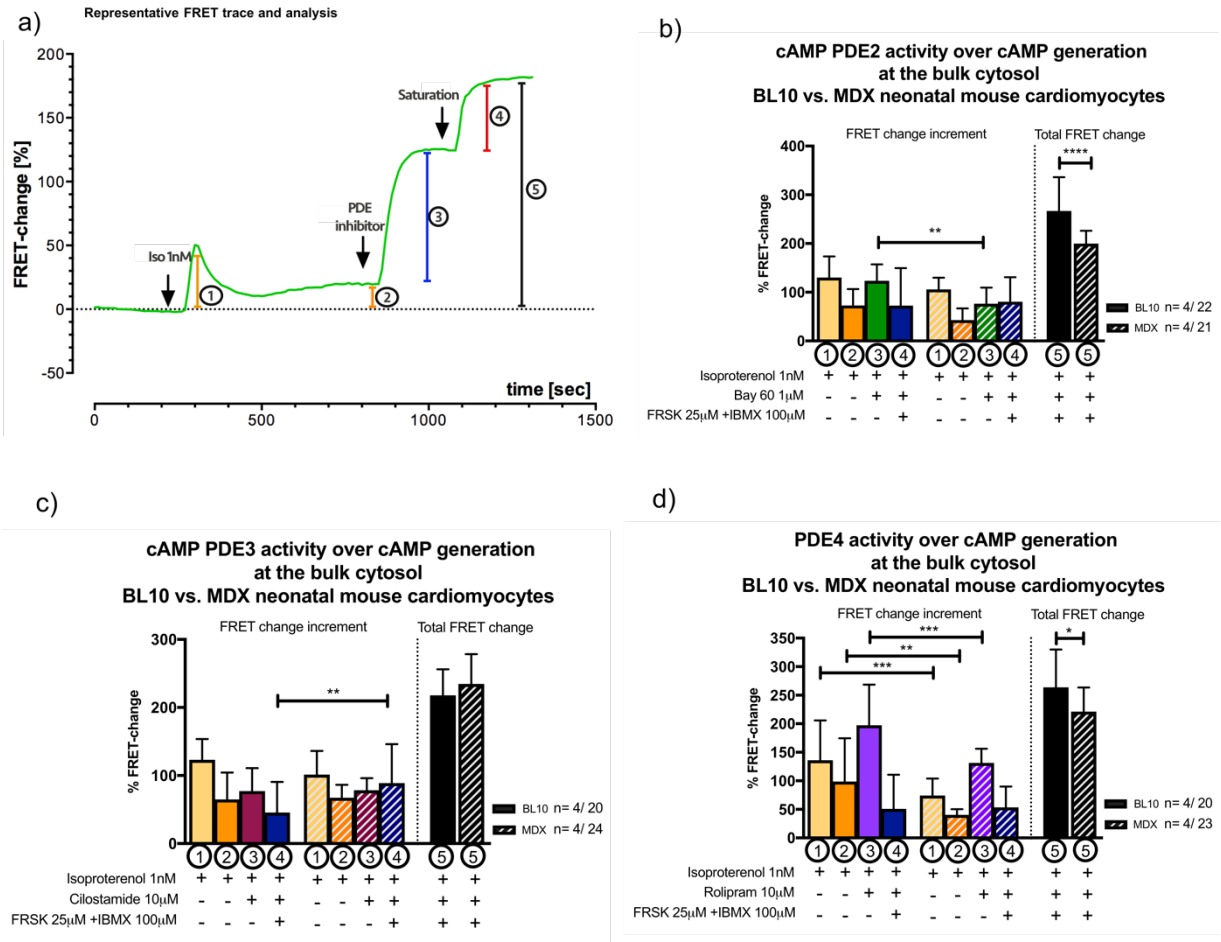
Figure 5.15.

Summary of FRET change recorded in mdx and C57BL/10ScSn neonatal cardiomyocytes individually expressing cytosolic cGMP FRET-based sensor, cGI 500, in response to bath application of NO donor S-Nitroso-N-Acetyl-D,L-Penicillamine (SNAP) in combination of 5μM of soluble guanylyl cyclase stimulator BAY 41-22721μM (a) followed by 1μM Bay 60 (c), 10μM Cilostamide (d), 10μM Sildenafil (e), 5μM PF-04447943 (f) or 100μM 3-isobutyl-1-methylxanthine (IBMX) (g) to fully inhibit PDEs. The FRET-change trace in graph (a) represents experimental protocol and analysis protocol. The numbers and arrows below the trace indicates how the analysis was performed and which areas of the trace are being represented in the bar graphs. The same number legend is used below each bar graph to facilitate understanding of the data. Graphs (b), (c), (d), (e) and (f) represent each experimental set separately, whereas graph (g) displays a summary of the relevant data from the individual sets. N number is indicated in each individual set as n= biological replicates/ individual cells. Error bars represent SEM; Tow-way ANOVA.

Although neonatal mdx cardiomyocytes responded as control cells to sGC stimulation and NO donor, they presented significantly lower generation of cAMP upon isoproterenol stimulation (Figures 5.16b – h or summary panel g), suggesting defective beta-adrenergic receptors and/or adenylyl cyclases activity as the generation of cAMP was also significantly lower upon different concentrations of the adenylyl cyclase activator forskolin (Figure 5.16j). Interestingly, cAMP PDE2 and PDE4 activity remained significantly lower in mdx neonatal cardiomyocytes after cAMP generation (Figure 5.16b and 5.16d respectively or 5.16g for summary figure), whereas PDE8 activity was found significantly higher (Figure 5.16e or 5.16g). Surprisingly, total PDE activity, measured upon IBMX application, showed significantly higher levels in the cytosol of mdx neonatal cardiomyocytes even though PDE2 and PDE4 appeared to be significantly less active,

suggesting that other mechanism which might be influenced by the total PDE inhibition might happen. Also, thi data suggests that mdx neonatal cardiomyocytes might present different compartmentalisation and PDE regulation.

Figure 5.16. cAMP PDE activity after cAMP generation in neonatal cardiomyocytes



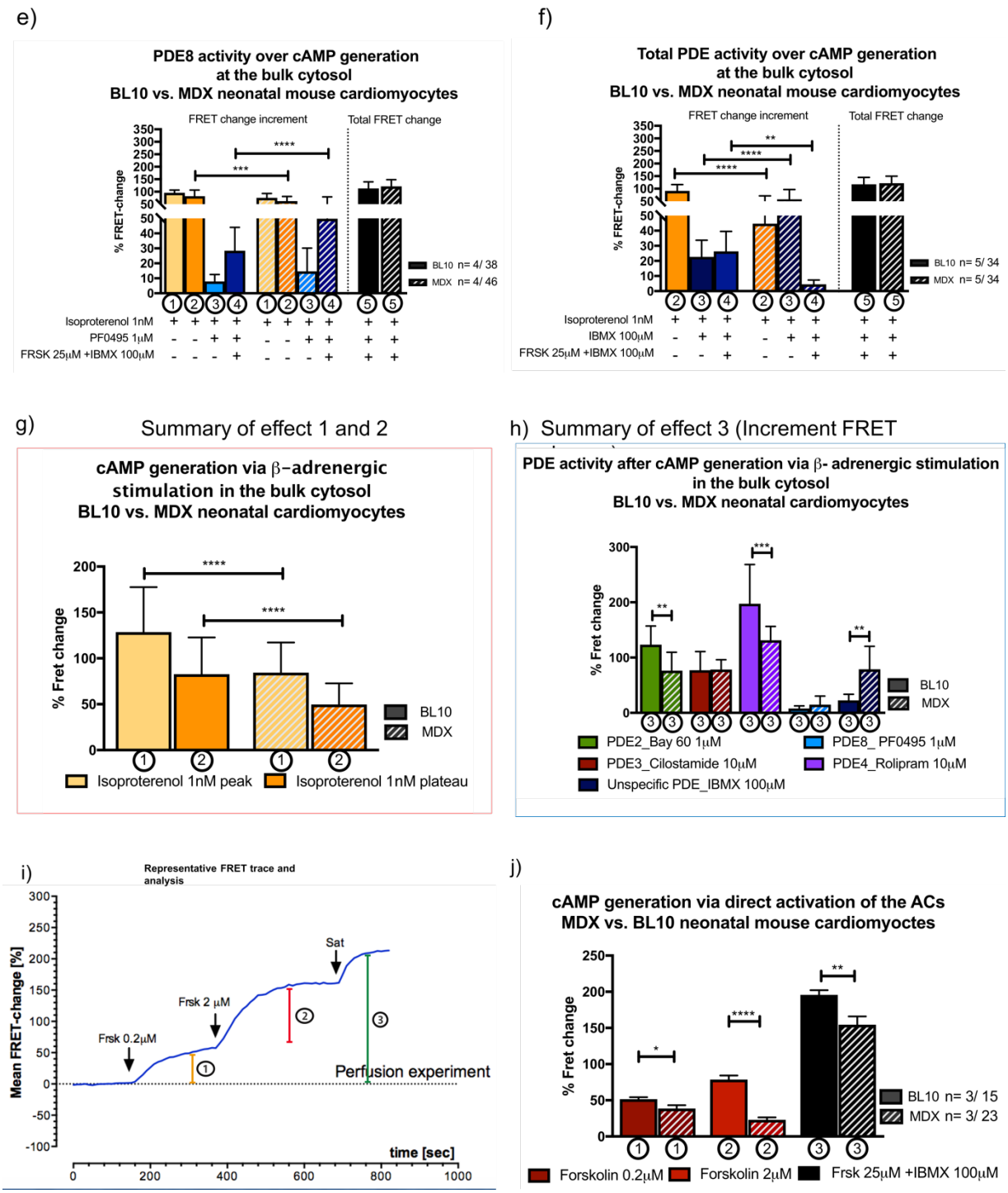
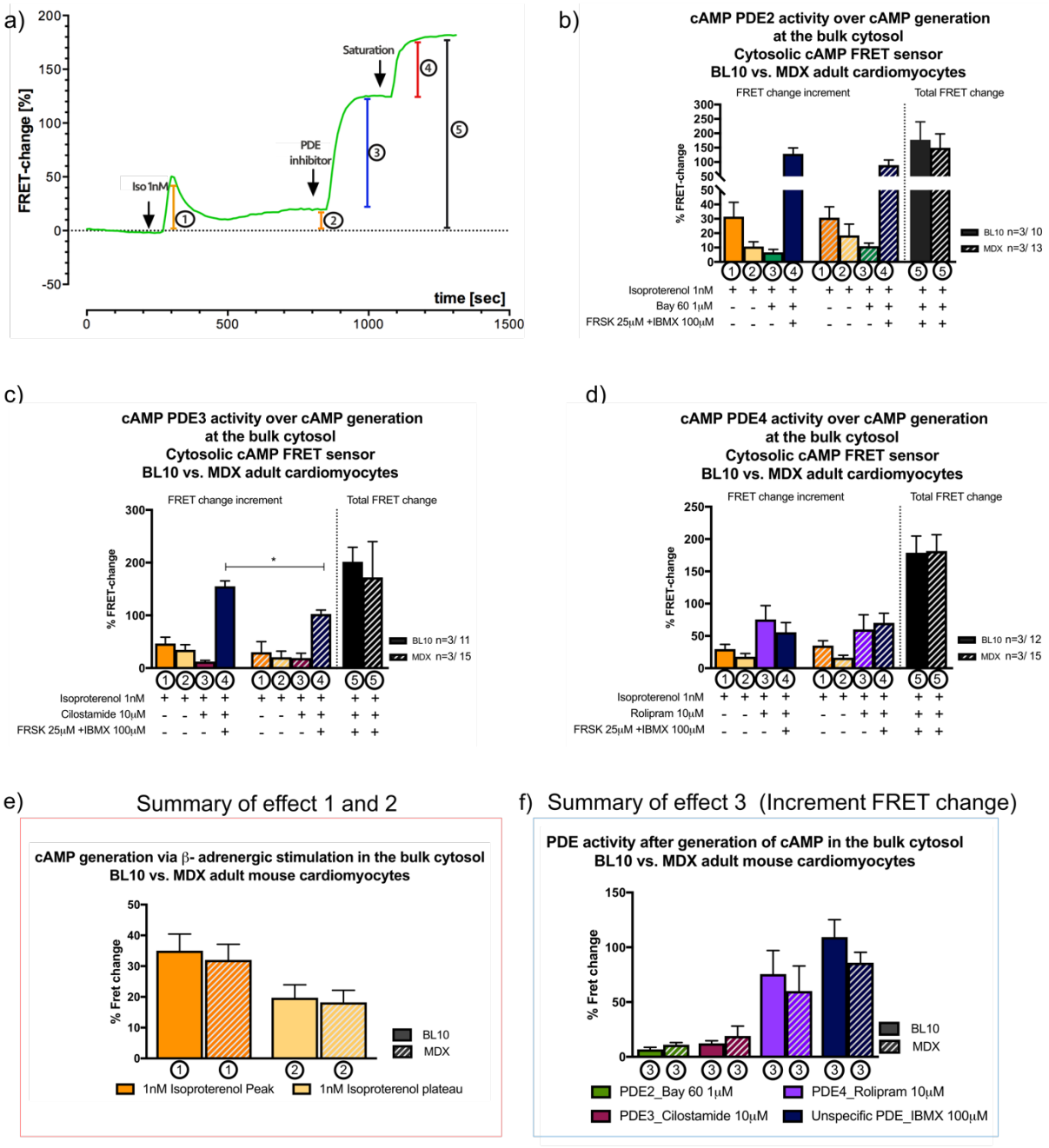


Figure 5.16.
Summary of FRET change recorded in mdx and C57BL/10ScSn neonatal cardiomyocytes individually expressing cytosolic cAMP FRET-based sensor, H187, in response to bath application of 1nM isoproterenol (a) followed by 1μM Bay 60 (c), 10μM Cilostamide (d), 10μM Rolipram (e), 1 μM PF-04957325 (f) and 100μM 3-isobutyl-1-methylxanthine (IBMX) (g) and 25μM of the adenylyl cyclase stimulator Forskolin (FRSK) in combination with 100μM 3-isobutyl-1-methylxanthine (IBMX) as saturation. Graph (j) represents Forskolin (FRSK) experiments where 0.2μM and 2μM were added by perfusion and in sequence, followed by saturating stimulus 25μM of the adenylyl cyclase stimulator Forskolin (FRSK) in combination with 100μM 3-isobutyl-1-methylxanthine (IBMX) and shown in representative trace on figure (i). The FRET-change trace in graph (a) and (i) represents experimental protocol and analysis protocol. The numbers and arrows below the trace indicates how the analysis was performed and which

areas of the trace are being represented in the bar graphs. The same number legend is used below each bar graph to facilitate understanding of the data. Graphs (b), (c), (d), (e) and (f) represent each experimental set separately, whereas graph (g) displays a summary of the response to NO donor + Bay 41 22-72 and graph (h) a summary of the single PDE inhibition effect. N number is indicated in each individual set as n= biological replicates/ individual cells. Error bars represent SEM; Two-way ANOVA, * = 0.05<p<0.01, ** = 0.01<p<0.001, ***= 0.001<p<0.0001, **** = p<0.0001.

Although most of the FRET experiments were performed in neonatal cardiomyocytes due to the limitations encountered in achieving reliable FRET measurements in adult cardiomyocytes (as discussed earlier), it was possible to replicate some of the experiments in isolated adult cardiac myocytes. Surprisingly, when compared to wt controls, mdx adult cardiomyocytes presented similar ability to generate cAMP upon isoproterenol stimulation and upon direct adenylyl cyclase stimulation (Figures 5.17 b and h). PDEs activity levels after cAMP generation were also found to be similar in mdx and control cells, even though higher mRNA levels were detected (Figure 5.14b). In order to elucidate whether mRNA levels of the two most abundant adenylyl cyclases (AC) in the heart, AC5 and AC6, were affected in mdx cardiomyocytes, qPCR experiments were performed in neonatal and adult samples. As shown in Figures 5.17i – 5.17j, AC5 and AC6 mRNA levels in mdx neonatal and adult cardiomyocytes were not different from the levels found in wt cells. AC5 is 0.5-fold higher in mdx adult cardiomyocytes, however, this increase does not reach statistical significance. This mRNA analysis suggests that the decreased levels of cAMP generated upon FRSK in mdx neonatal cardiomyocytes might be due to post-transcriptional regulation of the cyclase. A possible explanation is the presence of a negative feedback to the ACs as basal levels of cAMP are significantly higher in mdx cardiomyocytes.

Figure 5.17. cAMP PDE activity after cAMP generation in adult cardiomyocytes and mRNA analysis of AC 5 and 6



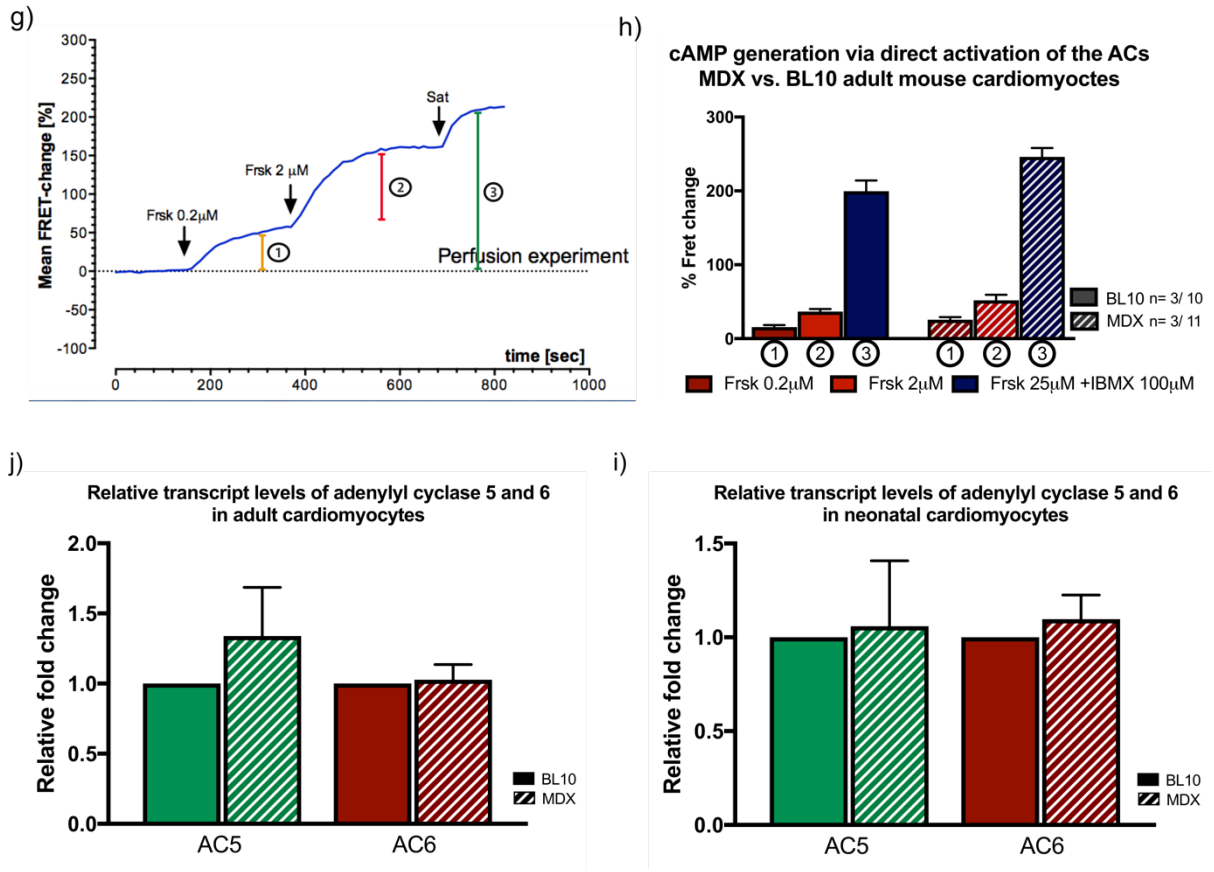


Figure 5.17. Summary of FRET change recorded in mdx and C57BL/10ScSn adult cardiomyocytes individually expressing cytosolic cAMP FRET-based sensor, H187, in response to bath application of 1nM isoproterenol (a) followed by 1μM Bay 60 (c), 10μM Cilostamide (d), 10μM Rolipram (e), followed by 25μM of the adenylyl cyclase stimulator Forskolin (FRSK) in combination with 100μM 3-isobutyl-1-methylxanthine (IBMX) as saturation. Graph (f) represents Forskolin (FRSK) experiments where 0.2μM and 2μM were added by perfusion and in sequence, followed by saturating stimulus 25μM of the adenylyl cyclase stimulator Forskolin (FRSK) in combination with 100μM 3-isobutyl-1-methylxanthine (IBMX). The FRET-change trace in graph (a) and (g) represents experimental protocol and analysis protocol. The numbers and arrows below the trace indicates how the analysis was performed and which areas of the trace are being represented in the bar graphs. The same number legend is used below each bar graph to facilitate understanding of the data. Graphs (b), (c), and (d) represent each experimental set separately, whereas graph (e) displays a summary of the cAMP generation data and graph (f) the summary of PDE inhibition responses. N = 3 biological replicates and ≥ 4 individual cells. Error bars represent SEM; Two-way ANOVA for all FRET experimental data. Analysis of adenylyl cyclase 5 (AC5) and adenylyl cyclase 6 (AC6) mRNA levels in neonatal cardiomyocytes (i) and adult cardiomyocytes (j) with T-test. qPCR graphs show means of 3 biological replicates measurements in triplicate and normalised related to wt levels.

5.3.5. Adult mdx cardiomyocytes present higher levels of NO insensitive $_{s}$GC

Soluble guanylyl cyclase (sGC) is a heterodimeric enzyme composed of two α and two β subunits (α 1, α 2, β 1, β 2) (Mergia et al. 2003). α2β1 is known to be recruited to the plasma membrane via its PSD-95 interaction with PDZ domains and plays a crucial role

in mediating NO actions on membrane targets by producing a membrane localised pool of cGMP. The α1β1 isoform is expressed in the cytosol and generates non-localised cGMP (Bellingham and Evans 2007). Interestingly, nNOS is recruited to α1 syntrophin at the dystrophin complex via the same mechanism, which suggests that α2β1 might also be co-localised at the dystrophin complex. In order to explore soluble guanylyl cyclases (sGC) expression levels and activity in adult cardiomyocytes without relying on FRET measurements, western blotting for the β1 subunit of sGC, which is part of both catalytically active heterodimers, and sGC activity assay were performed.

As shown in Figures 5.18a – 5.18b sGC β1 subunit protein level is significantly higher in adult mdx cardiomyocytes when compared to control, suggesting that there might be an up regulation of sGC in the mdx heart. This data is in agreement with previously reported data where up regulation of the α1 subunit in the mdx heart was encountered (Maya Khairallah et al. 2007). As β1 also complexes with the α2 subunit, the α2β1 enzyme which is recruited to the plasma membrane, could also be increased in the mdx heart.

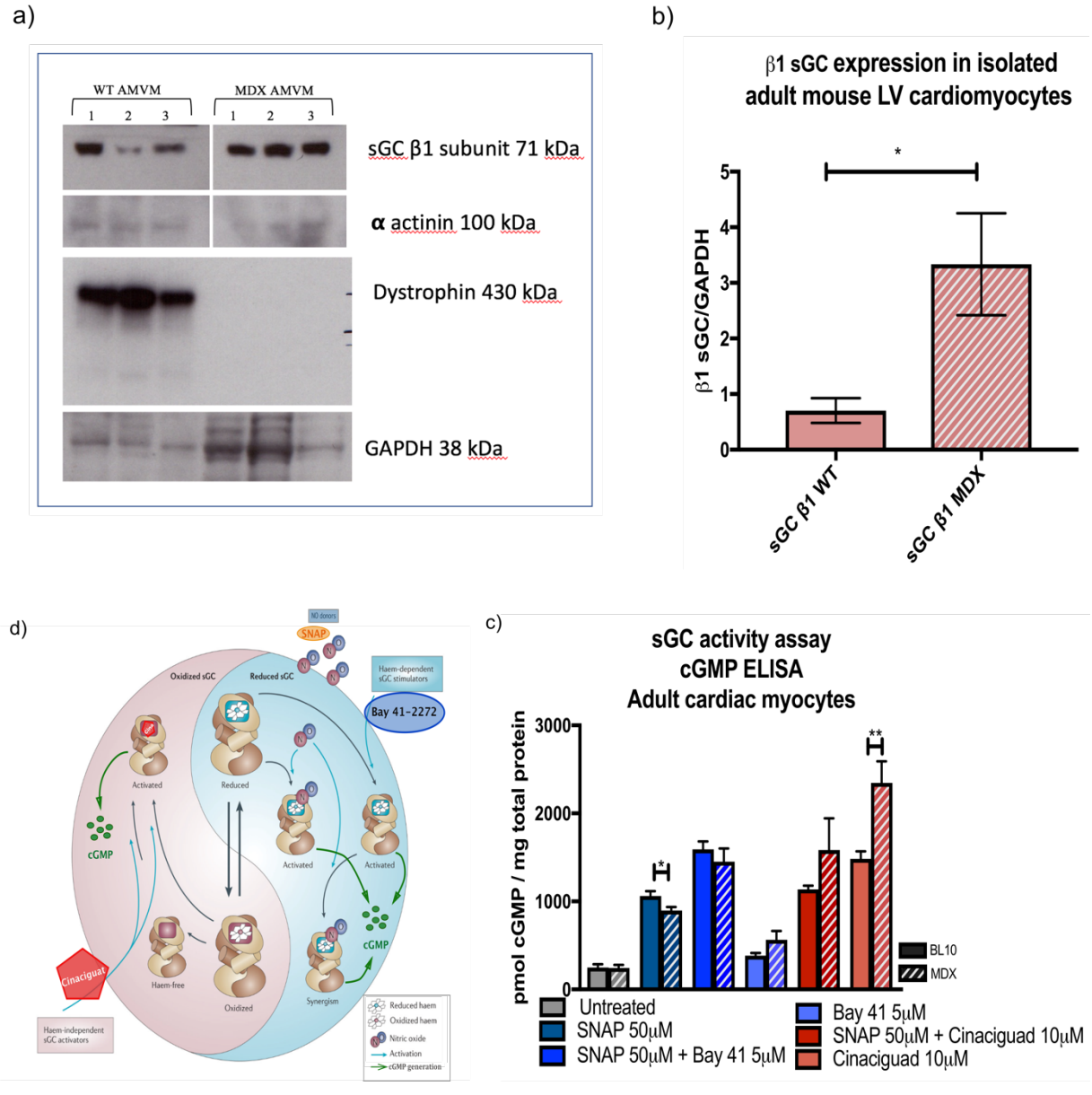
The presence of a prosthetic heme group is necessary for the sGC activation by NO. Although both subunits are required for proper binding and orientation of the heme group, β1 subunit plays a more important role in this process. In order to activate sGC, the uncharged NO radical binds to the reduced Fe^{2+} prosthetic heme group leading to a 200-fold increase in catalytic activity (Friebe and Koesling 2003). In addition to the removal of the heme group, heme oxidation leads to NO insensitive sGC. Oxidative stress, which generates reactive oxygen and nitrogen species, such as superoxide and peroxynitrite, can change the redox state of sGC, making it unresponsive to endogenous NO and NO-releasing drugs (Evgenov et al. 2006). It has been shown that mdx hearts present increased NADPH oxidase activity, which is a possible source of reactive oxygen species (ROS) (I. A. Williams and Allen 2007), as well as ROS-dependent nitrosylation (Fauconnier et al.

2010) and oxidation (Ullrich et al. 2009) of the RyR2s with contribution to increased Ca^{2+} from the SR and arrhythmias. Furthermore, increased ROS production was shown in stretched mdx cardiomyocytes (Prosser, Ward, and Lederer 2011). Therefore, it was important to assess whether mdx cardiomyocytes presented higher concentration of oxidised sGC. Figure 5.18c display schematic on the mechanism of action of Cinaciguat, drug which activated oxidised sGC.

sGC activity assay was performed by measuring the cGMP generated by adult cardiomyocytes under different treatments (by cGMP ELISA) (Figure 5.18d). The treatments included: (1) NO donor SNAP, (2) NO donor SNAP in combination with the sGC stimulator Bay 41-2272, a reduced heme-dependent but NO-independent sGC stimulator, (3) Bay 41-2272 alone, (4) NO donor SNAP in combination with Cinaciguat (also known as Bay 58-2667), which is a heme-independent sGC activator that activates the sGC by binding to the unoccupied heme-binding pocket or by replacing the weakly bound deficient or oxidised heme-group. Therefore, reduced sGC is unresponsive to this compound (Evgenov et al. 2006). Finally (5) Cinaciguat was used alone. The assay showed that adult mdx cardiomyocytes respond significantly more to the sGC activator Cinaciguat, and significantly less to the NO donor alone when compared to the wt cardiomyocytes. These results suggest that dystrophic adult cardiomyocytes present significantly more oxidised sGC as compared to controls. Interestingly, the response to the sGC stimulator Bay 41-2272 alone and in combination to SNAP, was not different between mdx and wt cardiomyocytes. The proportion of reduced and oxidised sGC in neonatal cardiomyocytes was assessed by measuring cGMP generation by FRET. As shown in Figure 5.18e and 5.18, fmdx neonatal cardiomyocytes seem to have similar amount of oxidised sGC in the cytosol than wt cells. It is important to keep in mind that

the FRET approach measures cGMP only at the cytosol, whereas the assay detected total cGMP within the cell as it takes use of cell lysates.

Figure 5.18. sGC activity and redox state in adult and neonatal mdx cardiomyocytes



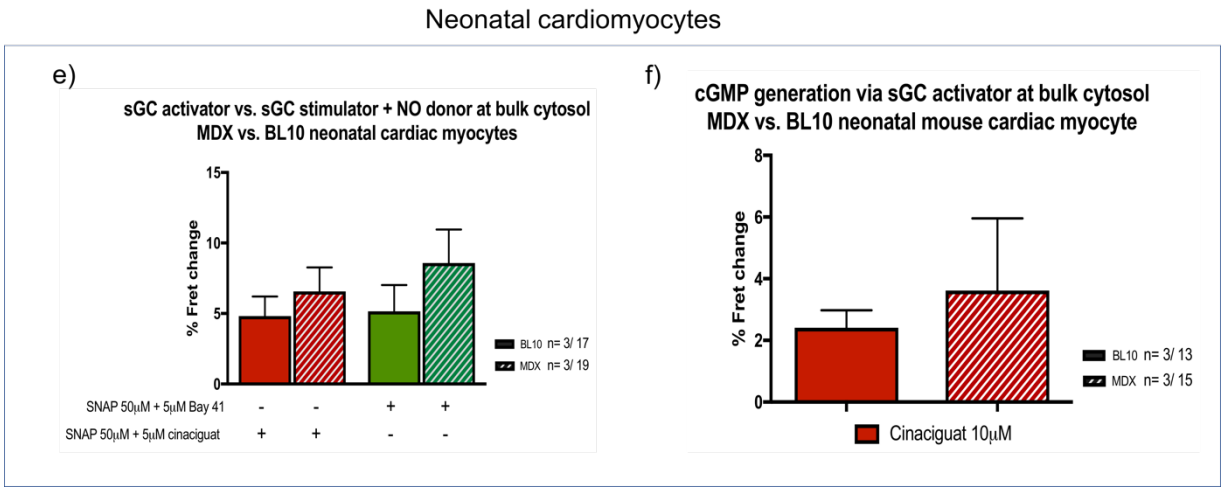


Figure 5.18.
Western blotting analysis of soluble guanylyl cyclase beta1 subunit (a and b). Quantification and analysis of Western blotting of isolated cardiomyocytes lysate from 12 weeks old mdx and C57BL/10ScSn mice (b) and representative western blotting membrane (a). (c) Schematic figure illustrating the intracellular redox equilibrium of the two sGC redox states, nitric oxide (NO)-sensitive reduced (blue) and NO-insensitive oxidized sGC (pink). Adapted from (Evgenov et al. 2006). Haem-independent sGC activators such as Cinaciguat activate the oxidized or haem-deficient form. By contrast, haem-dependent stimulators such as BAY 41-2272, can activate the reduced sGC and show a strong synergism when combined with NO; (d) Analysis of sGC activity assay where cGMP was measured by using direct cGMP ELISA kit from Enzo in untreated cells and after treatment with 50µM SNAP, 50µM SNAP + 5µM Bay 41-2272, 5µM Bay 41-2272, 50µM SNAP + 10µM Cinaciguat and 10µM Cinaciguat; Graphs show densitometric analysis and present the ratio value of total sGC β1 subunit protein after normalisation to the endogenous control GAPDH. Summary of FRET change recorded in mdx and C57BL/10ScSn neonatal cardiomyocytes individually expressing cytosolic cGMP FRET-based sensor, cGI500, in response to bath application of 50µM SNAP + 5µM Bay 41-2272 or 50µM SNAP + 10µM Cinaciguat (e), and 10µM Cinaciguat (f). N= 3 biological replicates for western blotting, sGC assay and FRET. Error bars represent SEM; Mann- Whitney applied for Western blot quantification analysis and T-test for FRET data, * = 0.05<p<0.01, ** = 0.01<p<0.001.

5.3.6. mdx neonatal cardiomyocytes present altered basal levels of $_{c}$AMP and $_{c}$GMP at specific subcellular compartments.

Concentrations of free basal cGMP and cAMP at the plasma membrane and the outer mitochondria membrane were measured by comparing the basal FRET ratios of neonatal and adult cardiomyocytes from mdx and BL10 mice expressing the specific targeted FRET-based sensors (discussed in Chapter 4). As presented in Figure 5.19a and b, basal concentrations of cAMP and cGMP at the plasma membrane, share similar relationship encountered in the cytosol (Figure 5.10 and 5.11): cGMP levels are significant lower in mdx neonatal cardiomyocytes but significantly higher in adults, and cAMP is significant

higher in mdx neonatal cardiomyocytes, maintaining higher levels at the plasma membrane of adult mdx cardiomyocytes.

Figure 5.19 Basal cAMP and cGMP concentration at the plasma membrane

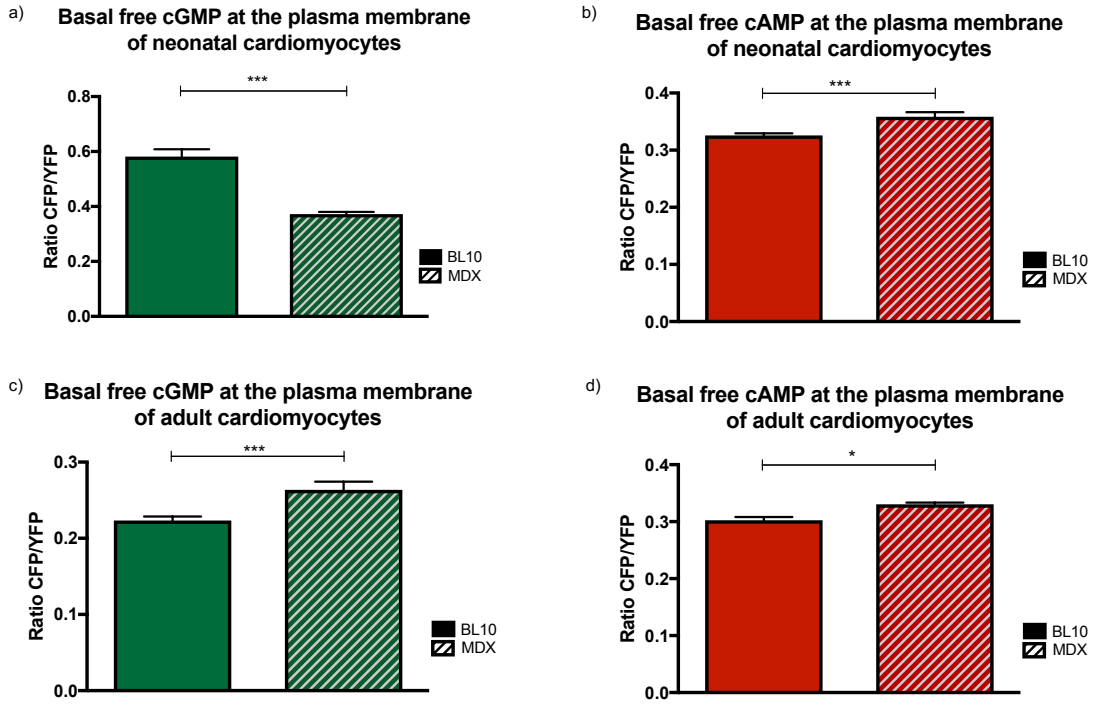


Figure 5.19.
Measurement of basal cGMP levels at the plasma membrane of isolated neonatal cardiomyocytes (a) and adult cardiomyocytes (c) by using basal FRET ratios of cells expressing the MPcGI500 FRET sensor; Measurement of basal cAMP levels at the plasma membrane of isolated neonatal cardiomyocytes (a) and adult cardiomyocytes (c) by using basal FRET ratios of cells expressing the MPH187 FRET sensor; Graphs show means basal rations of ≥ 20 cells per condition; Error bars represent SEM; T-test, * = 0.05<p<0.01, ** = 0.01<p<0.001, ***= 0.001<p<0.0001, **** = p<0.0001.

Interestingly, basal levels of cGMP at the outer mitochondria membrane (OMM) follow the same trend discussed above, with significantly lower levels in mdx neonatal cardiomyocytes and higher in adult cardiomyocytes, however, the cAMP basal levels at the OMM of mdx cardiomyocytes is significant lower at both ages analysed. These results suggest that, even though cGMP is compartmentalised, the basal cGMP levels suffer similar changes at all three cellular compartments of mdx cardiomyocytes

analysed whereas the cAMP signalling present different regulation at the distinct subcellular compartments explored.

Figure 5.20. Basal cAMP and cGMP concentration at the outer mitochondria membrane

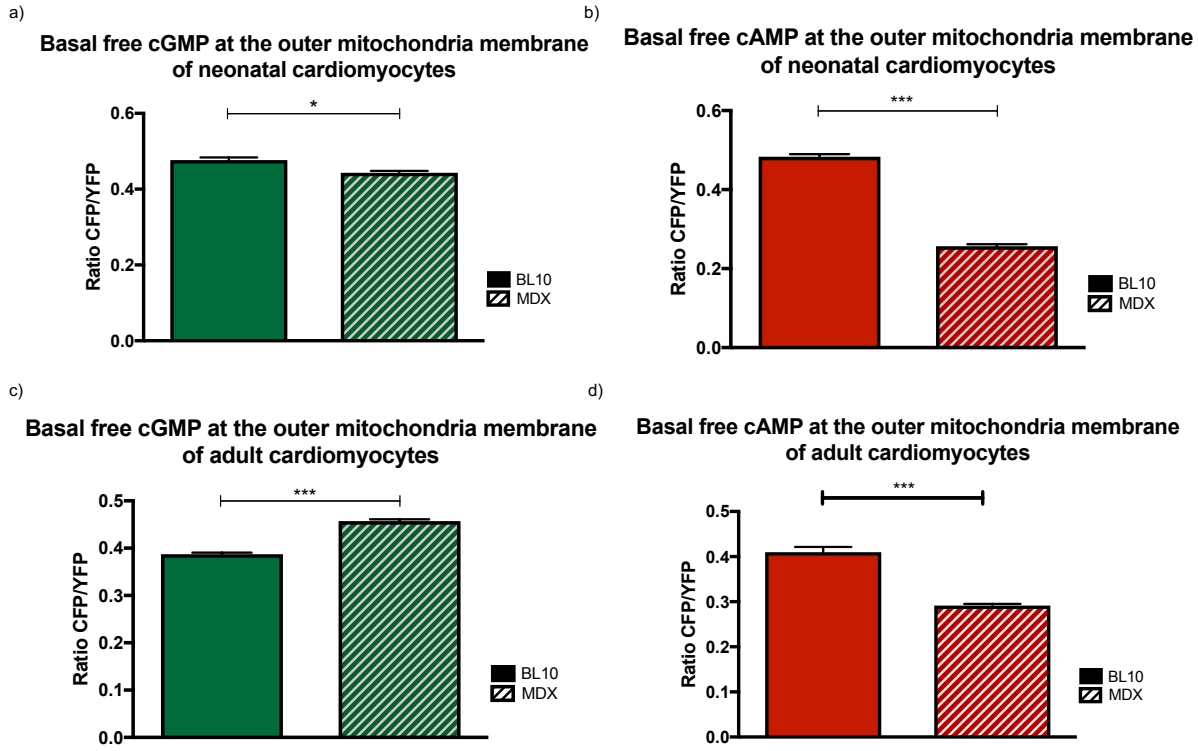


Figure 5.20.
Measurement of basal cGMP levels at the outer mitochondria membrane of isolated neonatal cardiomyocytes (a) and adult cardiomyocytes (c) by using basal FRET ratios of cells expressing the OMM ^{T}cGI500^{VV} FRET sensor; Measurement of basal cAMP levels at the outer mitochondria membrane of isolated neonatal cardiomyocytes (a) and adult cardiomyocytes (c) by using basal FRET ratios of cells expressing the OMM H187 FRET sensor; Graphs show means basal rations of ≥ 20 cells per condition; Error bars represent SEM; T-test, * = 0.05<p<0.01, ** = 0.01<p<0.001, ***= 0.001<p<0.0001, **** = p<0.0001.

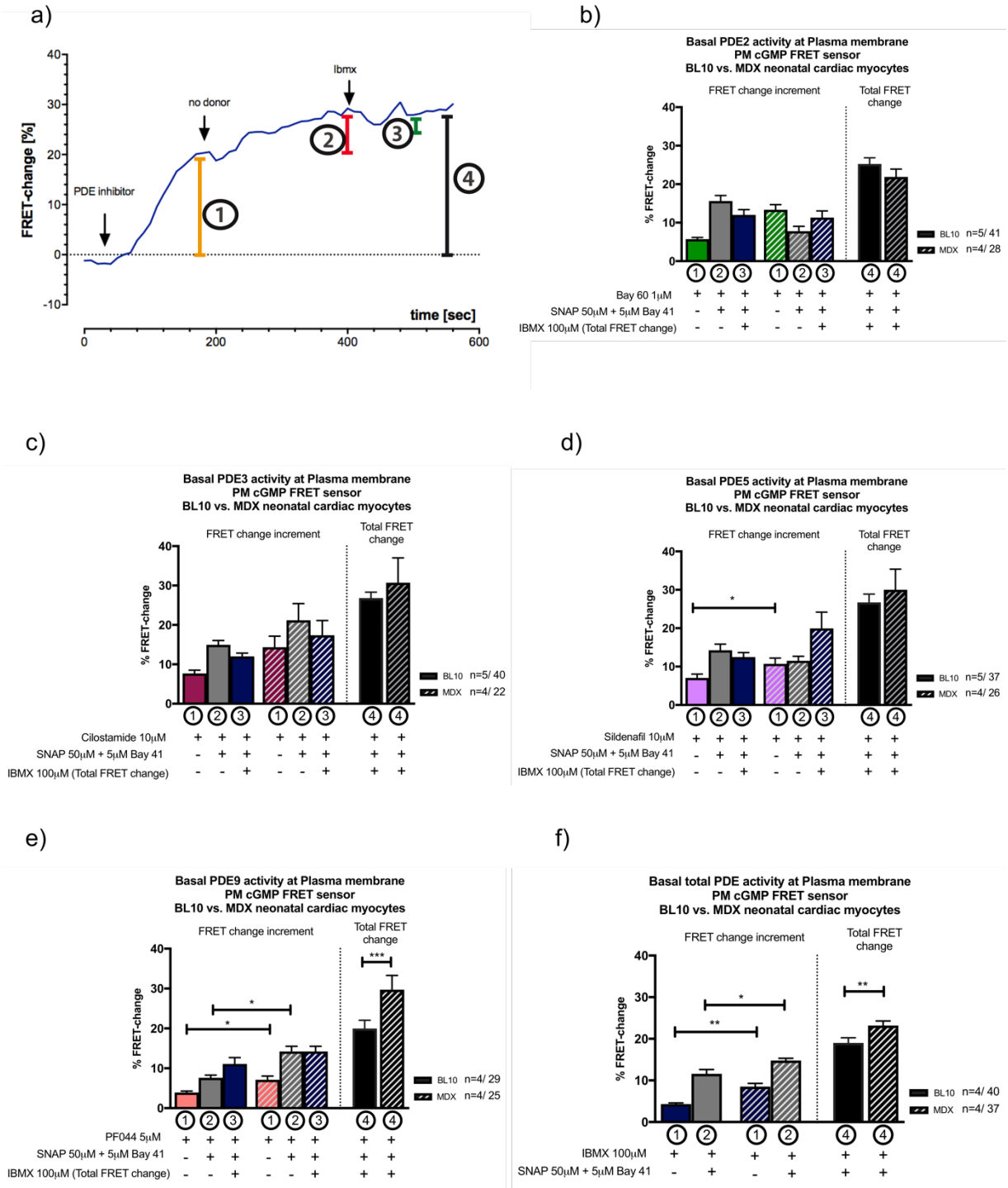
5.3.7. PDE activity is significantly altered at the plasma membrane of neonatal mdx cardiomyocytes

As the PDEs play important role in the regulation and compartmentalisation of the cAMP and cGMP signalling, a systematic analysis of the PDEs activity at both compartments discussed above, plasma membrane and outer mitochondria membrane, was performed by using FRET imaging. Unfortunately, this analysis was performed in neonatal cardiomyocytes only. Apart from the difficulties in measuring cGMP signalling in adult

cardiomyocytes, as already discussed, these experiments were not performed due to time limitations.

Analysis of compartmentalised CN signalling has never been performed in mdx cardiomyocytes before. As DMD is characterised by a membrane dysfunction due to the lack of dystrophin and disruption of the dystrophin complex, it was interesting to understand if the CN pathways were altered at this specific subcellular compartment of the mdx cardiomyocytes. As shown in Figure 5.21, the activity of most of the cGMP PDEs are significantly higher at the basal levels at the plasma membrane of neonatal mdx cardiomyocytes. This higher activity might possibly contribute to the significant low basal levels of cGMP encountered at the plasma membrane and also at other subcellular compartments of mdx neonatal cardiomyocytes.

Figure 5.21. Basal cGMP PDE activity at the plasma membrane of neonatal cardiomyocytes



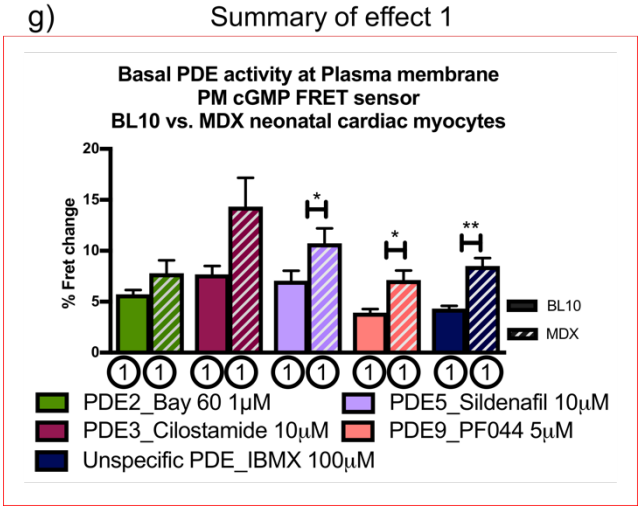
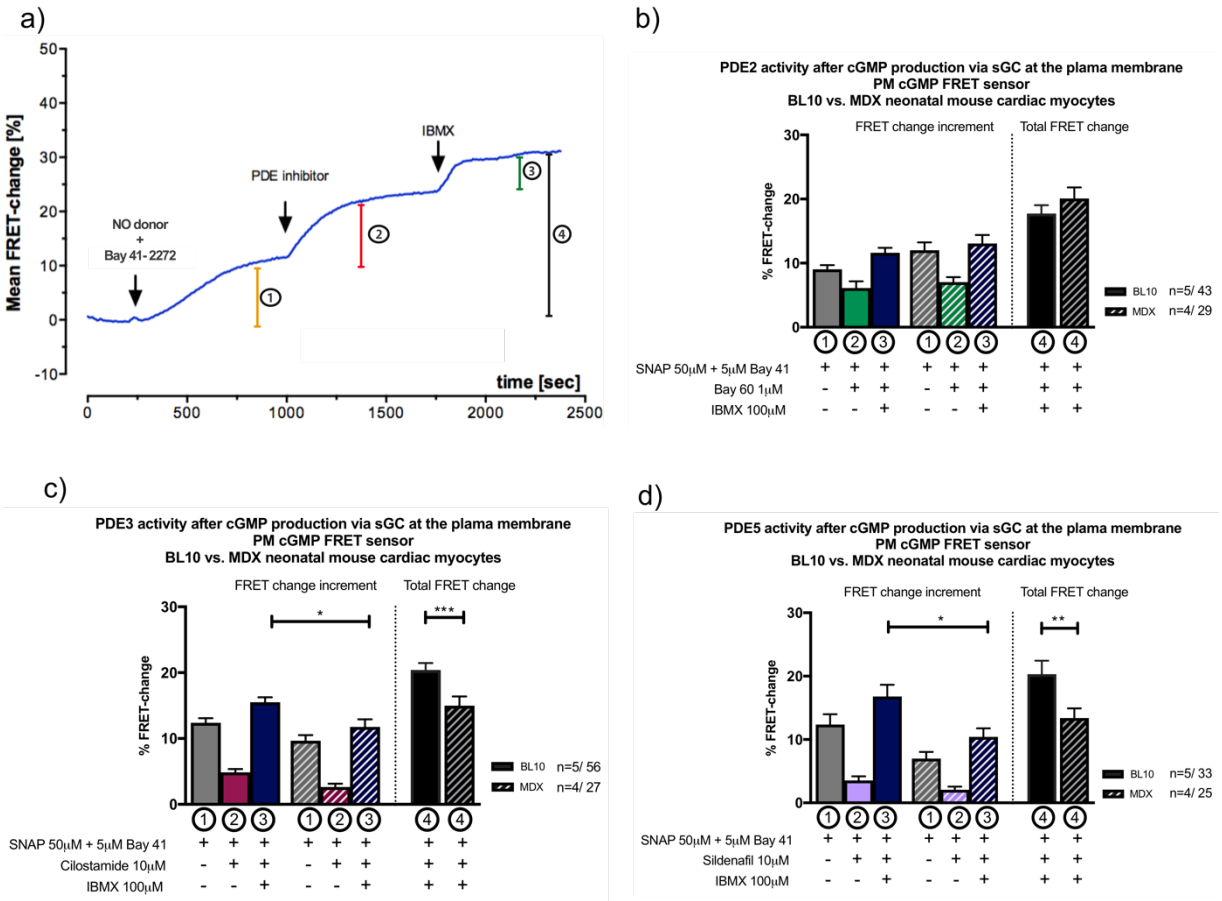


Figure 5.21.
Summary of FRET change recorded in mdx and C57BL/10ScSn individually expressing plasma membrane cGMP FRET-based sensor, MP cGI 500, in response to bath application of 1μM Bay 60 (b), 10μM Cilostamide (c), 10μM Sildenafil (d), 5μM PF-04447943 (e) and 100μM 3-isobutyl-1-methylxanthine (IBMX) (f) followed by 50μM of the NO donor S-Nitroso-N-Acetyl-D,L-Penicillamine (SNAP) in combination of 5 μM of soluble guanylyl cyclase stimulator BAY 41-2272 and 100μM 3-isobutyl-1-methylxanthine (IBMX). The FRET-change trace in graph (a) represents experimental protocol and analysis protocol. The numbers and arrows below the trace indicates how the analysis was performed and which areas of the trace are being represented in the bar graphs. The same number legend is used below each bar graph to facilitate understanding of the data. Graphs (b), (c), (d), (e) and (f) represent each experimental set separately, whereas graph (g) displays a summary of the relevant data from the individual sets. N number is indicated in each individual set as n= biological replicates/ individual cells. Error bars represent SEM; Two-way ANOVA, * = 0.05<p<0.01, ** = 0.01<p<0.001, ***= 0.001<p<0.0001.

The amount of cGMP generated upon NO donor in combination with the sGC stimulator at the plasma membrane of mdx neonatal cardiomyocytes was significantly lower than in wt cardiomyocytes (Figure 5.22b –f or summary panel g), suggesting that less NO sensitive sGC might be present at the dystrophic plasma membrane. In fact, when the cells were treated with the sGC activator, Cinaciguat, mdx neonatal cardiomyocytes responded significantly more than the wt control (Figure 5.22i). This data indicate that the lower basal cGMP observed in the plasma membrane of neonatal cardiomyocytes might be a consequence of higher oxidised sGC in the plasma membrane.

Another surprising finding is that the PDE activity, which was significantly higher at basal levels, is unchanged after cGMP generation at the plasma membrane of mdx cardiomyocytes. Although not completely understood, these data indicate that the high PDE activity recorded at basal levels might be partially a reflect of the activity of the pGC pathway at the plasma membrane of mdx cardiomyocytes.

Figure 5.22. cGMP PDE activity at the plasma membrane of neonatal cardiomyocytes after cGMP generation via sGC



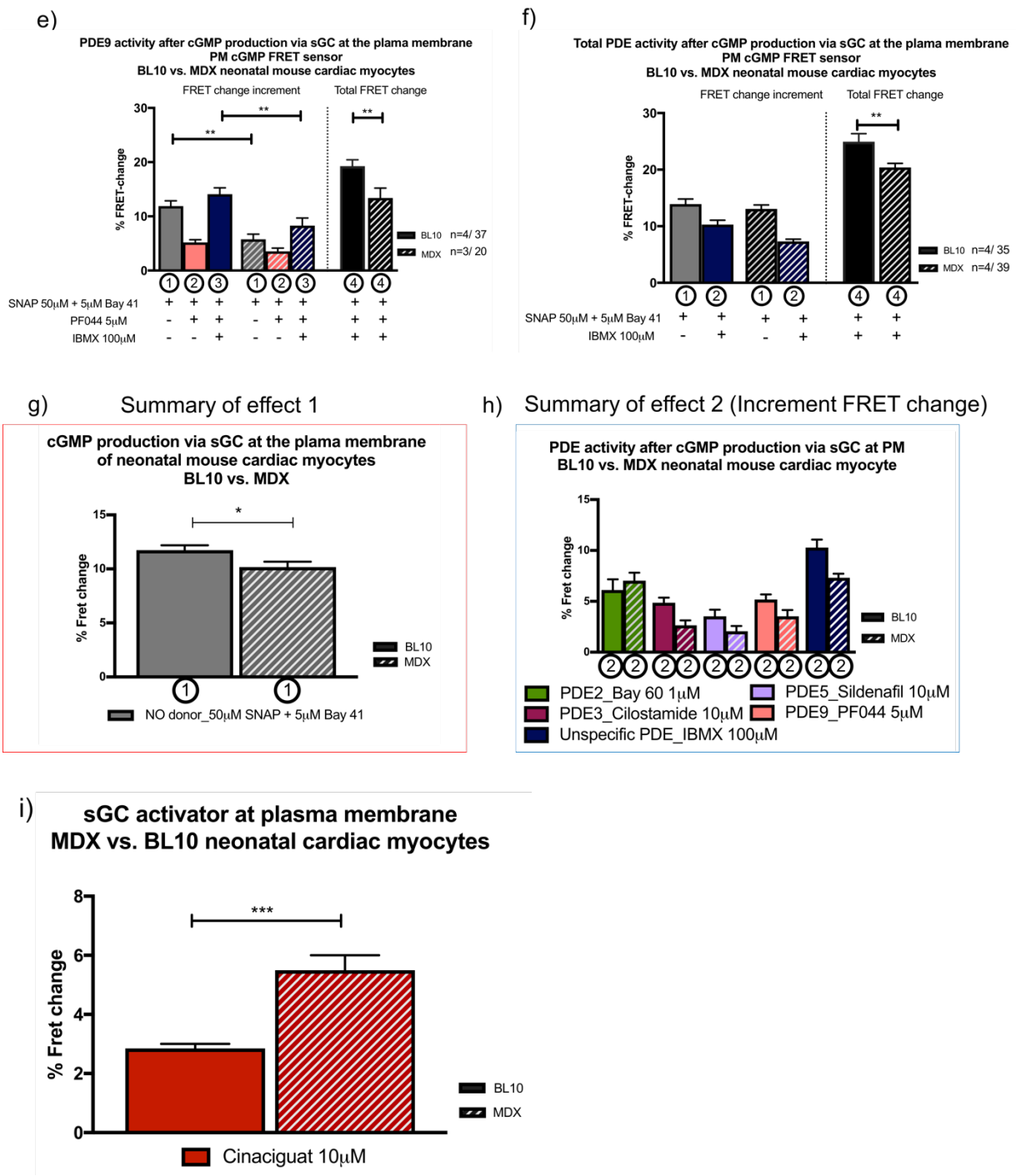
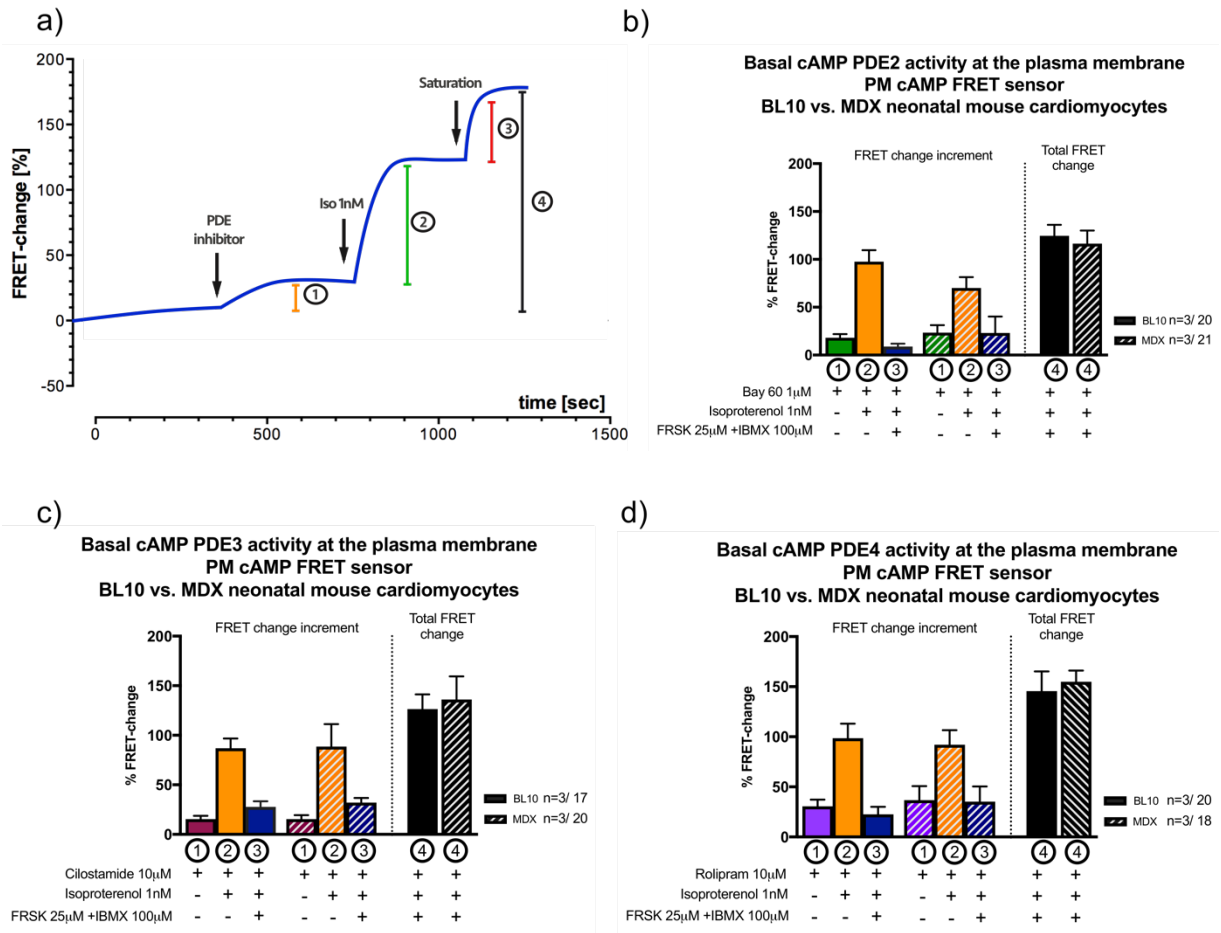


Figure 5.22.
Summary of FRET change recorded in mdx and C57BL/10ScSn neonatal cardiomyocytes individually expressing the plasma membrane cGMP FRET-based sensor, MP cGI 500, in response to bath application of NO donor S-Nitroso-N-Acetyl-D,L-Penicillamine (SNAP) in combination of 5µM of soluble guanylyl cyclase stimulator BAY 41-22721µM (a) followed by 1µM Bay 60 (c), 10µM Cilostamide (d), 10µM Sildenafil (e), 5µM PF-04447943 (f) and 100µM 3-isobutyl-1-methylxanthine (IBMX) (g) and 100µM 3-isobutyl-1-methylxanthine (IBMX) to fully inhibit PDEs, and 10µM Cinaciguat (h). The FRET-change trace in graph (a) represents experimental protocol and analysis protocol. The numbers and arrows below the trace indicates how the analysis was performed and which areas of the trace are being represented in the bar graphs. The same number legend is used below each bar graph to facilitate understanding of the data. Graphs (b), (c), (d), (e) and (f) represent each experimental set separately, whereas graph (g) displays a summary of NO donor + Bay 41 22-72 response and graph (h) a summary

of the single PDE inhibition data. N number is indicated in each individual set as n= biological replicates/ individual cells. Error bars represent SEM; Two-way ANOVA, * = 0.05<p<0.01, ** = 0.01<p<0.001, ***= 0.001<p<0.0001.

The basal cAMP-PDE activity at the plasma membrane of mdx neonatal cardiomyocytes does not seem to be as affected as the cGMP-PDE activity. As shown in Figure 5.23, the only PDE presenting significant alterations is the PDE8, which seems to be less active in mdx cells (Figures 5.23e and g).

Figure 5.23. Basal cAMP PDE activity at the plasma membrane of neonatal cardiomyocytes



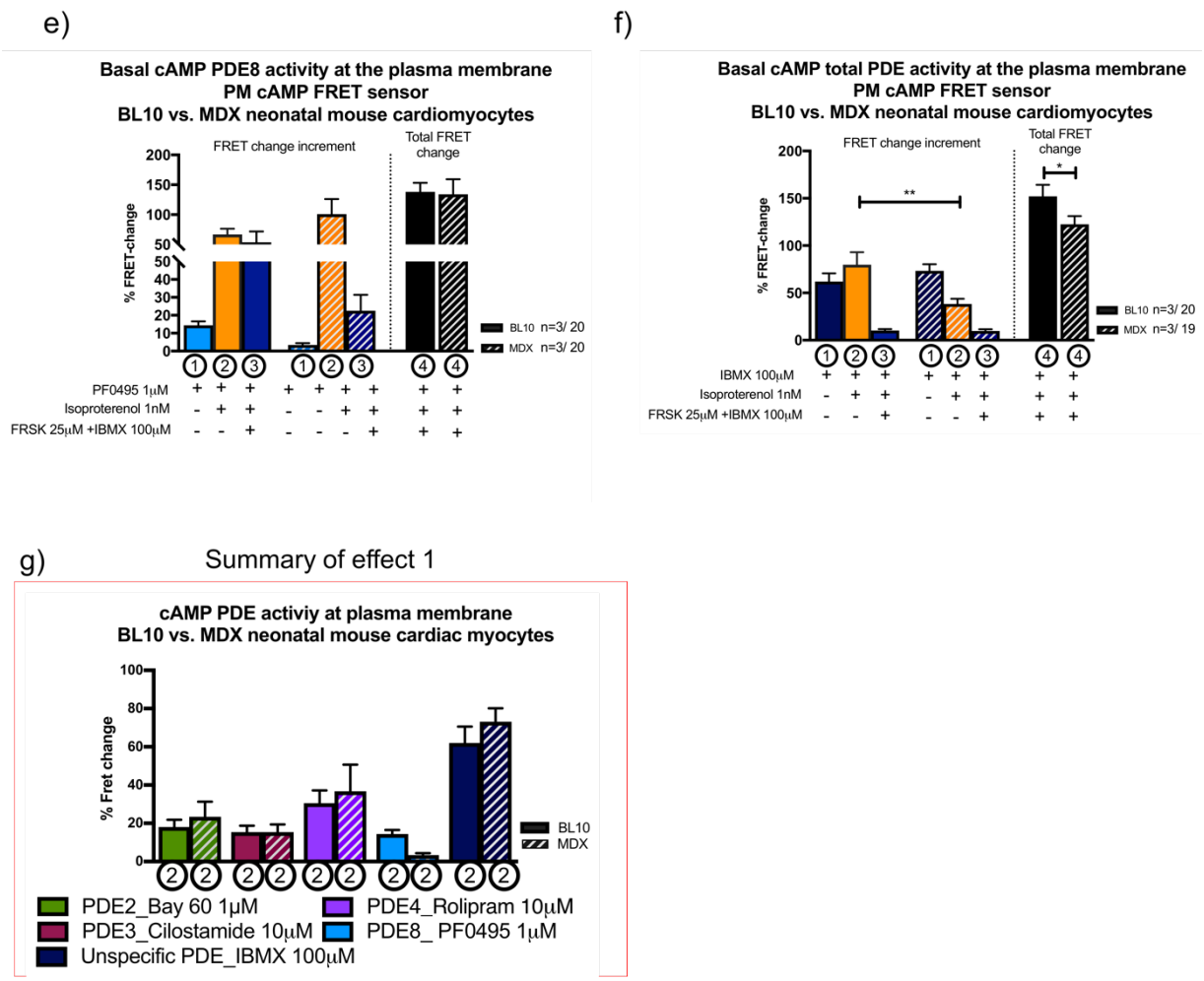
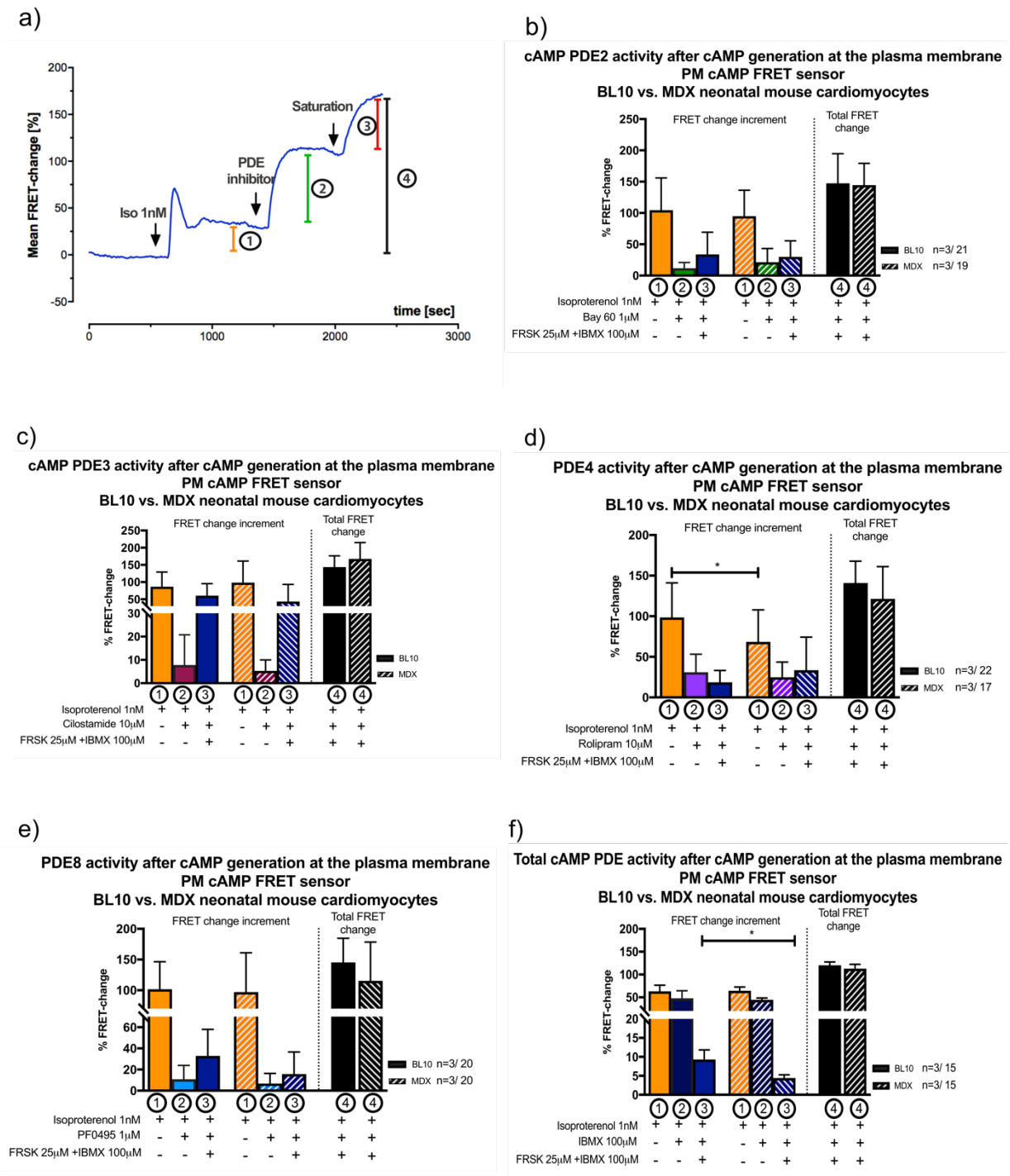


Figure 5.23.
Summary of FRET change recorded in mdx and C57BL/10ScSn individually expressing the plasma membrane cAMP FRET-based sensor, PM H187, in response to bath application of 1μM Bay 60 (b), 100μM 3-isobutyl-1-methylxanthine (IBMX) (c), 1 μM PF-04957325 (d), 10μM Cilostamide (e), and 10 μM Rolipram (f) followed by 1nM Isoproterenol and 25μM of the adenylyl cyclase stimulator Forskolin (FRSK) in combination with 100μM 3-isobutyl-1-methylxanthine (IBMX). The FRET-change trace in graph (a) represents experimental protocol and analysis protocol. The numbers and arrows below the trace indicates how the analysis was performed and which areas of the trace are being represented in the bar graphs. The same number legend is used below each bar graph to facilitate understanding of the data. Graphs (b), (c), (d), (e) and (f) represent each experimental set separately, whereas graph (g) displays a summary of the relevant data from the individual sets. N number is indicated in each individual set as n= biological replicates/ individual cells. Error bars represent SEM; Two-away ANOVA.

No differences were found in the ability to generate cAMP upon beta-adrenergic stimulation nor in the activity of PDEs after cAMP generation at the plasma membrane of mdx neonatal cardiomyocytes (Figure 5.24), suggesting that the higher basal cAMP levels observed at the plasma membrane might be a consequence of the reduced PDE8 basal activity at this specific subcellular compartment.

Figure 5.24. cAMP PDE activity at the plasma membrane of neonatal cardiomyocytes after cAMP generation



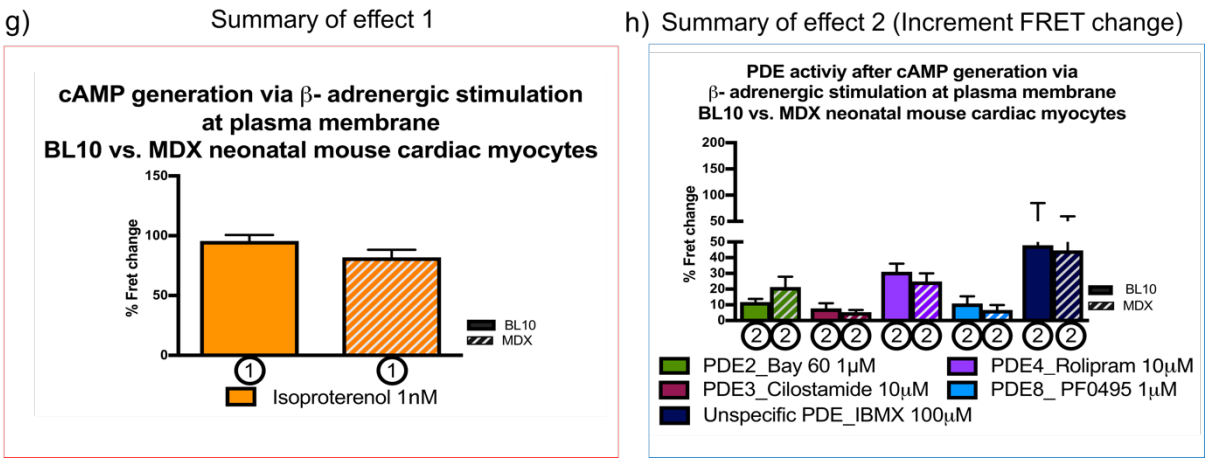


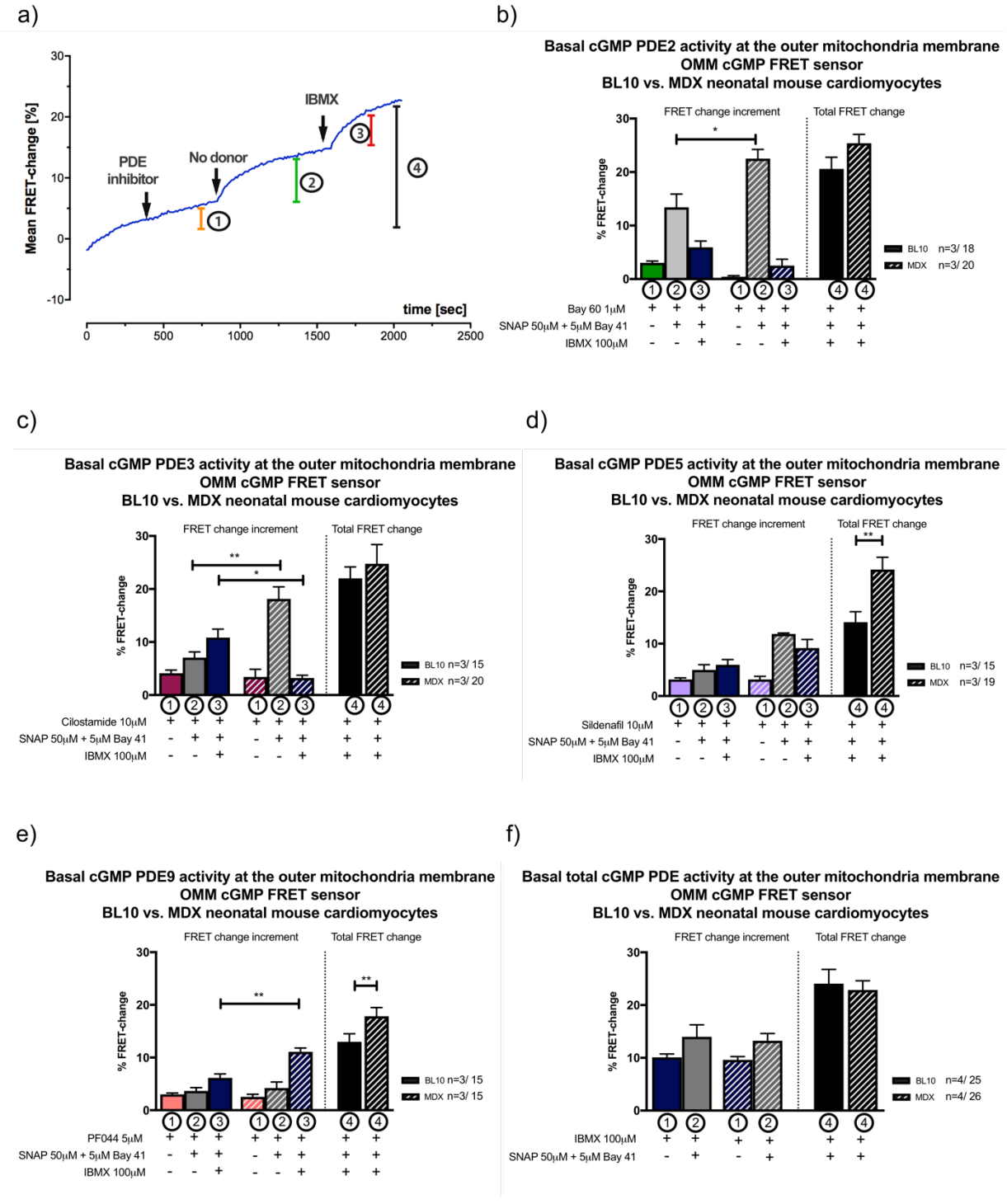
Figure 5.24.
Summary of FRET change recorded in mdx and C57BL/10ScSn neonatal cardiomyocytes individually expressing the plasma membrane cAMP FRET-based sensor, MP H187, in response to bath application of 1nM isoproterenol (a) followed by 1μM Bay 60 (c), 10μM Cilostamide (d), 10μM Rolipram (e), 1 μM PF-04957325 (f) and 100μM 3-isobutyl-1-methylxanthine (IBMX) (g) and 25μM of the adenylyl cyclase stimulator Forskolin (FRSK) in combination with 100μM 3-isobutyl-1-methylxanthine (IBMX) as saturation. The FRET-change trace in graph (a) represents experimental protocol and analysis protocol. The numbers and arrows below the trace indicates how the analysis was performed and which areas of the trace are being represented in the bar graphs. The same number legend is used below each bar graph to facilitate understanding of the data. Graphs (b), (c), (d), (e) and (f) represent each experimental set separately, whereas graph (g) displays a summary of the response to Isoproterenol and graph (h) a summary of the single PDE inhibition effect. N number is indicated in each individual set as n= biological replicates/ individual cells. Error bars represent SEM; Two-way ANOVA, * = 0.05<p<0.01.

5.3.8. The $_{c}$AMP pathway but not $_{c}$GMP is affected at the outer mitochondria membrane of mdx neonatal cardiomyocytes

The last subcellular compartment analysed was the outer mitochondria membrane (OMM) domain in isolated cardiomyocytes. When compared to wt control cells, the basal activity of most of the cGMP PDEs tested were not altered at the OMM of mdx cardiomyocytes, with exception of PDE2, which appeared to be less active (Figure 5.25). However, mdx cardiomyocytes generated significantly more cGMP upon NO donor after PDE3, PDE5 and PDE2 inhibition (Figure 5.25b, c and d). This data might suggest involvement of these PDEs in the regulation of sGC at the OMM of mdx cardiomyocytes. Interestingly, the response of IBMX was not different between both cell types, even

though PDE2 seemed to be substantially less active in the OMM of mdx cardiomyocytes at basal level.

Figure 5.25. Basal cGMP PDE activity at the outer mitochondria membrane of neonatal cardiomyocytes



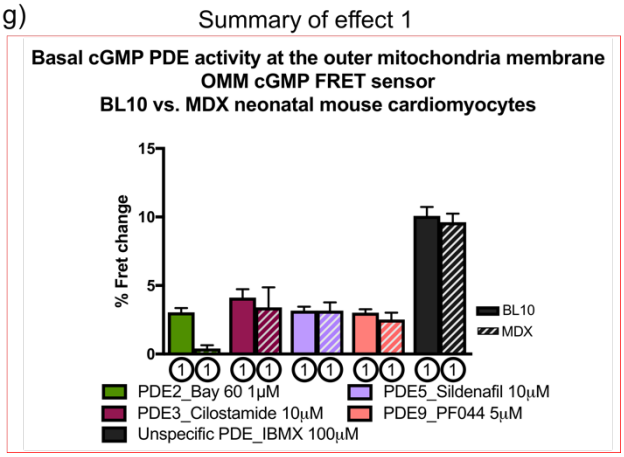
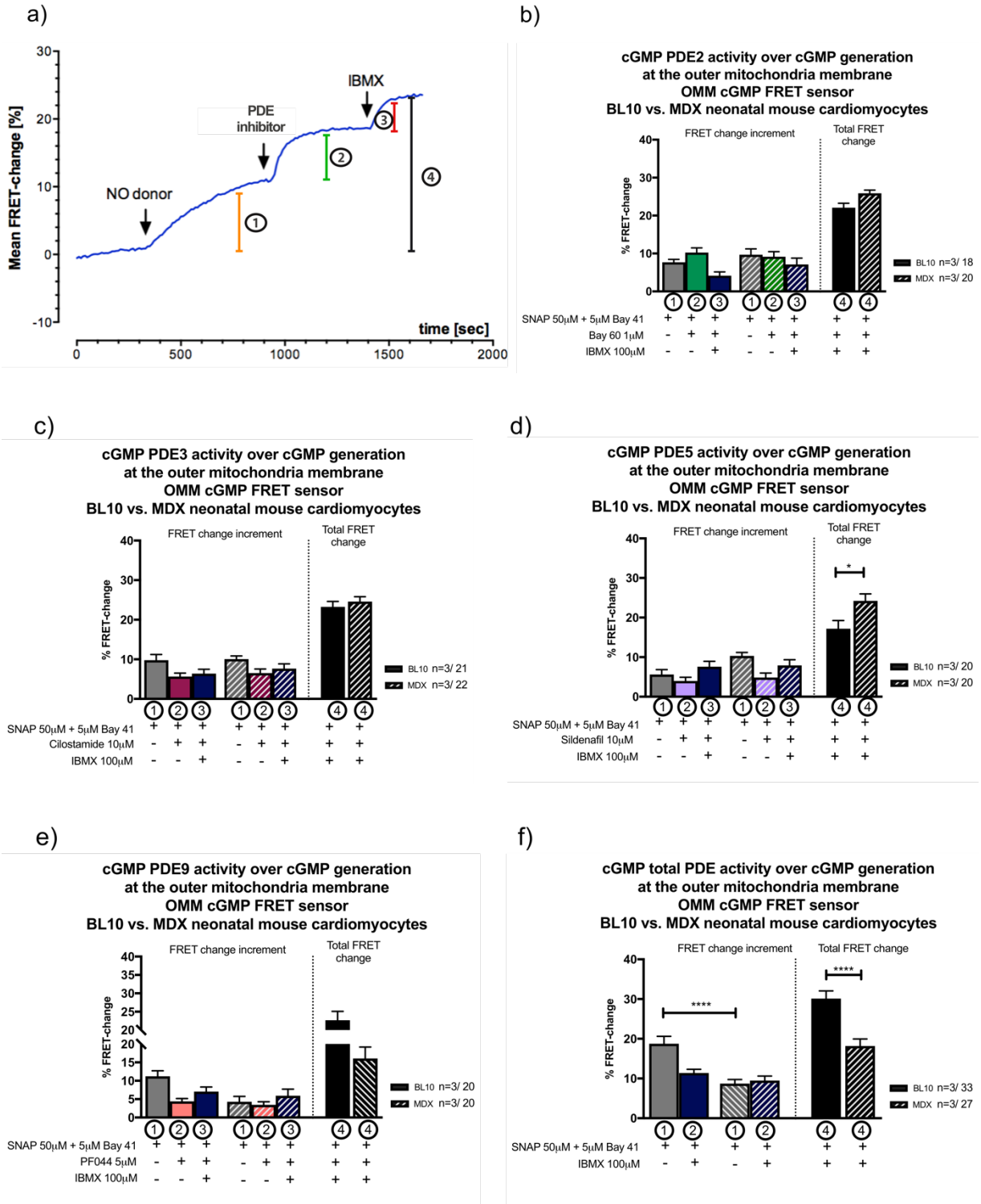


Figure 5.25.
Summary of FRET change recorded in mdx and C57BL/10ScSn individually expressing the outer mitochondria cGMP FRET-based sensor, OMM ^{T}cGI500^{VV}, in response to bath application of 1μM Bay 60 (b), 10μM Cilostamide (c), 10μM Sildenafil (d), 5μM PF-04447943 (e) and 100μM 3-isobutyl-1-methylxanthine (IBMX) (f) followed by 50μM of the NO donor S-Nitroso-N-Acetyl-D,L-Penicillamine (SNAP) in combination of 5 μM of soluble guanylyl cyclase stimulator BAY 41-2272 and 100μM 3-isobutyl-1-methylxanthine (IBMX). The FRET-change trace in graph (a) represents experimental protocol and analysis protocol. The numbers and arrows below the trace indicates how the analysis was performed and which areas of the trace are being represented in the bar graphs. The same number legend is used below each bar graph to facilitate understanding of the data. Graphs (b), (c), (d), (e) and (f) represent each experimental set separately, whereas graph (g) displays a summary of the relevant data from the individual sets. N number is indicated in each individual set as n= biological replicates/ individual cells. Error bars represent SEM; Two-way ANOVA, * = 0.05<p<0.01, ** = 0.01<p<0.001.

The ability to generate cGMP upon sGC stimulation and NO donor donor in combination with sGC stimulator showed to be significant lower in the OMM of mdx cardiomyocytes, as shown in Figure 5.26. The activity of all the PDEs tested after cGMP generation, including PDE2, which presented lower basal activity, are not different when compared to healthy cardiomyocytes.

Figure 5.26. cGMP PDE activity at the outer mitochondria membrane of neonatal cardiomyocytes after cGMP generation via sGC



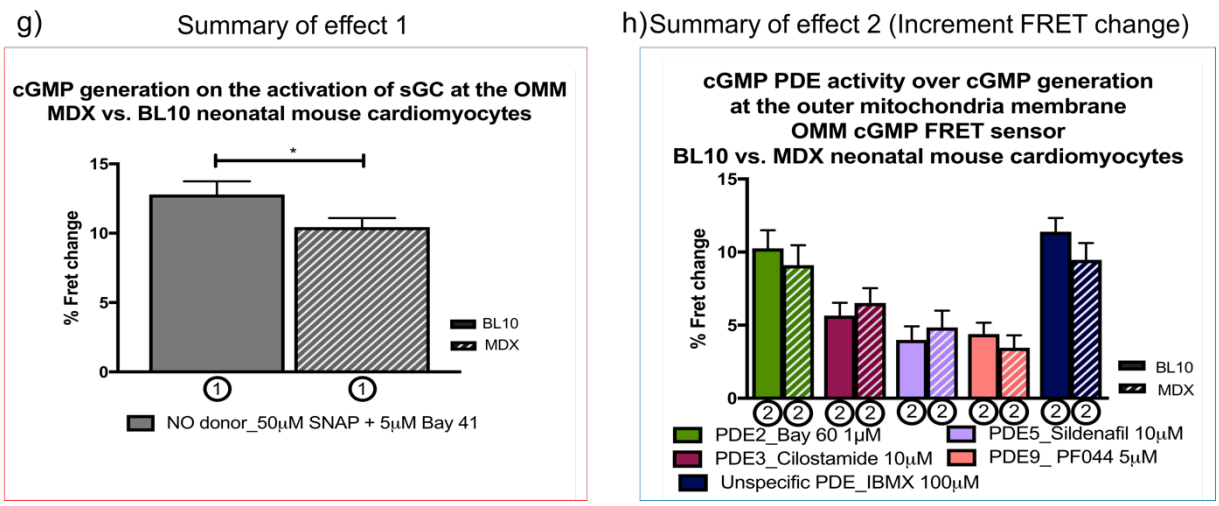


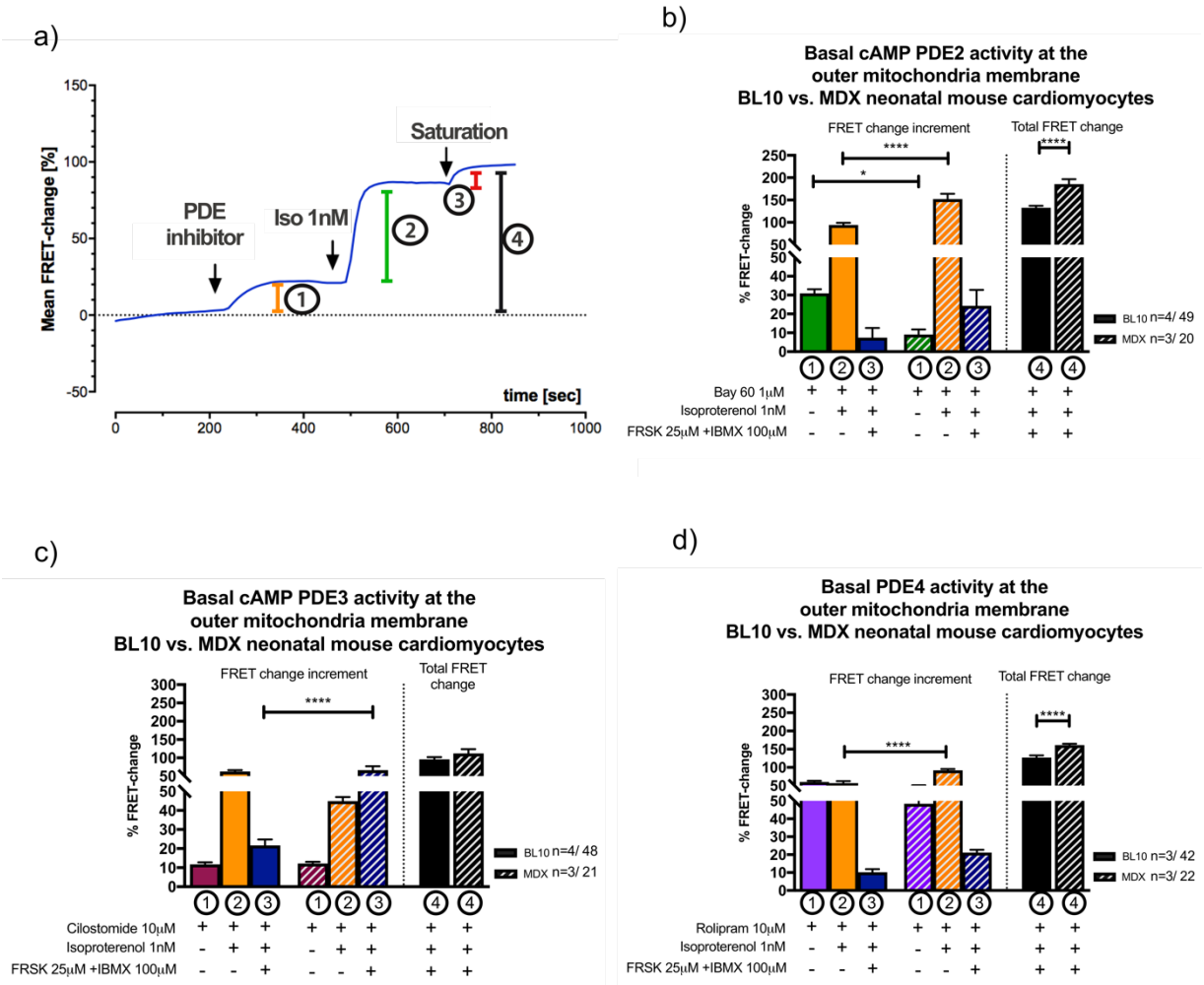
Figure 5.26.
Summary of FRET change recorded in mdx and C57BL/10ScSn neonatal cardiomyocytes individually expressing the outer mitochondria membrane cGMP FRET-based sensor, OMM ^{T}cGI500^{VV}, in response to bath application of NO donor S-Nitroso-N-Acetyl-D,L-Penicillamine (SNAP) in combination of 5μM of soluble guanylyl cyclase stimulator BAY 41-22721μM (a) followed by 1μM Bay 60 (c), 10μM Cilostamide (d), 10μM Sildenafil (e), 5μM PF-04447943 (f) and 100μM 3-isobutyl-1-methylxanthine (IBMX) (g) and 100μM 3-isobutyl-1-methylxanthine (IBMX) to fully inhibit PDEs, and 10μM Cinaciguat (h). The FRET-change trace in graph (a) represents experimental protocol and analysis protocol. The numbers and arrows below the trace indicates how the analysis was performed and which areas of the trace are being represented in the bar graphs. The same number legend is used below each bar graph to facilitate understanding of the data. Graphs (b), (c), (d), (e) and (f) represent each experimental set separately, whereas graph (g) displays a summary of NO donor + Bay 41 22-72 response and graph (h) a summary of the single PDE inhibition data. N number is indicated in each individual set as n= biological replicates/ individual cells. Error bars represent SEM; Two-way ANOVA, * = 0.05<p<0.01, ** = 0.01<p<0.001, ***= 0.001<p<0.0001, **** = p<0.0001.

cAMP PDE2 activity levels were also significantly lower at the OMM of mdx neonatal cardiomyocytes (Figure 5.27). It has been reported that PDE2A2 regulates local cAMP levels and PKA-dependent phosphorylation of the dynamin-related protein 1 (Drp1), which is involved in mitochondria fission. Furthermore, PDE2 inhibition results in mitochondria elongation and protection of cardiac myocytes from mitochondria-dependent cell death (Monterisi et al. 2017). Therefore, the decreased activity of PDE2 activity recorded in the OMM of mdx cardiomyocytes might be a cardioprotective mechanism of the dystrophic cell.

Apart from PDE2, basal PDE8 activity was significantly higher (Figure 5.27) at the OMM

of MDX. This data might suggest that PDE8 does not directly regulate basal levels of cAMP at the OMM as the basal levels of cAMP were found to be significantly higher at this specific subcellular compartment.

Figure 5.27. Basal cAMP PDE activity at the outer mitochondrial membrane of neonatal cardiomyocytes



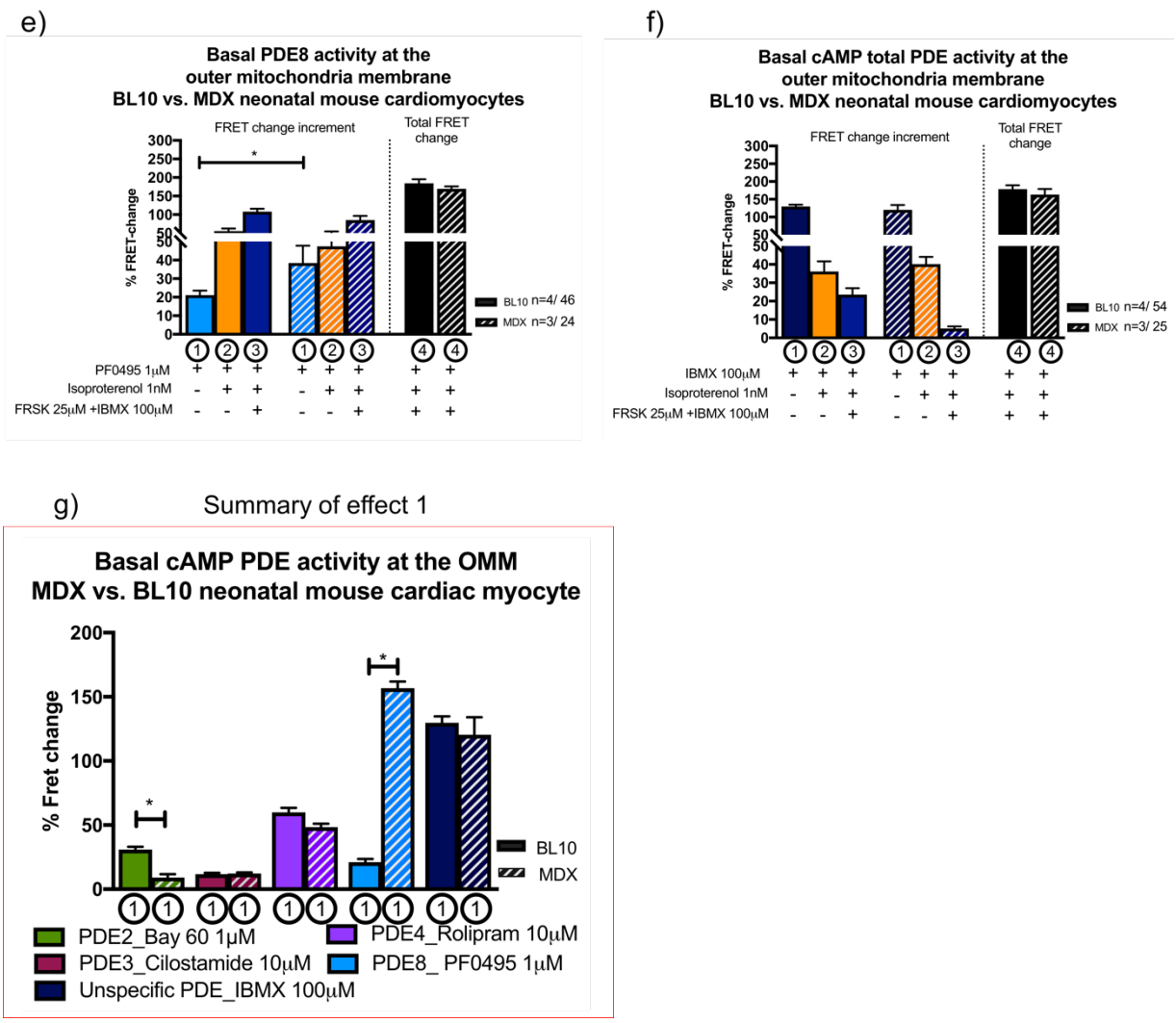
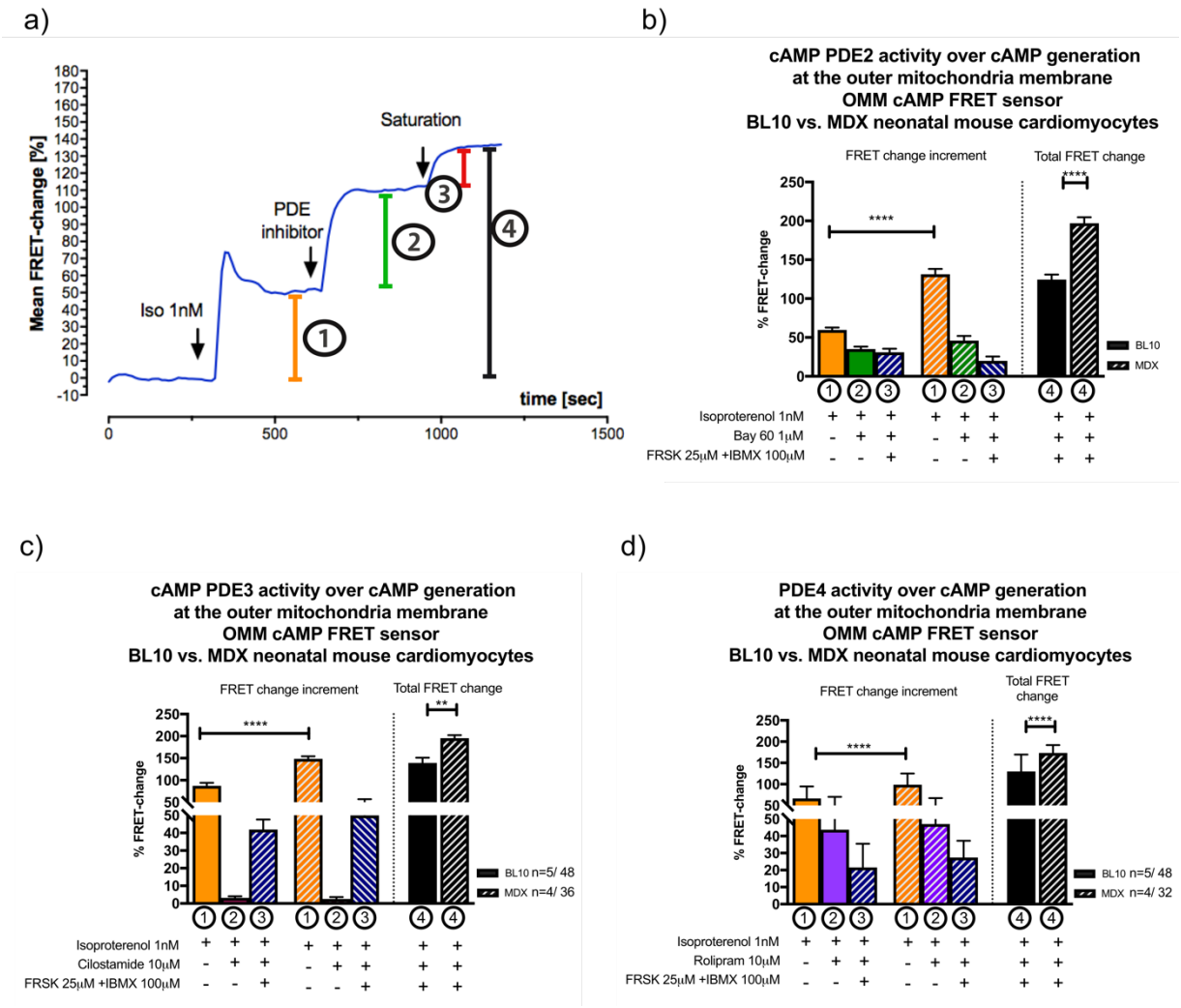


Figure 5.27.
Summary of FRET change recorded in mdx and C57BL/10ScSn individually expressing the outer mitochondria membrane cAMP FRET-based sensor, OMM H187, in response to bath application of 1μM Bay 60 (b), 100μM 3-isobutyl-1-methylxanthine (IBMX) (c), 1 μM PF-04957325 (d), 10μM Cilostamide (e), and 10 μM Rolipram (f) followed by 1nM Isoproterenol and 25μM of the adenylyl cyclase stimulator Forskolin (FRSK) in combination with 100μM 3-isobutyl-1-methylxanthine (IBMX). The FRET-change trace in graph (a) represents experimental protocol and analysis protocol. The numbers and arrows below the trace indicates how the analysis was performed and which areas of the trace are being represented in the bar graphs. The same number legend is used below each bar graph to facilitate understanding of the data. Graphs (b), (c), (d), (e) and (f) represent each experimental set separately, whereas graph (g) displays a summary of the individual PDE inhibition. N number is indicated in each individual set as n= biological replicates/ individual cells. Error bars represent SEM; Two-way ANOVA, * = 0.05<p<0.01, ** = 0.01<p<0.001, ***= 0.001<p<0.0001, **** = p<0.0001.

Furthermore, the treatment of mdx neonatal cardiomyocytes with isoproterenol resulted into a larger response in the OMM of mdx cardiomyocytes (Figure 5.28). Surprisingly,

the activity of most of the PDEs, except PDE8, was not found to be altered after cAMP generation in mdx cardiomyocytes. PDE8 inhibition, as well as total PDE upon IBMX, generated larger responses at the OMM of dystrophic cells.

Figure 5.28. cAMP PDE activity at the outer mitochondria membrane of neonatal cardiomyocytes after cAMP generation



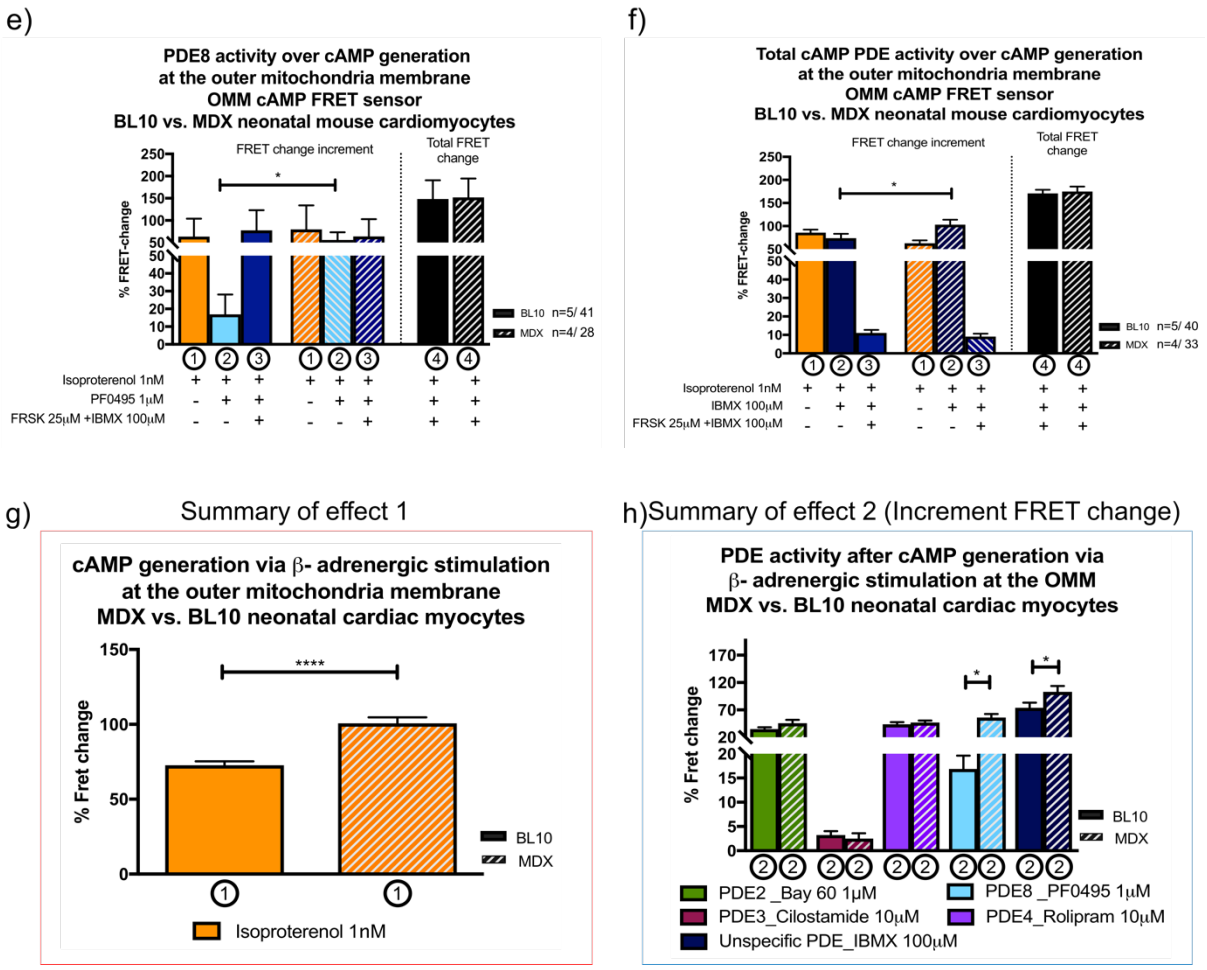


Figure 5.28.

Summary of FRET change recorded in mdx and C57BL/10ScSn neonatal cardiomyocytes individually expressing the outer mitochondria membrane cAMP FRET-based sensor, OMM H187, in response to bath application of 1nM isoproterenol (a) followed by 1μM Bay 60 (c), 10μM Cilostamide (d), 10μM Rolipram (e), 1 μM PF-04957325 (f) and 100μM 3-isobutyl-1-methylxanthine (IBMX) (g) and 25μM of the adenylyl cyclase stimulator Forskolin (FRSK) in combination with 100μM 3-isobutyl-1-methylxanthine (IBMX) as saturation. The FRET-change trace in graph (a) represents experimental protocol and analysis protocol. The numbers and arrows below the trace indicates how the analysis was performed and which areas of the trace are being represented in the bar graphs. The same number legend is used below each bar graph to facilitate understanding of the data. Graphs (b), (c), (d), (e) and (f) represent each experimental set separately, whereas graph (g) displays a summary of the response to Isoproterenol and graph (h) a summary of the single PDE inhibition effect. N number is indicated in each individual set as n= biological replicates/ individual cells. Error bars represent SEM; Two-way ANOVA, * = 0.05<p<0.01, ** = 0.01<p<0.001, ***= 0.001<p<0.0001, **** = p<0.0001.

5.4. SUMMARY AND DISCUSSION

This chapter presents a systematic analysis of the cGMP and cAMP levels in different subcellular compartments of the mdx cardiomyocytes and their comparison with control healthy cells. The data obtained are very complex and a schematic summarizing the main results is available on Figure 5.29. Due to the complexity of the multiple regulatory mechanisms associated with the signalling pathways explored (NO-cGMP-PDE-cAMP) and the interplay between these pathways, the range of possible implications and the hypothesis that can be formulated to explain these findings are multiple. Only the most substantial findings will be discussed below. As the main aim of this part of the project was to assess the hypothesis that disruption of the dystrophin complex at the PM may affect CN signalling in MDX cardiac myocytes, the majority of the work was performed using ventricular cardiac myocytes from neonatal MDX mice. This model, rather than cells from adult hearts, was considered more appropriate to investigate a possible direct involvement of the disruption of the dystrophin complex on CN signalling as it would allow to minimise confounding effects that may derive from myocardial remodelling that ensues at later time points when the cardiomyopathy becomes obvious in adult age. However, given some interesting results obtained when assessing the contractile properties of mdx myocytes vs control cells (see Chapter 6), selected sets of experiments were performed to investigate CN levels in adult cells as well. It is important to clarify that due to technical difficulties in performing FRET experiments in adult cardiomyocytes, especially when exploring cGMP dynamics, not all comparisons could be carried out in adult cells.

The main findings presented in this chapter are as follows:

- Neonatal mdx cardiomyocytes presented significantly lower basal levels of free cGMP and significantly higher levels of free cAMP in the bulk cytosol compared to control myocytes (Figure 5.10). An increased activity of PDE5 (Figure 5.12 g) may justify the reduced basal level of cGMP, whereas a reduction in the activity of PDE2, PDE3, PDE4 and PDE8 (Figure 5.13) would explain the significantly higher level of basal free cAMP. Interestingly, mRNA analysis of PDE isoforms shows no difference in the transcription level of any of these enzymes (Figure 5.14 a). Although level of mRNA does not necessarily correspond to protein level and some of the differences in PDE activity observed may still depend on different amount of protein, it is plausible that other mechanisms, such as regulation and/or disruption of compartmentalisation of individual PDEs may be responsible for the effects observed.
- While the reduced level of basal cGMP in neonatal mdx myocytes is found in all compartments analysed (Figure 5.10 a, Figure 5.19 a and Figure 5.20 a), the disruption of basal cAMP levels appears to be specific to different subcellular compartments as an increase compared to controls is observed in the cytosol and PL (Fig 5.10 b and Figure 5.19 b), but a very robust reduction of cAMP is detected at the mitochondria (Figure 5.20 b). Notably, this corresponds to a very substantial increase in PDE8 activity at this location (Figure 5.27 g).
- The data presented here shows that CN dynamics and regulation change significantly with age. Although CN basal concentrations also fluctuate with age in healthy cardiomyocytes, in adult mdx cardiac myocytes the alteration in the basal level of free CN observed in neonatal myocytes is completely reversed, at least in the bulk cytosol, and the levels of both cAMP and cGMP return to be the

same level as in adult control cells (Figure 5.11 a, b). Interestingly, these changes cannot be explained entirely by a change in the levels of PDEs (but the same caveat as above should be considered), as in adult mdx all PDEs seem to undergo transcriptional up-regulation (Figure 5.14 b), which would be expected to result in overall reduction of both cAMP and cGMP levels. Again, differences in the regulation and/or compartmentalisation of individual PDEs may be responsible for the normalisation of cytosolic basal CN levels in MDX. Interestingly disrupted cAMP and cGMP signalling persist in adult cardiac myocytes from MDX mice at the PM and at the mitochondria (Figures 5.19 and 5.20) Again, the effects seem to be compartment specific.

- nNOS levels were found significantly lower at the plasma membrane, ER and cytosol of adult mdx cardiomyocytes (Figures 5.3 – 5.7), supporting the hypothesis of nNOS-cGMP disruption in DMD. However, it is important to keep in mind that the deficiency in nNOS-NO-cGMP might not be only due to the loss of nNOS binding to the dystrophin complex but possibly to defects in its regulation.
- Additionally, adult mdx cardiomyocytes present significantly higher levels of oxidised sGC, a species that is not responsive to NO. This increase in the oxidised form of the enzyme might be due to increased levels of ROS previously described in mdx cardiomyocytes. Neonatal mdx cardiomyocyte also present higher oxidised sGC, however, only at the plasma membrane and not in the cytosol, again suggesting a progression with age in the disruption of the nNOS-cGMP signalling pathway

Figure 5.29a. Summary of findings in schematic figure – Neonatal cardiomyocyte

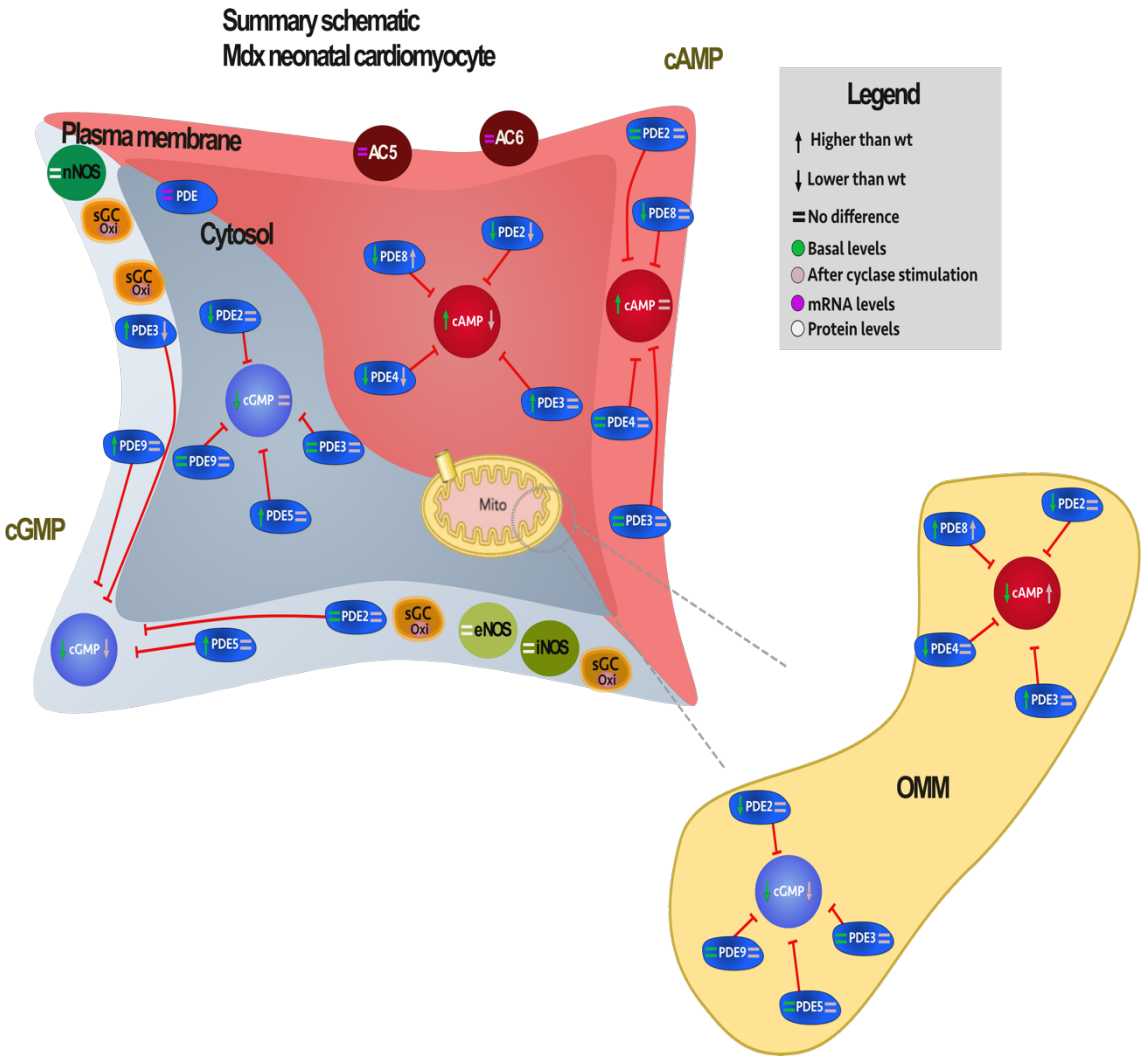


Figure 5.29b. Summary of findings in schematic figure – adult cardiomyocyte

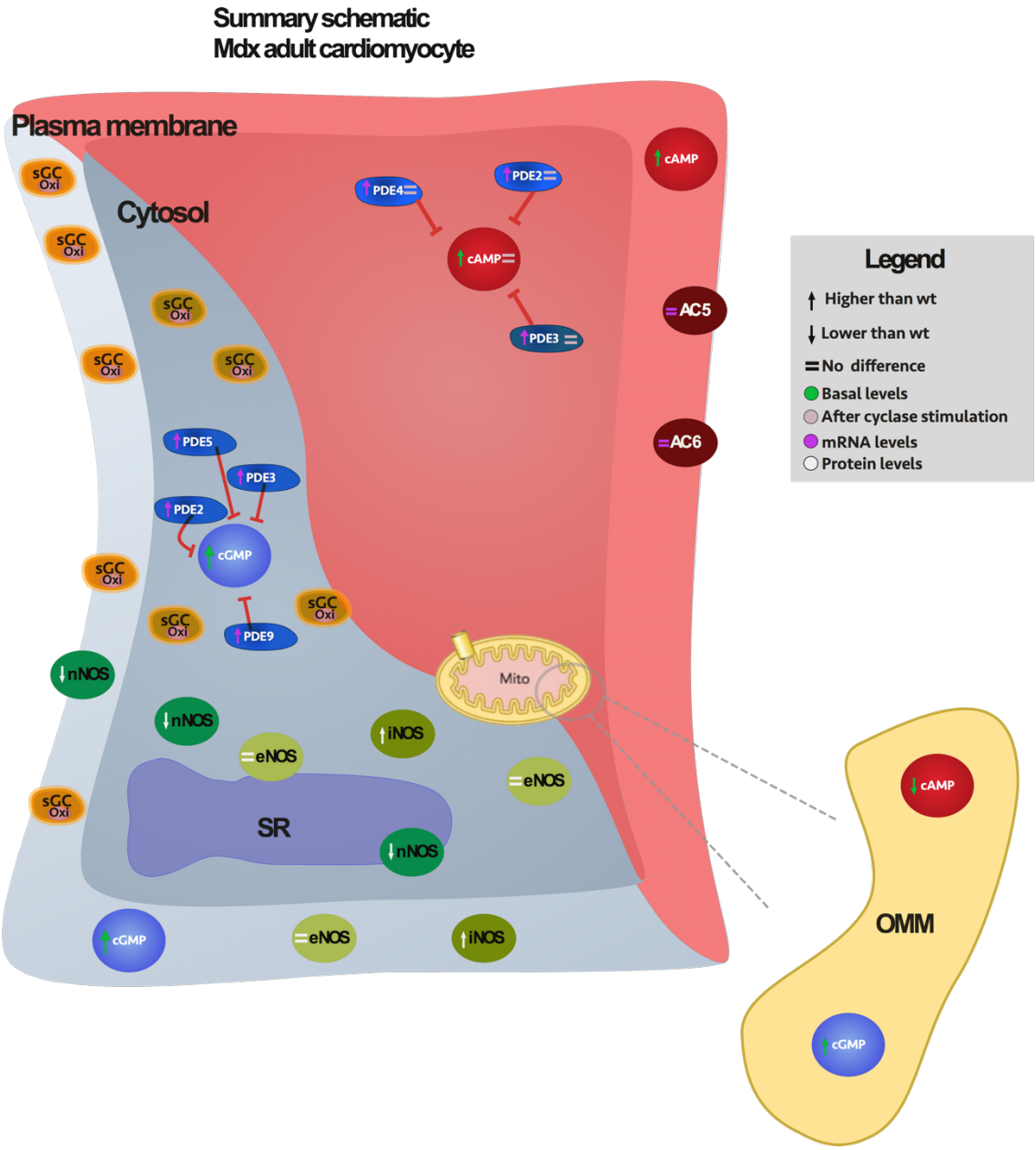


Figure 5.29.
Summary of the main findings in neonatal cardiomyocytes (a) and adult cardiomyocytes (b) discussed in this chapter. The figure illustrates a mdx cell and the differences when compared to the age matched control. Abbreviations: OMM: Outer mitochondria membrane; SR: Sarcoplasmic reticulum, PDE: phosphodiesterases; sGC oxi: oxidised soluble guanylyl cyclase; AC: Adenylyl cyclase; NOS: nitric oxide synthases.

In conclusion, the findings described in this chapter show an extensive disruption of both cAMP and cGMP signalling associated with the lack of an intact dystrophin complex at the PM. The results are compatible with the hypothesis that compensatory mechanisms are active in adult cardiomyocytes to overcome the altered levels and/or defective compartmentalisation of CN observed in neonatal cardiomyocytes. Increased levels of sGC beta1 subunit in combination with increased levels of ANP receptor have been previously reported. A plausible hypothesis is that they are up-regulated in response to defective NO-cGMP signalling (Maya Khairallah et al. 2007).

Additionally, the data show that not only NO-cGMP, but also the cAMP pathway is altered and may be involved in the pathogenesis of the cardiomyopathy that develops in adulthood. Although further investigations are necessary to fully understand the implications of such changes, manipulation of specific components of these pathways could potentially change the course of the disease.

5.5. REFERENCES

Adamo, Candace M, Dao-Fu Dai, Justin M Percival, Elina Minami, Monte S Willis, Enrico Patrucco, Stanley C Froehner, and Joseph A Beavo. 2010. "Sildenafil Reverses Cardiac Dysfunction in the Mdx Mouse Model of Duchenne Muscular Dystrophy." *Proceedings of the National Academy of Sciences* 107 (44): 19079–83.

Ascah, Alexis, Maya Khairallah, Frédéric Daussin, Céline Bourcier-Lucas, Richard Godin, Bruce G Allen, Basil J Petrof, Christine Des Rosiers, and Yan Burelle. 2011. "Stress-Induced Opening of the Permeability Transition Pore in the Dystrophin-Deficient Heart Is Attenuated by Acute Treatment with Sildenafil." *American Journal of Physiology-Heart and Circulatory Physiology* 300 (1): H144–53.

Bellingham, Michelle, and Thomas J Evans. 2007. "The α 2 β 1 Isoform of Guanylyl Cyclase Mediates Plasma Membrane Localized Nitric Oxide Signalling." *Cellular Signalling* 19 (10): 2183–93.

Bendall, Jennifer K, Thibaud Damy, Philippe Ratajczak, Xavier Loyer, Virginie Monceau, Isabelle Marty, Paul Milliez, Estelle Robidel, Françoise Marotte, and Jane-Lise Samuel. 2004. "Role of Myocardial Neuronal Nitric Oxide Synthase–derived Nitric Oxide in β-Adrenergic Hyporesponsiveness after Myocardial Infarction–induced Heart Failure in Rat." *Circulation* 110 (16): 2368–75.

Bia, Britta L, Paul J Cassidy, Martin E Young, Jill A Rafael, Brendan Leighton, Kay E Davies, George K Radda, and Kieran Clarke. 1999. "Decreased Myocardial nNOS, Increased iNOS and Abnormal ECGs in Mouse Models of Duchenne Muscular Dystrophy." *Journal of Molecular and Cellular Cardiology* 31 (10): 1857–62.

Brenman, Jay E, Daniel S Chao, Stephen H Gee, Aaron W McGee, Sarah E Craven, Daniel R Santillano, Ziqiang Wu, Fred Huang, Houhui Xia, and Matthew F Peters. 1996. "Interaction of Nitric Oxide Synthase with the Postsynaptic Density Protein PSD-95 and α1-Syntrophin Mediated by PDZ Domains." *Cell* 84 (5): 757–67.

Brenman, Jay E, Daniel S Chao, Houhui Xia, Ken Aldape, and David S Bredt. 1995. "Nitric Oxide Synthase Complexed with Dystrophin and Absent from Skeletal Muscle Sarcolemma in Duchenne Muscular Dystrophy." *Cell* 82 (5): 743–52.

Brescia, Marcella, and Manuela Zaccolo. 2016. "Modulation of Compartmentalised Cyclic Nucleotide Signalling via Local Inhibition of Phosphodiesterase Activity." *International Journal of Molecular Sciences* 17 (10): 1672.

Bridges, LR. 1986. "The Association of Cardiac Muscle Necrosis and Inflammation with the Degenerative and Persistent Myopathy of MDX Mice." *Journal of the Neurological Sciences* 72 (2): 147–57.

Canal, N, L Frattola, and S Smirne. 1975. "The Metabolism of Cyclic-3′-5′-Adenosine Monophosphate (cAMP) in Diseased Muscle." *Journal of Neurology* 208 (4): 259–65.

Carnicer, Ricardo, Silvia Suffredini, Xing Liu, Svetlana Reilly, Jillian N Simon, Nicoletta C Surdo, Yin H Zhang, Craig A Lygate, Keith M Channon, and Barbara Casadei. 2017. "The Subcellular Localization of Neuronal Nitric Oxide

Synthase Determines the Downstream Effects of NO on Myocardial Function." *Cardiovascular Research* 113 (3): 321–31.

Cerri, Cesare G, Joseph H Willner, and Armand F Miranda. 1982. "Adenylate Cyclase in Duchenne Fibroblasts." *Journal of the Neurological Sciences* 53 (2): 181–85.

Chang, Wen-Jinn, Susan T Iannaccone, Kim S Lau, BS Masters, Timothy J McCabe, Kirk McMillan, Roanna C Padre, Melissa J Spencer, James G Tidball, and James T Stull. 1996. "Neuronal Nitric Oxide Synthase and Dystrophin-Deficient Muscular Dystrophy." *Proceedings of the National Academy of Sciences* 93 (17): 9142–47.

Cho, Kyung-Ok, Carol A Hunt, and Mary B Kennedy. 1992. "The Rat Brain Postsynaptic Density Fraction Contains a Homolog of the Drosophila Discs-Large Tumor Suppressor Protein." *Neuron* 9 (5): 929–42.

Conti, Marco, Delphine Mika, and Wito Richter. 2014. "Cyclic AMP Compartments and Signaling Specificity: Role of Cyclic Nucleotide Phosphodiesterases." *The Journal of General Physiology* 143 (1): 29–38.

Damy, Thibaud, Philippe Ratajczak, Estelle Robidel, Jennifer K Bendall, Patricia Oliviéro, Jorge Boczkowski, Talin Ebrahimian, Françoise Marotte, Jane-Lise Samuel, and Christophe Heymes. 2003. "Up-Regulation of Cardiac Nitric Oxide Synthase 1-Derived Nitric Oxide after Myocardial Infarction in Senescent Rats." *The FASEB Journal* 17 (13): 1934–36.

Damy, Thibaud, Philippe Ratajczak, Ajay M Shah, Emmanuel Camors, Isabelle Marty, Gerd Hasenfuss, Françoise Marotte, Jane-Lise Samuel, and Christophe Heymes. 2004. "Increased Neuronal Nitric Oxide Synthase-Derived NO Production in the Failing Human Heart." *The Lancet* 363 (9418): 1365–67.

Evgenov, Oleg V, Pál Pacher, Peter M Schmidt, György Haskó, Harald HHW Schmidt, and Johannes-Peter Stasch. 2006. "NO-Independent Stimulators and Activators of Soluble Guanylate Cyclase: Discovery and Therapeutic Potential." *Nature Reviews. Drug Discovery* 5 (9): 755.

Fauconnier, Jérémy, Jérôme Thireau, Steven Reiken, Cécile Cassan, Sylvain Richard, Stefan Matecki, Andrew R Marks, and Alain Lacampagne. 2010. "Leaky RyR2 Trigger Ventricular Arrhythmias in Duchenne Muscular Dystrophy." *Proceedings of the National Academy of Sciences* 107 (4): 1559–64.

Fischer, S, M Tortolero, J-P Piau, J Delaunay, and G Schapira. 1978. "Protein Kinase and Adenylate Cyclase of Erythrocyte Membrane from Patients with Duchenne Muscular Dystrophy." *Clinica Chimica Acta* 88 (3): 437–40.

Friebe, Andreas, and Doris Koesling. 2003. "Regulation of Nitric Oxide-Sensitive Guanylyl Cyclase." *Circulation Research* 93 (2): 96–105.

Götz, Konrad R, and Viacheslav O Nikolaev. 2013. "Advances and Techniques to Measure cGMP in Intact Cardiomyocytes." *Guanylate Cyclase and Cyclic GMP: Methods and Protocols*, 121–29.

Götz, Konrad, Julia Sprenger, Ruwan K Perera, Julia H Steinbrecher, Stephan E Lehnart, Michaela Kuhn, Julia Gorelik, Jean-Luc Balligand, and Viacheslav O Nikolaev. 2014. "Transgenic Mice for Real Time Visualization of cGMP in Intact Adult Cardiomyocytes." *Circulation Research*, CIRCRESAHA-113.

Johnson, Eric K, Liwen Zhang, Marvin E Adams, Alistair Phillips, Michael A Freitas, Stanley C Froehner, Kari B Green-Church, and Federica Montanaro. 2012. "Proteomic Analysis Reveals New Cardiac-Specific Dystrophin-Associated Proteins." *PloS One* 7 (8): e43515.

Kanai, Anthony J, Linda L Pearce, Paula R Clemens, Lori A Birder, Michelle M VanBibber, So-Young Choi, William C de Groat, and Jim Peterson. 2001. "Identification of a Neuronal Nitric Oxide Synthase in Isolated Cardiac Mitochondria Using Electrochemical Detection." *Proceedings of the National Academy of Sciences* 98 (24): 14126–31.

Khairallah, M, RJ Khairallah, ME Young, BG Allen, MA Gillis, G Danialou, CF Deschepper, BJ Petrof, and C Des Rosiers. 2008. "Sildenafil and Cardiomyocyte-Specific cGMP Signaling Prevent Cardiomyopathic Changes Associated with Dystrophin Deficiency." *Proceedings of the National Academy of Sciences* 105 (19): 7028–33.

Khairallah, Maya, Ramzi Khairallah, Martin E Young, Jason RB Dyck, Basil J Petrof, and Christine Des Rosiers. 2007. "Metabolic and Signaling Alterations in Dystrophin-Deficient Hearts Precede Overt Cardiomyopathy." *Journal of Molecular and Cellular Cardiology* 43 (2): 119–29.

Lai, Yi, Gail D. Thomas, Yongping Yue, Hsiao T. Yang, Dejia Li, Chun Long, Luke Judge et al. "Dystrophins carrying spectrin-like repeats 16 and 17 anchor nNOS to the sarcolemma and enhance exercise performance in a mouse model of muscular dystrophy." *The Journal of clinical investigation* 119, no. 3 (2009): 624.

Leung, Doris G, Daniel A Herzka, W Reid Thompson, Bing He, Genila Bibat, Gihan Tennekoon, Stuart D Russell, Karl H Schuleri, Albert C Lardo, and David A Kass. 2014. "Sildenafil Does Not Improve Cardiomyopathy in Duchenne/Becker Muscular Dystrophy." *Annals of Neurology* 76 (4): 541–49.

Mawatari, Shiro, Michael Schonberg, and Marcelo Olarte. 1976. "Biochemical Abnormalities of Erythrocyte Membranes in Duchenne Dystrophy: Adenosine Triphosphatase and Adenyl Cyclase." *Archives of Neurology* 33 (7): 489–93.

McCormick, Kristie, and George S Baillie. 2014. "Compartmentalisation of Second Messenger Signalling Pathways." *Current Opinion in Genetics & Development* 27: 20–25.

Mergia, Evanthia, Michael Russwurm, Georg Zoidl, and Doris Koesling. 2003. "Major Occurrence of the New α 2 β 1 Isoform of NO-Sensitive Guanylyl Cyclase in Brain." *Cellular Signalling* 15 (2): 189–95.

Monterisi, Stefania, Miguel J Lobo, Craig Livie, John C Castle, Michael Weinberger, George Baillie, Nicoletta C Surdo, Nshunge Musheshe, Alessandra Stangherlin, and Eyal Gottlieb. 2017. "PDE2A2 Regulates Mitochondria Morphology and Apoptotic Cell Death via Local Modulation of cAMP/PKA Signalling." *eLife* 6.

Mungrue, Imran N, Robert Gros, Xiaomang You, Asif Pirani, Azar Azad, Tamas Csont, Richard Schulz, Jagdish Butany, Duncan J Stewart, and Mansoor Husain. 2002. "Cardiomyocyte Overexpression of iNOS in Mice Results in Peroxynitrite Generation, Heart Block, and Sudden Death." *The Journal of Clinical Investigation* 109 (6): 735.

Prosser, Benjamin L, Christopher W Ward, and WJ Lederer. 2011. "X-ROS Signaling: Rapid Mechano-Chemo Transduction in Heart." *Science* 333 (6048): 1440–45.

Ramachandran, Jayalakshmi, Joel S Schneider, Pierre-Antoine Crassous, Ruifang Zheng, James P Gonzalez, Lai-Hua Xie, Annie Beuve, Diego Fraidenraich, and R Daniel Peluffo. 2013. "Nitric Oxide Signalling Pathway in Duchenne Muscular Dystrophy Mice: Up-Regulation of L-Arginine Transporters." *Biochemical Journal* 449 (1): 133–42.

Recchia, Fabio A. 2002. "Role of Nitric Oxide in the Regulation of Substrate Metabolism in Heart Failure." *Heart Failure Reviews* 7 (2): 141–48.

Roses, Allen D, Michael H Herbstreith, and Stanley H Appel. 1975. "Membrane Protein Kinase Alteration in Duchenne Muscular Dystrophy." *Nature* 254 (5498): 350–51.

Seddon, Mike, Ajay M Shah, and Barbara Casadei. 2007. "Cardiomyocytes as Effectors of Nitric Oxide Signalling." *Cardiovascular Research* 75 (2): 315–26.

Silvagno, Francesca, Houhui Xia, and David S Bredt. 1996. "Neuronal Nitric-Oxide Synthase-, an Alternatively Spliced Isoform Expressed in Differentiated Skeletal Muscle." *Journal of Biological Chemistry* 271 (19): 11204–8.

Susheela, AK, RD Kaul, K Sachdeva, and Naunihal Singh. 1975. "Adenyl Cyclase Activity in Duchenne Dystrophic Muscle." *Journal of the Neurological Sciences* 24 (3): 361–63.

Ullrich, Nina D, Mohammed Fanchaouy, Konstantin Gusev, Natalia Shirokova, and Ernst Niggli. 2009. "Hypersensitivity of Excitation-Contraction Coupling in Dystrophic Cardiomyocytes." *American Journal of Physiology-Heart and Circulatory Physiology* 297 (6): H1992–2003.

Wacholtz, MC, DG Raible, S Jackowski, SB Rodan, GA Rodan, and RI Sha'afi. 1979. "Adenylate Cyclase and ATPase Activities in Red Cell Membranes of Patients and Genetic Carriers of Duchenne Muscular Dystrophy." *Clinica Chimica Acta* 96 (3): 255–59.

Wehling-Henricks, Michelle, Maria C Jordan, Kenneth P Roos, Bo Deng, and James G Tidball. 2005. "Cardiomyopathy in Dystrophin-Deficient Hearts Is Prevented by Expression of a Neuronal Nitric Oxide Synthase Transgene in the Myocardium." *Human Molecular Genetics* 14 (14): 1921–33.

Williams, Iwan A, and David G Allen. 2007. "The Role of Reactive Oxygen Species in the Hearts of Dystrophin-Deficient Mdx Mice." *American Journal of Physiology-Heart and Circulatory Physiology* 293 (3): H1969–77.

Williams, Judith C, Angel L Armesilla, Tamer MA Mohamed, Cassandra L Hagarty, Fiona H McIntyre, Sybille Schomburg, Aly O Zaki, Delvac Oceandy, Elizabeth J Cartwright, and Mamta H Buch. 2006. "The Sarcolemmal Calcium Pump, α-1 Syntrophin, and Neuronal Nitric-Oxide Synthase Are Parts of a Macromolecular Protein Complex." *Journal of Biological Chemistry* 281 (33): 23341–48.

Woods, Robyn L. 2004. "CARDIOPROTECTIVE FUNCTIONS OF ATRIAL NATRIURETIC PEPTIDE AND B-TYPE NATRIURETIC PEPTIDE: A BRIEF REVIEW." *Clinical and Experimental Pharmacology and Physiology* 31 (11): 791–94.

Xu, Kai Y, David L Huso, Ted M Dawson, David S Bredt, and Lewis C Becker. 1999. "Nitric Oxide Synthase in Cardiac Sarcoplasmic Reticulum." *Proceedings of the National Academy of Sciences* 96 (2): 657–62.

Zaccolo, Manuela, and Matthew A Movsesian. 2007. "cAMP and cGMP Signaling Cross-Talk." *Circulation Research* 100 (11): 1569–78.

Zhang, Yin Hua, and Barbara Casadei. 2012. "Sub-Cellular Targeting of Constitutive NOS in Health and Disease." *Journal of Molecular and Cellular Cardiology* 52 (2): 341–50.

Chapter 6. Contractility analysis of mdx cardiomyocyte upon cyclase stimulation

6.1. INTRODUCTION

6.1.1. Cardiomyocyte contractility

The important role of propelling the blood throughout the body is payed predominantly by contraction of the left ventricle cardiomyocytes. The process of excitation-contraction coupling of cardiomyocytes involves several mechanism and structures.

a) Organelles and structures

The sarcolemma is composed by the *surface sarcolemma*, which is the external membrane of the cells, and the *T-tubules*, which are tube-like invaginations of the sarcolemmal surface. Together, they form a permeability barrier between the intra and extracellular medium and provide strategic location for several ion channels, pumps and other membrane specific proteins. As T-tubules are deep invaginations, they bring the extracellular space closer to the interior of the cells and substantially increase the surface area of the cell, which is advantageous for extracellular stimuli to reach within the cardiomyocyte (Opie 2004). Furthermore, *L-type calcium channels* are present in the T-tubules structure. These channels play a crucial role in the excitation-contraction coupling process as they respond to electrical excitation and depolarisation of the membrane allowing the entry of calcium into the cell. Apart from the T-tubules, the sarcolemma also exhibits *caveolae*, which are small invaginations coated with the protein caveolin and rich in signalling molecules, such as eNOS and G-protein-coupled receptors (GPCRs) (Gratton, Bernatchez, and Sessa 2004). The point of connection between the sarcolemma of different cardiomyocytes is known as the *intercalated disk*. There are three differentiations of this region. The *gap junctions* are an important communication point

between the cells as they allow the direct contact between the cytoplasm of two adjacent cardiomyocytes via a pore constituted of connexins. The other two differentiated point of connection between the cardiomyocytes, the *intermediate junctions* and the *desmosomes*, are important in the mechanical connection between the cells. The *sarcoplasmic reticulum* (SR) plays a crucial role in regulating Ca^{2+} fluctuations within the cell as its main function is to release and sequestrate Ca^{2+} into and from the cytosol. A small amount of Ca^{2+} entered via the L-type Ca^{2+} (LTCC) channels can activate the SR Ca^{2+} release channels, called *ryanodine receptors* (RyR2), to release substantially more calcium. The increase in free intracellular Ca^{2+} triggers the myofilament cross-bridge cycle to start, and its decrease, by SR reuptake, causes relaxation. A specific region of the SR, called *cisterna*, is strategically located in close proximity to the T-tubules with the aim to facilitate the communication between the SR and the T-tubules and efficiently trigger the start of the contraction process by Ca^{2+} activation of the SR (Marx et al. 2000). This area, where the cisterna meets the T-tubule, called *diad*, closely connects both structures with the presence of *foot structures*, which are electron dense feet found at the coupling site (D. Bers 2001).

About 35% of the ventricular myocytes is occupied by *mitochondria*. Apart from the crucial role of generating more than 90% of the cardiac myocyte's ATP, the mitochondria are also the major source of reactive oxygen species (ROS) and can contribute to the cytosolic Ca^{2+} content (Murphy and Steenbergen 2007). They are found wedged in between the *myofilaments*, which are the contractile machinery of the cells.

The myofilaments are composed of *myosin* (thick filament), *actin* (thin filament) and other associated contractile and cytoskeletal elements. The fundamental contractile unit

is called *sarcomere.* The sarcomere is limited on each side by the Z-lines, where the actin filaments attach. The myosin filament extends from the centre of the sarcomere to the edges; however, it does not reach the Z-lines. An extremely long structural protein, called titin, attaches the myosin filaments to the Z-lines. The contraction occurs when the myosin heads crossbridges and interact with actin, a process called cross-bridge cycling. As they slide, the myofilaments pull together the edges of the sarcomere, shortening it. Apart from the Z-lines, the sarcomere is organised by other areas, such as the M-line, which represents the centre of the thick filaments; the A-band, which is the length of the thick filaments; the I-bands, which are areas where only thin filaments are present; and the H-bands, areas of the thick filaments where there is no overlap with the thin filaments (Opie 2004).

The sarcomere contraction would not lead to ventricular contraction if the sarcomeres where not connected to each other and to extracellular structures, therefore the cytoskeleton, which provides the connection of the sarcomere to the sarcolemma, is highly important to cardiac physiology. The major structural complexes of the cytoskeleton are the integrins, composed of actin, alpha-actin, vinculin, talin, paxillin, tensin, alpha and beta-integrins, laminin and collagen, and the dystrophin complex. Dystrophin, the core component of the complex, links the cytoplasmic actin to the transmembrane beta-dystroglycan and adjacent sarcoglycans. Alpha-dystroglycan, on the outer sarcolemma surface, binds to laminin in the extracellular matrix, therefore, the dystrophin complex has an important role in the mechanical stability of the sarcolemmal membrane during contraction (more details on the dystrophin complex are available in the introduction chapter) (Ervasti et al. 1990; Rybakova, Patel, and Ervasti 2000).

The myofilaments are not only composed of filaments, but contain several proteins which regulate the contractility process.

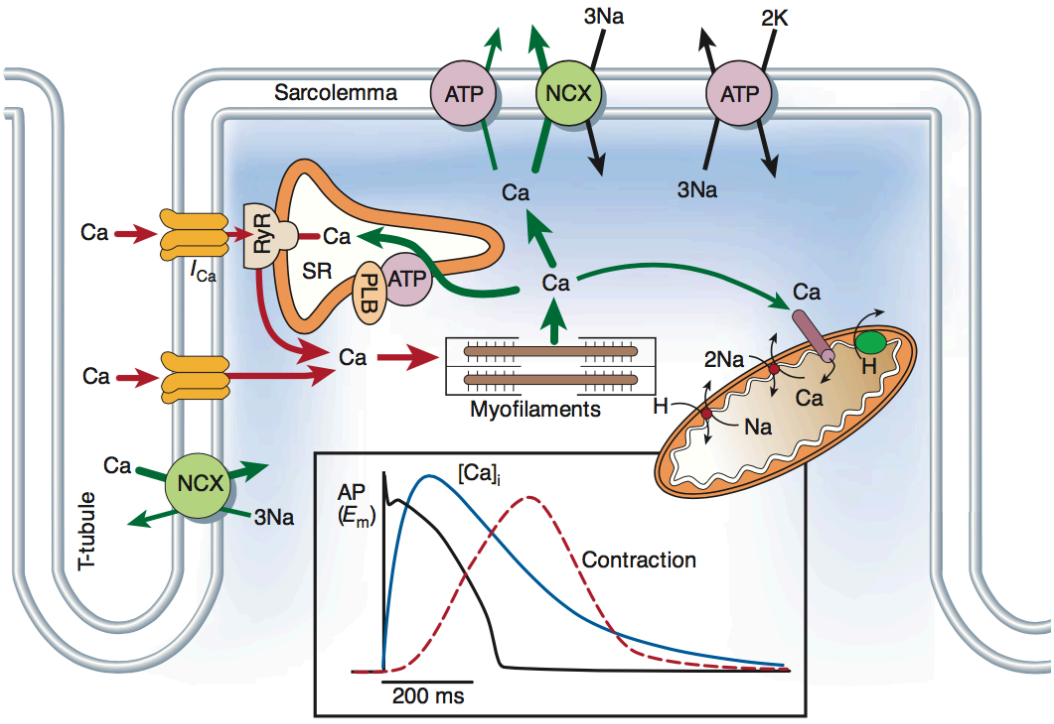
b) Excitation – contraction coupling

The cardiac excitation-contraction coupling initiates with the action potential (AP) and rapid propagation of the signal from the pacemaker cells of the sinus node to the ventricular cells. When the stimulus reaches the cells, voltage-induced ion channels open, influencing the intracellular calcium movement. In short, the initial depolarisation phase (+30mV) opens voltage-gated Na^+ and Ca^{2+} channels, reversing the negative resting polarity of the cell. Transient K^+ outward current, partially repolarise the cell to 0mV, driving a maximal Ca^{2+} current via the Ca^{2+} channels. The Ca^{2+} enters in the cells at the dyads and binds to regulatory calmodulin sites of the LTCC, inactivating the channel, until repolarisation occurs (-40mV). The Ca^{2+} which entered the cells, also binds to the Na^+/Ca^{2+} exchanger (NCX), activating it and facilitating the entry of more calcium via the reverse-mode of the channel. Importantly, the inflexed Ca^{2+} ions activate the ryanodine receptors at the SR, triggering a rapid and large flux of Ca^{2+} ions to the cytosol. This Ca^{2+} released travels a short distance to reach the myofilaments where it binds to Troponin C, one of the proteins of the troponin-tropomyosin complex on the actin filament, triggering the contractile machinery. Activated troponin C, binds to the inhibitory domain of troponin I which, when active, is associated with actin, inhibiting the interaction between actin and myosin. The inhibition of troponin I is sensed by troponin T, which moves tropomyosin away from the binding sites allowing myosin to interact with actin. In addition, troponin T activates the myosin ATPase, enzyme responsible for hydrolysing the ATP molecule transforming chemical energy into mechanical work. This ATPase is located at the head of myosin; therefore, it is called

myosin ATPase. The cross-bridge cycle consists of series of repetitive attachment and detachment of the myosin heads to and from actin. When the machinery is activated, the actin filaments slide through the thick myosin, bringing the Z-lines together and shortening the sarcomeres.

As contraction must be followed by relaxation, the intracellular Ca^{2+} concentration needs to decrease. The sarco(endo)plasmic Ca^{2+} ATPase 2 pump (SERCA2) present on the SR, is activated with the rapid cytosolic increase in Ca^{2+} and starts to sequestrate Ca^{2+} back to the SR. Additional calcium is removed from the cells by the NCX, which brings four Na^{+} back into the cell for each Ca^{2+} extrusion (Schematic available in Figure 6.1) (Opie 2004; D. Bers 2001; ter Keurs 2012).

Figure 6.1. Calcium transport in ventricular cardiomyocytes



(D. M. Bers 2002)

Figure 6.1.
Schematic representation of Ca^{2+} transport in ventricular myocytes including the channels and organelles involved in calcium influx, efflux and storage. The panel in the middle illustrates the time course of an action potential (in black), Ca^{2+} transient (in blue) and contraction (in red) measured in a rabbit ventricular myocyte at 37^{o}C. Abbreviations: NCX, Na+/Ca2+ exchange; ATP, ATPase; PLB, phospholamban; SR, sarcoplasmic reticulum. (D. M. Bers 2002).

6.1.2. Calcium modulation by beta-adrenergic stimulation

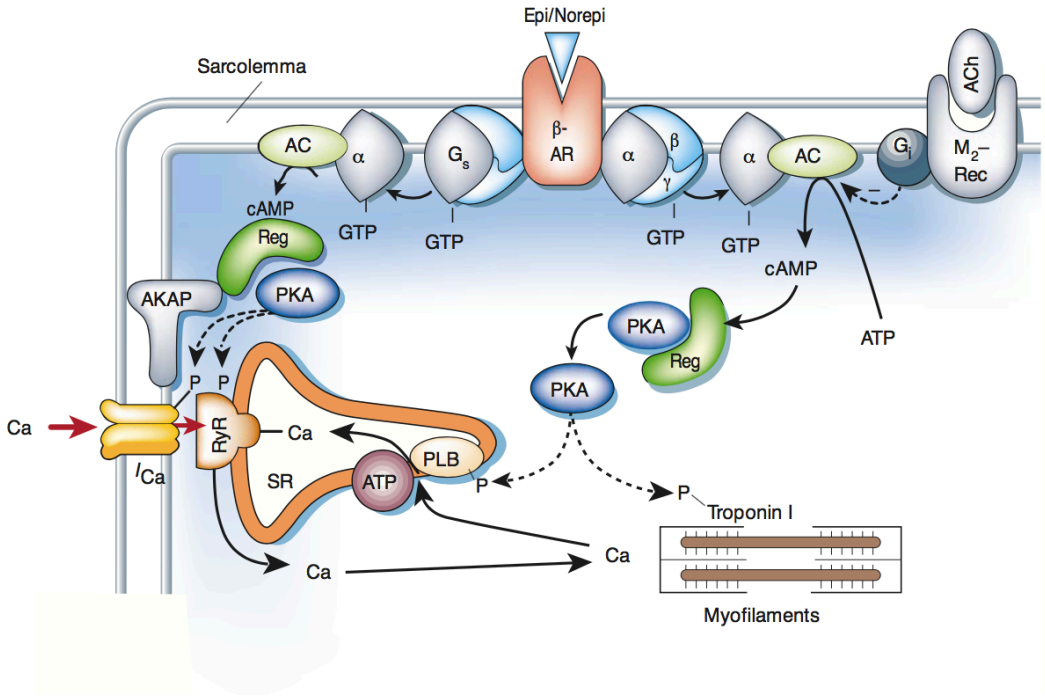
Physiological neurotransmitters, mainly norepinephrine and acetylcholine, travel short distances from the synaptic gaps to reach specific receptors at the plasma membrane and modulate the cardiac myocyte cellular responses. For example, as a response to stress, exercise or emotions, the sympathetic system releases catecholamines (norepinephrine and epinephrine) which are detected by the β-adrenergic receptors in the heart, increasing contractility (inotropic effect), accelerating relaxation (lusitropic effect) and increasing heart rate (chronotropic effect). As already discussed, the stimulation of β-adrenergic receptors activates the production of cAMP which in turn activates PKA. Therefore, cAMP has a crucial role in cardiac contractility via PKA phosphorylation of proteins involved in the excitation-contraction coupling mechanism, such as phospholamban (PLB) (MacLennan and Kranias 2003), LTCC (Gao et al. 1997), RyR (Marx et al. 2000), myosin binding protein C (MyBPC) (Gautel et al. 1995) and troponin I (Zhang et al. 1995). The phosphorylation of PLB, a protein that is localised to the SR in complex with SERCA, increases the rate of SR Ca^{2+} reuptake, accelerating the decline of Ca^{2+} concentration in the cytosol and mediating the lusitropic effect of β-adrenergic stimulation. Another contribution to this effect is given by the PKA-dependent phosphorylation of troponin I, as this speeds up the dissociation of Ca^{2+} from the filaments and decreases the Ca^{2+} sensitivity of troponin C (Layland, Solaro, and Shah 2005). The enhanced Ca^{2+} content in the SR together with PKA-dependent activation LTCC enhancing I_{ca}, substantially increases Ca^{2+} transient amplitude in the cells, creating

a positive inotropic effect. Furthermore, PKA can also modulate RyR gating (D. M. Bers 2008). Hyperphosphorilation of the RyR by PKA has been found to be involved in heart failure by affecting the closure of the channel and making it leaky (Wehrens et al. 2006).

The compartmentalisation of cAMP signalling plays a significant role in modulating the excitation-contraction coupling. The PKA effects discussed above are not achieved by all the hormones that lead to increase in cAMP levels. For example, it is known that prostaglandin, which also stimulates cAMP production, does not lead to positive inotropic effects (Hayes, Brunton, and Mayer 1980), yet, β1-AR activation leads to LTCC, PLB, RyR and TnI phosphorylation by PKA, causing the characteristic inotropic and lusitropic effects (Rockman, Koch, and Lefkowitz 2002; D. M. Bers 2002). The activation of β2-AR selectively stimulates calcium current, causing a smaller inotropic effect and no lusitropic effect (Kuschel et al. 1999; Petroff et al. 2001). The inotropic effect upon β-AR is transient, even in the continuous presence of catecholamines. The first reason is the spike in cAMP generation which happens at the beginning, followed by the enhancement of the phosphodiesterase 1 by calmodulin, which increases as a consequence of the high Ca^{2+} concentrations. Additionally, the high activity of the β-AR triggers inhibitory mechanisms, such as the β-agonist receptor kinase (β-ARK), which uncouples the receptors from the G protein complex and adenylyl cyclase. In addition, β-ARK stimulates the binding of β -arrestin to the receptors, which changes their molecular configuration disabling further interaction between the G proteins and the receptors (Opie 2004). In addition to receptor desensitization (process described above), β –arrestin was also shown to recruit PDEs to the activated β-AR, limiting the activation of PKA at the plasma membrane (Perry et al. 2002; Baillie et al. 2003).

The chronotropic effect achieved upon β-AR is partially consequence of the positive inotropic and lusitropic effect generated. Yet, it can also be explained by the fact that catecholamines increase the rate of contraction by stimulation of the pacemaker and increases the conductivity rate of the impulse down the atrioventricular node upon β1-AR stimulation (D. M. Bers 2008; D. Bers 2001).

Figure 6.2. PKA-mediated phosphorylation of excitation-contraction coupling proteins



(D. M. Bers 2002)

Figure 2.

Beta-adrenergic receptor activation and phosphorylation of targets relevant to excitation–contraction coupling such as the ryanodine receptors, Troponin I, LTCC and phospholamban. Abbreviations: AC, adenylyl cyclase; ACh, acetyl- choline; AKAP, A kinase anchor- ing protein; -AR, -adrenergic receptor; M2-Rec, M2-muscarinic receptor; PLB, phospholamban; Reg, PKA regulatory subunit; SR, sarcoplasmic reticulum. (D. M. Bers 2002).

6.1.3. Nitric oxide and $_{c}$GMP effect in cardiac contractility

The muscarinic cholinergic receptors in the heart are associated with the parasympathetic vagal system. Stimulation of this system is known to have inhibitory effects in the heart, opposing the adrenergic stimulation and decreasing heart rate (D. M. Bers 2002; D. Bers 2001). One of its mechanism of action is by interacting with the G inhibitory protein (Gi), decreasing the activity of the adenylyl cyclase and the generation of cAMP. It also acts on the pacemaking activity of the sinus node by direct inhibition, or by reducing cAMP levels (Tsai and Kass 2009). In addition, apart from inhibiting the formation of cAMP, the system has also been implicated to promote cGMP accumulation and activation of PKG (Fischmeister and Hartzell 1987) as muscarinic receptors activation by acetylcholine realise NO, which in turn stimulates sGC (Han, Shimoni, and Giles 1995; Opie 2004).

However, NO stimulation can also result in a positive inotropic effect by increasing cAMP, when in low concentrations by activating adenylyl cyclase (Vila-Petroff et al. 1999; Tsai and Kass 2009), and by cGMP-dependent PDE3 inhibition. The negative inotropic effect of NO is observed in high concentrations and it is partially due to cGMP-PKG signalling (Vila-Petroff et al. 1999; Layland, Li, and Shah 2002; Tsai and Kass 2009).

cGMP, via PKG, has the ability to reduce Ca^{2+} sensitivity of the myofilaments by phosphorylating troponin I (Brusq et al. 1999; Pfitzer et al. 1982). This PKG-mediated phosphorylation was also shown to increase resting myocyte cell length, to decrease sarcomere shortening amplitude and accelerate relaxation time of isolated rat cardiomyocytes upon NO-donor (Layland, Li, and Shah 2002). This effect was seen only

with active guanylyl cyclase and was achieved without affecting significantly the amplitude and kinetics of intracellular calcium, supporting the hypothesis that the myofilament response to calcium was decreased upon PKG-phosphorylation. Furthermore, PKG-mediated phosphorylation of LTCC has been shown to inhibit the channel calcium current (Yang et al. 2007). Apart from these mechanisms, cGMP also mediates decrease in cAMP levels by activating PDE2 (Massion et al. 2003) and regulates SR calcium reuptake by PKG- dependent phospholamban phosphorylation and consequent higher activity of SERCA2 (Raeymaekers, Hofmann, and Casteels 1988). PKG- mediated phosphorylation of the plasmalemma calcium ATPase also results in decreased intracellular calcium availability (Tsai and Kass 2009; Eggermont et al. 1988).

6.1.4. Sarcomere length, tension and force of contraction relationship

Increased force and rate of contraction is not only achieved by changes in intracellular calcium and phosphorylation of proteins involved in the excitation-contraction coupling. These effects can also be observed with the normal beat of the heart when the venous return increases, enhancing the tension and length of the cardiomyocytes and consequently, increasing left ventricle cardiac output (Starling Law). The relationship between sarcomere length and force of contraction can be partially (about 20%) explained by the concept that the maximal force of a sarcomere is determined by the degree of overlap between the thick and thin filaments. Therefore, the sarcomere can be stretched to an optimal length, achieving maximal number of crossbridges and therefore force generation; with over-stretch the force gradually declines as there is a decrease in overlap; when the cell is shrunk, the short sarcomere impedes the formation of effective crossbridges by cross over of the thin filaments and compressed thick filaments due to collision with the Z-lines (D. Bers 2001). As the steeper ascending tension-length

relationship encountered in cardiac myocytes when compared to skeletal muscle cells cannot be explained simply by the filaments overlay, other mechanisms are also known to play an important role. The greater proportion of the explanation for such relationship is given by the length dependence of myofilament Ca^{2+} sensitivity. The molecular process of how stretching mediates this length-dependent activation and the Frank-Starling law is not yet completely understood, however it appears to be complex as several synergistic mechanisms seem to be in place (Sequeira and van der Velden 2017).

6.2. SPECIFIC AIMS

Given the role of the cyclic nucleotides in controlling the excitation-contraction coupling, as well as the crucial role of the dystrophin complex in connecting the contractile machinery and cellular cytoskeleton to the extracellular matrix and in stabilising the sarcolemma against mechanical damage during contraction, and considering the defective cyclic nucleotide signalling encountered in mdx cardiomyocytes (Chapter 5), it became interesting to explore the contractile performance of adult mdx cardiomyocytes upon manipulation of cAMP and cGMP levels.

Available data suggest that stretch-activated channels (SACs) such as the transient receptor potential channels (TRPCs) are involved in the excessive Ca^{2+} influx observed in dystrophic cells (Aguettaz et al. 2016). Furthermore, mdx cardiomyocytes have been shown to significantly increase the production of ROS and increase Ca^{2+} waves oscillations when subject to stretched and physiological stretches was suggested to be a potential pathological trigger in mdx heart (Prosser, Ward, and Lederer 2011).

The experiments presented in this chapter had the aim to explore the contractile responses (sarcomere shortening and force generation) of mdx cardiomyocytes unloaded and under

tension upon beta-adrenergic stimulation with isoproterenol, inhibition of PDEs with IBMX and stimulation of soluble guanylyl cyclases with NO donors.

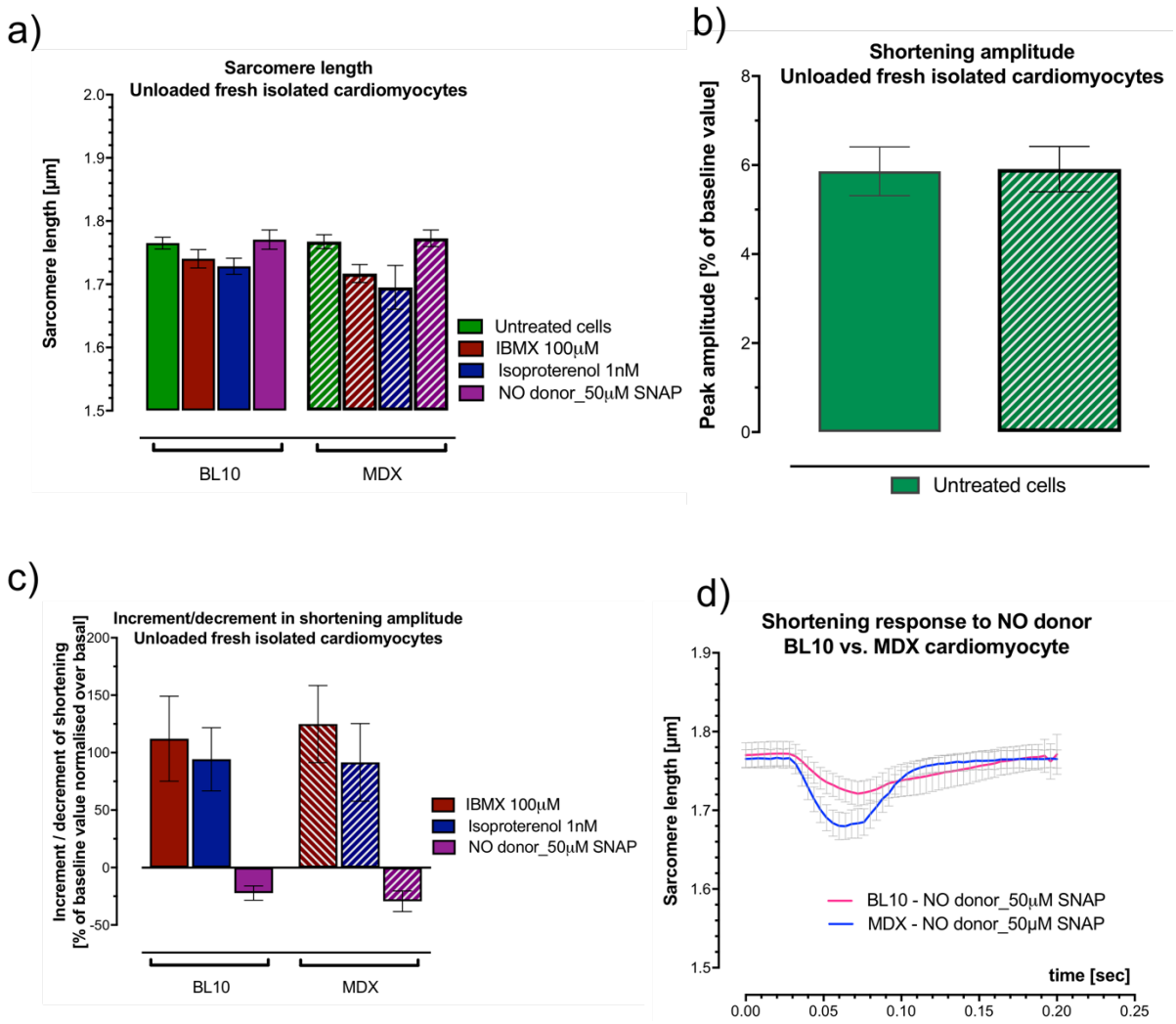
6.3. RESULTS

6.3.1. Unloaded mdx cardiomyocytes contracts similarly to healthy cells upon increase in cAMP however present defective relaxation upon NO donors application.

Unloaded freshly isolated cardiomyocytes from 12 weeks old mdx mice and aged-matched controls were paced at 5Hz at 37^{o}C and fractional shortening was measured either in untreated cells or after stimulation with 1nM of Isoproterenol, 100μM IBMX, or the NO donor SNAP 50 μM. At basal levels wt and mdx cells presented similar basal sarcomere lengths (Figure 6.3a) and fractional shortening at basal levels (Figure 6.3b). As expected, the increase in cAMP induced by treatment with isoproterenol or IBMX resulted in increased fractional shortening in both cell types (Figure 6.3c). The % increase, when compared to basal levels (untreated cells) was significantly higher, however, there was no difference between the two cell types. In addition, the increase in fractional shortening generated 100μM IBMX was not significantly different from the increase induced by 1nM Isoproterenol in both cell types (Figure 6.3c). The NO donor treatment also resulted in the expected effect as sarcomere shortening was decreased a few seconds after the application of the drug (shown as a decrement in Figure 6.3c). Although the fractional shortening data is not statistically significant, the mdx cells seems to be less responsive to the NO donor (normalised shortening traces shown in Figure 6.3d). As seen in Figures 6.1e and f, mdx cells do not get enhanced relaxation upon NO donor to the same extent as the wt cells. The measurement of the departure velocity (shortening velocity) and the return velocity (lengthening velocity) is significantly higher in mdx upon NO donor application, supporting the hypothesis that stimulation with NO

donor does not lead to the physiological negative inotropic and lusitropic effects as observed in wt cells. This might be due to defective NO-cGMP signalling present in dystrophic cardiomyocytes. Additionally, this data suggests that the although mdx cardiomyocytes present higher expression of beta1-subunit of the sGC, as shown in Chapter 5, these might not be sensitive to NO.

Figure 6.3. Sarcomere shortening analysis of unloaded cardiomyocytes



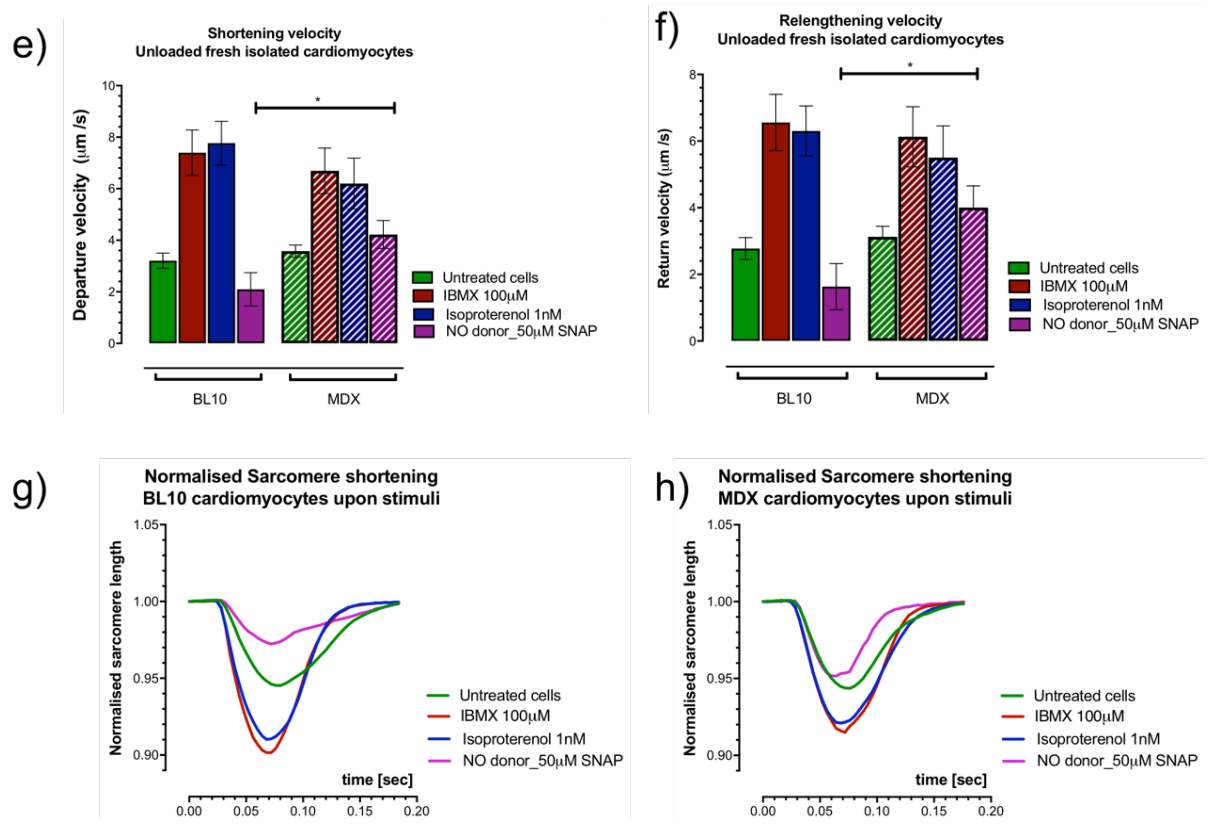


Figure 6.3.
Sarcomere shortening analysis of freshly isolated cardiomyocytes plated in laminin coverslips for 2 hours. Cells were paced at 5Hz, at 37oC and with pulse duration of 2ms. a) Sarcomere length, which represents the length of the sarcomere at relaxed state (baseline), under the different stimuli; b) Shortening departure velocity, which represents the systolic phase, under the different stimuli; c) Shortening return velocity which represents the lengthening velocity and relaxation phase under the different stimuli; d) Total shortening amplitude (from baseline to peak) in untreated cells. The shortening amplitude under the different stimuli were calculated as increment of shortening (e) for easier understanding as percent increment over control (before the stimulus) calculated as (D shortening / shortening control) * 100, where D shortening = (shortening stimulated – shortening control); f) Average shortening trace of BL10 and MDX upon the application of SNAP; g) Normalised sarcomere shortening trace of BL10 and mdx (h) cardiomyocytes at basal level (untreated) and after the application of each stimulus. Traces were normalised to initial baseline value to facilitate comparison between the shortening achieved with each drug. N = 3 biological replicates and ≥ 20 individual cells for all data set, except for SNAP experiments where only 6 cells were analysed. Error bars represent SEM; T-test, * = 0.05<p<0.01. Experiments are grouped in one graph to facilitate comparison; however, they were all performed separately.

6.3.2. mdx cardiomyocytes generate significantly lower force under tension

In the heart, the cardiomyocytes are closely connected and apply tension to one another. This characteristic is also important to adjust work output to external load. As discussed in the introduction, stretch-induced increase in force production has long been recognised.

Although the measurement of sarcomere shortening of unloaded cardiomyocytes provides useful information, applying tension to these cells while measuring contractility mimics better the physiological situation in the heart.

For the following experiments I have used a novel approach that allows the measurement of force of contraction of a single cardiomyocyte under tension by attaching two glass road (fibres) to the edges of each cell. One fibre is stiff, whereas the other is a flexible force transducer with known stiffness. The contraction movement of the cell deflects the force transducer which then translates the deflection into a measurement of force of contraction. By using a Piezo controller coupled to one of the rods, it is possible to apply controlled stretch steps to the cell while measuring its force of contraction (Figure 6.4a). This approach was applied to freshly isolated mdx and control cardiomyocytes to measure the force of contraction of untreated mdx cells under different conditions of stretch as well as upon application of isoproterenol or IBMX. Figure 6.4a shows the experimental protocol applied. The middle panel in Figure 6.4 (Figure 6.4b-e inside orange selection) shows the comparison between treatment and no treatment for each cell type. To facilitate comparison between wt and mdx, the same data is shown in the lower panel of Figure 6.4 (Figure 6.4f-i inside green selection) where each graph shows the comparison between wt and mdx cells under one specific condition (untreated, isoproterenol and IBMX).

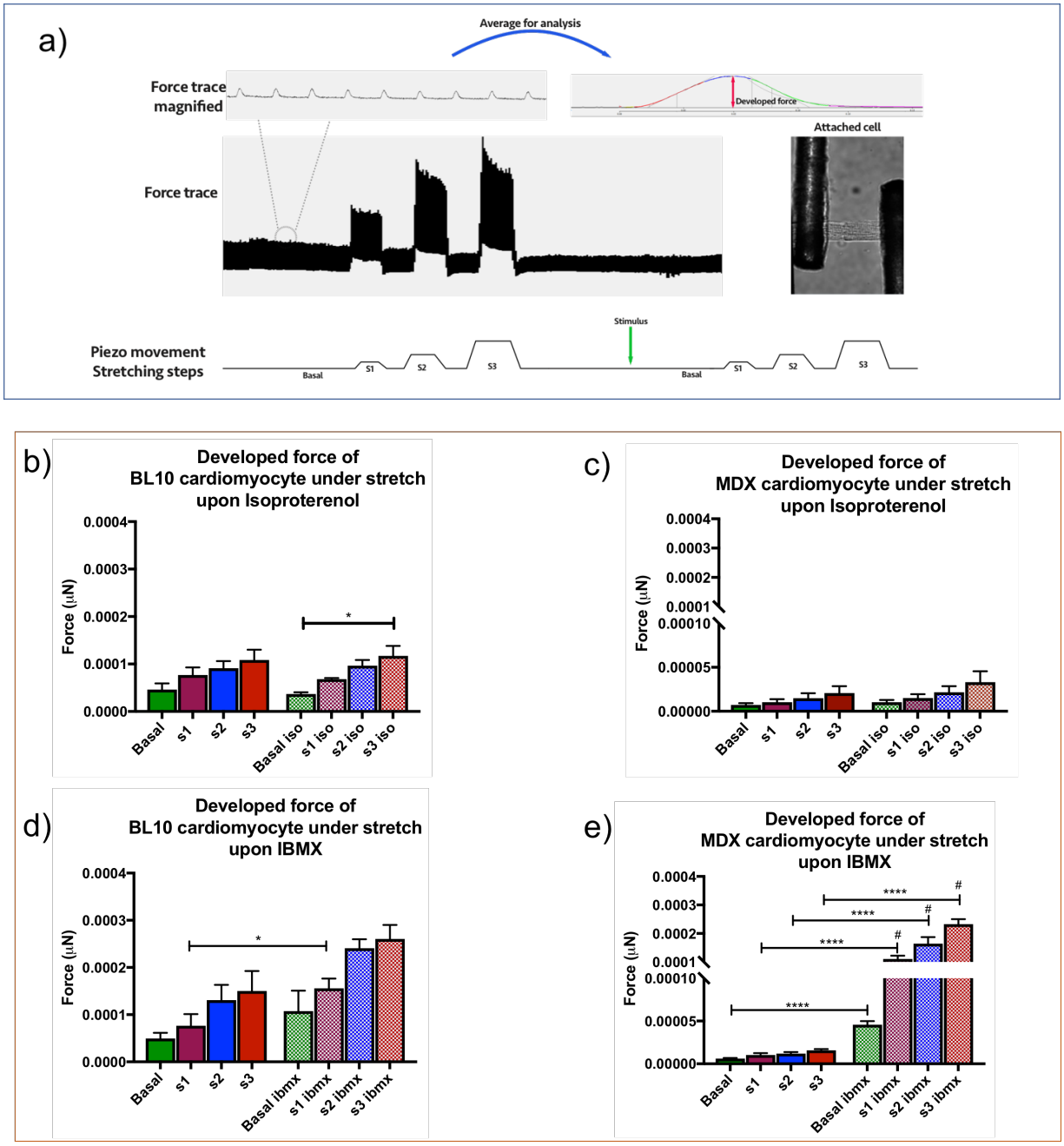
Both cell types generated increased force of contraction when the three stretch steps were applied. The developed force, although always greater after each stretch step, did not show statistically significant increment with each step. Treatment with 1nM isoproterenol generated only a small increase in force in both wt and mdx cardiomyocytes in un-stretched myocytes and upon stretch application (Figures 6.4b and c). This increase was not significantly higher than the force developed by untreated cells, suggesting that this concentration is not enough to produce a detectable inotropic effect. Treatment with

IBMX, on the other hand, significantly increased force of contraction in un-stretched and stretched mdx cells while no enhancement upon PDE inhibition was found in wt cells (Figures 6.4d and e). As shown in Figure 6.4f, the developed force of mdx cells under tension (simply attached to the rods, without stretch) and untreated was found to be significantly lower than control cells. Although untreated mdx cells showed increase in force with stretch application, the force generated was not significantly different when comparing the three stretching steps applied, however they were significantly lower when compared to the control cells across all the stretching steps (Figure 6.4g. significance star symbols represent comparison between control and mdx; # represent comparison between the control (basal) of the same group). The developed force of contraction upon isoproterenol was not significantly higher when compared to untreated cells (as already discussed), however, the forces generated by mdx cells under isoproterenol were significantly lower when compared to control cells (Figure 6.4h). Control cells significantly increased the developed force after the second stretching step when compared to basal levels (Figures 6.4g and h) as expected. IBMX treatment significantly increased the developed force of contraction in mdx cells (as already discussed and shown in Figure 6.4e). This increase was sufficiently high to abolish the differences found between untreated wt and mdx cells (Figure 6.4i), suggesting that mdx cardiomyocytes present higher PDE activity compared to wt. The elevated PDE mRNA levels found in mdx adult cardiomyocytes (shown in Chapter 5) supports this hypothesis. Initial FRET measurements to compare the responses achieved upon total inhibition of PDEs in both cell types upon IBMX were performed (Figure 6.4j). As sample size of this experiment is substantially low (n=3, 1 biological replicate), no significant difference is found upon IBMX between both cell types. However, there is a trend indicating high PDE activity in the mdx cardiomyocytes. Figure 6.4j also illustrates

that 1nM isoproterenol generates similar cAMP levels in both cells types. However, these are substantially lower than the level of cAMP generated upon 100 μM IBMX, supporting the hypothesis that cAMP generated upon this concentration of Isoproterenol is indeed not be sufficient to generate detectable positive inotropic effect with this technique.

It is known that the absence of the cytoskeletal protein dystrophin leads to changes in cellular stiffness and increased stretch-induced damage when compared to control cells (Allen et al 2010). Therefore, the results obtained in this experimental set could have been influenced by a different effect of stretch in the mdx cardiomyocytes. To control for this, the sarcomere length of mdx and wt cardiomyocytes were compared at each stretching step. As shown in Figure 6.4k, the sarcomere length of both cells responded similarly to each stretch step applied, suggesting that it is possible to directly compare the force developed in each cell after stretching.

Figure 6.4. Analysis of force developed upon stretch and isoproterenol and IBMX stimulation



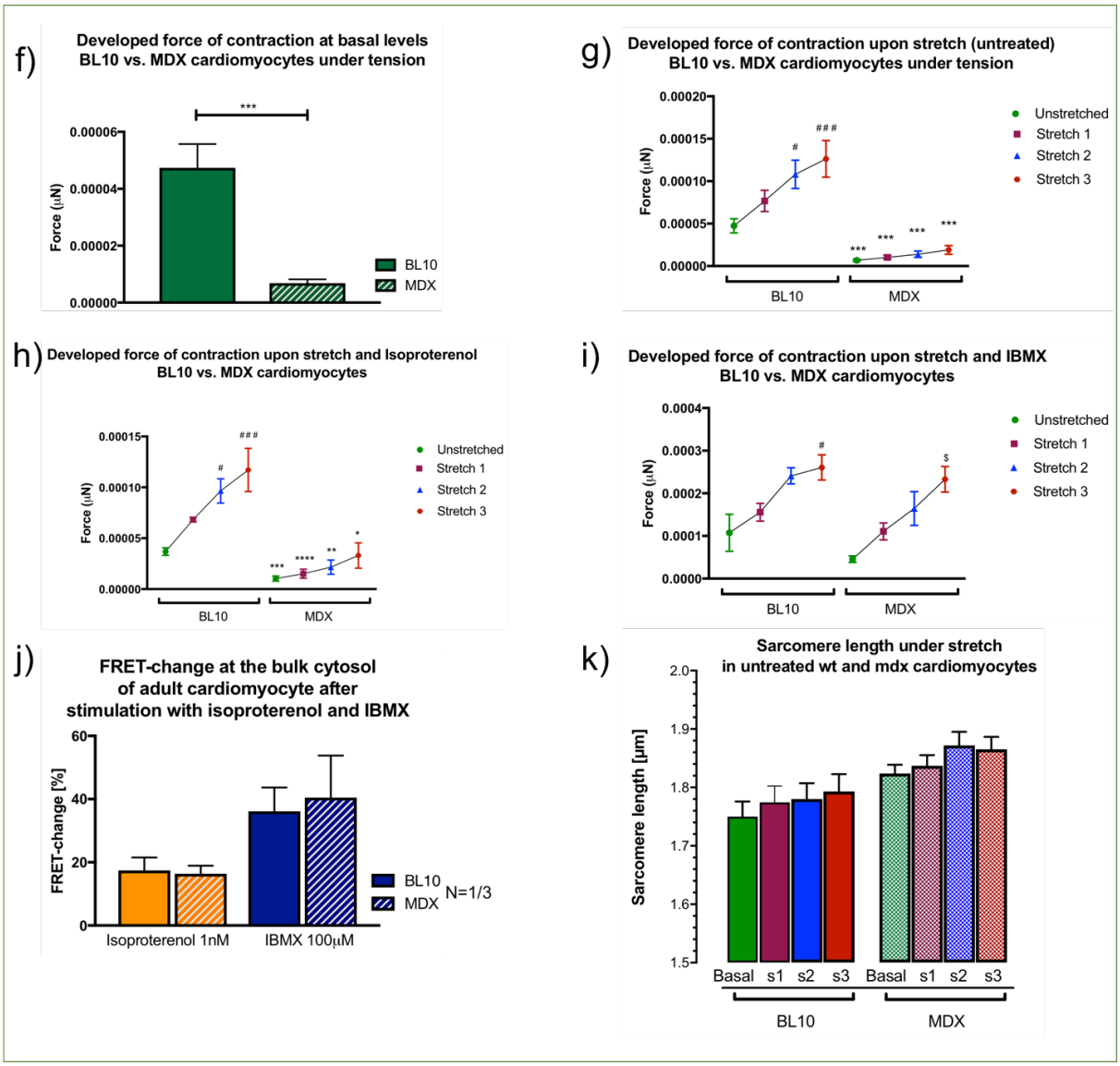


Figure 6.4.
The top panel (a) illustrates experimental protocol and analysis. Piezo controller moves accordingly to the protocol illustrated and force traces are recorded in real time. After the stretching sequence is completed (three sequential steps with increase stretch of 0.5 V each step), cells are put back to the initial length and stimulus is applied. The same stretching protocol is applied to the cells under stimulus. S1 represents the stretch step 1, S2 represents the stretch step 2 and S3 represents the stretch step 3. Basal represents force generated under no stretch. An area corresponding to at least 10 transients (shown in magnified force trace) were analysed by averaging the transient peaks (shown in magnified force trace after average). The peak amplitude or developed force parameter was used for comparison between treatments and cells (shown by the red arrow in averaged peak image). The analysis of the characteristics of the transient was done by using the IonOptix software. The image on the right show acardiomyocyte attached to the rods where one rod is fixed and one is the force transducer. For comparison, the developed force measured in each experiment was normalised by the cross-sectional area of the cardiomyocyte under study. The middle panel (panels b) to e)) shows the individual experimental sets: Force developed upon stretch and isoproterenol in control cells (b) and in mdx cells (c); Force developed upon stretch and IBMX in control cells (d) and mdx cells (e). Lower panel (panels f) to j)) shows the comparison between wt and mdx developed force at basal levels (f) where cells are not stretched and are not treated; developed force of untreated wt vs. mdx cells upon stretch where * represent t-test between the same stretch step of wt and mdx, and # represent t-test between stretch step and basal for the set of experiment with wt cells (g); developed force of wt vs. mdx cells upon stretch and isoproterenol

where * represent t-test between the same stretch step of wt and mdx, and # represent t-test between stretch step and basal within the wt set of experiment (h); developed force of wt vs. mdx cells upon stretch and IBMX where # represent t-test between stretch step and basal within only the wt set of experiment and $ represent t-test between stretch step and basal within the mdx set of experiment (i); FRET-change response of adult cardiomyocytes expressing the cytosolic cAMP FRET sensor H187 upon 1nM isoproterenol and 100μM IBMX. N = 3 biological replicates and ≥ 4 individual cells. K) Comparison of sarcomere length increase with stretch in untreated conditions. Two-way ANOVA applied for comparison. Error bars represent SEM; T-test applied when comparison between only two independent experimental sets and Mann Whitney test applied to compare IBMX and Iso data (n=3), $^{*, \#, \$}$ = 0.05<p<0.01, ** = 0.01<p<0.001, *** $^{, \#\#\#}$ = 0.001<p<0.0001, **** = p<0.0001.

6.4. DISCUSSION

Several studies have focused on exploring contractility properties of the mdx heart (M Khairallah et al. 2008; Bia et al. 1999; Chu et al. 2002; Wehling-Henricks et al. 2005), however, most of them were developed in whole heart. The data presented in this chapter show to our knowledge for the first time the contractile characteristics of the mdx heart at the level of single cardiomyocyte. By using the IonOptix sarcomere shortening recording system and the IonOptix force transducer apparatus, the contractility and force of contraction of freshly isolated cardiomyocytes from 12 weeks old mdx mice were analysed using cells under tension and upon stretch, as well as unloaded cells (sarcomere shortening only) upon different stimuli.

The main findings were:

- Cardiomyocytes from 12 weeks old mdx mice present significantly reduced force development when compared to wt cardiomyocytes. This effect was observed not only at basal levels but also upon isoproterenol stimulation and under different degree of stretch (Figure 6.4). It is important to note that the treatment with 1nM isoproterenol was not sufficient to generate significantly higher forces even in wt cardiomyocytes (Figure 6.4b). This observation is interesting as substantial increase in fractional shortening in unloaded cells was recorded upon

administration of the same amount of isoproterenol. Also, the fractional shortening recorded in unloaded mdx cardiomyocytes was not different from wt cells, indicating that unloaded shortening might not be a direct accurate readout of force of contraction and that the cardiomyocytes respond differently when under tension.

- mdx cardiomyocytes treated with IBMX generated a significantly greater force when compared to Isoproterenol (Figure 6.4e). This data can be explained by the higher concentrations of cAMP achieved after total blockage of PDEs by using 100μM IBMX when compared to the level of cAMP generated by 1nM isoproterenol (Figure 6.4j). The increase in force upon IBMX application in the mdx cells was detected at basal levels (non-stretched) as well as with each stretch step applied. While the wt cells presented low level of significance between each stretching step upon IBMX (only visible at the first step), the mdx cells showed significantly enhanced force of contraction upon IBMX application at each stretching step. This effect resulted into restored contractility as the force developed by mdx cells in basal un-stretched conditions and upon stretch was not significantly different from wt cells treated with IBMX (Figure 6.4i). This finding suggests that the PDEs might be significantly more active in the mdx cardiomyocytes and may be responsible for blunting the cAMP signal which may then result in reduced force of contraction. Due to time limitations, it was not possible to perform a complete set of FRET experiments exploring the cAMP responses of each cell type to IBMX. Nonetheless, preliminary experiments show trend for higher PDE activity in the mdx, which is supported by the significantly

higher mRNA levels found for the majority of the PDEs in mdx adult cardiomyocytes (data in Chapter 5 Figure 5.14)

- A small set of experiments to explore the effects of the NO donor SNAP on the contractile properties of mdx cells was conducted in unloaded cells. Although the sample size was small, the data suggests that SNAP is significantly less effective in promoting negative inotropic effects in the mdx cardiomyocytes, as they present significantly higher departure and return velocities when compared to wt treated with SNAP (Figure 6.3).

The force measurement presented here are technically extremely demanding and hampered by extreme fragility of the force transducer probe, challenging calibration and tricky cell attachment. As a consequence, it was not possible to further develop this analysis by assessing the effect of inhibition of individual PDEs and stimulation of the cGMP pathway.

In conclusion, data from this chapter suggests that even at a young age (12 weeks), when the cardiomyopathy is not obviously established (Maya Khairallah et al. 2007), the developed force of contraction is significantly reduced in isolated mdx cardiomyocytes compared to age matched control cells. Furthermore, mdx cells do not seem to be able to substantially increase the force of contraction upon stretch. As IBMX treatment was able to restore the force developed by mdx cardiomyocytes to the same levels of control cells, altered PDEs activity and possible altered regulation of the excitation-contraction coupling in mdx cardiomyocytes is a plausible explanation for the compromised force generation found in the mdx model.

6.5. REFERENCES

Aguettaz, E, JJ Lopez, A Krzesiak, L Lipskaia, S Adnot, RJ Hajjar, C Cognard, B Constantin, and S Sebille. 2016. “Axial Stretch-Dependent Cation Entry in Dystrophic Cardiomyopathy: Involvement of Several TRPs Channels.” *Cell Calcium* 59 (4): 145–55.

Allen, David G., Bao-ting Zhang, and Nicholas P. Whitehead. "Stretch-induced membrane damage in muscle: comparison of wild-type and mdx mice." In *Muscle Biophysics*, pp. 297-313. Springer New York, 2010.

Baillie, George S, Arvind Sood, Ian McPhee, Irene Gall, Stephen J Perry, Robert J Lefkowitz, and Miles D Houslay. 2003. “β-Arrestin-Mediated PDE4 cAMP Phosphodiesterase Recruitment Regulates β-Adrenoceptor Switching from Gs to Gi.” *Proceedings of the National Academy of Sciences* 100 (3): 940–45.

Bers, Donald. 2001. *Excitation-Contraction Coupling and Cardiac Contractile Force*. Vol. 237. Springer Science & Business Media.

Bers, Donald M. 2002. “Cardiac Excitation–contraction Coupling.” *Nature* 415 (6868): 198–205.

———. 2008. “Calcium Cycling and Signaling in Cardiac Myocytes.” *Annu. Rev. Physiol.* 70: 23–49.

Bia, Britta L, Paul J Cassidy, Martin E Young, Jill A Rafael, Brendan Leighton, Kay E Davies, George K Radda, and Kieran Clarke. 1999. “Decreased Myocardial nNOS, Increased iNOS and Abnormal ECGs in Mouse Models of Duchenne Muscular Dystrophy.” *Journal of Molecular and Cellular Cardiology* 31 (10): 1857–62.

Brusq, Jean-Marie, Eric Mayoux, Laurent Guigui, and Jorge Kirilovsky. 1999. “Effects of C-type Natriuretic Peptide on Rat Cardiac Contractility.” *British Journal of Pharmacology* 128 (1): 206–12.

Chu, Victor, Jose M Otero, Orlando Lopez, Matthew F Sullivan, James P Morgan, Ivo Amende, and Thomas G Hampton. 2002. “Electrocardiographic Findings in Mdx Mice: A Cardiac Phenotype of Duchenne Muscular Dystrophy.” *Muscle & Nerve* 26 (4): 513–19.

Eggermont, Jan A, Matty Vrolix, Luc Raeymaekers, Frank Wuytack, and Rik Casteels. 1988. “Ca2+-Transport ATPases of Vascular Smooth Muscle.” *Circulation Research* 62 (2): 266–78.

Ervasti, James M, Kay Ohlendieck, Steven D Kahl, Mitchell G Gaver, and Kevin P Campbell. 1990. “Deficiency of a Glycoprotein Component of the Dystrophin Complex in Dystrophic Muscle.” *Nature* 345 (6273): 315–19.

Fischmeister, R, and HC Hartzell. 1987. “Cyclic Guanosine 3’, 5’-monophosphate Regulates the Calcium Current in Single Cells from Frog Ventricle.” *The Journal of Physiology* 387 (1): 453–72.

Gao, Tianyan, Atsuko Yatani, Mark L Dell’Acqua, Hidenori Sako, Stuart A Green, Nathan Dascal, John D Scott, and M Marlene Hosey. 1997. “cAMP-Dependent Regulation of Cardiac L-Type Ca 2+ Channels Requires Membrane Targeting of PKA and Phosphorylation of Channel Subunits.” *Neuron* 19 (1): 185–96.

Gautel, M, Orsetta Zuffardi, A Freiburg, and S Labeit. 1995. “Phosphorylation Switches Specific for the Cardiac Isoform of Myosin Binding Protein-C: A Modulator of Cardiac Contraction?” *The EMBO Journal* 14 (9): 1952.

Gratton, Jean-Philippe, Pascal Bernatchez, and William C Sessa. 2004. “Caveolae and Caveolins in the Cardiovascular System.” *Circulation Research* 94 (11): 1408–17.

Han, X, Y Shimoni, and WR Giles. 1995. “A Cellular Mechanism for Nitric Oxide-Mediated Cholinergic Control of Mammalian Heart Rate.” *The Journal of General Physiology* 106 (1): 45–65.

Hayes, J Scott, Laurence L Brunton, and Steven E Mayer. 1980. “Selective Activation of Particulate cAMP-Dependent Protein Kinase by Isoproterenol and Prostaglandin E1.” *Journal of Biological Chemistry* 255 (11): 5113–19.

Keurs, Hendrick EDJ ter. 2012. “The Interaction of Ca 2+ with Sarcomeric Proteins: Role in Function and Dysfunction of the Heart.” *American Journal of Physiology-Heart and Circulatory Physiology* 302 (1): H38–50.

Khairallah, M, RJ Khairallah, ME Young, BG Allen, MA Gillis, G Danialou, CF Deschepper, BJ Petrof, and C Des Rosiers. 2008. “Sildenafil and Cardiomyocyte-Specific cGMP Signaling Prevent Cardiomyopathic Changes Associated with Dystrophin Deficiency.” *Proceedings of the National Academy of Sciences* 105 (19): 7028–33.

Khairallah, Maya, Ramzi Khairallah, Martin E Young, Jason RB Dyck, Basil J Petrof, and Christine Des Rosiers. 2007. “Metabolic and Signaling Alterations in Dystrophin-Deficient Hearts Precede Overt Cardiomyopathy.” *Journal of Molecular and Cellular Cardiology* 43 (2): 119–29.

Kuschel, Meike, Ying-Ying Zhou, Harold A Spurgeon, Sabine Bartel, Peter Karczewski, Sheng-Jun Zhang, Ernst-Georg Krause, Edward G Lakatta, and Rui-Ping Xiao. 1999. “β 2-Adrenergic cAMP Signaling Is Uncoupled from Phosphorylation of Cytoplasmic Proteins in Canine Heart.” *Circulation* 99 (18): 2458–65.

Layland, Joanne, Jian-Mei Li, and Ajay M Shah. 2002. “Role of Cyclic GMP-dependent Protein Kinase in the Contractile Response to Exogenous Nitric Oxide in Rat Cardiac Myocytes.” *The Journal of Physiology* 540 (2): 457–67.

Layland, Joanne, R John Solaro, and Ajay M Shah. 2005. “Regulation of Cardiac Contractile Function by Troponin I Phosphorylation.” *Cardiovascular Research* 66 (1): 12–21.

MacLennan, David H, and Evangelia G Kranias. 2003. “Phospholamban: A Crucial Regulator of Cardiac Contractility.” *Nature Reviews. Molecular Cell Biology* 4 (7): 566.

Marx, Steven O, Steven Reiken, Yuji Hisamatsu, Thotalla Jayaraman, Daniel Burkhoff, Nora Rosemblit, and Andrew R Marks. 2000. “PKA Phosphorylation Dissociates FKBP12. 6 from the Calcium Release Channel (Ryanodine Receptor): Defective Regulation in Failing Hearts.” *Cell* 101 (4): 365–76.

Massion, PB, Olivier Feron, Chantal Dessy, and J-L Balligand. 2003. “Nitric Oxide and Cardiac Function: Ten Years After, and Continuing.” *Circulation Research* 93 (5): 388–98.

Murphy, Elizabeth, and Charles Steenbergen. 2007. “Preconditioning: The Mitochondrial Connection.” *Annu. Rev. Physiol.* 69: 51–67.

Opie, Lionel H. 2004. *Heart Physiology: From Cell to Circulation*. Lippincott Williams & Wilkins.

Perry, Stephen J, George S Baillie, Trudy A Kohout, Ian McPhee, Maria M Magiera, Kok Long Ang, William E Miller, Alison J McLean, Marco Conti, and Miles D Houslay. 2002. “Targeting of Cyclic AMP Degradation to β2-Adrenergic Receptors by β-Arrestins.” *Science* 298 (5594): 834–36.

Petroff, Martín G Vila, Josephine M Egan, Xiaolin Wang, and Steven J Sollott. 2001. “Glucagon-like Peptide-1 Increases cAMP but Fails to Augment Contraction in Adult Rat Cardiac Myocytes.” *Circulation Research* 89 (5): 445–52.

Pfitzer, G, JC Rüegg, V Flockerzi, and F Hofmann. 1982. “cGMP-Dependent Protein Kinase Decreases Calcium Sensitivity of Skinned Cardiac Fibers.” *FEBS Letters* 149 (2): 171–75.

Prosser, Benjamin L, Christopher W Ward, and WJ Lederer. 2011. “X-ROS Signaling: Rapid Mechano-Chemo Transduction in Heart.” *Science* 333 (6048): 1440–45.

Raeymaekers, Luc, Ft Hofmann, and Rik Casteels. 1988. “Cyclic GMP-Dependent Protein Kinase Phosphorylates Phospholamban in Isolated Sarcoplasmic Reticulum from Cardiac and Smooth Muscle.” *Biochemical Journal* 252 (1): 269–73.

Rockman, Howard A, Walter J Koch, and Robert J Lefkowitz. 2002. “Seven-Transmembrane-Spanning Receptors and Heart Function.” *Nature* 415 (6868): 206–12.

Rybakova, Inna N, Jitandrakumar R Patel, and James M Ervasti. 2000. “The Dystrophin Complex Forms a Mechanically Strong Link between the Sarcolemma and Costameric Actin.” *The Journal of Cell Biology* 150 (5): 1209–14.

Sequeira, Vasco, and Jolanda van der Velden. 2017. “The Frank–Starling Law: A Jigsaw of Titin Proportions.” *Biophysical Reviews* 9 (3): 259.

Tsai, Emily J, and David A Kass. 2009. “Cyclic GMP Signaling in Cardiovascular Pathophysiology and Therapeutics.” *Pharmacology & Therapeutics* 122 (3): 216–38.

Vila-Petroff, Martin G, Antoine Younes, Josephine Egan, Edward G Lakatta, and Steven J Sollott. 1999. “Activation of Distinct cAMP-Dependent and cGMP-Dependent Pathways by Nitric Oxide in Cardiac Myocytes.” *Circulation Research* 84 (9): 1020–31.

Wehling-Henricks, Michelle, Maria C Jordan, Kenneth P Roos, Bo Deng, and James G Tidball. 2005. “Cardiomyopathy in Dystrophin-Deficient Hearts Is Prevented by Expression of a Neuronal Nitric Oxide Synthase Transgene in the Myocardium.” *Human Molecular Genetics* 14 (14): 1921–33.

Wehrens, Xander HT, Stephan E Lehnart, Steven Reiken, John A Vest, Anetta Wronska, and Andrew R Marks. 2006. “Ryanodine Receptor/Calcium Release Channel PKA Phosphorylation: A Critical Mediator of Heart Failure Progression.” *Proceedings of the National Academy of Sciences of the United States of America* 103 (3): 511–18.

Yang, Lin, Guoxia Liu, Sergey I Zakharov, Andrew M Bellinger, Marco Mongillo, and Steven O Marx. 2007. “Protein Kinase G Phosphorylates Cav1. 2 α1c and β2 Subunits.” *Circulation Research* 101 (5): 465–74.

Zhang, Ren, Jiaju Zhao, Alan Mandveno, and James D Potter. 1995. “Cardiac Troponin I Phosphorylation Increases the Rate of Cardiac Muscle Relaxation.” *Circulation Research* 76 (6): 1028–35.

Chapter 7. Concluding remarks

The data presented in this thesis constitute an exhaustive investigation of the cAMP and cGMP signalling and regulation by PDEs in three different subcellular compartments of control and mdx cardiomyocytes: the bulk cytosol, the plasma membrane and the outer mitochondrial membrane. The first main hypothesis at the basis of this project was that mdx cardiomyocytes present defective cGMP and/or cAMP signalling. Experimental data presented in this thesis supports this hypothesis for the following four reasons. First, the initial experimental data indicated that basal free cGMP and cAMP levels at all three subcellular compartments were found to be significantly altered in mdx neonatal cardiomyocytes when compared to controls. Interestingly, these levels were substantially different in adult cardiomyocytes. Second, although mdx neonatal cardiomyocytes presented similar levels of mRNA for all PDEs tested, significant alterations in activity were observed in all the subcellular compartment analysed. Furthermore, the ability to generate cGMP and cAMP were found significantly altered in some of the subcellular compartments. Third, nNOS and iNOS expression levels were found to be significantly altered in the mdx cardiomyocytes compared to controls. Fourth, mdx cardiomyocytes presented significantly more oxidised sGC at the plasma membrane when compared to wt myocytes.

The data collected and the comparison between neonatal and adult MDX cardiac myocytes and their age-matched counterparts suggest that compensatory mechanisms that aim at re-establishing normal levels on free CNs occur with age. The two following experimental findings support this hypothesis. First, basal levels of free and total cyclic nucleotide significantly changed with age, nearly abolishing the difference encountered in neonatal cardiomyocytes. Second, cAMP and cGMP PDE mRNA levels were found to

be significantly higher in mdx adult cardiomyocytes when compared to age-matched control cells. This difference was not present in neonatal cardiomyocytes.

Taking into consideration the data as a whole it is possible to hypothesise that defective cyclic nucleotide signalling may be involved in the cardiomyopathy associated with DMD. Functional analysis of cardiac myocyte contractility supports this hypothesis as mdx cardiomyocytes develop significantly lower force of the contraction at basal levels and also under stretch. Treatment with IBMX completely restores the force of contraction as well as the force-stretch relationship in the mdx cardiomyocytes. The combination of this data and the higher levels of PDEs (as inferred from mRNA levels) in adult mdx cardiac myocytes suggest that higher PDE activity and expression in these cells might be involved in the development of the cardiomyopathy associated with the disease.

Appendix 1. Solutions and reagents

Tyrode Buffer Solution (pH 7.4; Filter sterilise)

Stock	Molarity	500 ml 1x	For 500ml 10x	
NaCl 4M	130.0 mM	16.25 ml	162.5 ml	
KCl 2M	5.6 mM	1.4 ml	14.0 ml	
$MgCl_2$ 1M	3.5 mM	1.75 ml	17.5 ml	
Hepes MW 238.3 (Sigma : H4034-25g)	5.0 mM	595 mg	5.95 g	
Sodium Phosphate dibasic (Na_2HPO_4) MW 141.96 (Sigma : S9763-100g)	0.4 mM	28.4 mg	0.284 g	
Glucose MW 180.16 (Sigma : G7528-250g)	10.0 mM	0.9 g	Add on reconstitution	180 mg per 100 ml
Taurine MW 125.15 (Sigma : T0624-100mg)	20.0 mM	1.25 g	12.5g	
H_2O (ml)	-			

Digestion Enzyme	Concentration/mg of enzyme	Volume of Tyrode Buffer	Concentration of $CaCl_2$
Liberase TH (Roche : 5401151001	50µg / ml	20mL	0.1mM
Collagenese type 2, Worthington 220-265 U/mg_ LS004176	25mg	25mL	50uM

MEM Culture Medium (as derived from Li et al. (2003).)

For adenoviral infection

	Mass for 500ml in Cell Culture Water
MEM with Hank's salts (Sigma : M1018-10L)	5.37 g
$NaHCO_3$ (9mM) MW 84.1	375 mg
L- Glutamine (1%)	5 ml
Penicillin / Streptomycin (1%)	5 ml

M-199 Culture Medium *(Louch, Sheehan and Wolska* - J Mol Cell Cardiol. 2011 September; 51(3): 288–298)

Medium 199 – no glutamine

Supplemented with Creatine-Carnitine-Taurine (CCT):

	Mass for 100ml	Mass for 200ml	Mass for 500ml
Creatine (5mM) *MW 131.13*	0.066 g	0.131 g	328 mg
L-Carnitine (2mM) *MW 197.66*	0.040 g	0.079 g	198 mg
Taurine (5mM) *MW 125.15*	0.063 g	0.125 g	313 mg
$NaHCO_3$ (10mM) *MW 84.1*	0.084 g	0.168 g	421 mg
HEPES (10mM) *MW 238.3*	0.238 g	0.477 g	1,192 mg (1.19 g)

Modified in light of Pavlovic D 2010 – 2mM Taurine

	Mass for 50ml	Mass for 100ml
Creatine (5mM) *MW 131.13*	33 mg	0.066 g
L-Carnitine (2mM) *MW 197.66*	20 mg	0.040 g
Taurine (2mM) *MW 125.15*	13 mg	0.025 g

ADS 10x – 250mL

NaCl	1060mM	15.4g
Hepes	200mM	11.9g
NaH_2PO_4	8mM	0.284g
KCl	53mM	0.988g
$MgSO_4$	4mM	0.247g
Glucose	50mM	2.253g
pH 7.4 and filter sterilise		

Collagenese Buffer – 50mL:

Collagenese (Roche 10103586001)	22.5mg
Pancreatin (Sigma P1750 25mg)	62.5mg

Stir for 5 minutes, filter sterilise and keep in ice.

Medium Day 1 (M1) – 100mL

D-Mem 25mM Hepes (Invitrogen 42430025)	67ml
M-199 (Invitrogen 31150022)	17.5ml
Horse serum (HS)	10ml
Newborn Calf Serum (NCS)	5ml
Glutamin 200mM	1ml
Pen/strep	100µl
Insulin-Transferrin-Selenium-X Supplement (100X)	1ml

Medium Day 2 (M2) – 100mL

D-Mem 25mM Hepes (Invitrogen 42430025)	75ml
M-199 (Invitrogen 31150022)	17ml
Horse serum (HS)	5ml
Newborn Calf Serum (NCS)	0.5ml
Glutamin 200mM	1ml
Pen/strep	100l
Insulin-Transferrin-Selenium-X Supplement (100X)	1ml

FRET Saline - Doses for 1 liter.

NaCl	125mM	7.3g
KCl	5mM	0.372g
Na3PO4	1mM	0.38g
MgSO4	1mM	0.246g
Hepes	20mM	4.74g
Glucose	5.5 mM	1g
CaCl2	1mM	

Antibodies

Antibody	**Company and code**	**Dilution**
Mouse Anti eNOS	BD laboratories 610296	1:1000

Mouse Anti nNOS – NOSI (A-11)	Santa Cruz 5302	1:500
Mouse Anti iNOS	Abcam ab49999	1:1000
Mouse Anti Dystrophin NCL- DYs1	Leica 2018-01	1:50
Mouse Anti NKA α	Santa Cruz 28800	1:500
Rabbit anti Soluble Guanyly cyclase beta1 subunit	Abcam ab154841	1:1000
Rabbit Anti β2-AR	Santa Cruz 570	1:1000
Mouse Anti IP3R-3	DB laboratories 610313	1:500
Mouse Anti GAPDH	Protein tech	1:2000
Mouse anti α-actinin Antibody (H-2)	Santa Cruz 17829	1:2000
Mouse anti rabbit IgG HRP	Santa Cruz 2357	1:10000
Anti mouse IgG HRP	Promega w4028	1:20000
Alexa fluor 488 goat anti-mouse	Thermo Fisher Scientific A11001	1:1000
Alexa fluor 647 goat anti mouse	Thermo Fisher Scientific A21255	1:1000